NUMERICAL STUDY OF INFLUENCE OF AIR CEILING DIFFUSERS ON ROOM AIR FLOW CHARACTERISTICS

MEHDI CHOWAID

January 2016

NUMERICAL STUDY OF INFLUENCE OF AIR CEILING DIFFUSERS ON ROOM AIR FLOW CHARACTERISTICS

A THESIS SUBMITTED TO
THE GRADUATE SCHOOL OF NATURAL AND APPLIED SCIENCES OF
ÇANKAYA UNIVERSITY

BY
MEHDI CHOWAID

IN PARTIAL FULFILLMENT OF THE REQUIREMENTS FOR THE DEGREE OF
MASTER OF SCIENCE
IN
THE DEPARTMENT OF
MECHANICAL ENGINEERING

January 2016

Title of the Thesis: **Numerical Study Of Influence Of Air Ceiling Diffusers On Room Air Flow Characteristics.**

Submitted by **Mehdi CHOWAID**

Approval of the Graduate School of Natural and Applied Sciences, Çankaya University.

Prof. Dr. Halil Tanyer EYYUBOĞLU
Director

I certify that this thesis satisfies all the requirements as a thesis for the degree of Master of Science.

Prof. Dr. Sıtkı Kemal İDER
Head of Department

This is to certify that we have read this thesis and that in our opinion it is fully adequate, in scope and quality, as a thesis for the degree of Master of Science.

Prof. Dr. Taner ALTUNOK
Supervisor

Examination Date: 08.01.2016

Examining Committee Members

Prof. Dr. Taner ALTUNOK	(THK)
Asst Prof. Dr. Özgün SELVI	(Çankaya University)
Prof. Dr. Adem ACIR	(Gazi University)

STATEMENT OF NON-PLAGIARISM PAGE

I hereby declare that all information in this document has been obtained and presented in accordance with academic rules and ethical conduct. I also declare that, as required by these rules and conduct, I have fully cited and referenced all material and results that are not original to this work.

Name, Last Name : **Mehdi CHOWAID**
Signature :
Date : **08.01.2016**

ABSTRACT

NUMERICAL STUDY OF INFLUENCE OF AIR CEILING DIFFUSERS ON ROOM AIR FLOW CHARACTERISTICS

CHOWAID, Mehdi
M.Sc., Department of Mechanical Engineering
Supervisor: Prof. Dr. Taner ALTUNOK

January 2016, 129 pages

A theoretical study includes details flow turbulence in air-conditioned Turkey spaces with the determination of the boundary conditions depending on the Code of cooling is done in this thesis.

Two kinds of two-dimensional and three-dimensional ventilation problems have been considered. Isothermal ventilation in simple rooms. And non-isothermal ventilation with coupled heat or mass transfer.

The investigation has studied the flow and thermal boundary conditions for four different diffusers (displacement, grille, slot, and square diffusers). The dimensions of the physical model are (5.16×3.65 m) with (2.43 m high). The supply condition for four diffusers are (displacement (0.0768 kg/s), grille (0.0768 kg/s), slot (0.1410kg/s), square (0.750kg/s)) and temperature at supply for all types is (15° C), the return considered as the type of diffusers has been imposed zero flow pressure and temperature at (24° C).

A modified version of a three-dimensional computer program (fluent 6.3.26) by using finite-volume method was used to simulate the complex flow with buoyant inside the model room. They have been investigated numerically by using several turbulence models and the method solution by using k-ε and k-ω models.

The numerical results can be divided into:

1. Results which compared with the measured ones obtained from ASHRAE RP-1009 three-dimensional as non-Isothermal and two cases of two-dimensional as Isothermal.
2. There is a good agreement with (k-ω) model gives more accurate fitting and closer to reality, the reason for this is due to the overall average error for displacement ventilation (19.87 % at velocity carves) and (14.20 % at temperature carve).
3. The Effective Draft Temperature (EDT) for four types of diffusers for three orientations simulating the Iraqi condition (east, south, and west) for these models are as follow:

The EDT performance of various commonly used turbulence models for complex airflows and temperature distributions with forced ventilation conditions for different buildings in Iraq, also obtain displacement outlet is better than other types. The accuracy of the results can be found at different levels in terms of average temperature.

Keywords: Surface Diffraction, Edge Diffraction, Fringe Waves.

ÖZ

TAVAN DİFUZORLERİNİN ODADAKİ HAVA AKIM ÖZELLİKLERİNE ETKİSİ ÜZERİNE SAYISAL ÇALIŞMA

CHOWAID, Mehdi
Yüksek Lisans, Makine Mühendisliği Anabilim Dalı
Tez Yöneticisi: Prof. Dr. Taner ALTUNOK

Ocak 2016, 129 sayfa

Bu araştırmada, soğutma kurallarına bağlı olarak sınır koşulları belli olan klimalı alanlardaki hava akış türbülanslarını içeren kuramsal bir çalışma yapılmıştır.
İki boyutlu ve üç boyutlu olmak üzere iki tür havalandırma sorunu ele alınmıştır: Sade odalarda izotermal havalandırma ve ısı veya kütle transferi ile gerçekleşen izotermal olmayan havalandırma.
Araştırmada, dört farklı dağıtıcı için (deplasman, ızgara, kesik tip ve kare anemostatları) akım ve termal sınır koşulları üzerine çalışma yapılmıştır. Fiziksel modelin boyutları (2.43 metre yüksekliğe sahip olarak) (5.16 x 3.65 metredir). Dört anemostat için tedarik koşulu deplasman için (0.0768 kg/s), ızgara için (0.0768 kg/s), kesik tip için (0.1410 kg/s) ve kare anemostat için (0.750 kg/s) ayrıca tüm tipler için tedarik sıcaklığı (15° C) ve anemostat türlerine ilişkin dönüş ise sıfır akım basıncı ve (24° C) olarak değerlendirilmiştir.
Sınırlı hacim yöntemini kullanarak üç boyutlu bir bilgisayar programının (Fluent 6.3.26) modifiye edilmiş bir sürümü, model odadaki hareketli kompleks akışı simüle

etmek adına kullanılmıştır. Bunlar, birkaç türbülans modeli ayrıca $k\text{-}_E$ ve $k\text{-}_w$ modellerini kullanan yöntem çözümü kullanarak sayısal olarak incelenmiştir.

Sayısal sonuçlar aşağıdaki gruplara ayrılabilir:

1. İzotermal olmayan üç boyutlu ve izotermal olan iki boyutlu iki vaka olarak ASHRAE RP-1009'dan alınan ölçülmüş değerler ile karşılaştırılan sonuçlar,
2. ($k\text{-}_w$) modelinin daha doğru ve gerçeğe daha yakın olduğu görülmektedir, bunun nedeni deplasman havalandırması (hız eğrilerinde %19.87) ve (sıcaklık eğrisinde %14.20) genel ortalama hata payıdır.
3. Bu modeller için Irak koşullarını (doğu, güney ve batı) simüle eden üç yön için dört farklı anemostata ilişkin Geçerli Taslak Sıcaklıklar (EDT) aşağıdaki gibidir:

Deplasman çıkışından alınan Irak'taki farklı binalar için zorunlu havalandırma koşulları ile kompleks hava akışı ve sıcaklık dağılımları için yaygın olarak kullanılan türbülans modellerinin EDT performansı, diğer türlerden daha iyidir. Bu sonuçların doğruluğu, ortalama sıcaklık koşullarında farklı seviyelerde bulunabilir.

Anahtar Kelimeler: Yüzey Kırılması, Kenar Kırılması, Saçak Dalgaları.

ACKNOWLEDGEMENTS

I would like to express my sincere gratitude to Prof. Dr. Taner ALTUNOK for his supervision, special guidance, suggestions, and encouragement through the development of this thesis.

It is a pleasure to express my special thanks to my family for their valuable support.

TABLE OF CONTENTS

STATEMENT OF NON PLAGIARISM..... iii
ABSTRACT..... iv
ÖZ..... vi
ACKNOWLEDGEMENTS..... viii
TABLE OF CONTENTS..... ix
LIST OF FIGURES..... xiv
LIST OF TABLES..... xxvi

CHAPTERS:

1. INTRODUCTION..... 1
- **1.1.** Brief History of Air Conditioning..... 1
- **1.2.** The Meaning of Air Conditioning..... 2
- **1.3.** Ventilation Requirements..... 2
- **1.4** Ventilation Process..... 3
- **1.5** Types of Ventilation..... 3
  - **1.5.1** Local Exhaust Ventilation (LEV)..... 3
  - **1.5.2** Piston Ventilation (Unidirectional)..... 4
  - **1.5.3** Mixing Ventilation (Dilution)..... 4
  - **1.5.4** Displacement Ventilation..... 5
- **1.6** Thermal and Environment Comfort..... 6
- **1.7** Basic Flow Patterns..... 8
  - **1.7.1** Outlet Types..... 8
- **1.8** The Reason of Study Air Distribution..... 10
- **1.9** Types of Diffusers..... 10
- **1.10** Objectives of the Present Work..... 11

2. LITERATURE REVIEW..... 12
- **2.1.** Experimental Works..... 12

2.2. Numerical Simulations..... 15
2.3. Experimental and Numerical Studies..... 20
2.4. Summary of Literature Review..... 25
2.5 Scope of the Present Work..... 28
3. THEORETICAL FORMULATION..... 33
3.1. Introduction about CFD..... 33
3.1.1 General..... 33
3.1.2 Types of Prediction Models and CFD Preference..... 34
3.2. Assumptions for 2D and 3D models..... 35
3.3. Turbulence Models..... 35
3.3.1 The standard k-ε model..... 35
3.3.2 The RNG k-ε model..... 37
3.3.3 The Realizable k-ε model..... 39
3.3.4 The k-ω Model..... 41
3.4 Numerical Modeling..... 43
3.4.1 Room geometry..... 43
3.4.2 Mesh generation..... 43
3.4.2.1 Surface mesh generation..... 43
3.4.2.2 Volume mesh generation..... 43
3.5 Numerical Cases Setup in Fluent 6.3.26..... 44
3.5.1 Setup for 2D ventilation..... 44
3.5.1.1 General setup..... 44
3.5.1.2 Materials setup..... 44
3.5.1.3 Solution controls..... 45
3.5.1.4 Convergence criteria..... 45
3.5.2 Setup for 3D ventilation..... 46
3.5.2.1 General setup..... 46
3.5.2.2 Materials setup..... 46
3.5.2.3 Solution controls..... 46

3.5.2.4 Convergence criteria..... 46
3.6 Data Analysis Method..... 47
3.7 Effective Draft Temperature (EDT)..... 47
4. VALIDATION STUDY FOR 3D AND 2D VENTILATION..... 49
4.1. Validation study of 2D Isothermal Ceiling Jet..... 49
4.1.1 First case..... 49
4.1.1.1 Boundary conditions..... 49
4.1.1.2 Results and discussion..... 50
4.1.2 Second case..... 50
4.2 Validation study of IEA Annex 20..... 50
4.2.1 Boundary conditions..... 51
4.2.2 Numerical simulation with different k-ε turbulence models... 51
4.2.2.1 Prediction with standard k-ε turbulence model..... 51
4.2.2.2 Prediction with RNG k-ε model and Realizable k-ε model..... 51
4.3 3D Ventilation Flows with Heat and Mass Transfer..... 52
4.3.1 Displacement ventilation..... 52
4.3.1.1 Modeling and simulation..... 53
4.3.2 Ceiling slot ventilation..... 55
4.3.2.1 Test conditions..... 55
4.3.2.2 Modeling and simulation..... 56
4.3.3 Ceiling square ventilation..... 57
4.3.3.1 Test conditions..... 57
4.3.3.2 Modeling and simulation..... 58
4.4 Illustrations list..... 59
5. RESULTS AND DISCUSSION..... 75
5.1. Case Studies Suggestion..... 75
5.2. Boundary Conditions..... 76
5.2.1. Modeling and simulation……..... 76

5.2.1.1 Turbulence modeling……..... 76
5.2.1.2 Computation meshes……..... 76
5.2.1.3 Numerical schemes……..... 77
5.3 Displacement Diffuser..... 77
5.3.1 Boundary conditions..... 77
5.3.2 Summary of boundary conditions..... 77
5.3.3 Simulation results..... 78
5.4 Grille Diffuser..... 78
5.4.1 Boundary conditions..... 78
5.4.2 Summary of boundary conditions..... 78
5.4.3 Simulation results..... 79
5.5 Slot Diffuser..... 79
5.5.1 Boundary conditions..... 79
5.5.2 Summary of boundary conditions..... 79
5.5.3 Simulation results..... 80
5.6 Square diffuser..... 80
5.6.1 Boundary conditions..... 80
5.6.2 Summary of boundary conditions..... 81
5.6.3 Simulation results..... 81
6. CONCLUSIONS AND SUGGESTIONS FOR FUTURE WORKS..... 129
6.1 Conclusions..... 129
6.2 Suggestions for Future Works..... 130
REFERENCES..... R1
CURRICULUM VITAE..... A1

LIST OF FIGURES

FIGURES

Figure 1.1	Schematic representing a LEV.....	4
Figure 1.2.a	Schematic representing Piston ventilation (Unidirectional).....	5
Figure 1.2.b	Schematic representing Mixing Ventilation.....	5
Figure 1.3	Schematic representing displacement ventilation.....	6
Figure 1.4	Acceptable ranges of operative temperature and humidity for people in typical summer and winter clothing during light and primarily sedentary activity (≤ 1.2 met).....	7
Figure 1.5	Air motion characteristics of Group A outlet.....	8
Figure 1.6	Air motion characteristics of Group B outlet.....	9
Figure 1.7	Air motion characteristics of Group C outlet.....	9
Figure 1.8	Air motion characteristics of Group D outlet.....	9
Figure 1.9	Air motion characteristics of Group E outlet.....	10
Figure 1.10	Eight commonly used air supply diffusers.....	11
Figure 1.10.a	Grille.....	10
Figure 1.10.b	Nozzle.....	10
Figure 1.10.c	Valve.....	11
Figure 1.10.d	Displacement.....	11
Figure 1.10.e	Slot.....	11
Figure 1.10.f	Square Ceiling.....	11
Figure 1.10.g	Round Ceiling.....	11
Figure 1.10.h	Vortex.....	11
Figure 2.1	The full-scale section of the Boeing 767-300 aircraft cabin.....	28
Figure 2.2	Furnishings and heat load in the full-scale room.....	29
Figure 2.3	A photograph of the test chamber configured for 4 heat sources and showing the air temperature sensor assembly.....	29

FIGURES

Figure 2.4	Physical model of ceiling air-supply.....	30
Figure 2.5	The models of outlets.....	30
Figure 2.6	An air channel along the cross section of fuselage to insulate an aircraft.....	31
Figure 2.7	Environmental chamber and diffusers used for the TDV and UFAD systems.....	32
Figure 2.7.a	Environmental chamber.....	31
Figure 2.7.b	Environmental chamber.....	31
Figure 2.7.c	Perforated-corner diffuser.....	31
Figure 2.7.d	Swirl diffuser.....	31
Figure 2.7.e	Linear diffuser.....	31
Figure 2.7.f	Perforated-floor panel diffuser.....	32
Figure 2.8	The small-scale experimental test facility of an airliner cabin in a water tank.....	32
Figure 3.1	The meshed model for displacement and square ventilation.....	48
Figure 4.1	Dimension and Layout of the Room.....	60
Figure 4.2	Air Velocity in a Vertical Line (Supply Position).....	61
Figure 4.3	Air Velocity in a Vertical Line (0.75 m from the Supply).....	61
Figure 4.4	Air Velocity in a Vertical Line (Return Position).....	61
Figure 4.5	Air velocity profile, a- conventional method, b- k-ε (SWF).....	62
Figure 4.6	A comparison between predicted results with experimental data using standard k-ε model at X=3 m.....	62
Figure 4.7	A comparison between predicted results with experimental data using standard k-ε model at X=6 m.....	63
Figure 4.8	Comparison between predicted results using different k-ε models with experimental data, a- X=3m, b- X=6m.....	63
Figure 4.9	Configuration of the displacement ventilation test case.....	64

FIGURES

Figure 4.10 The positions of the measuring poles for the displacement ventilation test case..... 64

Figure 4.11 Prediction of the air velocity with Realizable k-ε model and Enhancement Wall Treatment and SST k-ω, (Z=height/total room height (H), U=velocity/supply velocity (U0), H=2.43m, U0=0.35m/s)..... 65

Figure 4.12 Prediction of the air temperature with Realizable k-ε model and Enhancement Wall Treatment and SST k-ω, (*Z=height/total room height (H), □=(T-Tin/Tout-Tin), H=2.43m, Tin=13.0ºC, Tout=22.2ºC*)..... 66

Figure 4.13 Configuration of ceiling slot ventilation test case..... 67

Figure 4.14 The positions of the measuring poles for the ceiling slot ventilation test case..... 67

Figure 4.15.a Details of the slot diffuser..... 67

Figure 4.15.b Inflow direction..... 68

Figure 4.15 Installation and details of the slot diffuser..... 68

Figure 4.16 Prediction of the air velocity with Realizable k-ε model and Enhancement Wall Treatment and SST k-ω, (*Z=height/total room height (H), U=velocity/supply velocity (U0), H=2.43m, U0=3.9m/s*)..... 69

Figure 4.17 Prediction of the air temperature with Realizable k-ε model and Enhancement Wall Treatment and SST k-ω, (*Z=height/total room height (H), □=(T-Tin/Tout-Tin), H=2.43m, Tin=16.3ºC, Tout=21.4ºC*)..... 70

Figure 4.18 Configuration of ceiling slot ventilation test case..... 70

FIGURES

Figure 4.19 The positions of the measuring poles for the ceiling slot ventilation test case..... 71

Figure 4.20 Modeling of the square diffuser..... 71

Figure 4.21 Prediction of the air velocity with Realizable k-ε and SST k-ω model compared with box and momentum, (*Z=height/total room height (H), U=velocity/supply velocity (U0), H=2.43m, U0=5.2m/s*)..... 72

Figure 4.22 Prediction of the air temperature with Realizable k-ε and SST k-ω model compared with box and momentum, (*Z=height/total room height (H), □=(T-Tin/Tout-Tin), H=2.43m, Tin=14.5ºC, Tout=24.1ºC*)..... 73

Figure 4.23 Fig. (4.23) Prediction of the air temperature with Realizable k-ε and SST k-ω model compared with box and momentum, (*Z=height/total room height (H),* $\theta=(T-T_{in}/T_{out}-T_{in})$*, H=2.43m,* $T_{in}=14.5^{\circ}C$*,* $T_{out}=24.1^{\circ}C$)..... 74

Figure 5.1 Element of test room and positions of the supply diffusers (1- person, 2- computer, 3- table, 4- cabinet, 5- fluorescent lamp, 6- window, 7- exhaust for the displacement diffuser, 8- exhaust for the mixing diffusers)..... 82

Figure 5.2 The positions of the measuring poles..... 82

Figure 5.2.a The displacement ventilation test case..... 82

Figure 5.2.b The ceiling slot ventilation test case..... 82

Figure 5.3 Configuration of the displacement ventilation test case..... 83

Figure 5.4 Displacement diffuser (case 1) prediction of the air velocity by Realizable k-ε model with Enhancement Wall Treatment and SST k-ω, (*Z=height/total room height (H), U=velocity/supply velocity (U0), H=2.43m, U0=0.35m/s*)..... 84

Figure 5.5 Displacement diffuser (case 1) prediction of the air temperature by Realizable k-ε model with Enhancement Wall Treatment and SST k-ω, 86 (Z=height/total room height (H), θ=(T-Tin/Tout-Tin), H=2.43m, Tin=15.0ºC, Tout=24ºC)..... 85

FIGURES

Figure 5.6 Displacement diffuser (case 2) prediction of the air velocity by Realizable k-ε model with Enhancement Wall Treatment and SST k-ω, (*Z=height/total room height (H), U=velocity/supply velocity (U0), H=2.43m, U0=0.35m/s*)..... 86

Figure 5.7 Displacement diffuser (case 2) prediction of the air temperature by Realizable k-ε model with Enhancement Wall Treatment and SST k-ω, (Z=height/total room height (H), θ=(T-Tin/Tout-Tin), H=2.43m, Tin=15.0ºC, Tout=24ºC)..... 87

Figure 5.8 Displacement diffuser (case 3) prediction of the air velocity by Realizable k-ε model with Enhancement Wall Treatment and SST k-ω, (*Z=height/total room height (H), U=velocity/supply velocity (U0), H=2.43m, U0=0.35m/s*)..... 88

Figure 5.9 Displacement diffuser (case 3) prediction of the air temperature by Realizable k-ε model with Enhancement Wall Treatment and SST k-ω, (Z=height/total room height (H), θ=(T-Tin/Tout-Tin), H=2.43m, Tin=15.0ºC, Tout=24ºC)..... 89

Figure 5.10 Distribution of calculation air temperature contours with k-ε , (case1)..... 89

Figure 5.10.a Plane at z=1.825m..... 89

Figure 5.10.b Plane at z=0.4m..... 89

Figure 5.11 Distribution of calculation air temperature contours with k-ω, (case 1)..... 90

Figure 5.11.a Plane at z=1.825m..... 90

Figure 5.11.b Plane at z=0.4m..... 90
Figure 5.12 Distribution of calculation air temperature contours with k-ε , (case 2)..... 91
Figure 5.12.a Plane at z=1.825m..... 90
Figure 5.12.b Plane at z=0.4m..... 91
Figure 5.13 Distribution of calculation air temperature contours with k-ω , (case 2)..... 91
Figure 5.13.a Plane at z=1.825m..... 91
Figure 5.13.b Plane at z=0.4m..... 91
Figure 5.14 Distribution of calculation air temperature contours with k-ε , (case3)..... 92
Figure 5.14.a Plane at z=1.825m..... 92
Figure 5.14.b Plane at z=0.4m..... 92
Figure 5.15 Distribution of calculation air temperature contours with k-ω , (case 3) 93
Figure 5.15.a Plane at z=1.825m..... 92
Figure 5.15.b Plane at z=0.4m..... 93
Figure 5.16 Effect draft temperature for k-ε and k-ω models..... 94
Figure 5.16.a Case1..... 93
Figure 5.16.b Case2..... 93
Figure 5.16.c Case3..... 94
Figure 5.17 Configuration of grille ventilation test case..... 94
Figure 5.18 Grille diffuser (case 1) prediction of the air velocity by Realizable k-ε model with Enhancement Wall Treatment and SST k-ω, (*Z=height/total room height (H), U=velocity/supply velocity (U0), H=2.43m, U0=2.7m/s*)..... 95
Figure 5.19 Grille diffuser (case 1) prediction of the air temperature by Realizable k-ε model with Enhancement Wall Treatment and SST k-ω, (Z=height/total room height (H), θ=(T-Tin/Tout- 96

Tin), H=2.43m, Tin=15.0ºC, Tout=24ºC).....

Figure 5.20 Grille diffuser (case 2) prediction of the air velocity by Realizable k-ε model with Enhancement Wall Treatment and SST k-ω, (*Z=height/total room height (H), U=velocity/supply velocity (U0), H=2.43m, U0=2.7m/s*)..... 97

Figure 5.21 Grille diffuser (case 2) prediction of the air temperature by Realizable k-ε model with Enhancement Wall Treatment and SST k-ω, (Z=height/total room height (H), θ=(T-Tin/Tout-Tin), H=2.43m, Tin=15.0ºC, Tout=24ºC)..... 98

Figure 5.22 Grille diffuser (case 3) prediction of the air velocity by Realizable k-ε model with Enhancement Wall Treatment and SST k-ω, (*Z=height/total room height (H), U=velocity/supply velocity (U0), H=2.43m, U0=2.7m/s*)..... 99

Figure 5.23 Grille diffuser (case 3) prediction of the air temperature by Realizable k-ε model with Enhancement Wall Treatment and SST k-ω, (Z=height/total room height (H), θ=(T-Tin/Tout-Tin), H=2.43m, Tin=15.0ºC, Tout=24ºC)..... 100

Figure 5.24 Distribution of calculation air temperature contours with k-ε , (case 1)..... 101

Figure 5.24.a Plane at z=1.825m..... 101

Figure 5.24.b Plane at z=0.4m..... 101

Figure 5.25 Distribution of calculation air temperature contours with k-ω , (case 1)..... 102

Figure 5.25.a Plane at z=1.825m..... 101

Figure 5.25.b Plane at z=0.4m..... 102

Figure 5.26 Distribution of calculation air temperature contours with k-ε , (case 2)..... 102

Figure 5.26.a Plane at z=1.825m..... 102

Figure 5.26.b Plane at z=0.4m..... 102

Figure 5.27 Distribution of calculation air temperature contours with k-ω , (case 2)..... 103
Figure 5.27.a Plane at z=1.825m..... 103
Figure 5.27.b Plane at z=0.4m..... 103
Figure 5.28 Distribution of calculation air temperature contours with k-ε , (case 3)..... 104
Figure 5.28.a Plane at z=1.825m..... 103
Figure 5.28.b Plane at z=0.4m..... 104
Figure 5.29 Distribution of calculation air temperature contours with k-ω , (case 3)..... 104
Figure 5.29.a Plane at z=1.825m..... 104
Figure 5.29.b Plane at z=0.4m..... 104
Figure 5.30 Grille effect draft temperature for k-ε and k-ω models..... 105
Figure 5.30.a Case1..... 105
Figure 5.30.b Case2..... 105
Figure 5.30.c Case3..... 105
Figure 5.31 Configuration of ceiling slot ventilation test case..... 106
Figure 5.32 Slot diffuser (case 1) prediction of the air velocity by Realizable k-ε model with Enhancement Wall Treatment and SST k-ω, (*Z=height/total room height (H), U=velocity/supply velocity (U0), H=2.43m, U0=3.9m/s*)..... 107
Figure 5.33 Slot diffuser (case 1) prediction of the air temperature by Realizable k-ε model with Enhancement Wall Treatment and SST k-ω, (Z=height/total room height (H), θ=(T-Tin/Tout-Tin), H=2.43m, Tin=15.0ºC, Tout=24ºC)..... 108
Figure 5.34 Slot diffuser (case 2) prediction of the air velocity by Realizable k-ε model with Enhancement Wall Treatment and SST k-ω, (*Z=height/total room height (H), U=velocity/supply velocity (U0), H=2.43m, U0=3.9m/s*)..... 109

Figure 5.35 Slot diffuser (case 2) prediction of the air temperature by Realizable k-ε model with Enhancement Wall Treatment and SST k-ω, (Z=height/total room height (H), θ=(T-Tin/Tout-Tin), H=2.43m, Tin=15.0ºC, Tout=24ºC)..... 110
Figure 5.36 Slot diffuser (case 3) prediction of the air velocity by Realizable k-ε model with Enhancement Wall Treatment and SST k-ω, (*Z=height/total room height (H), U=velocity/supply velocity (U0), H=2.43m, U0=3.9m/s*)..... 111
Figure 5.37 Slot diffuser (case 3) prediction of the air temperature by Realizable k-ε model with Enhancement Wall Treatment and SST k-ω, (Z=height/total room height (H), θ=(T-Tin/Tout-Tin), H=2.43m, Tin=15.0ºC, Tout=24ºC)..... 112
Figure 5.38 Distribution of calculation air temperature contours with k-ε , (case 1)..... 112
Figure 5.38.a Plane at z=1.825m..... 112
Figure 5.38.b Plane at z=0.4m..... 112
Figure 5.39 Distribution of calculation air temperature contours with k-ω, (case 1)..... 113
Figure 5.39.a Plane at z=1.825m..... 113
Figure 5.39.b Plane at z=0.4m..... 113
Figure 5.40 Distribution of calculation air temperature contours with k-ε , (case 2)..... 114
Figure 5.40.a Plane at z=1.825m..... 113
Figure 5.40.b Plane at z=0.4m..... 114
Figure 5.41 Distribution of calculation air temperature contours with k-ω , (case 2)..... 114
Figure 5.41.a Plane at z=1.825m..... 114
Figure 5.41.b Plane at z=0.4m..... 114
Figure 5.42 Distribution of calculation air temperature contours with k-ε , 115

(case 3).....
Figure 5.42.a Plane at z=1.825m..... 115
Figure 5.42.b Plane at z=0.4m..... 115
Figure 5.43 Distribution of calculation air temperature contours with k-ω , (case 3)..... 116
Figure 5.43.a Plane at z=1.825m..... 115
Figure 5.43.b Plane at z=0..... 116
Figure 5.44 Slot effect draft temperature for k-ε and k-ω models..... 116
Figure 5.44.a Case1..... 116
Figure 5.44.b Case2..... 116
Figure 5.44.c Case3..... 117
Figure 5.45 Configuration of ceiling slot ventilation test case..... 117
Figure 5.46 Square diffuser (case 1) prediction of the air velocity by Realizable k-ε model with Enhancement Wall Treatment and SST k-ω, (*Z=height/total room height (H), U=velocity/supply velocity (U0), H=2.43m, U0=5.2m/s*)..... 119
Figure 5.47 Square diffuser (case 1) prediction of the air temperature by Realizable k-ε model with Enhancement Wall Treatment and SST k-ω, (Z=height/total room height (H), θ=(T-Tin/Tout-Tin), H=2.43m, Tin=15.0ºC, Tout=24ºC)..... 119
Figure 5.48 Square diffuser (case 2) prediction of the air velocity by Realizable k-ε model with Enhancement Wall Treatment and SST k-ω, (*Z=height/total room height (H), U=velocity/supply velocity (U0), H=2.43m, U0=5.2m/s*)..... 120
Figure 5.49 Square diffuser (case 2) prediction of the air temperature by Realizable k-ε model with Enhancement Wall Treatment and SST k-ω, (Z=height/total room height (H), θ=(T-Tin/Tout-Tin), H=2.43m, Tin=15.0ºC, Tout=24ºC)..... 121
Figure 5.50 Square diffuser (case 3) prediction of the air velocity by 122

Realizable k-ε model with Enhancement Wall Treatment and SST k-ω, (*Z=height/total room height (H), U=velocity/supply velocity (U0), H=2.43m, U0=5.2m/s*).....

Figure 5.51 Square diffuser (case 3) prediction of the air temperature by Realizable k-ε model with Enhancement Wall Treatment and SST k-ω, (Z=height/total room height (H), θ=(T-Tin/Tout-Tin), H=2.43m, Tin=15.0ºC, Tout=24ºC)..... 123

Figure 5.52 Distribution of calculation air temperature contours with k-ε , (case 1)..... 124

Figure 5.52.a Plane at z=1.825m..... 124

Figure 5.52.b Plane at z=0.4m..... 124

Figure 5.53 Distribution of calculation air temperature contours with k-ω , (case 1)..... 125

Figure 5.53.a Plane at z=1.825m..... 124

Figure 5.53.b Plane at z=0.4m..... 125

Figure 5.54 Distribution of calculation air temperature contours with k-ε , (case 2)..... 125

Figure 5.54.a Plane at z=1.825m..... 125

FIGURES

Figure 5.54.b Plane at z=0.4m..... 125

Figure 5.55 Distribution of calculation air temperature contours with k-ω , (case 2)..... 126

Figure 5.55.a Plane at z=1.825m..... 126

Figure 5.55.b Plane at z=0.4m..... 126

Figure 5.56 Distribution of calculation air temperature contours with k-ε , (case 3)..... 127

Figure 5.56.a Plane at z=1.825m..... 126

Figure 5.56.b Plane at z=0.4m..... 127

Figure 5.57 Distribution of calculation air temperature contours with k-ω , (case 3)..... 127
Figure 5.57.a Plane at z=1.825m..... 127
Figure 5.57.b Plane at z=0.4 m..... 127
Figure 5.58 Slot effect draft temperature for k-ε and k-ω models..... 128
Figure 5.58.a Case1..... 128
Figure 5.58.b Case2..... 128
Figure 5.58.c Case3..... 128

LIST OF TABLES

TABLES

Table 1	Summary of Experimental Researches.....	25
Table 2	Summary of Numerical Researches.....	26
Table 3	Summary of Experimental and Numerical Researches.....	28
Table 4	Comparison of approaches.....	35
Table 5	Two-Dimensional surface mesh specifications.....	43
Table 6	Two-Dimensional surface mesh parameters.....	44
Table 7	Air properties.....	45
Table 8	Under-Relaxation Factors.....	45
Table 9	Under-Relaxation Factors.....	46
Table 10	Size and position of the displacement and exhaust diffusers.....	52
Table 11	Configuration of the test chamber.....	53
Table 12	Position and size of the slot and exhaust diffusers.....	55
Table 13	Position and size of the square and exhaust diffusers.....	57
Table 14	Outdoor data for Iraq.....	75
Table 15	Indoor conditions.....	75
Table 16	Size of cells.....	77
Table 17	Summarize boundary conditions.....	77
Table 18	Summarize boundary conditions.....	79
Table 19	Summarize boundary conditions.....	80
Table 20	Summarize boundary conditions.....	81

LIST OF ABBREVIATIONS

EDT	Effective Draft Temperature
BRS	Building Related Sickness
SBS	Sick Building Syndrome
LEV	Local Exhaust Ventilation
ACH	Air Change Per Hour
HVAC	Heating, Ventilation, And Air Conditioning
CFD	Computational Fluid Dynamics
VEF	Ventilation Effectiveness Factor
VPTV	Volumetric Particle Tracking Velocimetry
FVGL	Flow Visualization With Green Laser
PEE	Personal Exposure Effectiveness
SIMPLEC	Semi Implicit Method For Pressure Linked Equation-Consistent
EPD	Effective Penetration Depth
MMLA	Micro/Macro-Level Approach
RSM	Reynolds Stress Model
UFAD	Underfloor Air Distribution
LMA	Local Mean Age Of Air
LDA	Laser Doppler Anemometry
PIV	Particle İmage Velocimetry
TDV	Traditional Displacement Ventilation
UFAD	Under-Floor Air Distribution
RNG	Re-Normalization Group
PDE	Partial Differential Equations
SST	Shear-Stress Transport
IEA	International Energy Agency
SWF	Standard Wall-Function
NEWF	Non-Equilibrium Wall Function
PRESTO	PREssure STaggering Option
EDF	Effect Draft Temperature

CHAPTER 1

INTRODUCTION

1.1 Brief History of Air Conditioning

The art of air conditioning developed only gradually form the predecessor art of cooling, cleaning, heating and ventilation. Leonardo Da Vinci had built a ventilating fan by the end of the 15th century. The first text on heating and ventilating was written by Robertson Buchanan, a Glasgow civil engineer, in 1815, [1].

Towards the latter half of the 19th century, the development in the art of humidifying air went along with the progress of textile industry in England devices for measuring pressure, temperature, humidity and flow air were perfected during this period, [1].

It is worth mentioning here the name of A. R. Wolff who designed an air-conditioning system for as many as hundred buildings during his life-time. But it is W. H. Carrier (1876-1950) who is known as the "father of Air Conditioning" while working with Buffalo Forg Co., he developed formulae for optimizing the application of forced-draft fan, developed ratings of pipe-coil heaters and set up a research laboratory. He engineered and installed the first year-round Air Conditioning system, providing for four major functions of heating, cooling, humidifying and dehumidifying, [1].

In 1902, Carrier discovered the relationship between temperature and humidity and how to control them. In 1904, he developed the air washer, a chamber installed with several banks of water sprays for air humidification and cleaning. His method of temperature and humidity regulation, achieved by controlling the dew point of supply air, is still used in many industrial applications, such as lithographic printing plants and textile mills, [2].

Perhaps the first air-conditioned office was the Larkin Administration Building, designed by Frank L. Wright and completed in 1906. Ducts handled air that was drawn in and exhausted at roof level. Wright specified a refrigeration plant which distributed 10°C cooling water to air-cooling coils in air-handling systems, [2].

The U.S. Capitol was air-conditioned in 1929. Conditioned air was supplied from overhead diffusers to maintain a temperature of 75°F (23.9°C) and a relative humidity of 40 percent during summer, and 80°F (26.7°C) and 50 percent during winter. The volume of supply air was controlled by a pressure regulator to prevent cold drafts in the occupied zone, [2].

Perhaps the first fully air conditioned office building was the Milan Building in San Antonio, Texas, which was designed by George Willis in 1928. This air conditioning system consisted of one centralized plant to serve the lower floors and many small units to serve the top office floors, [2].

In 1937, Carrier developed the conduit induction system for multi room buildings, in which recirculation of space air is induced through a heating/cooling coil by a high-velocity discharging airstream. This system supplies only a limited amount of outdoor air for the occupants, [2].

1.2 The Meaning of Air Conditioning

Full air conditioning implies the automatic control of environment either for the comfort of human beings or animals or for the proper performance of some industrial or scientific process. The adjective 'full' demands that the purity, movement, temperature and relative humidity of the air be controlled, within the limits imposed by the design specification. (It is possible that, for certain applications, the pressure of the air in the environment may also have to be controlled), [3].

1.3 Ventilation Requirements

UP to 90% of a typical person’s time is spent indoors, and a large fraction of that time is spent in a residential or commercial environment.

Ventilation occupies an important position in the building design process as building occupants expect good standards of indoor air quality and comfort. People have become more aware of the effect of the indoor environment on health as a result of media publicity surrounding building related sickness (BRS) and the sick building syndrome (SBS). SBS is fundamentally a complaint about the indoor air quality of a building which appears to be more common in air-conditioned buildings than in naturally ventilated buildings. BRS comprises the sensation of stuffy, stale and unacceptable indoor air, irritation of mucous membranes, headache, lethargy and so forth, [4].

ventilation for acceptable indoor air quality shall be considered acceptable if the required rates of acceptable outdoor air are provided for the occupied space, [42].

1.4 Ventilation Process

Ventilation can be either fully 'natural', induced by wind or temperature, fully 'mechanical', where air movement results from power drive applied to a fan or fans or it can be a combination of natural or mechanical. Where a combination of natural and mechanical ventilation is intermittently, this is known as a mixed mode or hybrid system.

The options for ventilation system are described under the following sub-headings [5]:

1. Natural inlet and outlet
2. Natural inlet and mechanical outlet
3. Mechanical inlet and natural outlet
4. Mechanical inlet and outlet

1.5 Types of Ventilation

There are many means to ventilate a room. They may be classified according to their flow conditions or according to the way it ventilates a room. For instance, the flow may be classified as isothermal flow, or as a local exhaust ventilation system. It may confuse at start, but both terms may be used, [6].

1.5.1 Local exhaust ventilation (LEV)

This method of ventilation is based on the principle of capturing the contaminant at source before it spreads into the room air, Figure 1.1. An LEV capture device or extract hood is used, and its shape and flow characteristics are important elements of this method of ventilation. LEV is the most effective method of contaminant extraction, and it is widely used in industrial ventilation, particularly where localized sources of hazardous contaminants are present.

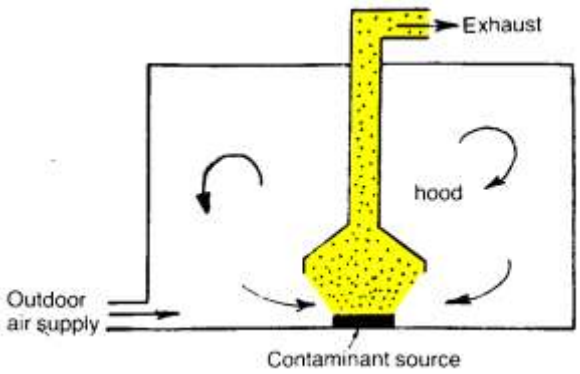

Figure 1.1 Schematic representing a LEV, [6]

1.5.2 Piston ventilation (Unidirectional)

This describes a unidirectional flow of air in which outdoor air propels the contaminated room air ahead of it like a front, Figure (1-2a). The room air is continuously 'swept' by outdoor air, and little spread of contamination generated within the room takes place before this is carried by the outdoor air to the extract duct. This method of ventilation is employed in 'clean rooms', but to be effective the air turbulence must be reduced to a minimum so that contaminant dispersion is minimized.

1.5.3. Mixing ventilation (Dilution)

In mixing ventilation, fresh air is supplied at a high momentum to induce overall recirculation and promote sufficient mixture of contaminants and fresh air. It is thus aimed at diluting the contamination level down to an acceptable level. To avoid sensible air draught in the occupied zone, the supply opening (usually a slot or a diffuser) is often installed at the ceiling level. In most of the cases, the inflow forms a wall jet. As the initial momentum is large enough, the wall jet is able to reach the opposite wall and consequently becomes an impinging jet, see Figure 1.2 b.

Although the wall jet is generally characterized by fully developed turbulence, the air motion in the occupied zone is often characterized by low velocities induced as a result of jet entrainment and air recirculation. Nielsen (1989) showed that the maximum velocity in the occupied zone is linearly proportional to supply air flow rate for isothermal mixing ventilation flows. If the ventilation air flow rate is lower than 4 ACH (air change per hour), however, this proportionality no longer holds and the velocity decays more sharply, [7].

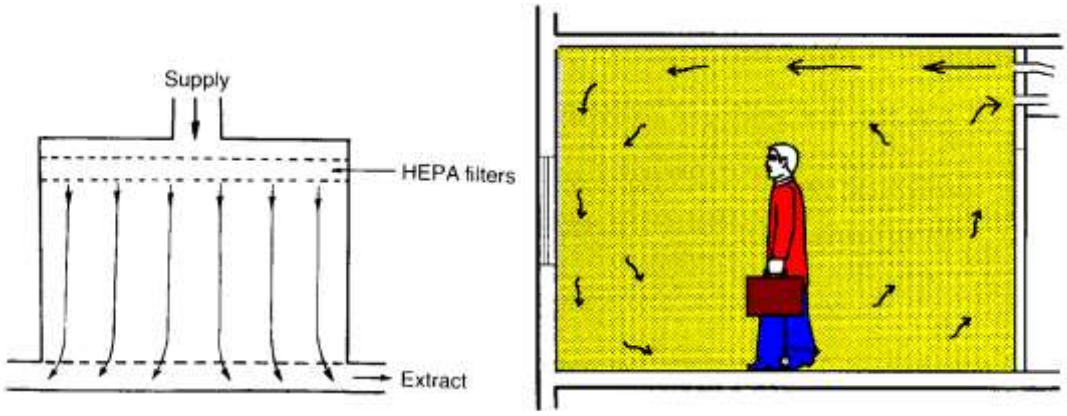

Figure 1.2 a. Schematic representing Piston ventilation (Unidirectional).

b. Schematic representing Mixing Ventilation, [6].

1.5.4. Displacement ventilation

In displacement ventilation, cooled fresh air is supplied at floor level with low momentum. Upward buoyant convection created by indoor heat sources carries contaminants into the upper zone, where recirculation and mixture occur and contaminated air and/or excess heat are exhausted, Figure 1.3. This system thus aims at directly delivering fresh air into the occupied zone without inducing significant mixture with contaminants. Therefore, the buoyancy is the virtual origin of the air motion. Displacement ventilation can be used in cooling conditions only. In displacement ventilation, the mechanism of inducing buoyancy relies on the behavior of both air supply and heat sources. To investigate the performance of such a system, special attention must be paid to the air supply, buoyant convection, and their interaction. Since the air is supplied at a low velocity and at a temperature of usually 2~4 °C lower than the mean room air temperature, the inflow forms a gravity current due to buoyancy and spreads over the floor surface. On the other hand, heat sources (e. g., people, lamps and computers, etc.) create upward thermal plumes which then entrain surrounding ambient air and rise to the upper zone, [7].

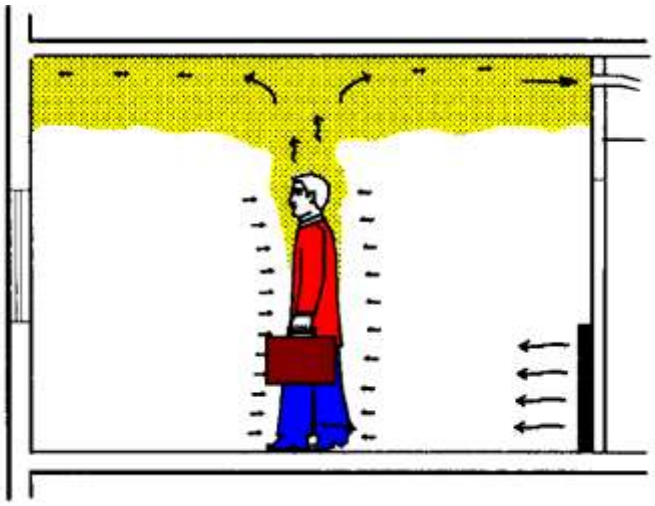

Figure 1.3 Schematic representing displacement ventilation, [6].

1.6 Thermal and Environment Comfort

Iraqi standard for cooling related to the ASHRAE Standard 55 "Thermal Environmental Conditions for Human Occupancy" and ISO Standard 7730 was applied to the thesis.

Metabolic activities of the body result almost completely in heat that must be continuously dissipated and regulated to maintain normal body temperatures. Skin temperatures associated with comfort at sedentary activities are 33 to 34°C and decrease with increasing activity (Fanger 1967). In contrast, internal temperatures rise with activity. The temperature regulatory center in the brain is about 36.8°C at rest in comfort and increases to about 37.4°C when walking and 37.9°C when jogging. An internal temperature less than about 28°C can lead to serious cardiac arrhythmia and death, and a temperature greater than 46°C can cause irreversible brain damage. Therefore, careful regulation of body temperature is critical to comfort and health. A resting adult produces about 100 W of heat. Because most of this is transferred to the environment through the skin, it is often convenient to characterize metabolic activity in terms of heat production per unit area of skin. For a resting person, this is about 58 W/m2 and is called (1 met), [8].

The environmental factors that affect a person's thermal balance and therefore influence thermal comfort are:

1. The dry bulb temperature of the surrounding air.
2. The humidity of the surrounding air.
3. The relative velocity of the surrounding air.

4. The temperature of any surfaces that can directly view any part of the body and thus exchange radiation.

In addition, the personal variables that influence thermal comfort are activity and clothing, [9].

Acceptable ranges of operative temperature and humidity for people in typical summer and winter clothing during light and primarily sedentary activity (≤ 1.2 met) are given in Figure 1.4.

In Figure 1.4, the upper and lower humidity limits are based on considerations of dry skin, eye irritation, respiratory health, microbial growth, and other moisture-related phenomena. In selecting indoor design conditions, care must also be taken to avoid condensation on building surfaces and materials by adjusting indoor dew points and by controlling critical surface temperatures.

It can be seen that the winter and summer comfort zones overlap. In this region, people in summer dress tend to approach a slightly cool sensation, but those in winter clothing would be near a slightly warm sensation, [9].

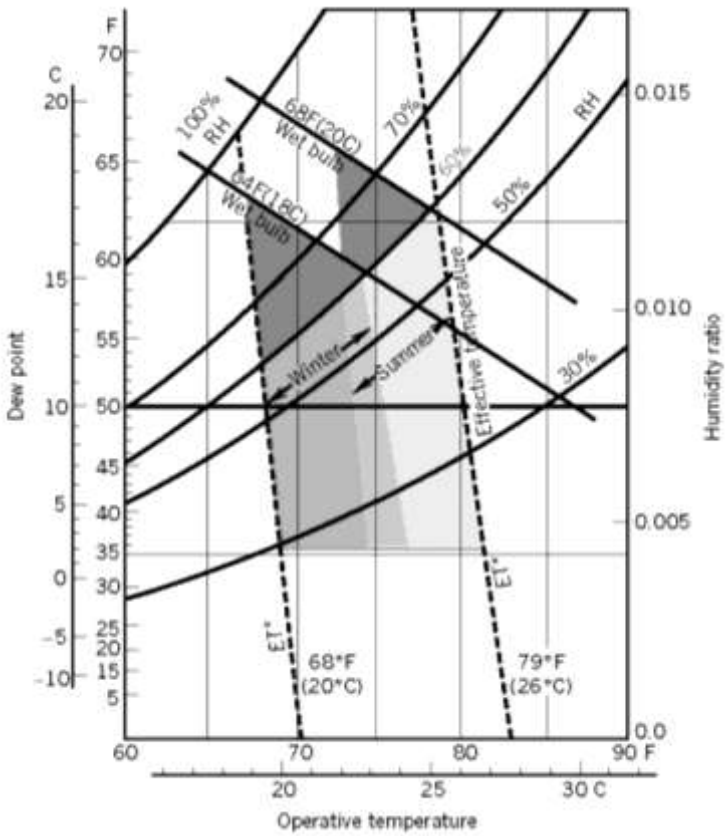

Figure 1.4 Acceptable ranges of operative temperature and humidity for people in typical summer and winter clothing during light and primarily sedentary activity (≤ 1.2 met), [9]

1.7 Basic Flow Patterns

In mixed-air systems, high-velocity supply jets from air outlets maintain comfort by mixing room air with supply air. This air mixing, heat transfer, and resultant velocity reduction should occur outside the occupied zone. Occupant comfort is maintained not directly by motion of air from the outlets, but from secondary air motion that results from mixing in the unoccupied zone. Comfort is maximized when uniform temperature distribution and room air velocities of less than 0.25 m/s are maintained in the occupied zone, [8].

1.7.1 Outlet types

Outlets have been classified into five groups:

Group A: Outlets mounted in or near the ceiling that discharge air horizontally as shown in Figure 1.5.

Group B: Outlets mounted in or near the floor that discharge air vertically in a nonspreading jet as shown in Figure 1.6.

Group C: Outlets mounted in or near the floor that discharge air vertically in a spreading jet as shown in Figure 1.7.

Group D: Outlets mounted in or near the floor that discharge air horizontally as shown in Figure 1.8.

Group E: Outlets mounted in or near the ceiling that project primary air vertically as shown in Figure 1.9.

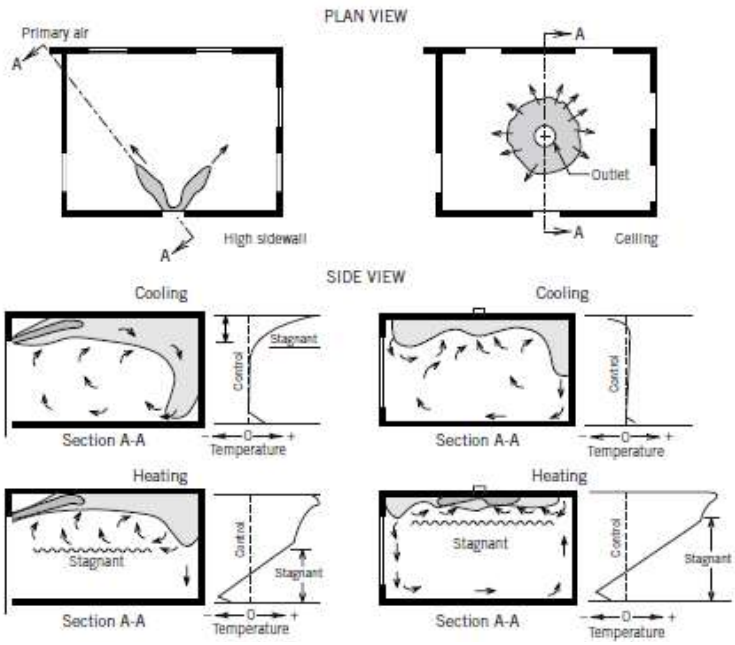

Figure 1.5 Air motion characteristics of Group A outlet, [8].

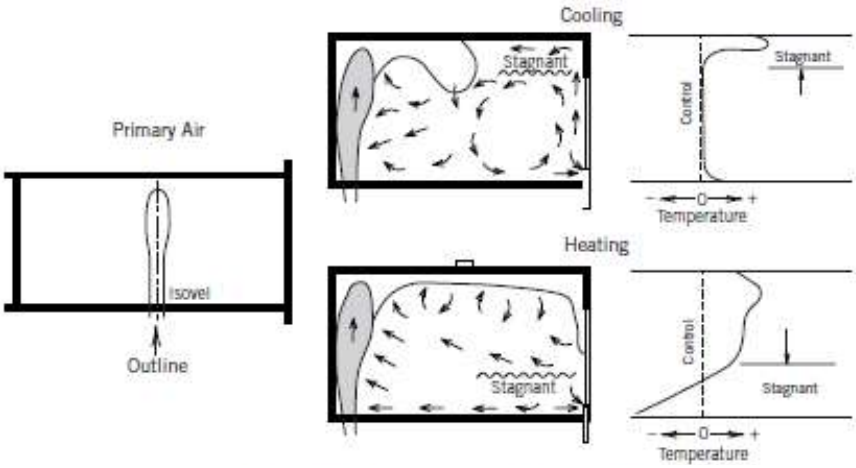

Figure 1.6 Air motion characteristics of Group B outlet,[8].

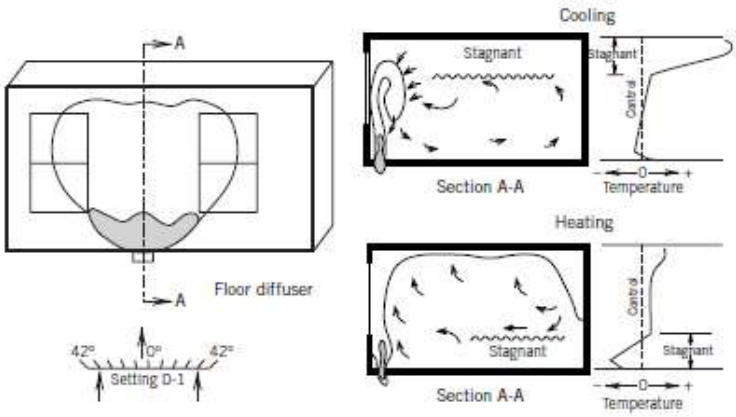

Figure 1.7 Air motion characteristics of Group C outlet,[8].

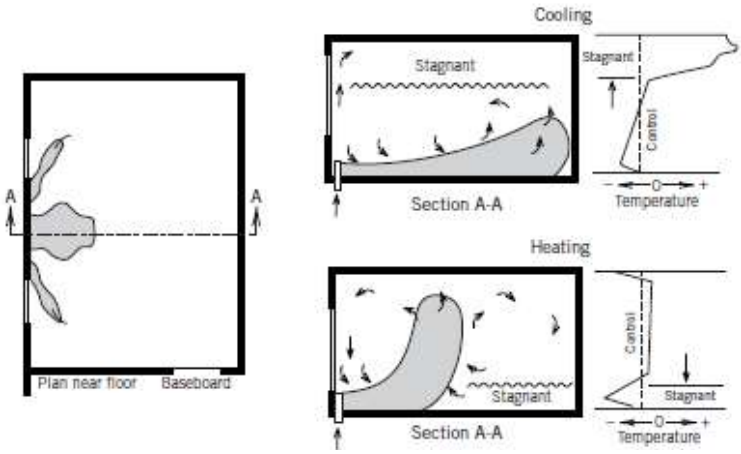

Figure 1.8 Air motion characteristics of Group D outlet,[8].

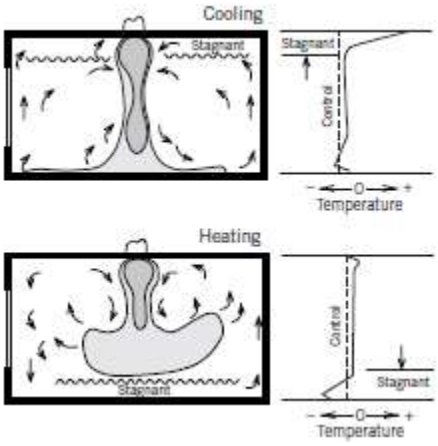

Figure 1.9 Air motion characteristics of Group E outlet,[8].

1.8 The Reason of Study Air Distribution

Ventilation of buildings has become one of the main topics in building services now. In the past, the buildings were designed as to be naturally ventilated. The buildings had high ceilings and the location and size of windows was in such a way to avoid excess heat in from sun radiation, and to supply enough air in. In the last decade, the drive to produce more energy efficient buildings led to the design of highly insulated buildings that are air tight. Since then, the need of mechanical ventilation increased considerably. However, incorrect application of mechanical ventilation systems may lead to the presence of badly ventilated space or to high energy demands. To avoid incorrect application of mechanical ventilation systems, the study of heat, ventilation and air conditioning (HVAC) became necessary, [6].

1.9 Types of Diffusers

Different types of diffusers generate different airflow distributions, and may have fundamental differences in the jet flow structure. The eight different diffusers are: nozzle diffuser, slot (linear) diffuser, valve diffuser, displacement diffuser, round ceiling diffuser, square ceiling diffuser, vortex diffuser, and grille diffuser, as shown in Figure 1.10, [10].

a b

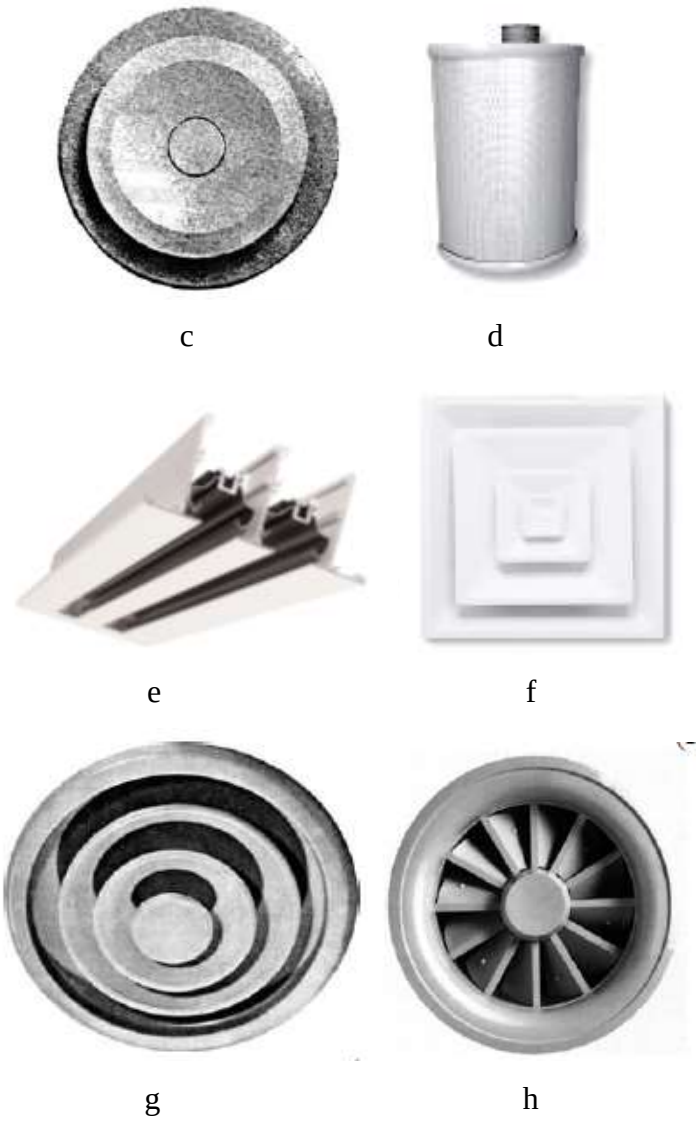

Figure 1.10 Eight commonly used air supply diffusers: (a) grille, (b) nozzle, (c) valve, (d) displacement, (e) slot, (f) square ceiling, (g) round ceiling, and (h) vortex. [10]

1.10 Objectives of the Present Work

1. To carry out computational fluid dynamics (CFD) analysis for room air distribution at the design flow rate of the outlet and validate it with -0- experimental data.
2. The investigate the possibility of using the Different Supply Patterns as an air distribution system in an office building.
3. To study the effects of changing the locations of inlets and outlets on the flow patterns.
4. Study the effect the of differents turbulence models k-ε and k-ω.

CHAPTER 2

LITERATURE REVIEW

This chapter presents brief description of the published literature and recorded experimental results in the field of room parameters. Although the list should not be considered exhaustive, the review should sufficiently represent the advances, findings, and contributions which are of particular relevance to this project. This review is subdivided into three main topics Experimental Works, Numerical Simulations and Experimental and Numerical Studies.

2.1 Experimental Works

Barber et. al. (1972) [11], described the development of an experimental small-scale modeling technique for conducting simulations of air distribution patterns in full-sized rooms. The technique was applied to simulate the motion of air in a single-room survival shelter. The parameters that describe and must satisfy the tile principles of dynamic similarity for a comparison of convection between a model and a full-scale room were determined. The main parameters were the Grashof and Prandtl numbers of the fluid and the aspect ratio of the room. High temperature water was used in place of air as the fluid in the model. The model was (6" x 6") (width x height) and (18") (depth). Experimental results presented the effect of the increased temperature on predicted fluid motion. Since the effect of the higher temperature is to lower the viscosity of the water, the same temperature differentials across the model operated at a higher temperature level will have high velocities. The higher velocities would increase the ventilation rate and turbulent level. Further, when the ventilation rate is high, the temperature difference between the floor and ceiling is smaller as was observed here.

Zhang et. al. (1992) [12], developed two-dimensional isothermal and non-isothermal air flows measured in a full-scale room (24 ft × 18 ft × 8 ft). Measurements included the flow patterns of the room air, the profiles of air velocity and turbulent kinetic energy at the diffuser, velocities, turbulent kinetic energies, and temperatures at

(205) locations within the room. The measurement grid was non-uniform, with higher grid density in flow regions where relatively high velocity gradients were expected (e.g., the diffuser jet region). Such detailed measurements are useful for evaluating numerical simulation models as well as for understanding the behavior of the room ventilation air flows.

Wang et. al. (2006) [13], investigated a full-scale section of a Boeing 767 aircraft cabin containing thirty five mannequins as shown in the Figure 2.1, for evaluating the ventilation effectiveness and characterizing the air distribution. Each mannequin was attached with a body heater and an outlet of carbon dioxide to simulate breathing. A set of experiment trials was conducted to measure the local mean age of air and the ventilation effectiveness factor (VEF) at the breathing level of the passengers. Carbon dioxide was used as the trace gas to determine the local mean age of air and the VEF.

The air velocity profiles measured using a volumetric particle tracking velocimetry (VPTV) system, were used to generate the airflow patterns and investigate the underlying mechanism affecting the local mean age of air and the VEF. The VPTV technique has been successfully used to characterize the airflows cameras from two different locations, a three-dimensional description of the air distribution can be obtained after data processing. In addition, measurements were conducted at different air supply rates to examine its effect on the ventilation performance.

The results showed that the local mean age of air was affected not only by the velocity magnitude, but also by the local airflow patterns, such as jet and recirculation. Except for the recirculation regions, the higher mean air velocity corresponded to a lower local mean age of air, indicating a higher net air exchange rate. In the strong air recirculation regions, the higher air velocity did not lead to the lower local mean age of air. This was because the ‘‘old’’ air was kept in the recirculation area, and no sufficient freshly supplied air was introduced. In these regions, the efficiency for heat dissipation and pollutant removal was also low. The VEF at most of the different locations in three rows was larger than one, indicating better ventilation effectiveness than complete mixing conditions in terms of contaminant removal

Nielsen (2007) [14], compared addresses for five air distribution systems in all, namely mixing ventilation from a wall-mounted terminal, mixing ventilation from a ceiling-mounted diffuser, mixing ventilation from a ceiling-mounted diffuser with a

swirling flow, displacement ventilation from a wall-mounted low velocity diffuser and a low impulse system based on a textile terminal. The systems are all tested in the same full-scale room.

The dimensions of the room with length, width and height equal to (4.2 m, 3.6 m and 2.5 m), respectively. Figure 2.2 shows the furnishings and the heat load of the room (office layout). The heat load consists of two PCs, two desk lamps and two manikins producing a total heat load of 480 W. It is possible to make a direct comparison between the five different air distribution systems, because they are tested in the same room.

The comparison showing air distribution systems based on mixing ventilation and ceiling-mounted diffusers are able to generate comfortable conditions up to a thermal load which is slightly superior to systems with mixing ventilation from wall-mounted diffusers, displacement ventilation with a wall-mounted low velocity diffuser or vertical ventilation systems with ceiling-mounted textile terminals. The measurements showed that the temperature gradient and asymmetric radiation are only important for displacement ventilation.

Van Hooff et. al. (2012) [15], presented a detailed and systematic experimental analysis of a transitional plane wall jet in a confined space. A water-filled experimental model has been built to perform flow visualizations and PIV measurements. It consists of the water column to drive the flow by hydrostatic pressure, a flow conditioning section, and a cubic test section having edges of L = 0.3 m constructed from glass plates. The inlet width is (0.3 m), and inlet height (0.03 m). The height of the outlet is fixed at (0.005 m).

Based on the flow visualizations, PIV measurements were conducted for seven Reynolds numbers, ranging from (800 to 2500). For each value of Re, two sets of measurements were obtained: one of the flow pattern in the entire cross-section of the cube (region of interest = L*L) and one with a smaller region of interest near the inlet (0.6L*0.4L) to increase the measurement resolution in this area with large velocity gradients.

Rees et. al. (2012) [16], studied by making temperature and air flow measurements in a test chamber over a range of operating parameters typical of office applications. The size of test chamber has internal dimensions of (5.43 m long, 3.08 m wide and 2.78 m high). The general arrangement is shown in Figure 2.3. The displacement ventilation system air supply was via a semicylindrical diffuser (700 mm high and

400 mm diameter), and the ventilation system extract was via a (125 mm high and 575 mm long) grille above the door. The chilled ceiling has dimensions of (1.65 m long and 0.3 m wide).

The results showed linear temperature gradients in the lower part of the room, in all cases, to be driven by convection from the adjacent walls. Significant mixing, indicated by reduced temperature gradients, was evident in the upper part of the room in the chilled ceiling results at higher levels of heat gain.

Pang et. al. (2013) [17], presented results by using the Flow Visualization with Green Laser (FVGL) technology used to analyze the air flow. The top-in-side bottom-out pattern may have the disadvantages of an indirect path to deliver fresh air to passengers, a low fresh air utilization ratio and the potential to widely spreading airborne infectious diseases. The bottom-in-top-out pattern can overcome these disadvantages very well, but it also faces the stratification of contaminated air above the head of the passengers. The improved pattern may overcome the above challenges quite well while also delivering good ventilation performance.

The modified Personal Exposure Effectiveness (PEE) was measured to compare their performances with regard to inhaled air quality. The measured results suggest that the personalized inlet should be designed to adjust its supply air angle according to the height of the passenger's face to provide a higher fresh air utilization effectiveness and better air quality for passengers in the improved pattern.

2.2 Numerical Simulations

Kondo et. al. (1998) [18], simulated the results which present the airflow and thermal fields for the modeled kitchen under the cooling condition. An airflow analysis was carried out based on the standard k-□□turbulence model with a wall function type boundary condition. Spatial coordinate (X1, X2, X3) to specification of Kitchen model was divided into (18 (X1) ×57 (X2) ×37 (X3) =37,962) meshes. The surface temperature of an object, such as walls was obtained by solving the heat balance equation, in which the convective and radiative heat transfer were combined. The modeled kitchen with dimension (a depth of 3.0 m, a width of 1.5 m and a height of 2.2 m), and the amount of heat from the cooking range is assumed to be 5.8kW(5000kcal/h).

The numerical simulations were conducted for the kitchen space under the cooling condition in which 400 m3/h of conditioned air at 15°C, and the same volume of

outdoor air at 30 °C was supplied. The obtained results for the hot outdoor air (30°C) were supplied at the position near the cooking range, such as the lower faces of the hood or the upper faces of the cooking equipment, the power of the outdoor air is not strong in the working space. It is possible to maintain a comfortable environment in the working area.

Sinha et. al. (1999) [19], investigated a velocity and temperature distribution in a room heated by a warm air stream introduced at various levels. Numerical solutions of Navier Stokes equations and energy equation were obtained by SIMPLE, and Semi Implicit Method for Pressure Linked Equation-Consistent SIMPLEC algorithms steady, laminar, and incompressible flow under Boussinesq's approximation was considered. A rectangular room (2.5 m long and 3 m high) with four locations of inlet and outlet was assumed. No slip and impermeability boundary conditions were used on all walls except at inlets and outlets. Solutions were presented for various locations of inlets and outlets, and for different values of Grashof number and Reynolds number. An increase in Gr increases the intensity of recirculation and yields uniform temperature distribution. Location of outlet at higher level than the inlet leads to better temperature distribution.

Charvat et. al. (2001) [20], studied the CFD modeling of airflow and temperature fields inside a glazed attic, and made comparison of results with experimentally obtained data. The main goal is to find optimal locations of ventilation system inlets in order to increase the efficiency of solar energy utilization. The CFD modeling of airflow and temperature fields in the glazed attic represents a complicated 3-D transient problem involving solar radiation induced natural convection in enclosed space. Considering the complexity and computational difficulties of the task, only 2D cross-sectional area of the attic was solved. This simplification is justified by the dimensions of the attic, which are ($L \times W \times H = 29 \times 9.1 \times 3.3$ m).

Both measurements and CFD modeling revealed significant temperature stratification inside the attic. The laminar model does not seem to be quite relevant for the solution, in spite of this fact there is only a small difference between temperature fields obtained from the laminar and turbulent model. The results imply that the inlets of the ventilation system should be located just underneath the roof. However, application of a 3D-model involving suction of solar preheated air into the ventilation system and infiltration of outdoor air through the ventilating slot will be necessary for determination of optimal inlet locations along the length of the attic.

Song et. al. (2006) [21], reported the development of a new zoning approach based on room air age, a parameter that indicates the mixing condition of the air. Zoning criteria were developed based on the deviation ratio of air age as well as location of the key source that is of concern (e.g., temperature, air pollutant). The dynamic characteristics of indoor parameters, such as air temperature, humidity, and pollutant concentrations can be simulated.

A case study was presented for a displacement ventilated room, and simulation results using the new zonal model were compared with those using a computational fluid dynamics (CFD) model and a conventional zonal model. The new approach is that zoning should be based on the distributions of flow field, and the zoning results should indicate the uniformity of zones in the space.

Comparisons showed that the new approach can calculate the room temperature distributions more accurately than a conventional zoning method. The disadvantage of the current zoning method is the reliance on CFD in zoning and obtaining air exchange rates between zones. Thus, it is suitable for long-time dynamic simulations of indoor environmental parameters.

Zhu et. al. (2006) [22], simulated a three-dimensional incompressible turbulence of indoor air by turbulence model. To simplify the issue, the models assumed the indoor air was incompressible, invariable property, steady-state flow and coincidence with the basic assumption of Boussinesq. Heat-transfer in walls was equable and it was considered as steady-state. Air leakage was not considered. The door and windows were assumed to be closed when air supplying and their sealing performance was good. Glass scattering to solar radiation and the impact of interior heat-transfer surfaces were not considered. There was no internal heat source indoors.

The turbulence model, considering the influence of buoyant force, adopted two-equation model with high-Reynolds against little air-supply quantity and low air velocity in air-conditioned space, and simulative computation was combined with the wall-function method. The size of the room is (7200 mm×5600 mm×3200 mm) (length×width×height). It has two steel sashes in the south with size 2350 mm×1750 mm (width × height), and the rest three walls are all interior ones. The ceiling air-outlet was (2.8 m) high above which the air distribution was not influenced greatly, so the physical model's height was (2.8 m). Here, two kinds of air-outlets made of aluminum alloy were used as ceiling air-outlets which were rectangular air

distributors and as wall air supply which were double louver air-outlets. Where return air intake-linear grille and wall air-outlets laid were interior walls.

The results showed that the air fallout is easily generated, and the air detention area and eddy current are existent. The same case occurs with both ceiling and wall air supply.

Steeman et. al. (2009) [23], compared simulations made with a traditional well-mixed model and a CFD model in search for the limitations of the well- mixed model. The experimental setup is a rectangular room (3.1 m×3.1 m×2.5 m) with an air inlet and outlet. The air was supplied to the inlet and removed from the outlet using circular ducts. The temperature at the outer surface of the wall at the air inlet, called inlet wall, was controlled. The temperatures in the other spaces adjacent to the test rooms were maintained at 20 ºC.

To allow for a good comparison between both models, the CFD model was extended with an effective penetration depth (EPD) model for the moisture buffering in the walls, an approach which is also used in the well-mixed model. The average indoor climate and the average relative humidity in the walls predicted by the CFD–EPD model and the well- mixed model with standard surface transfer coefficients agree quite well for the studied test case. The use of CFD generated surface transfer coefficients in the well-mixed model was able to improve the well-mixed results significantly in case of a stable, and physically relevant surface transfer coefficient could be related to the average indoor air conditions. The CFD generated average surface water vapor transfer coefficient for the total wall area over longer periods of time. This indicates that it is not always necessary to use the fully coupled CFD–EPD model to predict the average indoor climate.

Cai et. al. (2010) [24], have investigated the method of CFD for air distribution and comfort in a typical room with cold air diffusion. A mathematics model was established, and the air distribution was stimulated. The velocity and temperature fields of the airstreams in the room at different conditions were analyzed. The room size for simulation is of 7.2 m×5.6 m×3.2 m (long×wide×high) as shown in Figure 2.4. The ceiling air-outlet was (2.8 m) high above the floor. The models of outlets are shown as Figure 2.5. To assure the direction of air-current possibly close to practice, the rectangular air distributors, which used basic model, adopted (4) simple apertures in different directions, and the degree of the direction of air flow and the ceiling was (45º). The result showed that the air fallout is easily generated, and the air detention

area and eddy current are existent. The same case occurs with both ceiling and wall air supply.

Cehlin et. al. (2010) [25], used a micro/macro-level approach (MMLA) to predict the flow and thermal behavior of the air in the near-zone of a complex low-velocity diffuser. A series of experiments was carried out to validate the numerical predictions in order to ensure that the simulations can be used with confidence to predict indoor airflow. The predictions were performed by means of steady Reynolds Stress Model (RSM), and the results had a good agreement, both qualitatively and quantitatively, with the measurements. However, measurements indicated that the diffusion of the velocity and temperature was to some extent under- predicted by the RSM, which might be related to high instability of the airflow close to the diffuser. This effect might be captured by employing unsteady RSM. The present study also showed the importance of detailed inlet supply modeling in the accuracy of indoor air prediction.

Ho et. al. (2011) [26], compared the thermal environment of two air distribution systems in an office setting. Airflow, heat and mass (water vapor and contaminant gas) transfer in steady-state condition were modeled for an underfloor air distribution system and an overhead air distribution system. The models include a typical cubicle in a large office floor with a chair, a desk with a personal computer on top, and heat sources, such as seated person, desktop computer, and lights.

The comparison of simulation results for the two systems showed that UFAD system has some advantages over overhead system. Improvement in indoor air quality is expected in the breathing zone near the occupant by delivering the fresh supply air near the occupant at floor level, allowing an overall floor-to-ceiling airflow pattern to more efficiently remove contaminants from the occupied zone of the cubicle. Simulation results also showed an energy saving of 20-30% for UFAD system compared to overhead system which provides the same thermal comfort condition. Comparison to experimental data showed a good agreement among the systems of similar airflow characteristics.

Al-Sanea et. al. (2012) [27], used a CFD to simulate turbulent flow and heat-transfer inside mechanically ventilated rooms, using mixing air-distribution system, under forced convection conditions. Air enters the room from the side wall opening flush with isothermal ceiling and leaves through port in opposite wall flush with floor.

Velocity and temperature distributions were determined by using a finite volume method employing the k-ε turbulence model.

The model was then used to investigate the effects of supply Reynolds number (Red = 4000 to 10,000, where d is supply port height) and room aspect ratio (L/H = 0.5 - 6) on flow and heat-transfer characteristics within the room. Variation of convection coefficient hx along the ceiling was compared with the isolated flat plate correlation.

The results showed that the ceiling averaged convection coefficient (hav) increases with Red and decreases with L/H. Correlations for hav were constructed in terms of Red and L/H. Streamline plots showed that flow pattern is independent of Red but strongly dependent on L/H. A single contour map of speed with values normalized by supply velocity is therefore sufficient to describe all speeds inside the room for different supply Reynolds numbers.

Zhang et. al. (2012) [28], proposed to insulate an aircraft by an air stream barrier running through an annular channel along the cross section of the fuselage. Hot air is supplied to the channel entry at the lower lobe of the aircraft to heat the aircraft before it is finally delivered into the passenger cabin. As both channel surfaces are neither in uniform temperature nor uniform heat flux, the existent correlation formulas cannot be applied to fulfill the insulation design, as shown in Figure 2.6. This investigation applied a computational fluid dynamics (CFD) program to model a two-dimensional aircraft section insulated by such an air channel. A partial aircraft cabin mockup was constructed and put to a psychrometric chamber that was conditioned to -19 ºC for experimental test. The results revealed that the air channel is effective to insulate an airplane. The highly asymmetric temperature profiles across the channel also lead to asymmetric velocity profiles. In the near-window region of the passenger cabin, temperature is much elevated due to the channel, and thus cold sidewall and draft that have been repetitiously experienced by passengers seated near windows can be much alleviated.

2.3 Experimental and Numerical Studies

Huo (1997) [29], studied the supplied air that was uniformly distributed in the ventilated area under various conditions. Experimental study was first conducted to obtain more general information about the ventilation effect on indoor air quality problems in partitioned offices. The controlled environment consists of two interconnected rooms, the dimensions of each room are (4.9 m×4.8 m×2.9 m high).

At the same time, the contaminant distribution was influenced by almost all kinds of parameters in the office. It was the room air flow pattern but not the uniformity of the supplied air distribution which influenced the contaminant distribution in the office.

The results also indicated that the contaminant distribution in a mechanically ventilated partitioned office need to be studied individually according to the different cases. CFD simulation is an efficient tool for such kind of studies. The air inflow condition is one of the most important parameters affecting the air flow pattern and contaminant distribution in a mechanically ventilated room. Because of the complex geometry of the supply air diffuser and computer capacity, the conventional method of describing the supply air diffuser boundary conditions in CFD simulation may not well define the air inflow condition. The inaccurate description to the air inflow condition could be a totally unrealistic simulation result of the air flow inside the office.

A new method to correctly describe the diffuser boundary conditions in CFD simulation was proposed in this thesis. The model prediction was validated with the experimental data in a literature and the results from the experimental part of this thesis. The CFD predictions applying the new method were in good agreement with the experimental results.

Bartak et. al. (2001) [30], presented results from experimental and numerical study of a room with mixing ventilation, the test room (4.2, 3.6, 3 m) (L, W, H) and the supply opining (0.3*0.2 m) was placed symmetrically on the west wall having the bottom edge 2.05 m above the floor. The study focused on the local mean age of air (LMA). The measurements were performed using the tracer gas concentration decay method. The numerical predictions were obtained from the computational fluid dynamics (CFD) module of the latest version of the ESP-r software. In order to address the requirement for a proper choice of the number of control volumes in CFD, the analysis was made by comparing the results from two consequently finer numerical grids. Some guidelines for practicing engineers are given concerning the number of numerical grid points and their distribution, reasonable for buildings energy simulations. The guidelines are based on common CFD rules supported by examples from the presented computations. Both the fine and the coarse grid computations gave results, which were very close to the measurements.

Srebric et. al. (2002) [31], studied how to find simplified methods that can be used to describe flow and thermal information from eight commonly used diffusers (nozzle

diffuser, slot (linear) diffuser, valve diffuser, displacement diffuser, round ceiling diffuser, square ceiling diffuser, vortex diffuser, and grille diffuser). The objective of this research was to develop a simplified methodology to specify the boundary conditions of air supply diffusers for CFD simulations. Two simplified methods, the momentum and box methods, were validated with the measured data in order to assess their accuracy and reliability. The measured data were obtained from a state-of-the-art experimental facility.

The investigation used the box and momentum methods. The box method works for most of the diffusers with an appropriate box size. The momentum method performs well for five diffusers. Since the momentum method is simpler than the box method, the momentum method should be used, whenever it is applicable.

Posner et. al. (2003) [32], compared the results from relatively simple three-dimensional numerical simulations (CFD) with laser Doppler anemometry (LDA) and particle image velocimetry (PIV) experimental measurements of indoor air flows in a one-tenth sub-scale model room. The sub-scale model room is made from anodized aluminum and has four plane glass windows which provide adequate optical access; it is (91.4 cm long, 45.7 cm wide, and 30.5 cm high). A single inlet vent and outlet vent, both on the ceiling, supply and remove ventilation air. The inlet and exit are both (10.1 cm2).

A large partition is laminar, k-ε turbulence, and RNG k-ε. Turbulence numerical models were used and evaluated with respect to their performance in simulating the flow in the model room, and results of the numerical simulations and velocimetry measurements showed how obstructions can greatly influence the air flow and contaminant transport in a room. It is important, therefore, that obstructions be considered in ventilation design room obstructions.

Of the flow models examined, the RNG k-ε model showed best agreement with experiments, but all of the simulations predicted the measured trends in the model room very well, with relative errors never much larger than 20%. The RNG model most accurately predicts the flow in a partitioned room, capturing the gross effects of a large flow obstruction.

Akoua et. al. (2006) [33], obtained Computational Fluids Dynamics (CFD) results in a real environment. Experimental tests were undertaken in a room (2.5, 5.15, 2.53 m) (H, L, W) and in a kitchen (2.5, 4.15, 2.6 m) (H, L, W) of an experimental house. Although the wall surface temperatures and the air intake temperature were not

imposed, the air change rates were controlled during the measurements. Moreover, since measurements were carried out in a real environment, air leakage occurred at the walls.

Thereafter, measurements were used to define the boundary conditions of CFD simulations. A CFD code based on “Finite Volume Method” (FLUENT) was used to numerically explore the internal flows. The effects of turbulence on the flow were dealt with a “realizable” k- ε model. This is an improvement of the standard k-ε model. As a result, it can be stated that as long as air leakage is slight during the experimental tests, satisfactory agreement is observed between CFD results and in situ experimental results.

However, in the case where experimental tests were carried out in a room with significant air leakage, the quality of the numerical results was decreased since this phenomenon was not considered in the CFD model. For this case, a simplified hypothesis of modeling was proposed and validated to deal with air leakage effects and thus to improve the accuracy of CFD results.

Mei et. al. (2009) [34], explained the results of an experimental system for measuring the performance of air conditioning unit designed, constructed and numerically simulated at three-dimensional distribution of testing room with the computational fluid dynamics technique. The testing room, which is 5m long, 3 m wide and 3 m high. Three tuyeres were located at the side wall behind the testing unit to supply preconditioning air. The twenty-one measuring points were located isometrically at the intersection lines of three horizontal and three vertical used to measure the velocity and temperature. All the measuring points after the air environment were steady. The computational fluid dynamics software FLUENT was used in this study based on the k–ε turbulence model, the air flow and heat transfer problems were resolved by finite volume method. The number of meshes was 30×30×50. The experimental data and simulation results proved that the velocity and temperature of testing room distribute homogenously, and the indoor air environment meets the testing request of air conditioning unit. The simulation results showed that supply air parameters and the location of testing unit have an obvious effect on the air distribution

Lee et. al. (2009) [35], compared experimentally the TDV (Traditional displacement ventilation) with UFAD (under-floor air distribution) systems that use four different diffusers (perforated TDV diffusers, swirl diffusers, linear diffusers, and perforated-

floor-panel diffusers) in an environmental chamber (4.2 m wide × 4.8 m long× 2.73 m high), Figure 2.7, that can simulate different indoor spaces of the same size. The experimental results showed that the perforated-corner TDV diffuser, swirl diffuser, and perforated-floor- panel diffuser created low air velocity in the occupied zone. However, the perforated-corner TDV and perforated-floor-panel diffusers could generate a high temperature difference between the head and ankle level of an occupant.

The TDV and UFAD systems had better ventilation performance than the mixing ventilation system in cooling mode. For heating mode, the TDV and UFAD system created mixing conditions except in the vicinity of the floor. The systems with low-height-throw diffusers (all except the linear diffusers) were better. This investigation used a validated CFD program [The turbulent kinetic energy (k), and dissipation rate of turbulent kinetic energy (ε) modeled by the Re-Normalization Group (RNG) k-ε model]. The differential equations were solved by the CFD program with the finite volume.

Chen et. al. (2010) [36], investigated seven types of models (analytical, empirical, small scale experimental, full-scale experimental, multizone network, zonal, and CFD) for predicting the ventilation performance in buildings, which can be different in details according to the model type. The analytical model could give an overall assessment of a ventilation system if the flow approximated to obtain an analytical solution. The empirical model is similar to the analytical model in terms of its capacities but is developed with a database. The small-scale model could be useful to examine complex ventilation problems if flow designed following similarity analysis, in which the relevant dimensionless flow parameters are identical between small- and full-scale (e.g., Reynolds, Grashof, Prandtl numbers), and it can be maintained between the scaled model and reality, as shown in Figure 2.8.

Reynders et. al. (2011) [37], presented a focuses on the intra-zonal airflow in a standard laboratory set-up. The airflow and ventilation efficiency was computed with Computational Fluid Dynamics (CFD), and an extensive in-situ experimental case, in which different ventilation strategies were evaluated, was conducted. The size of laboratory used for the experimental study is (8.40, 3.40, 3.40 m) (L, W, H), laboratory tables are placed at both sides of the room has a height of 1.10 m and a width of 0.90 m.

The results indicated that the current design standards, which impose a minimal number of air changes per hour, cannot guarantee an optimal, energy efficient design. An optimal design starts from a comprehensive risk analysis. The CFD-simulations and experimental study showed that an optimal design should not only be based on a minimal ventilation rate, but also has to include an analysis of the impact of the location and type of the ventilation inlet and outlet, the room geometry and ideally the influence of occupants and laboratory appliances.

2.4 Summary of Literature Review

Researches that have been reviewed previously are summarized in the following Tables (1 & 2), as shown below, where they were divided into the Experimental Researches, Numerical Researches, and Experimental and Numerical Researches.

No	Author	Detail	Working fluid	Dimension L×W×H
1	E. M. Barber et. al.	small-scale modeling technique	Water	18" × 6" × 6"
2	J.S. Zhang et. al.	Two-dimensional isothermal and non-isothermal air flows were measured in a full-scale room	Air	18′ × 6′ × 6′
3	A. Wang et. al.	full-scale section of a Boeing 767	Air	aircraft cabin
4	P. V. Nielsen	five air distribution systems for full-scale	Air	4.2 × 3.6 × 2.5 m
5	T. van Hooff et. al.	Small-scale	water	0.3 × 0.3 × 0.3 m
6	S. J. Rees et. al.	test chamber for scale	Air	5.43 × 3.08 × 2.78 m
7	L. Pang et. al.	aircraft cabin	Air	aircraft cabin

Table 1 Summary of Experimental Researches

No	Author	Flow regime	Dimension L×W×H	Methodology	Grid
1.	Y. Kondo et. al.	Turbulent	3×1.5×2.2 m	Standard k-ε turbulence model	(18×57×37) 37,962 meshes
2.	S.Sinha et. al.	laminar	2-D 2.5×3 m (L×H)	----	(90×98)
3.	P.Charvat et. al.	Laminar and turbulent	2-D 29×9.1×3.3 m	Laminar and turbulent RNG k-ε	3500 cell
4.	F. Song et. al.	Turbulent	5.16×3.65×2.4 m	zoning approach	---
5.	L. Zhu et. al.	Turbulent	7.2×5.6×3.2 m	Standard k-ε turbulence model	the main meshes was 0.15m
6.	H.J. Steeman et. al.	Turbulent	3.1×3.1×2.5 m	Standard k-ε turbulence model	683,590 cells
7.	W. Cai et. al.	Turbulent	7.2×5.6×3.2 m	Standard k-ε turbulence model	---
8.	M. Cehlin et. al.	Turbulent	4.1×3.4×2.7 m L×W×H	RSM	1,330,754
9.	S. H. Ho et. al.	laminar	2 × 2.7 m L × H	----	---
10.	S.Al-Sanea et. al.	Turbulent	9.3 × 3 m L × H	k-ε turbulence model	20×20, 40×40, 60×60 and 90×90
11.	T. Zhang	Turbulent	aircraft	the RANS	cell numbers are 588, 595 and 590

Table 2 Summary of Numerical Researches

No	Author	Flow regime	Detail	Working fluid	Dimension L×W×H	Methodology	Grid
1.	Y. Huo	Turbulent	full-scale modeling technique	Air	4.9×4.8×2.9 m	The k-ε model	(16×26×22) grid
2.	M. Bartak et. al.	Turbulent	full-scale modeling for mixing ventilation	Air	4.2×3.6×3 m	k-ε turbulence model	(11×9×11) (30×27×30)
3.	J. Srebric et. al.	Turbulent	full-scale modeling technique	Air	5.16m×3.65 m×2.43 m	Box and Momentum	Different grid depend on type of diffuser
4.	J.D. Posner et. al.	Turbulent and Laminar	one-tenth sub-scale model room	Air	91.4 × 45.7× 30.5 cm	the standard k-ε and RNG k-ε turbulence models	---
5.	J. J. A. A. Akoua et. al.	turbulent and non-isothermal	five air distribution systems for full-scale	Air	2.5×5.15×2.53 m 2.5×4.15×2.6 m	Standard k-ε turbulence model	---
6.	Y. Mei et. al.	Turbulent	Measurements in the room	Air	5×3×3 m	k-ε turbulence model	30×30×50
7.	K. Lee et. al.	Turbulent	full-scale	Air	4.8×4.2×2.73 m	(RNG) k-ε model	---
8.	Q.Chan et. al.	Turbulent	Analytical small scale, full-scale, multizone network, zonal CDF	Water and Air	one-tenth scale for small-scale 2.44×2.44×2.44 m for full-scale 3.1×3.1×2.5 m for CFD	Contamanint (RNG) k-ε model	---

9.	G. Reynders et. al.	Turbulent	Full-scale	Air	8.4×3.4×3.4 m	standard k-ε, RNG-k-ε, Realizable k-ε, standard k-ε and SST k-ε models	98 700 elements

Table 3 Summary of Experimental and Numerical Researches

2.5 Scope of the Present Work

From the above review where the theoretical and experimental studies are stated in the previous sections, the scope of the present work will be:

1. Modeling of air outlet of the types (slot, square, displacement and grille).
2. Analyzing the effect of actual heat load inside the space, such as human, computer and wall temperature.
3. Comparing the prediction results of physical model to air velocity and temperature with other experimental one's previous work.
4. Obtaining the results based on the standard conditions under the Turkey Code of cooling.

Figure 2.1 The full-scale section of the Boeing 767-300 aircraft cabin, [16].

Figure 2.2 Furnishings and heat load in the full-scale room, [17]

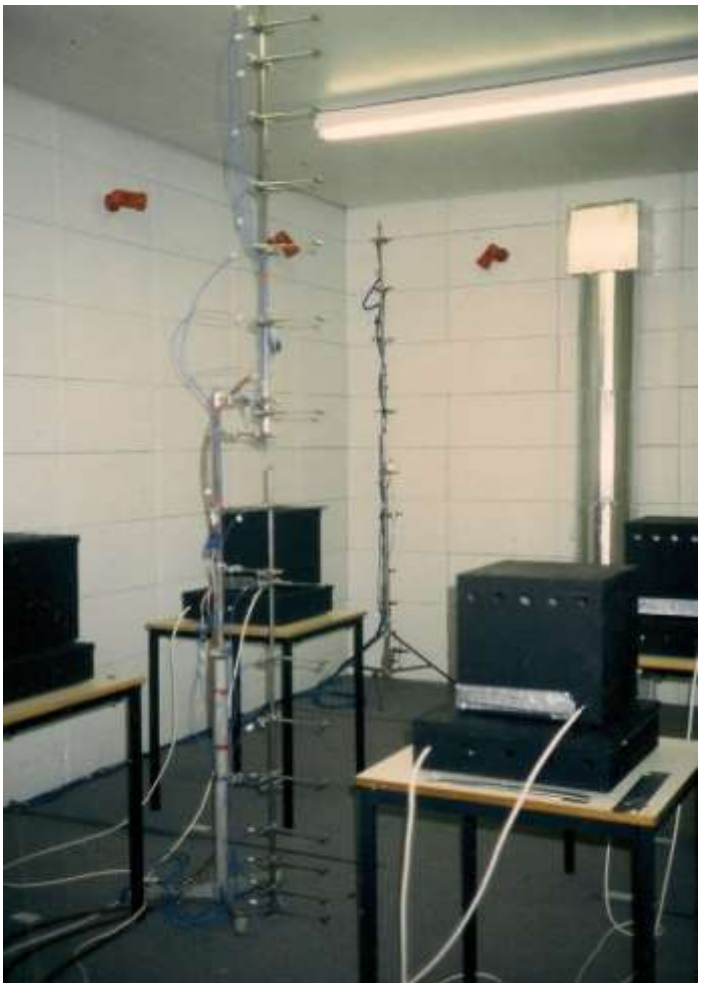

Figure 2.3 A photograph of the test chamber configured for 4 heat sources and showing the air temperature sensor assembly [19].

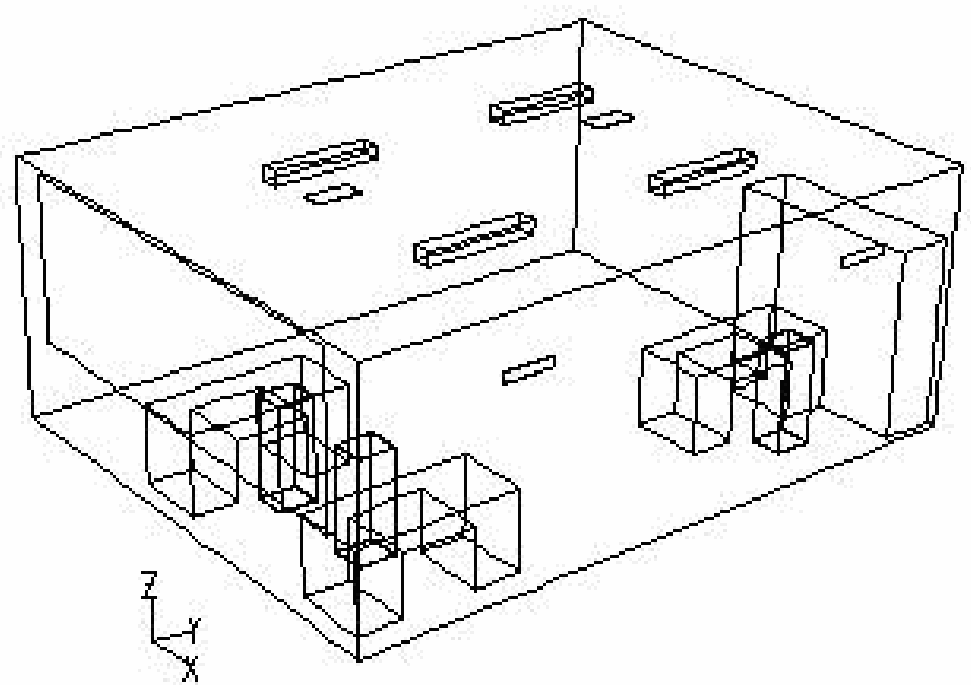

Figure 2.4 Physical model of ceiling air-supply, [27].

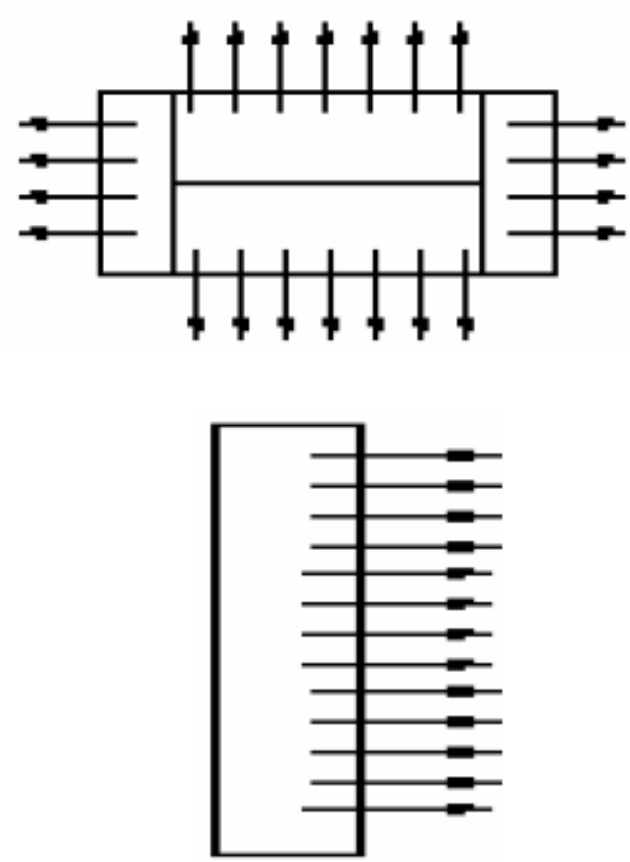

Figure 2.5 The models of outlets, [27].

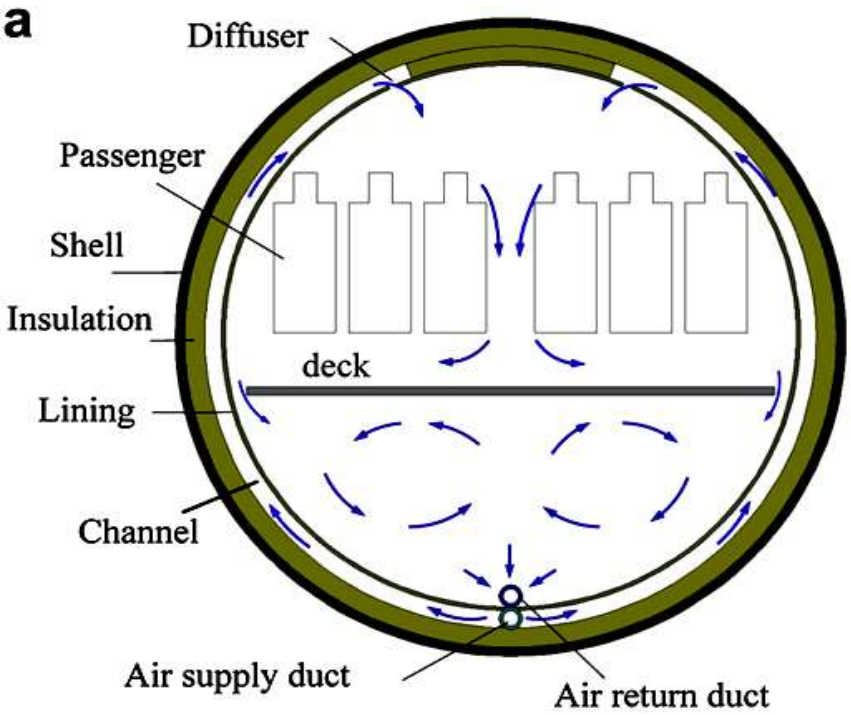

Figure 2.6 An air channel along the cross section of fuselage to insulate an aircraft, [31].

a b

c d e

f

Figure 2.7 Environmental chamber and diffusers used for the TDV and UFAD systems: (a) and (b) environmental chamber, (c) perforated-corner diffuser, (d) swirl diffuser, (e) linear diffuser, and (f) perforated-floor panel diffuser, Ref. [38].

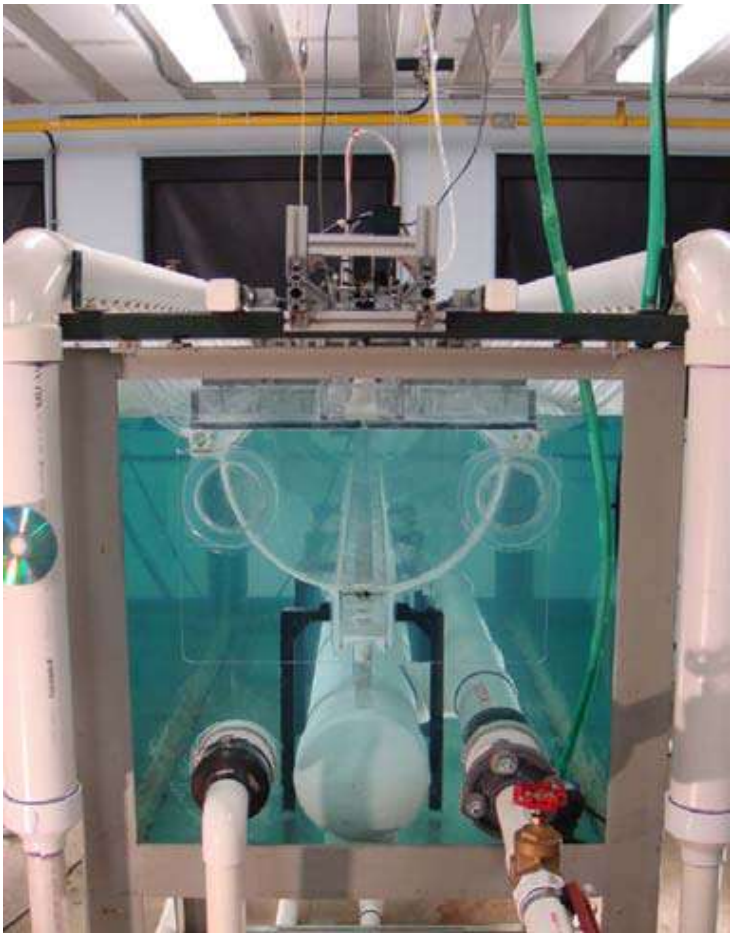

Figure 2.8 The small-scale experimental test facility of an airliner cabin in a water tank, Ref. [39].

CHAPTER 3

THEORETICAL FORMULATION

3.1 Introduction about CFD

3.1.1 General

The task of obtaining solutions to the governing equations of fluid mechanics represents one of the most challenging problems in science and engineering. In most instances, the mathematical formulations of the fundamental laws of fluid mechanics are expressed as partial differential equations (PDE). Second-order partial differential equations appear frequently and, therefore, are of particular interest in fluid mechanics and heat transfer.

Generally, the governing equations of fluid mechanics form a set of coupled, nonlinear PDEs which must be solved within an irregular domain subject to various initial and boundary conditions.

In many instances, analytical solutions of the equations of fluid mechanics are limited. This is further restricted due to the imposed boundary conditions. For example, a PDE subject to a Dirichlet boundary condition (i.e., values of the dependent variable on the boundary are specified) may have an analytical solution. However, the same PDE subject to a Neumann boundary condition (where normal gradients of the dependent variable on the boundary are specified) may not have an analytical solution.

Experimental fluid mechanics can provide some information regarding a particular flow field. However, the limitation on the hardware, such as the model and tunnel size and the difficulty in adequately simulating the prototype flow field, makes it an impractical means of obtaining flow fields for many problems. Nevertheless, the flow field information from experiments are valuable in validating mathematical solution of the governing equations. Thus, experimental data is used along with computational solutions of the equations for design purposes.

A technique that has gained popularity in recent years is computational (numerical) fluid dynamics. Of course, numerical analysis has been around

For many years. However, improvements in computer hardware, resulting in increased memory and efficiency, have made it possible to solve equations in fluid mechanics using a variety of numerical techniques. This has stimulated the introduction of newer numerical techniques which are being proposed almost on a daily basis. Unlike experimental fluid mechanics, the geometry and flow conditions can be easily varied to obtain various design goals. The solution that any such numerical program generated should be validated by comparing it to a set of experimental data; but once its validity has been established, the program can be used for various design purposes, within the limits imposed by the assumptions on which it was based, [38].

3.1.2 Types of Prediction Models and CFD Preference

Designing ventilation systems for buildings require a suitable tool to assess the system performance. Seven types of models assessed (analytical, empirical, small-scale experimental, full-scale experimental, multizone network, zonal, and CFD) for predicting ventilation performance in buildings, which can be different in details according to the model types, [39].

Some of the advantages and disadvantages of the three approaches are summarized in Table 4, [40].

The analytical model could give an overall assessment of a ventilation system if the flow approximated to obtain an analytical solution. The empirical model is similar to the analytical model in terms of its capacities but is developed with a database. The small-scale model could be useful to examine complex ventilation problems if the flow similarity maintained between the scaled model and reality. The full-scale model is the most reliable in predicting ventilation performance, but it is expensive and time consuming. The multizone model is a useful tool for ventilation design in a whole building, but it cannot provide detailed flow information in a room. The zonal model can be useful when a user has prior knowledge of the flow in a room. The CFD models provided the most detailed information about the performance of ventilation systems in a zone, and were the most accurate of the numerical models, but they are sophisticated and require very dedicated training of a user. Although it is possible to apply the CFD models to a whole building, the computing time would be extremely long – too long for design. Since the CFD models use approximations, it is essential to validate the models. A validated CFD model is a powerful tool for

conducting a parametric study or for optimizing the design of ventilation systems in buildings, [11].

Approach	Advantages	Disadvantages
Experimental	1. Capable of being most realistic	1. Equipment required. 2. Scaling problems. 3. Tunnel corrections. 4. Measurement difficulties. 5. Operating costs.
Theoretical (Analytical)	Clean, general information Which is usually in formula form	1. Restricted to simple geometry and physics. 2. Usually restricted to linear problems.
Numerical	1. No restriction to linearity. 2. Complicated physical can be treated. 3. Time evolution of flow can be obtained.	1. Truncation errors. 2. Boundary condition problems. 3. Computer costs

Table 4 Comparison of approaches, [12].

3.2 Assumptions for 2D and 3D Models

The following assumptions are used to simplify the proposed model solution:

1. Steady state flow.
2. Incompressible flow of air.
3. Two and three dimensional fluid, which includes dry air with buoyancy force.
4. The fluid properties are considered as constants except the density f(T) for buoyancy term in the momentum equation.
5. Thermal conductivity is scalar.
6. No chemical reaction.
7. Turbulent flow.

3.3 Turbulence Models

3.3.1 The standard k-ε model

The two-equation k-ε turbulence model was first developed by Launder and Spalding (1974), which remains as the most widely used turbulence model for a range of engineering flows and is often referred to as the standard k-ε model.

For incompressible flows, the model has the following form, [7]:

$$\frac{\partial}{\partial t}(\rho k) + \frac{\partial}{\partial x_i}(\rho k u_i) = \frac{\partial}{\partial x_j}\left[\left(\mu + \frac{\mu_t}{\sigma_k}\right)\frac{\partial k}{\partial x_j}\right] + G_k + G_b - \rho\varepsilon + S_k \tag{3.1}$$

$$\frac{\partial}{\partial t}(\rho \varepsilon) + \frac{\partial}{\partial x_i}(\rho \varepsilon u_i) = \frac{\partial}{\partial x_j}\left[\left(\mu + \frac{\mu_t}{\sigma_\varepsilon}\right)\frac{\partial \varepsilon}{\partial x_j}\right] + C_{1\varepsilon}\frac{k}{\varepsilon}(G_k + C_{3\varepsilon}G_b) - C_{2\varepsilon}\rho\frac{\varepsilon^3}{k} + S_\varepsilon \tag{3.2}$$

Where:

σ_k *and* $\sigma_\varepsilon$are turbulent Prandtl numbers for k and ε, respectively; $S_k$and $S_\varepsilon$are the source terms$G_k$represents the generation of turbulent kinetic energy due to the mean velocity gradients:

$$G_k = -\rho\overline{u_i'u_j'}\frac{\partial u_j}{\partial x_i} = \mu_t\left(\frac{\partial u_i}{\partial x_j} + \frac{\partial u_j}{\partial x_i}\right)\frac{\partial u_j}{\partial x_i} \tag{3.3}$$

and $G_b$represents the production of turbulent kinetic energy due to buoyancy:

$$G_b = \beta g_i \frac{\mu_t}{\sigma_t}\frac{\partial T}{\partial x_i} \tag{3.4}$$

$g_i$is the component of the gravitational vector in i-direction, and β is the thermal expansion coefficient defined as:

$$\beta = -\frac{1}{\rho}\left(\frac{\partial \rho}{\partial T}\right)_p \tag{3.5}$$

For ideal gas, equation (3.4) reduces to:

$$G_b = -g_i \frac{\mu_t}{\rho\sigma_t}\frac{\partial \rho}{\partial x_i} \tag{3.6}$$

The turbulent (eddy) viscosity μ_t is obtained by combining k and ε as follows:

$$\mu_t = \rho C_\mu \frac{k^2}{\varepsilon} \tag{3.7}$$

C_μ,$C_{1\varepsilon}$, $C_{2\varepsilon}$, $C_{3\varepsilon}$, σ_k, *and* $\sigma_\varepsilon$are model coefficients constants and,

$$C_\mu = 0.09, C_{1\varepsilon} = 1.44, C_{2\varepsilon} = 1.92, \sigma_k = 1.0, \sigma_\varepsilon = 1.3$$

$C_{3\varepsilon}$ is determined from the equation

$$C_{3\varepsilon} = \tanh\left|\frac{v}{u}\right| \tag{3.8}$$

Where,v is the component of the flow velocity parallel to the gravitational vector, and u is the component of the flow velocity perpendicular to the gravitational vector.

3.3.2 The RNG k-ε model

The RNG k-ε turbulence model is derived from the instantaneous Navier-Stokes equations by using a mathematical technique called "Re-Normalization Group" (RNG) method. The analytical derivation results in a model with constants, different from those in the standard k-ε model, additional terms and functions in the transport equations for k and ε. The RNG k-ε model is very similar in form to the standard k-ε model. For incompressible flows, the transport equations for k and ε are as follows [7],

$$\frac{\partial}{\partial t}(\rho k) + \frac{\partial}{\partial x_i}(\rho k u_i) = \frac{\partial}{\partial x_j}\left[\left(\alpha_k \mu_{eff}\right)\frac{\partial k}{\partial x_j}\right] + G_k + G_b - \rho\varepsilon + S_k \tag{3.9}$$

$$\frac{\partial}{\partial t}(\rho \varepsilon) + \frac{\partial}{\partial x_i}(\rho \varepsilon u_i) = \frac{\partial}{\partial x_j}\left[\left(\alpha_\varepsilon \mu_{eff}\right)\frac{\partial \varepsilon}{\partial x_j}\right] + C_{1\varepsilon}\frac{k}{\varepsilon}(G_k + C_{3\varepsilon}G_b) - C_{2\varepsilon}\rho\frac{\varepsilon^2}{k} - R_\varepsilon + S_\varepsilon \tag{3.10}$$

As with the standard k-ε model, the $G_k$and $G_b$terms in the above equations represent the generation of turbulence kinetic energy due to the mean velocity gradients and due to buoyancy, respectively, they are calculated using the same equations (3.3) and (3.4) as in the standard k-ε model. The quantities of $\alpha_k$and $\alpha_\varepsilon$are the inverse effective Prandtl numbers for k and ε, respectively; $S_k$and $S_\varepsilon$are the source terms for k and ε, respectively.

The scale elimination procedure in RNG theory results in a differential equation for turbulent viscosity:

$$d\left(\frac{\rho^2 k}{\sqrt{\varepsilon\mu}}\right) = 1.72\frac{\hat{v}}{\sqrt{\hat{v}^3 - 1 + C_v}}\,d\hat{v} \tag{3.11}$$

Where,$\hat{v} = \mu_{eff}/\mu$, $C_v \approx 100$.

By integrating equation (3.11), an accurate description of how the effective turbulence transport varies with the effective Reynolds number (or eddy scale) can be obtained, which allows the model to better handle low-Reynolds number and near-wall flows. In the high-Reynolds number limit, the equation (3.2) gives the same form for computing the turbulent viscosity but with a slightly different coefficientC_μ=0.0845, which was derived by using RNG theory. The inverse

effective Prandtl numbers $\alpha_k$and $\alpha_\varepsilon$are computed using the following formula derived by the RNG theory:

$$\left|\frac{\alpha-1.3929}{\alpha_0-1.3929}\right|^{0.6321}\left|\frac{\alpha+2.3929}{\alpha_0-2.3929}\right|^{0.6321}=\frac{\mu_{mol}}{\mu_{eff}} \tag{3.12}$$

Where $\alpha=1/\sigma_k=1/\sigma_\varepsilon=1/\sigma_t$ andα_0=1.0. In the high-Reynolds number limit (μ/μ_{eff}<<1), $\alpha_k=\alpha_\varepsilon\approx$1.393, that means the effective Prandtl numbers for k and ε are about 0.7178. The main difference between the RNG and standard k-ε models lies in the additional term in the ε equation given by:

$$R_\varepsilon=\frac{C_\mu\rho\eta^3\left(1-\frac{\eta}{\eta_0}\right)}{1+\beta\eta^3}\frac{\varepsilon^2}{k} \tag{3.13}$$

Where,$\eta\equiv\frac{Sk}{\varepsilon},\eta_0=4.38, and\ \beta=0.012$

The ε equation can be rewritten as:

$$\frac{\partial}{\partial t}(\rho\varepsilon)+\frac{\partial}{\partial x_i}(\rho\varepsilon U_i)=\frac{\partial}{\partial x_j}\left[\left(\alpha_\varepsilon\sigma_\varepsilon\mu_{eff}\right)\frac{\partial\varepsilon}{\partial x_j}\right]+C_{1\varepsilon}\frac{k}{\varepsilon}(G_k+C_{3\varepsilon}G_b)-C^*_{2\varepsilon}\rho\frac{\varepsilon^2}{k}+S_\varepsilon \tag{3.14}$$

Where,$C^*_{2\varepsilon}$ is given by

$$C^*_{2\varepsilon}=C_{2\varepsilon}+\frac{C_\mu\eta^3(1-\frac{\eta}{\eta_0})}{1+\beta\eta^3} \tag{3.15}$$

In regions where $\eta<\eta_0$, the R term makes a positive contribution, and $C^*_{2\varepsilon}$becomes larger than $C_{2\varepsilon}$. In the logarithmic layer, for instance, it can be shown that η≈3.0, giving $C^*_{2\varepsilon}\approx$ 2, which is close in magnitude to its value in the standard k-ε model (1.92). As a result, for weakly to moderately strained flows, the RNGmodel tends to give results largely comparable to the standard k-ε model. In regions of large strain rate($\eta>\eta_0$), however, the R term makes a negative contribution, making the value of $C^*_{2\varepsilon}$less than $C_{2\varepsilon}$. In comparison with the standard k-ε model, the smaller destruction of ε augments ε, reducing *k* and, eventually, the effective viscosity. As a result, in rapidly strained flows, the RNG model yields a lower turbulent viscosity than the standard k-ε model. Thus, the RNG model is more responsive to the effects of rapid strain and streamlines curvature than the standard k-ε model, which explains the superior performance of the RNG model for certain classes of flows, [7].

The model constants in equation (3.14) are the following values:

$C_{1\varepsilon}$=1.42 and $C_{2\varepsilon}$=1.68

The coefficient $C_{3\varepsilon}$is determined by equation (3.18).

3.3.3 The Realizable k-ε model

The realizable k-ε model is a relatively recent development and differs from the standard k-ε model in two important ways:

1. The realizable k-ε model contains a new formulation for the turbulent viscosity.
2. A new transport equation for the dissipation rate ε, has been derived from an exact equation for the transport of the mean-square vorticity fluctuation.

The term "realizable" means that the model satisfies certain mathematical constraints on the Reynolds stresses, consistent with the physics of turbulent flows. Neither the standard k-ε model nor the RNG k-ε model is realizable.

An immediate benefit of the realizable k-ε model is that it more accurately predicts the spreading rate of both planar and round jets. It is also likely to provide superior performance for flows involving rotation, boundary layers under strong adverse pressure gradients, separation, and recirculation.

To understand the mathematics behind the realizable k-ε model, consider combining the Boussinesq relationship and the eddy viscosity definition equation (3.16) to obtain the following expression for the normal Reynolds stress in an incompressible strained mean flow:

$$\mu_t = C_\mu \rho k^2/\varepsilon \tag{3.16}$$

$$\overline{u^2} = \frac{2}{3}k - 2v_t\frac{\partial U}{\partial x} \tag{3.17}$$

Using Equation (3.16) for $v_t \equiv \eta_t/\rho$, one obtains the result that the normal stress $\overline{u^2}$, which by definition is a positive quantity, becomes negative, i.e., "non-realizable", when the strain is large enough to satisfy.

$$\frac{k}{\varepsilon}\frac{\partial U}{\partial x} > \frac{1}{3C_\mu} \approx 3.7 \tag{3.18}$$

Similarly, it can also be shown that the Schwarz inequality for shear stresses ($\overline{u_\alpha u_\beta}^2 \leq \overline{u_\alpha^2 u_\beta^2}$); no summation over (αand β) can be violated when the mean strain rate is large. The most straightforward way to ensure the realizability (positivity of normal stresses and Schwarz inequality for shear stresses) is to make$C_\mu$variable by sensitizing it to the mean flow (mean deformation) and the turbulence (k, ε). The notion of variable $C_\mu$is suggested by many modelers, including Reynolds, and is well substantiated by experimental evidence. For example, $C_\mu$is found to be around 0.09

in the inertial sublayer of equilibrium boundary layers, and 0.05 in a strong homogeneous shear flow.

Both the realizable and RNG (k, ε) models have shown substantial improvements over the standard (k, ε) model, where the flow features include strong streamline curvature, vortices, and rotation. Since the model is still relatively new, it is not clear in exactly which instances the realizable (k, ε) model consistently outperforms the RNG model. However, initial studies have shown that the realizable model provides the best performance of all the (k, ε) model versions for several validations of separated flows and flows with complex secondary flow features.

One of the weaknesses of the standard (k, ε) model or other traditional (k, ε) models lies with the modeled equation for the dissipation rate (ε). The well-known round-jet anomaly (named based on the finding that the spreading rate in planar jets is predicted reasonably well, but prediction of the spreading rate for axisymmetric jets is unexpectedly poor) is considered to be mainly due to the modeled dissipation equation.

One limitation of the realizable (k, ε) model is that it produces non-physical turbulent viscosities in situations when the computational domain contains both rotating and stationary fluid zones (e.g., multiple reference frames, rotating sliding meshes). This is due to the fact that the realizable (k, ε) model includes the effects of mean rotation in the definition of the turbulent viscosity. This extra rotation effect has been tested on single rotating reference frame systems and showed superior behavior over the standard (k, ε) model. However, due to the nature of this modification, its application to multiple reference frame systems should be taken with some caution.

The modeled transport equations for *k*and εin the realizable (k, ε) model are

$$\frac{\partial}{\partial t}(\rho k) + \frac{\partial}{\partial x_j}(\rho k u_j) = \frac{\partial}{\partial x_j}\left[\left(\mu + \frac{\mu_t}{\sigma_k}\right)\frac{\partial k}{\partial x_j}\right] + G_k + G_b - \rho\varepsilon - Y_M + S_k \tag{3.19}$$

$$\frac{\partial}{\partial t}(\rho \varepsilon) + \frac{\partial}{\partial x_j}(\rho \varepsilon u_j) = \frac{\partial}{\partial x_j}\left[\left(\mu + \frac{\mu_t}{\sigma_\varepsilon}\right)\frac{\partial \varepsilon}{\partial x_j}\right] + \rho C_1 S_\varepsilon - \rho C_2 \frac{\varepsilon^2}{k+\sqrt{v\varepsilon}} + C_{1\varepsilon}\frac{\varepsilon}{k} C_{3\varepsilon} G_b + S_\varepsilon \tag{3.20}$$

Where,

$$C_1 = max\left[0.43, \frac{\eta}{\eta+5}\right], and\ \eta = S\frac{k}{\varepsilon}, S\sqrt{2S_{ij}S_{ij}}$$

In these equations, $G_k$represents the generation of turbulence kinetic energy due to the mean velocity gradients. $G_b$is the generation of turbulence kinetic energy due to buoyancy. $Y_M$represents the contribution of the fluctuating dilatation in compressible

turbulence to the overall dissipation rate. $C_2$and $C_{1\varepsilon}$are constants. $\sigma_k$and $\sigma_k$are the turbulent Prandtl numbers for $k$and ε, respectively. $S_k$and $S_\varepsilon$are user-defined source terms.

The model constantsC_2, σ_k, and $\sigma_\varepsilon$have been established to ensure that the model performs well for certain canonical flows. The model constants are

$C_{1\varepsilon}$=1.44, C_2=1.9, σ_k=1.0 and σ_ε=1.2

3.3.4 The k-ω model

The shear-stress transport (SST) k-ωmodel was developed by Menter to effectively blend the robust and accurate formulation of the k-ωmodel in the near-wall region with the free-stream independence of the k-ε model in the far field. To achieve this, the k-ε model is converted into a k-ωformulation. The SST k-ωmodel is similar to the standard k-ωmodel. These features make the SST k-ωmodel more accurate and reliable for a wider class of flows (e.g., adverse pressure gradient flows, airfoils, transonic shock waves) than the standard k-ω model. Other modifications include the addition of a cross-diffusion term in the ωequation and a blending function to ensure that the model equations behave appropriately in both the near-wall and far-field zones.

The SST k-ωmodel has a similar form to the standard k-ωmodel:

$$\frac{\partial}{\partial t}(\rho k) + \frac{\partial}{\partial x_i}(\rho k u_i) = \frac{\partial}{\partial x_j}\left[\Gamma_k \frac{\partial k}{\partial x_j}\right] + \tilde{G}_k + -Y_k + S_k \tag{3.21}$$

$$\frac{\partial}{\partial t}(\rho \omega) + \frac{\partial}{\partial x_i}(\rho \omega u_i) = \frac{\partial}{\partial x_j}\left[\Gamma_\omega \frac{\partial \omega}{\partial x_j}\right] + G_\omega - Y_\omega + D_\omega + S_\omega \tag{3.22}$$

In these equations, $\tilde{G}_k$represents the generation of turbulence kinetic energy due to mean velocity gradients, calculated as described in eq. (3.3) that represents the generation of ω, calculated as

$$G_\omega = \alpha \frac{\omega}{k} G_k \tag{3.23}$$

The Γ_k and Γ_ω represent the effective diffusivity of k and ω, respectively, which are calculated as described below. $Y_k$and $Y_\omega$represent the dissipation of k-ε and ωdue to turbulence, calculated as described in Fluent documentation. $D_\omega$represents the cross-diffusion term, calculated as described below. $S_k$and $S_\omega$are user-defined source terms.

$$\Gamma_k = \mu + \frac{\mu_t}{\sigma_k} \tag{3.24}$$

$$\Gamma_\omega = \mu + \frac{\mu_t}{\sigma_\omega} \tag{3.25}$$

Where,$\sigma_k$and $\sigma_\omega$are the turbulent Prandtl numbers for k and ω, respectively. The turbulent viscosity,μ_t, is computed as follows:

$$\mu_t = \frac{\rho k}{\omega} \frac{1}{\max\left[\frac{1}{\alpha^*}, \frac{SF_2}{\alpha_1 \omega}\right]} \tag{3.26}$$

$$\sigma_k = \frac{1}{\frac{F_1}{\sigma_{k,1}} + (1-F_1)/\sigma_{k,2}} \tag{3.27}$$

$$\sigma_\omega = \frac{1}{\frac{F_1}{\sigma_{\omega,1}} + (1-F_1)/\sigma_{\omega,2}} \tag{3.28}$$

The coefficient α^*damps the turbulent viscosity causing a low-Reynolds-number correction. It is given by:

$$\alpha^* = \alpha_\infty^* \left(\frac{\alpha_0^* + R_{et}/R_k}{1 + R_{et}/R_k}\right) \tag{3.29}$$

$$R_{et} = \frac{\rho k}{\mu \omega} \tag{3.30}$$

$$R_k = 6 \tag{3.31}$$

$$\alpha_0^* = \frac{\beta_i}{3} \tag{3.32}$$

$$\beta_i = 0.072 \tag{3.33}$$

The blending functions, $F_1$and F_2, are given by

$$F_1 = \tanh(\Phi_1^4) \tag{3.34}$$

$$\Phi_1 = min\left[max\left(\frac{\sqrt{k}}{0.09\omega y}, \frac{500\mu}{\rho y^2 \omega}\right), \frac{4\rho k}{\sigma_{\omega,2} D_\omega^+ y^2}\right] \tag{3.35}$$

$$D_\omega^+ = max\left[2\rho \frac{1}{\sigma_{\omega,2}} \frac{1}{\omega} \frac{\partial k}{\partial x_j} \frac{\partial \omega}{\partial x_j}, 10^{-10}\right] \tag{3.36}$$

$$F_2 = \tanh(\Phi_2^2) \tag{3.37}$$

$$\Phi_2 = max\left[2\frac{\sqrt{k}}{0.09\omega y}, \frac{500\mu}{\rho y^2 \omega}\right] \tag{3.38}$$

Where,yis the distance to the next surface, and $D_\omega^+$is the positive portion of the cross-diffusion term.

$$D_\omega = 2(1 - F_1)\rho\sigma_{\omega,2} \frac{1}{\omega} \frac{\partial k}{\partial x_j} \frac{\partial \omega}{\partial x_j} \tag{3.39}$$

$\sigma_{k,1}$=1.176, $\sigma_{\omega,1}$=2.0, $\sigma_{k,2}$=1.0, $\sigma_{\omega,2}$=1.168, α_1=0.31, $\beta_{i,1}$=0.075, and $\beta_{i,2}$=0.0828

3.4 Numerical Modeling

3.4.1 Room geometry

The geometry is generated by using **GAMBIT 2.2.30** to build the physical model surface and other constructions and then to generate a three-dimensional and two dimensional models.

The Gambit software was used to mesh both models to prepare them for solution stage by using Fluent code.

3.4.2 Mesh generation

The way that such a grid is determined is called grid generation. The matter of grid generation is a significant consideration in CFD, the type of grid you choose for a given problem can make or break the numerical solution. Because of this, grid generation has become an entity by itself in CFD. The generation of an appropriate grid or mesh is one thing, the solution of the governing flow equations over such a grid is quite another thing. Assume that (for reasons to be discussed later) we construct a nonuniform grid in our flow field.

3.4.2.1Surface mesh generation

Surface mesh is created for the model room geometry on the corrugated panel surface with specifications as shown in Table 5. Two types meshes used, to get the required accuracy use quadrilateral type in 2D Isothermal Ceiling Jet and triangular type in IEA Annex 20.

2D isothermal	Element Shape	Mesh Type	Cell size (cm)
Ceiling Jet [32]	Quadrilateral	Map	15.38
IEA Annex 20 [41]	Triangular	Pave	13.29

Table 5 Two-Dimensional surface mesh specifications

3.4.2.2 Volume mesh generation

In three-dimensional, hexahedral, tetrahedral, pyramid, wedge, and polyhedral cells can be used, depicts each of these cell types. Both single-block and multi-block structured meshes, as well as hybrid meshes containing quadrilateral and triangular cells or hexahedral, tetrahedral, pyramid, and wedge cells are acceptable. FLUENT

also accepts grids with hanging nodes (i.e., nodes on edges and faces that are not vertices of all the cells sharing those edges or faces).

Building the mesh requires fine cells in area near the panel surface. On the other hand, using this element size in the whole domain would lead to an enormous number of elements. That is why it was decided to use a fine mesh in the region near to the panel surface and use coarse meshes as the distance from the surface grows as shown in Table 6. Figure 3.1 show the meshed models.

3D Ventilation Flows	Element Shape	Mesh Type	Cell size (cm)
Displacement ventilation	Tetrahedron	TGrid	0.02 to 0.2
Grille ventilation	Tetrahedron	TGrid	0.02 to 0.1
Ceiling slot ventilation	Tetrahedron	TGrid	0.05 to 0.1
Ceiling square ventilation	Tetrahedron	TGrid	0.05 to 0.1

Table 6 Two-Dimensional surface mesh parameters

3.5 Numerical Cases Setup in Fluent 6.3.26

3.5.1Setup for 2D ventilation

3.5.1.1 General setup:

1. **Pressure-Based** solver type.
2. **Absolute** velocity formulation.
3. **Steady** state for time consideration.
4. **Green-Gauss cell based Gradient option.**
5. **Implicit formulation.**

3.5.1.2 Materials setup

It is very important to specify the model construction parts materials properties, and the properties of the medium fluid, so the solution will be more accurate and more convergent. Table 7 shows air properties.

Parameter	Unit	Value
Density (ρ)	(kg/m^3)	1.22
Specific Heat (C_p)	(J/kg. K)	1006.43
Thermal Conductivity (k)	(W/m. K)	0.0242
Viscosity (μ)	kg/m. s	1.7894×10^{-5}

Table 7 Air properties.

3.5.1.3 Solution controls

It is necessary to control the change of the primary variable, because of the pressure-velocity coupling and nonlinearity of the equation set to be solved by FLUENT. This is typically achieved by **under-relaxation**, which reduces the change of primary variable produced during iterations. The values of **under-relaxation factors** used in the present work to solve the momentum equation and other scalar quantities are listed in Table 8.

	Under-Relaxation Factor
Pressure	0.3
Density	1
Momentum	0.7
Turbulent Kinetic Energy	0.8
Turbulent Dissipation Rate	0.8
Turbulent Viscosity	1

Table 8 Under-Relaxation Factors.

3.5.1.4 Convergence criteria

This is the group of residual values, under which, when the average residuals fall, the solver terminates itself. Residuals are the error of the computation.

It is accepted that when the residuals for flow, including continuity, momentum fall below (1×10^{-3})**,** the computational error may be ignored. Average minimum convergences were (1×10^{-4}) for continuity and velocities equations. Figure 3.2 show convergence history for continuity, momentum and also kandε for turbulent flow case.

3.5.2 Setup for 3D ventilation

3.5.2.1 General setup:

As in section **3.5.1.1.**

3.5.2.2 Materials setup

As in section **3.5.1.2.**

3.5.2.3 Solution controls

It is necessary to control the change of the primary variable, because of the pressure-velocity coupling and nonlinearity of the equation set to be solved by FLUENT. This is typically achieved by **under-relaxation**, which reduces the change of primary variable produced during iterations. The values of **under-relaxation factors** used in the present work to solve the momentum equation and other scalar quantities are listed in Table 9

	Under-Relaxation Factor
Pressure	0.3
Density	1
Body Force	1
Momentum	0.5
Turbulent Kinetic Energy	0.8
Turbulent Dissipation Rate	0.8
Turbulent Viscosity	1
Energy	0.9

Table 9 Under-Relaxation Factors.

3.5.2.4 Convergence criteria

The residuals for turbulent flow, including continuity, momentum fall below (1×10^{-3}) and the energy falls below (1×10^{-6}), the computational error may be ignored. Average minimum convergences were (1×10^{-4}, 1×10^{-4} and 1×10^{-8}) for continuity, velocities and energy equations respectively, and for kandε are (2×10^{-4} and 9×10^{-4}) for turbulent flow cases.

3.6 Data Analysis Method

Upon collecting all the actual measurement data, the data was analyzed using a few methods. As each room was divided into five zones with fifty points to comparing with measured data, which consists of ten points. The actual results were compared with the simulated results by using overall average error calculations.

The equations (3.40) are overall average error [42]:

$$E = \frac{\left|X^i_{CFD} - X^i_{exp}\right|}{X^i_{exp}} \times 100\% \tag{3.40}$$

Where X can be either air velocity or air temperature. $\left|X^i_{CFD} - X^i_{exp}\right|$ is the absolute difference between simulated values and actual measurement values for variable X.

3.7 Effective Draft Temperature (EDT)

The Effective Draft Temperature (EDT) was evaluated for each point using the air velocity and air temperature obtained. To define the effective draft temperature (EDT) (difference in temperature between any point in the occupied zone and the control condition), the investigators using the equation (3.41) accounts for the feeling of coolness produced by air motion [8].

$$\text{EDT} = (T_x - T_c) - 8^{x} (V_x - 0.15) \tag{3.41}$$

where

EDT = effective draft temperature, K.

T_x = local airstream dry-bulb temperature, °C.

T_c = average (control) room dry-bulb temperature, °C.

V_x = local airstream centerline velocity, m/s.

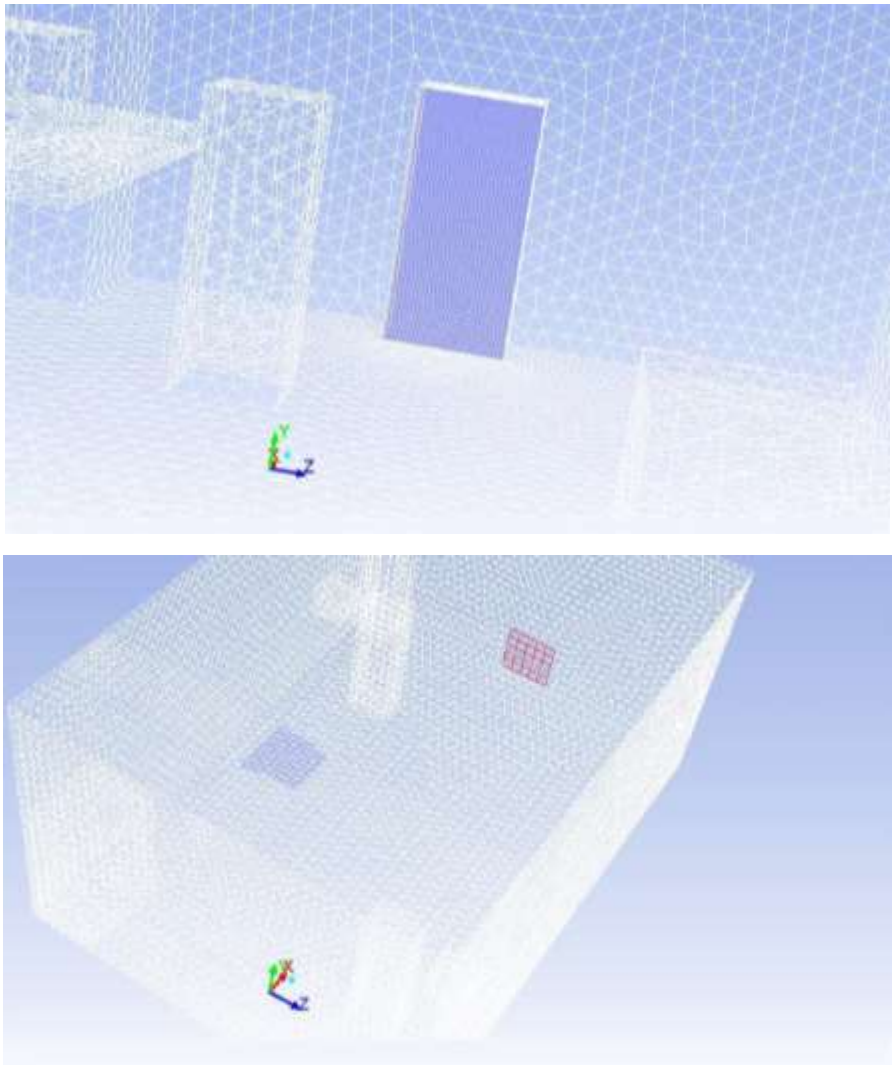

Figure 3.1 The meshed model for displacement and square ventilation.

CHAPTER 4

VALIDATION STUDY FOR 3D AND 2D VENTILATION

4.1 Validation study of 2D Isothermal Ceiling Jet

In this section, two isothermal ventilation test cases, cases for 2D ventilation in a partitioned model room, are studied to validate the numerical models and simulation results.

4.1.1 First Case

In this case, a simple linear ceiling jet under a two-dimensional isothermal condition was studied. This case is used to validate the CFD simulation applicable to a model room with vertically discharged jet. The published studied was a thorough simulation of this case using EXACT3 code, [29]. These results were compared with the published studied. Figure 4.1 shows the dimensions and layout of the model and linear jet.

The standard k-ε model was used in order to illustrate the influence of choosing the grids in model. In previous studies, the grid (16×36) was used, but in the present work, (20×40) is used to obtain more accurate results, was selected to simulate the pattern of the room.

4.1.1.1 Boundary conditions

The boundary conditions for this test case can be summarized as:

Dimension of Layout room are (5.9436 m×2.8575 m) (L×H)

Inlet: velocity inlet

U_o=0 m/s, V_o= 1 m/s

Where, U_o the horizontal velocity component, V_o the vertical velocity component at the inlet and outlet.

k_o, ε_o as defined in equations:

$$K_o = 1.5\,(0.04 \times V_o)^2 \tag{4.1}$$

$$\varepsilon_o = k_o^{1.5} / l_o \tag{4.2}$$

Where, l_o is the length scale of the inlet, l_o = h/10. The above inlet conditions correspond to a turbulence intensity of 4%, [41].

Outlet:

U_o=0 m/s, V_o= -1 m/s

4.1.1.2 Result and discussion

To further compare these results, the velocity along a vertical line at the supply position is shown in Figure 4.2. This investigation deals with the velocity provided slightly acceptable results, by using overall average error equation, the error not exceed (12.59 %). However, the method with same model (standard k-ε) provided good results.

The comparison of the velocity along a vertical line at distance (0.75 m) from the supply is depicted in Figure 4.3. The two-dimensional models can give a good indication about trends in the model room. There are some differences in the region close to the ceiling. A comparison of the velocity along a vertical line at the return position is shown m Figure 4.4. Both of these methods have the same behavior as possible be considered very close results and the overall average error is (10.98 %).

4.1.2 Second case

The second case was similar to the first one. The only difference was that the direction of the supply air was not perpendicular to the ceiling but at an angle of 60 degrees. It indicates that the air flow pattern inside the room is reasonable, no large discrepancies can be seen directly. The velocity vector for published studied is illustrated in Figure 4.5 a, and the simulation for present study is shown in Figure 4.5 b.

4.2 Validation Study of IEA Annex 20

Researchers from thirteen countries have participated in this project. Within a research period of three years and a half (May 1, 1988 ~ Nov. 1, 1991). Many full scale experiments on forced convection, mixed convection and natural convection were conducted by different research groups in an identical three-dimensional experiment configuration in International Energy Agency (IEA Annex 20 Standard Test Room) on different sites. Many useful experimental data acquired and compiled, and relevant numerical simulations carried out.

In the IEA Annex 20 Test Case B project, a simple 2D test case is shown in Figure 4.6 with L/H=3.0, h/H=0.056 and t/H=0.16, where H=3.0 m, L=9.0 m, h=0.168 m and t=0.48 m, [41].

Experimental data for this test case were obtained from a scale model room using laser-Doppler anemometry (LDA). The data included the measured horizontal velocity component U at two vertical lines of x=H (x= 3 m) and x= 2H (x= 6 m), [41].

The experimental data are expressed in terms of dimensionless horizontal velocity U/Uo where Uo is the supply air velocity at the inlet, and U is the horizontal velocity.

4.2.1 Boundary conditions

The boundary conditions for this test case can be summarized as:

Inlet: velocity inlet Uo

Uo = 0.455 m/s, Vo=0 m/s

ko, εo as defined in equations (4.1) and (4.2).

Outlet:

outflow, i.e., dp/dx=0

Where, (Vo) is the vertical velocity component at the inlet, and (p) is pressure.

4.2.2 Numerical simulation with different k-ε turbulence models

4.2.2.1 Prediction with standard k-ε turbulence model

The most widely used standard k-ε model was used as a baseline model for this test case. For the predicted flow pattern using the standard k-ε model and a mesh grid of (50×28), comparisons with experimental data of the prediction results using standard k-ε model and three different near-wall treatments (standard wall-function (SWF), non-equilibrium wall function (NEWF) and enhanced wall treatment (EWF) are plotted in Figures. 4.7 and (4.8) at X=3 m and X=6 m. It can be seen that the predicted results from these three different near-wall treatments are nearly the same.

4.2.2.2 Prediction with RNG k-ε model and Realizable k-ε model

The predictions using RNG k-ε model and Realizable k-ε model together with SWF are shown in Figure 4.9. The mesh grid used is also (50×28). As a baseline result, the prediction using standard k-ε model and SWF is also depicted in Figure 4.9. It can be

seen that the predictions from the standard k-ε model and the RNG k-ε have a very little deviation, the Realizable k-ε predicts better the jet flow at X=6m.

4.3 3D Ventilation Flows with Heat and Mass Transfer

Three typical ventilation flow cases are considered (displacement, slot ceiling, and square ceiling) ventilation in summer cooling condition. In the former case, the ventilation flow is mainly driven by buoyancy created by the temperature differences between the supplied air and the internal heat sources; in the latter case the air flow is driven by forced convection which has more relevance to the ventilation flow in a spacecraft cabin. The three test cases are taken from a recent report ASHRAE RP-1009, [10].

4.3.1 Displacement ventilation

The displacement ventilation test case was carried out under a ventilation rate of (5ACH). The inlet diffuser is located near the west wall, and the exhaust opening is at the center of the ceiling, as shown in Figure 4.10. The size and position of the inlet and outlet diffusers are listed in Table 10. The positions of the five poles carrying the anemometers are shown in Figure 4.11. All the other objects (human simulators, computers, tables, lamps and cabinets) in the flow field are the same as in the displacement ventilation test case, their dimension and position as well as heat generating rate are presented in Table 10.

	Size (m)			**Location**			**Temp.**
	ΔX (m)	**ΔZ (m)**	**ΔY (m)**	**ΔX (m)**	**ΔZ (m)**	**ΔY (m)**	**T (ºC)**
Supply	0.28	0.53	1.1	0.28	1.56	0.03	13.0
Return	0.43	0.43	0.0	2.365	1.16	2.43	22.2

Table 10 Size and position of the displacement and exhaust diffusers [10]

	Size			**Location**			**Heat**
	ΔX (m)	**ΔY (m)**	**ΔZ (m)**	**X (m)**	**Y (m)**	**Z (m)**	**Q (W)**
Room	5.16	2.43	3.65	0.0	0.0	0.0	-
Window	0.0	1.16	3.65	5.16	0.94	0.0	-
Person 1	0.4	1.1	0.35	1.1	0.0	0.95	75
Person 2	0.4	1.1	0.35	3.9	0.0	2.4	75
Computer 1	0.4	0.35	0.35	1.1	0.75	0.1	108

Computer 2	0.4	0.35	0.35	3.9	0.75	3.2	173
Table 1	1.47	0.1	0.75	0.58	0.74	0.0	-
Table 2	1.47	0.1	0.75	3.69	0.74	2.9	-
Lamp 1	0.1	0.0	1.2	1.03	2.43	0.15	34
Lamp 2	0.1	0.0	1.2	3.61	2.43	0.15	34
Lamp 3	0.1	0.0	1.2	1.03	2.43	0.15	34
Lamp 4	0.1	0.0	1.2	3.61	2.43	0.15	34
Cabinet 1	0.58	1.32	0.33	0.0	0.0	0.0	-
Cabinet 2	0.95	1.24	0.58	4.21	0.0	0.0	-

Table 11 Configuration of the test chamber [10]

4.3.1.1 Modeling and simulation

a- Boundary conditions

- *Supply diffuser:* The supply air was discharged horizontally from the front surface of the diffuser; this corresponds to a discharge velocity of (0.11m/s). Because the front surface of the inlet diffuser is covered with a perforated metal sheet, the actual flow area is less than the gross area of the surface, and the actual discharge velocity from the diffuser is 0.35 m/s. At the front surface of the diffuser, a mass flow rate of 0.0768 kg/s and a turbulence intensity of 4% are specified. The inlet air temperature is (13°C). The turbulence quantities (k, ε or ω) at the inlet are calculated using equations (4.1) and,

$$\varepsilon = \frac{C_{\mu}^{3/4} k_0^{3/2}}{l_0} \tag{4.3}$$

Where: l_0=0.1L is the length scale. L normally equals to the characteristic length of the diffuser

Return: The outlet is specified as pressure outlet, i.e., the gauge pressure at the outlet is specified as zero.

Thermal conditions: Temperature or heat flux at the walls is used to specify the thermal conditions for different objects in the flow field:

The thermal conditions of the following objects are specified as heat flux given from published studied [10]:

- Computer 1: 171.43 W/m^2

- Computer 2: 274.6 W/m^2
- Human simulators: 41.9 W/m^2
- Lamps: 37.78 W/m^2

The average of the measured temperatures at the walls is used to specify the thermal condition for the walls:

- Ceiling: 295 K (22°C)
- Floor: 292 K (19°C)
- West wall: 294 K (21°C)
- East Wall: 296 K (23°C)
- South and North walls: 294 K (21°C)
- Table 1: 293 K (20°C)
- Table 2: 294 K (21°C)

b- Turbulence modeling

Applying that the Realizable k-ε and the SST k-ω models can give reasonable prediction for ventilation flows coupled with heat transfer, these models are further evaluated in this test case.

c- Computation meshes

Because there are many flow obstacles in the flow field, using a structured mesh will result in lots of unnecessary mesh cells in the regions far from the walls, so an unstructured mesh is used instead. Depending on many testing meshes, it is found that the size of (1,480,232) cells is acceptable.

d- Numerical schemes

The convection terms are discretized using the second-order upwind scheme. For the discretization of pressure, the PRESTO! (PREssure STaggering Option) scheme is used. The SIMPLEC scheme is used for the pressure-velocity coupling. When working with unstructured meshes, a high-order scheme is preferred for the discretization of convection terms to minimize the discretization errors.

e- Simulation results

Figures 4.12 and (4.13) show comparisons of the predicted air velocity and temperature profiles using Realizable k-ε and SST k-ω models with the experimental

measurements, respectively. Showed a comparison between the experimental and turbulence models in this case that the model (k-ω) is better because of that overall average error are (28.37 %) for k-ε and (19.87 %) for k-ω for velocity prediction, and overall average error are (20.92 %) for k-ε and (14.2 %) for k-ω for temperature prediction. The predicted temperatures have some discrepancies with the measured data near the ceiling and floor level, this may be a consequence of the imposed thermal boundary conditions at the ceiling and the floor. Experimentally, the measured temperature near the diffuser (17.42°C at X= 0.8 m) has 3°C difference with the temperature recorded as near the west wall and (20.43°C at X=4.36 m) has 1.313 °C difference at the floor, by imposing an average temperature (23°C) at the floor, thus the predicted temperature is lower than the measured value. Figure 4.13 presents the predicted temperatures near the floor which are generally lower than the measured ones. At the ceiling region, the imposed averaged temperature is close to temperature near the west wall which enhances the heat exchange between the ceiling and the air in that region, thus the predicted air temperature is slightly higher than the measured value in this region. Despite the discrepancies, the vertical temperature gradient in the middle of the room is well predicted, which is an important parameter influencing the thermal comfort for displacement ventilation.

4.3.2 Ceiling slot ventilation

4.3.2.1 Test conditions

The ceiling slot ventilation test case was carried out under a ventilation rate of (9.2 ACH). The inlet diffuser is installed on the ceiling and (0.15 m) from south wall, and the exhaust opening is on the west wall and 0.02 m above the floor, as shown in Figure 4.14. The size and position of the inlet and outlet diffusers are listed in Table 12. The positions of the five poles carrying the anemometers are shown in Figure 4.15.

	size			Location			Temp.
	ΔX (m)	ΔZ (m)	ΔY (m)	ΔX (m)	ΔZ (m)	ΔY (m)	T (ºC)
Supply	0.10	1.15	0.0	2.53	0.15	2.43	16.3
Exhaust	0.00	0.43	0.43	0.00	1.16	0.02	21.4

Table 12 Position and size of the slot and exhaust diffusers [10]

4.3.2.2 Modeling and simulation

a- Boundary conditions

Inlet diffuser:

The slot diffuser consists of three opening each one (1.143 m x 0.019 m) and the inflow passes through the two openings to enter the test room (Figure 4.16a). In the experiment, it was observed by smoke visualization that the inlet flow from the slot diffuser turned 45° downwards toward the west wall (Figure 4.16b).

At the supply opening, a mass flow rate of (0.138 kg/s) and a turbulence intensity of 5% are specified. The boundary condition for the turbulence quantities (k, ε or ω) are calculated using equations (4.1) and (4.3), the temperature of the inlet air is 289.3 K (16.3°C).

Outlet:

The outlet is specified as pressure outlet, i.e., the gauge pressure at the outlet is specified as zero.

Thermal conditions:

As in the displacement ventilation case in section 4.3.1.1

b- Turbulence modeling

As in section 4.3, the influence of turbulence on the mean flow is modeled using the Realizable k-ε and the SST k-ω models. The non-equilibrium wall function or the enhanced wall treatment is used when working with the two k-ε models.

c- Computation meshes

As in a section 4.3, an unstructured mesh is used to discretize the flow domain. Several different mesh sizes are tested it is found that the predicted velocity and temperature profiles change much less as the mesh resolution changes. After some tests, a mesh size of (1,071,118) cells is chosen as the main computation mesh which represents a good compromise between the mesh resolution requirements and the available computational resources.

d- Numerical schemes

The discretization schemes are the same as in item (d) in section 4.3.1.1.

e- Simulation results

The Figures. 4.17 and 4.18 give comparisons of the predicted air velocity and temperature profiles using Realizable k-ε and SST k-ω models with experimental data, respectively. It can be seen that the predicted profiles correspond reasonably well with measured ones ASHRAE RP-1009 [10].

Showed a comparison between the experimental and turbulence models in this case that the model (k-ω) is better because of that overall average error are (20.69 %) for k-ε and (17.12 %) for k-ω for velocity prediction, and overall average error are (9.49 %) for k-ε and (7.08 %) for k-ω for temperature prediction.

In Figures. 4.17 and 4.18, the predicted air velocity and temperature profiles at X=1.78 m, and X=2.51 m have some big discrepancies compared with measured data in the ceiling region. This is likely due to the momentum model used for the inlet diffuser, because ASHRAE RP-1009 [10] when using the momentum model for the diffuser, they obtained the same results for the predicted temperature profiles, the discrepancies at X=3.36 still exists. When it is used with the k-ε or k-ω models, it may also contribute to some degree to the discrepancies between the predicted temperature profiles and the measured ones. In the occupied zone, thus the prediction using the model for the diffuser is acceptable for practical purposes.

4.3.3 Ceiling square ventilation

4.3.3.1 Test conditions

The ceiling square ventilation test case was carried out under a ventilation rate of (4.9 ACH). The inlet diffuser is installed on the ceiling, and the exhaust opening is on the west wall and 0.02 m above the floor, as shown in Figure 4.19. The size and position of the inlet and outlet diffusers are listed in Table 13. All the other objects (human simulators, computers, tables, lamps and cabinets) in the flow field are the same as in the displacement ventilation test case, their dimension and position as well as heat generating rate are presented in Table 13 and the positions of the five poles carrying the anemometers are shown in Figure 4.20.

	Size			Location			Temp.
	ΔX	ΔZ	ΔY	ΔX	ΔZ	ΔY	T (ºC)
Supply	0.30	0.30	0.00	3.69	1.68	2.41	14.5
Exhaust	0.00	0.43	0.43	0.00	1.16	0.02	24.1

Table 13 Position and size of the square and exhaust diffusers, [10].

4.3.3.2 Modeling and simulation

a- Boundary conditions

Inlet diffuser: The square diffuser has nine 0.1m x 0.1m openings and the inflow passes through the eight openings to enter the test room Figure 4.21. In the experiment, it was observed by smoke visualization that the inlet flow from the square diffuser attached the ceiling wall. To assure the correct flow from the diffuser, the Realizable k-ε and k-ω method are used to model the square diffuser.

At the supply opening, a mass flow rate is 0.075 kg/s and a turbulence intensity of 5% are specified. The boundary condition for the turbulence quantities (k, ε or ω) are calculated using equations (4.1) and (4.3), and the hydraulic diameter of the inlet opening is about 0.1 m. The temperature of the inlet air is 287.5 K (14.5°C)

Outlet:

The outlet is specified as pressure outlet, i.e., the gauge pressure at the outlet is specified as zero.

Thermal conditions:

As in the displacement ventilation case in section 4.3.

b- Turbulence modeling

As in section 4.2, the influence of turbulence on the mean flow is modeled using the Realizable k-ε and the SST k-ω models. The non-equilibrium wall function or the enhanced wall treatment is used when working with the two k-ε models.

c- Computation meshes

As in section 4.2, an unstructured mesh is used to discretize the flow domain. Several different mesh sizes are tested, it is found that the predicted tracer gas profiles are more sensitive to the mesh size used, and the predicted velocity and temperature profiles change much less as the mesh resolution changes. After some tests, a mesh size of (1,751,500) cells is chosen as the main computation mesh which represents a good compromise between the mesh resolution requirements and the available computational resources.

d- Numerical schemes

The discretization schemes are the same as in item (d) in section 4.3.1.1.

e- Simulation results

Simulations were carried out with the Realizable k-ε models and the SST k-ω model with Box and Momentum method published. Figures. 4.22 and 4.23 give comparisons of the predicted air velocity, temperature profiles using Realizable k-ε and SST k-ω models with experimental data, respectively. It can be seen that the predicted profiles correspond reasonably well with measured ones. In Figure 4.22, the predicted air velocity profiles at X=0.8 m, have some big discrepancies compared with measured data in the ceiling region, and in Figure 4.23, the predicted air temperatures at X=0.8 m have some big discrepancies compared with measured date in the floor region, this is due to selected model used for the inlet diffuser. It is noted that the prediction, that we have, is better than the way from Box and Momentum method.

4.4 Illustrations list

Dimension and Layout of the Room given in Figure 4.1. Figure 4.2 explains Air Velocity in a Vertical Line (Supply Position). Figure 4.3 shows Air Velocity in a Vertical Line (0.75m from the Supply). Air Velocity in a Vertical tine (Return Position) given if Figure 4.4. Figure 4.5 illustrates Air velocity profile, a- conventional method b- k-ε (SWF). Figure 4.6 shows the IEA Annex 20 project, a simple 2D test case. Figure 4.7 explaines comparison of the predicted results with experimental data using standard k-ε model at X=3 m. Figure 4.8 shows comparison of the predicted results with experimental data using standard k-ε model at X=6 m. Figure 4.9 explaines comparison of predicted results using different k-ε models with experimental data, a- X=3m, b- X=6m. Figure 4.10 shows configuration of the displacement ventilation test case. Figure 4.11 illustrates the positions of the measuring poles for the displacement ventilation test case (Chen et al. 2001). Figure 4.12 shows prediction of the air velocity with Realizable k-ε model and Enhancement Wall Treatment and SST k-ω, Z=height/total room height (H), U=velocity/supply velocity (U0), H=2.43m, U0=0.35m/s. Figure 4.13 explaines prediction of the air temperature with Realizable k-ε model and Enhancement Wall Treatment and SST k-ω, Z=height/total room height (H), □ = (T-Tin/Tout-Tin), H=2.43m, Tin=13.0ºC, Tout=22.2ºC. Figure 4.14 shows configuration of ceiling slot ventilation test case. Figure 4.15 explaines the positions of the measuring poles for the ceiling slot ventilation test case (Chen et al. 2001). Figure 4.16 Installates and

details of the slot diffuser (Chen et al. 2001). Figure 4.17 Prediction of the air velocity with Realizable k-ε model and Enhancement Wall Treatment and SST k-ω, Z=height/total room height (H), U=velocity/supply velocity (U0), H=2.43m, U0=3.9m/s. Figure 4.18 shows prediction of the air temperature with Realizable k-ε model and Enhancement Wall Treatment and SST k-ω, Z=height/total room height (H), □ = (T-Tin/Tout-Tin), H=2.43m, Tin=16.3ºC, Tout=21.4ºC. Figure 4.19 shows configuration of ceiling slot ventilation test case. Figure 4.20 shows the positions of the measuring poles for the ceiling slot ventilation test case (Chen et al. 2001). Figure 4.21 shows modeling of the square diffuser Figure. Figure 4.22 shows prediction of the air velocity with Realizable k-ε and SST k-ω model compared with box and momentum, Z=height/total room height (H), U=velocity/supply velocity (U0), H=2.43m, U0=5.2m/s. Figure 4.23 shows prediction of the air temperature with Realizable k-ε and SST k-ω model compared with box and momentum, Z=height/total room height (H), □=(T-Tin/Tout-Tin), H=2.43m, Tin=14.5ºC, Tout=24.1ºC.

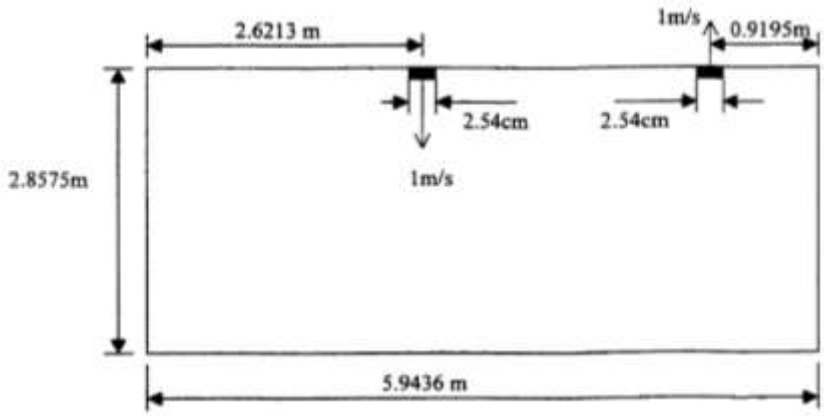

Figure 4.1 Dimension and Layout of the Room, [29].

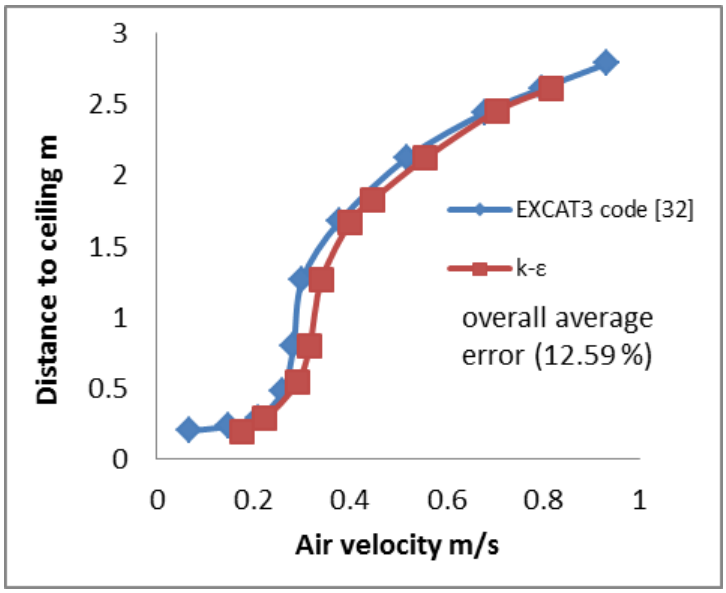

Figure 4.2 Air Velocity in a Vertical Line (Supply Position)

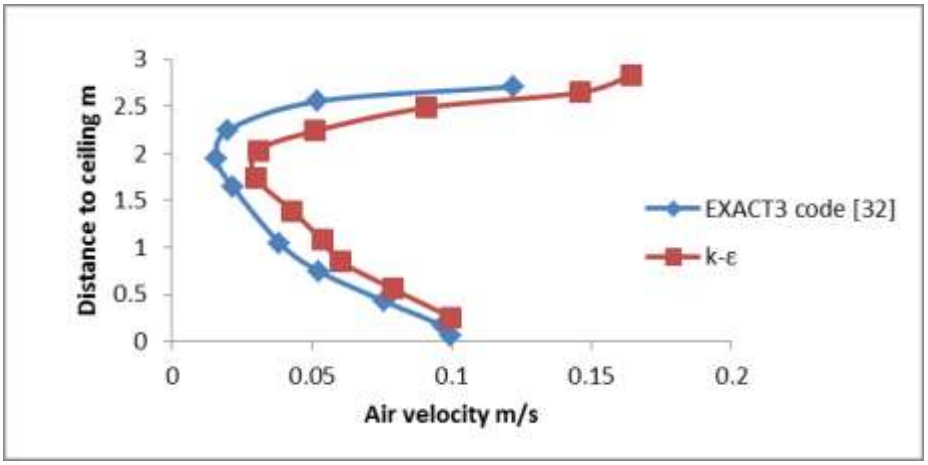

Figure 4.3 Air Velocity in a Vertical Line (0.75 m from the Supply)

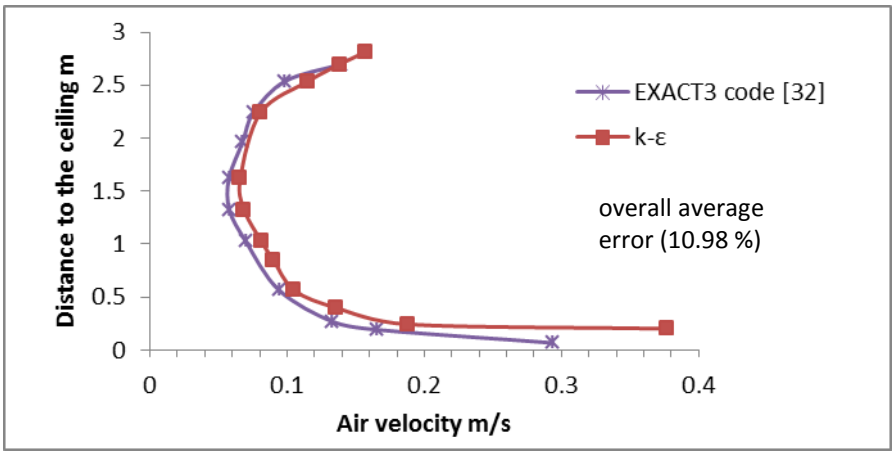

Figure 4.4 Air Velocity in a Vertical Line (Return Position)

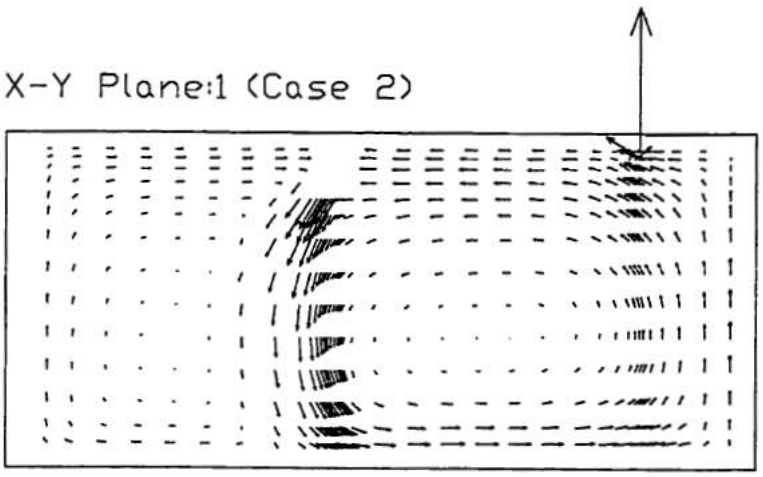

a

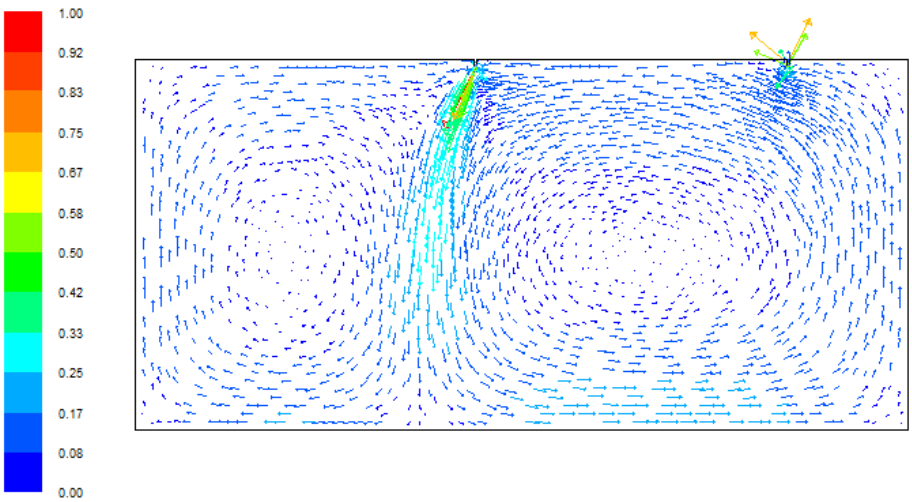

b

Figure 4.5 Air velocity profile, a- conventional method, b- k-ε (SWF)

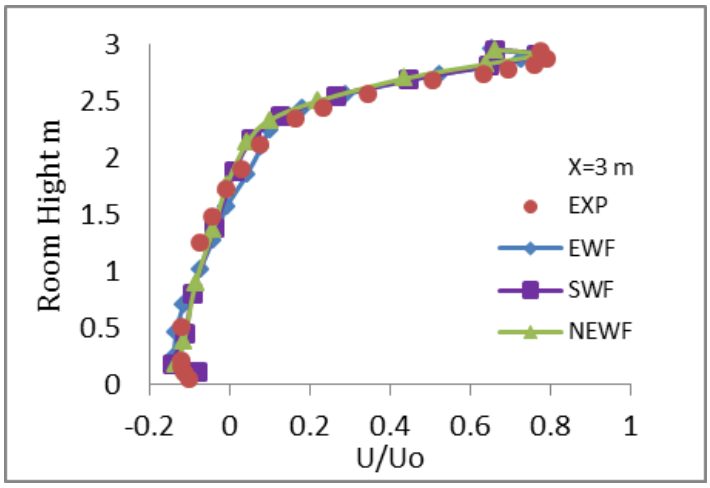

Figure 4.6 A comparison between predicted results with experimental data using standard k-ε model at X=3 m

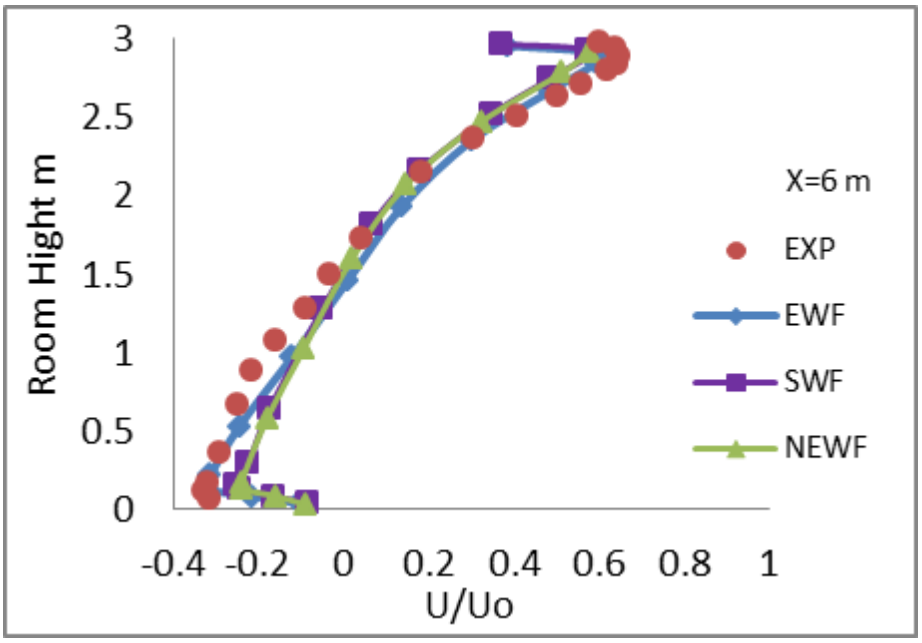

Figure 4.7 A comparison between predicted results with experimental data using standard k-ε model at X=6 m

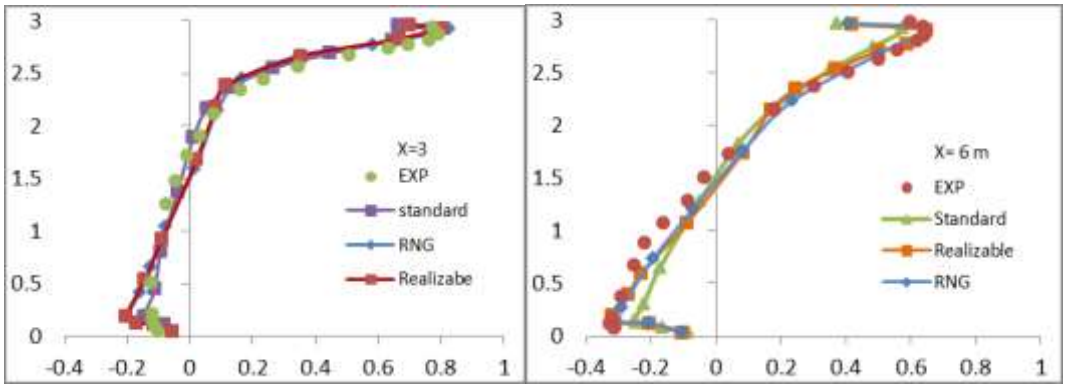

a b

Figure 4.8 A comparison between predicted results using different k-ε models with experimental data, a- X=3m, b- X=6m.

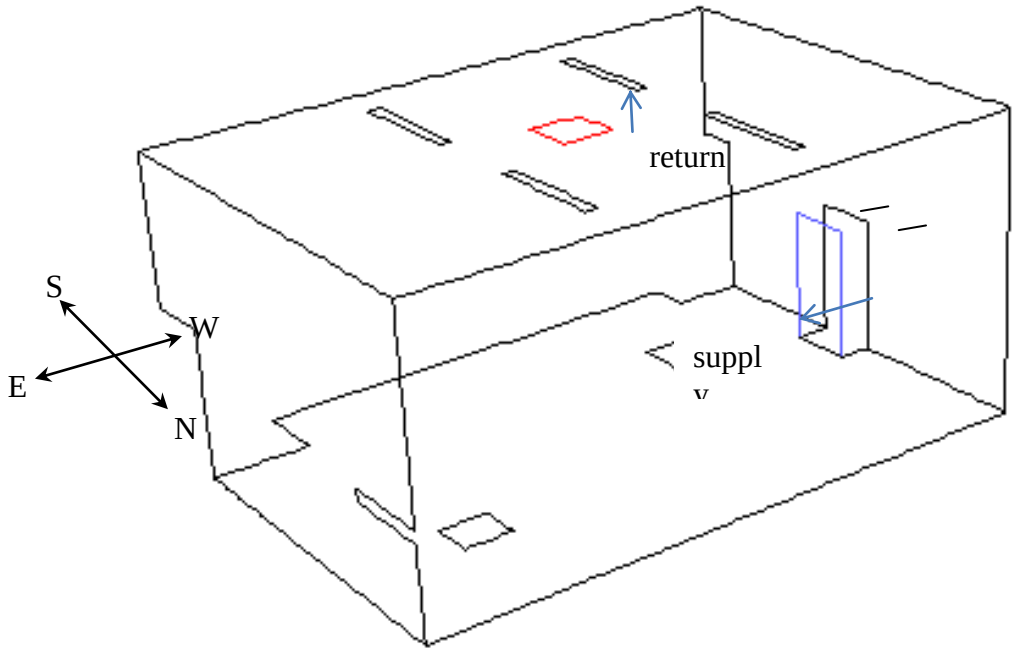

Figure 4.9 Configuration of the displacement ventilation test case.

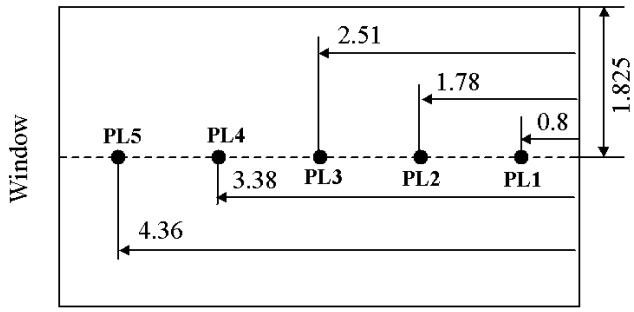

Figure 4.10 The positions of the measuring poles for the displacement ventilation test case [10]

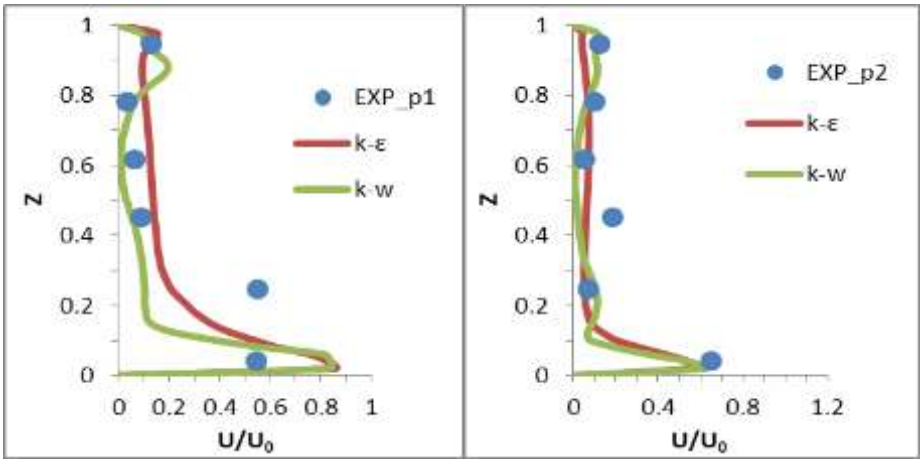

a b

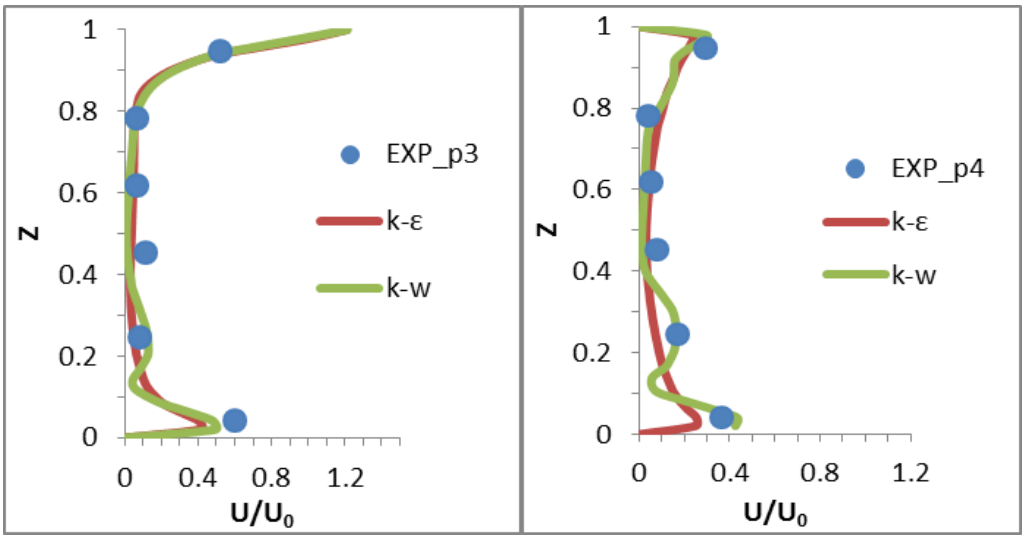

c d

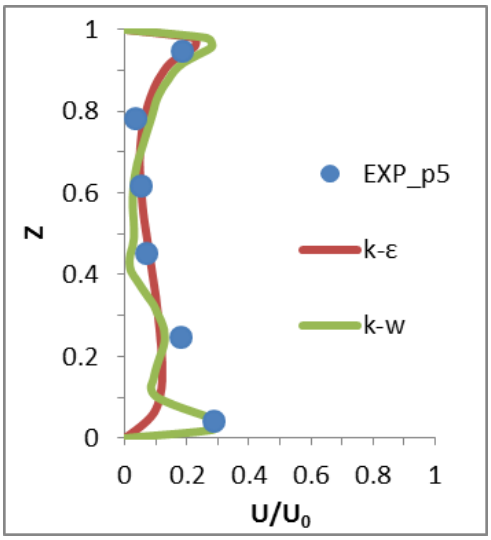

e

The overall average error for two models with experimental data:

K-ε and exp. Error (28.37 %)

k-ω and exp. Error (19.87 %)

Figure 4.11 Prediction of the air velocity with Realizable k-ε model and Enhancement Wall Treatment and SST k-ω, (Z=height/total room height (H), U=velocity/supply velocity (U0), H=2.43m, U0=0.35m/s).

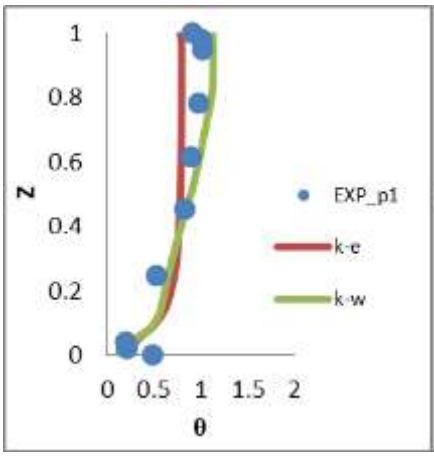

a

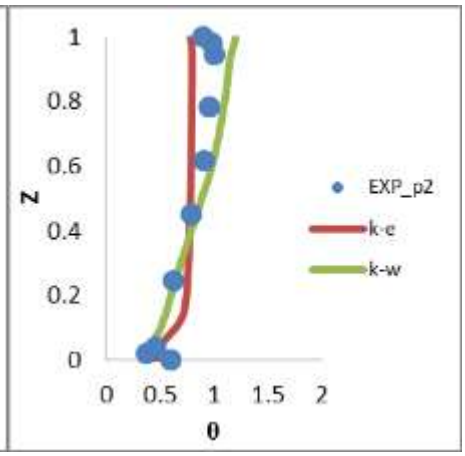

b

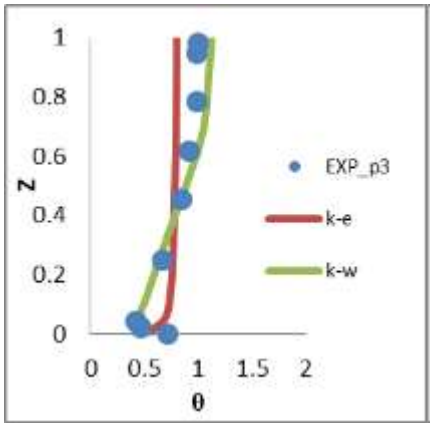

c

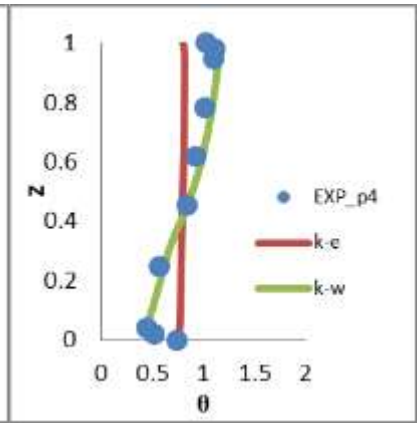

d

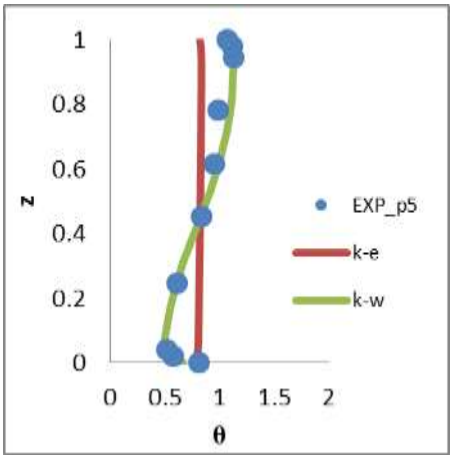

e

The overall average error for two models with experimental data:

K-ε and exp. Error (20.92 %)

k-ω and exp. Error (14.2 %)

Figure 4.12 Prediction of the air temperature with Realizable k-ε model and Enhancement Wall Treatment and SST k-ω, (*Z=height/total room height (H)*, $\theta=(T-T_{in}/T_{out}-T_{in})$, *H=2.43m*, $T_{in}=13.0^{o}C$, $T_{out}=22.2^{o}C$).

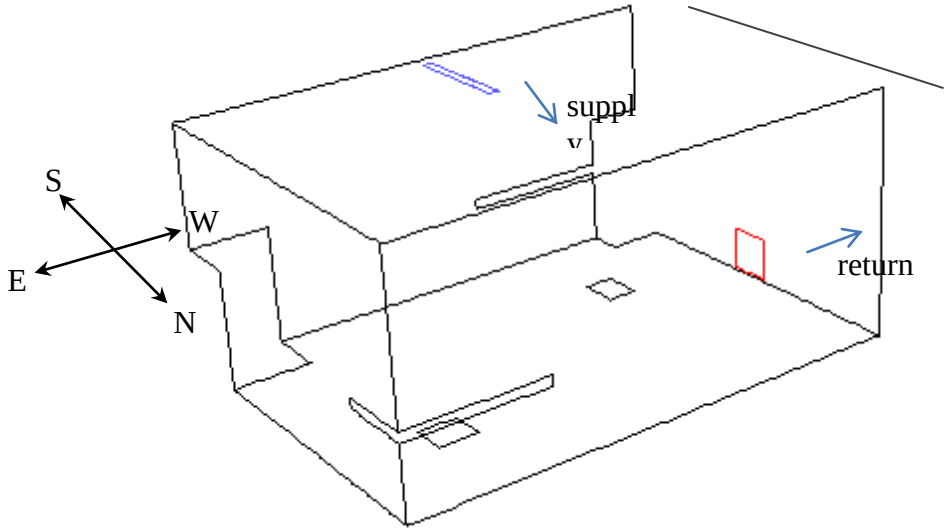

Figure 4.13 Configuration of ceiling slot ventilation test case

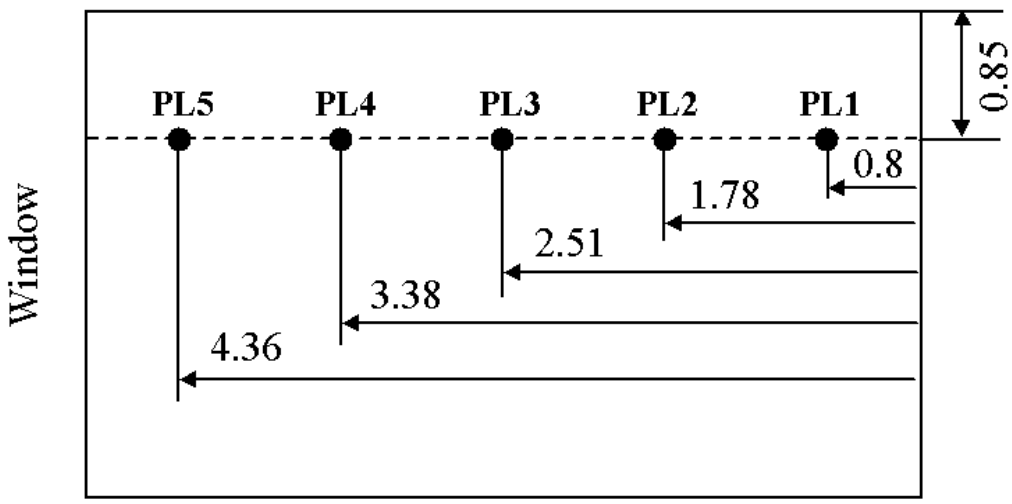

Figure 4.14 The positions of the measuring poles for the ceiling slot ventilation test case [10]

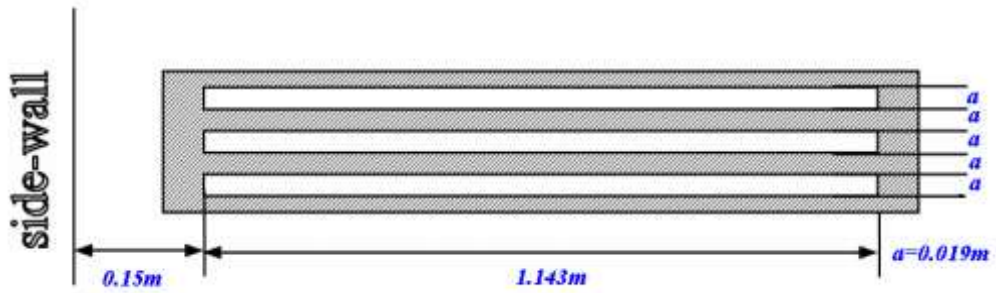

(a) Details of the slot diffuser

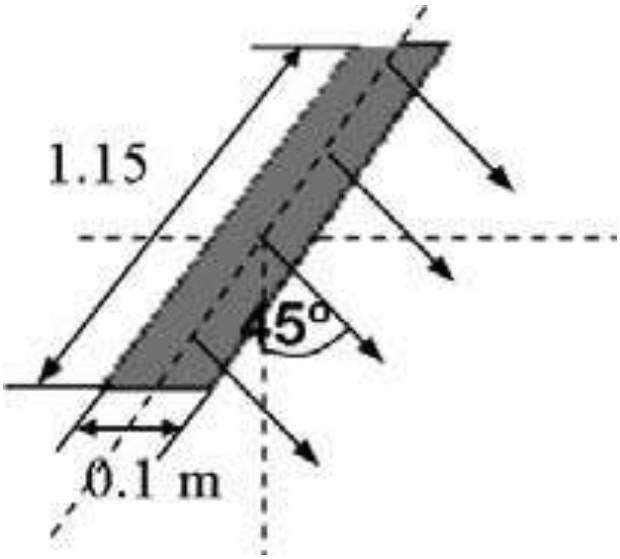

(b) Inflow direction

Figure 4.15 Installation and details of the slot diffuser [10]

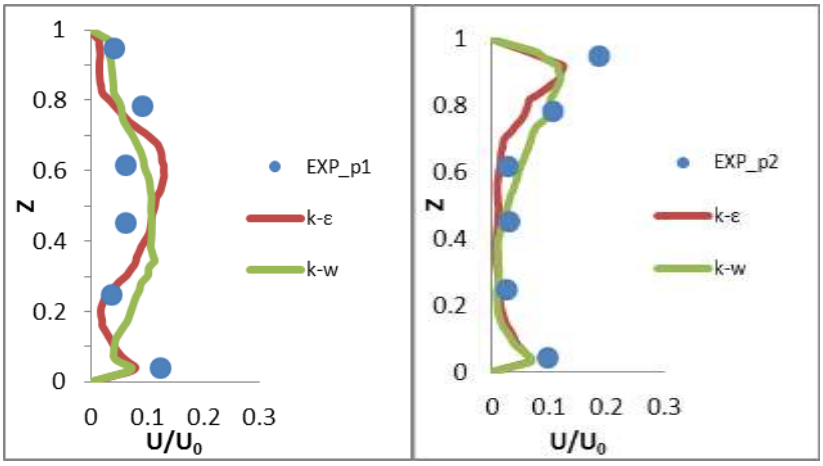

a b

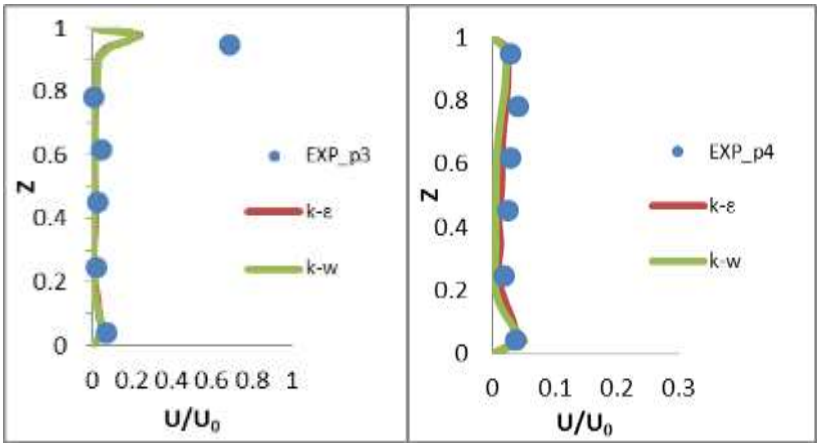

c e

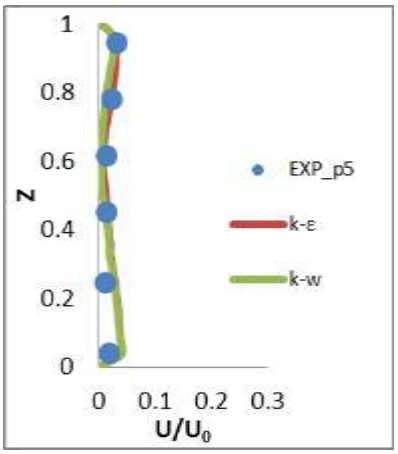

e

The overall average error for two models with experimental data:

K-ε and exp. Error (20.69 %)

k-ω and exp. Error (17.12 %)

Figure 4.16 Prediction of the air velocity with Realizable k-ε model and Enhancement Wall Treatment and SST k-ω, (*Z=height/total room height (H), U=velocity/supply velocity (U_0), H=2.43m, U_0=3.9m/s*)

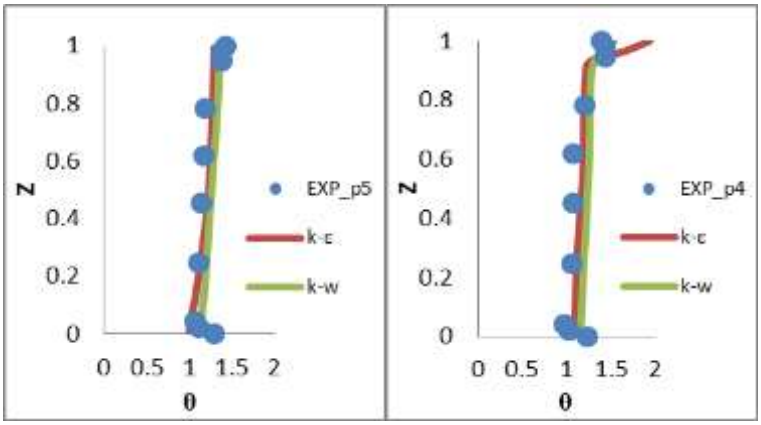

a

b

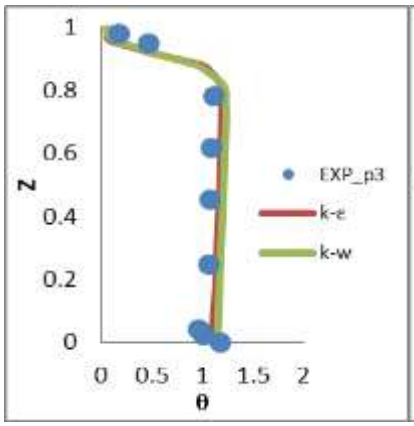

c

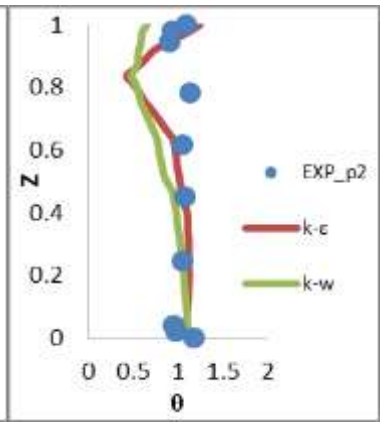

d

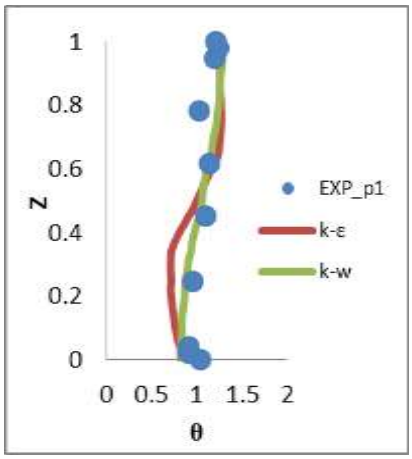

e

The overall average error for two models with experimental data:

K-ε and exp. Error (9.49 %)

k-ω and exp. Error (7.08 %)

Figure 4.17 Prediction of the air temperature with Realizable k-ε model and Enhancement Wall Treatment and SST k-ω, (*Z=height/total room height (H)*, $\theta=(T-T_{in}/T_{out}-T_{in})$, $H=2.43m$, $T_{in}=16.3^{o}C$, $T_{out}=21.4^{o}C$).

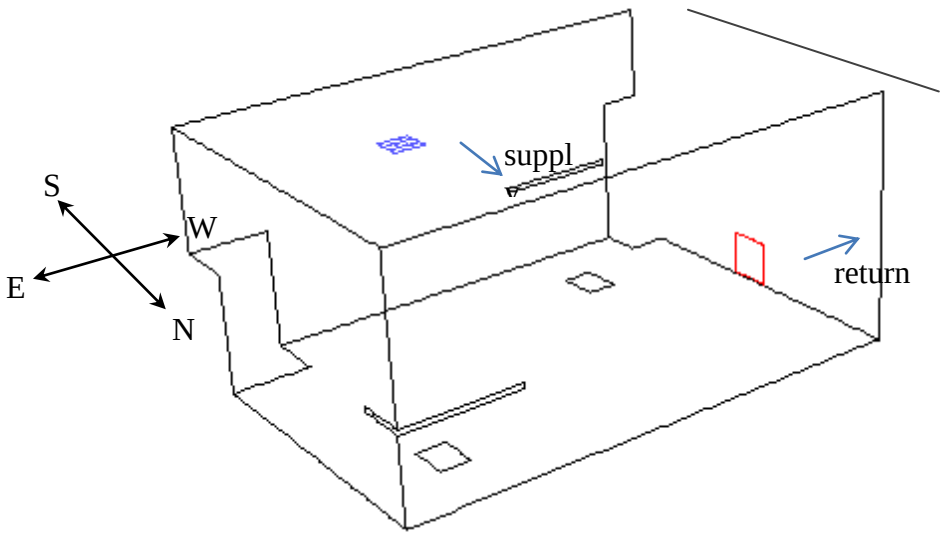

Figure 4.18 Configuration of ceiling slot ventilation test case

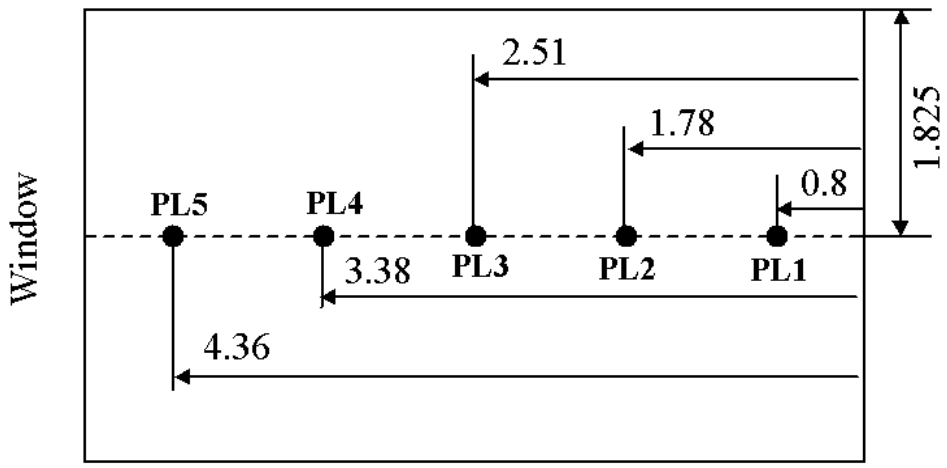

Figure 4.19 The positions of the measuring poles for the ceiling slot ventilation test case [10]

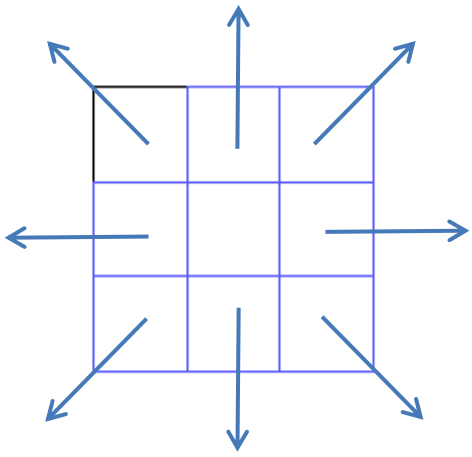

Figure 4.20 Modeling of the square diffuser

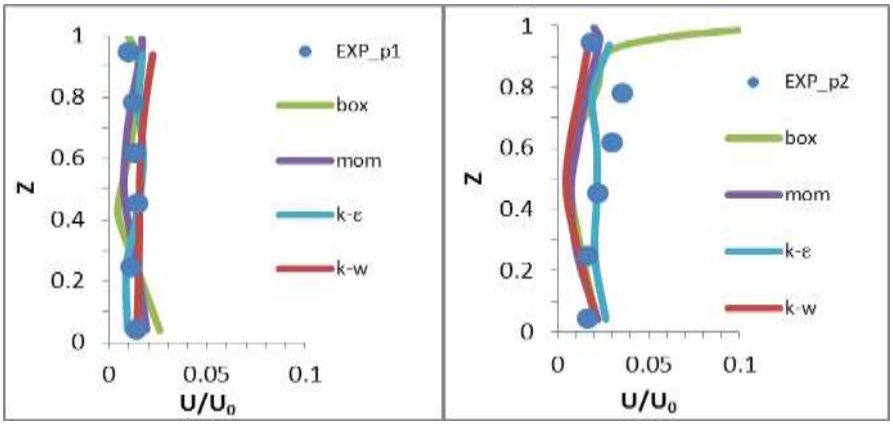

a b

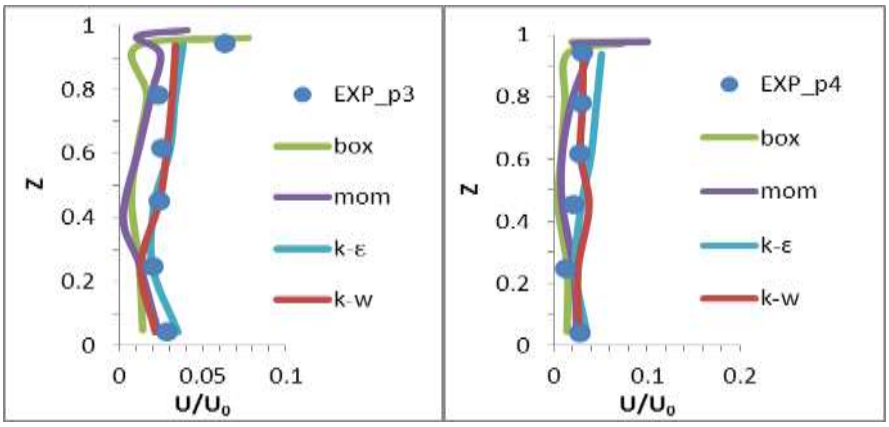

c e

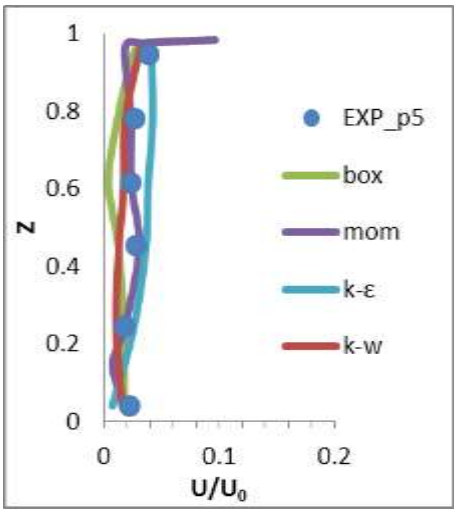

e

Figure 4.21 Prediction of the air velocity with Realizable k-ε and SST k-ω model compared with box and momentum, (*Z=height/total room height (H), U=velocity/supply velocity (U_0), H=2.43m, U_0=5.2m/s*).

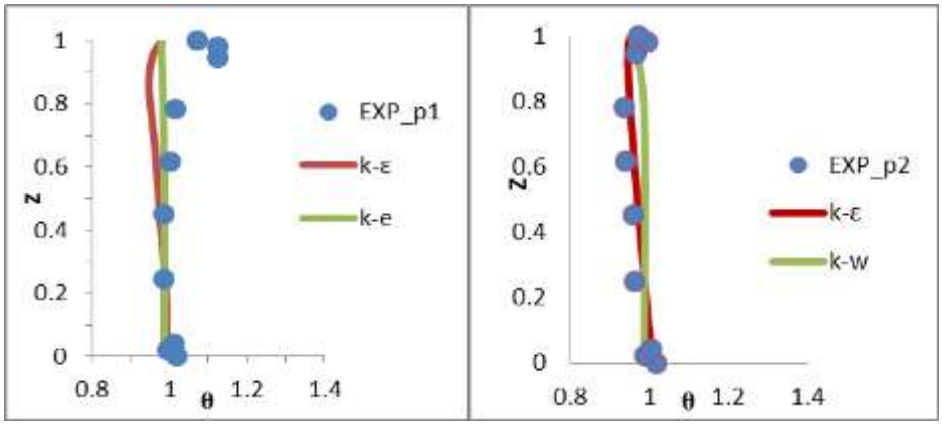

a b

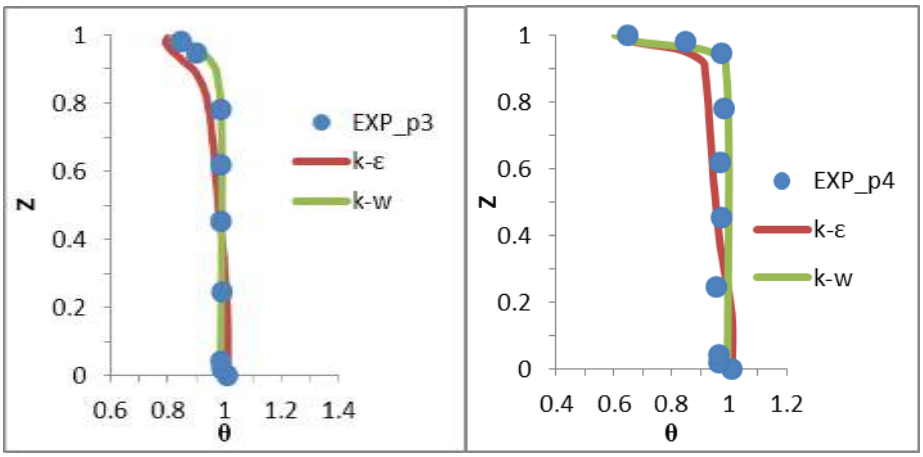

c d

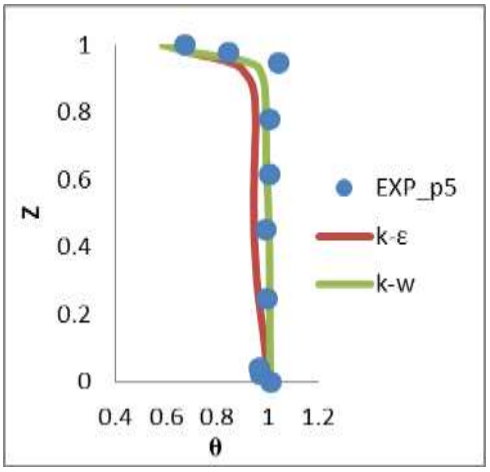

e

Figure 4.22 Prediction of the air temperature with Realizable k-ε and SST k-ω model compared with box and momentum, (*Z=height/total room height (H)*, $\theta=(T-T_{in}/T_{out}-T_{in})$, *H=2.43m*, $T_{in}=14.5^{\circ}C$, $T_{out}=24.1^{\circ}C$).

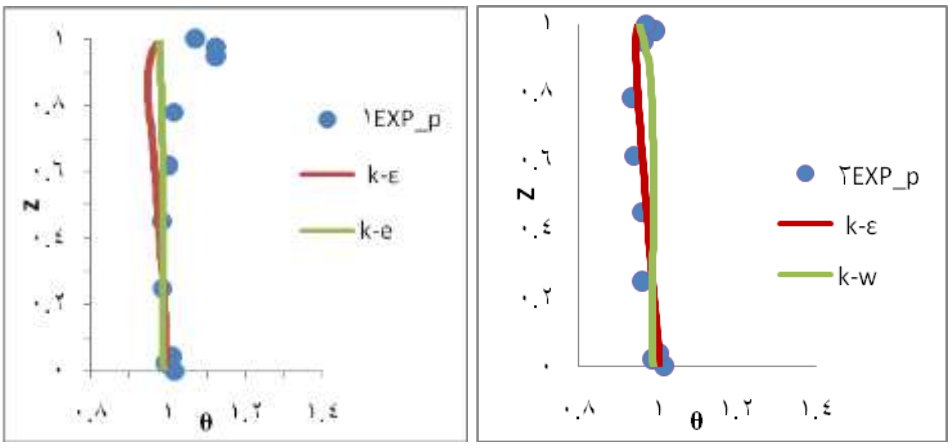

a b

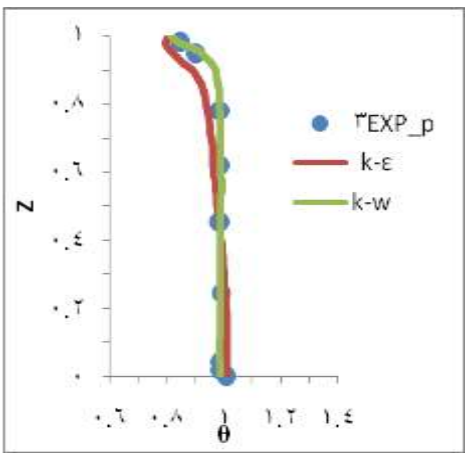

c

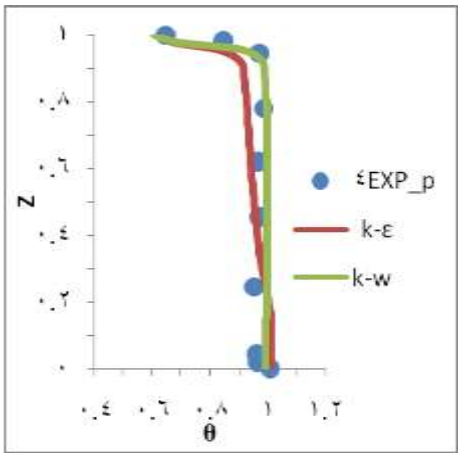

d

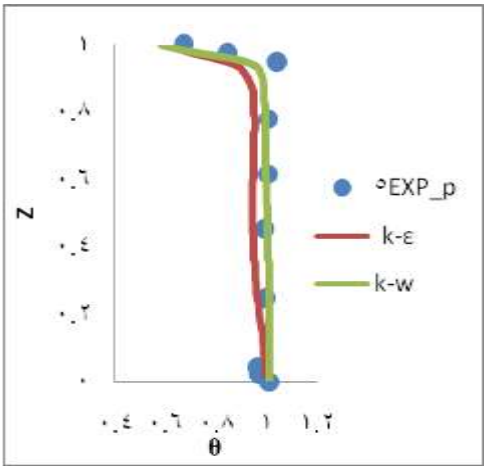

e

Fig. (4.23) Prediction of the air temperature with Realizable k-ε and SST k-ω model compared with box and momentum, (*Z=height/total room height (H)*, $\theta=(T-T_{in}/T_{out}-T_{in})$, *H=2.43m*, $T_{in}=14.5^{\circ}C$, $T_{out}=24.1^{\circ}C$).

CHAPTER 5

RESULTS AND DISCUSSION

5.1 Case Studies Suggestion

In chapter four, four types of diffusers (displacement, slot, grille, square), as shown in Figure 5.1, were simulated using k-ε and k-ω models. In this chapter, also same diffusers are suggestion but with different boundary conditions for suitable climate in Turkey building, this is done by referring to Turkey Code of cooling [42].

The Turkey Code of Cooling limited the outdoor and indoor conditions for Istanbul are listed in Table14 and Table 15 respectively.

Region	**DBT in summer (ºC)**	**RH % in summer**	**The daily range (ºC)**	**Altitude (m)**	**Latitude N**	**Longitude E**
Istanbul	37	16	18.7	34.1	33.32	44.33

Table 14 Outdoor data for Iraq

	DBT in summer (ºC)	**RH % in summer**	**Air velocity (m/s)**
Human comfort	19 - 24	40 - 60	1.8 – 2
Recommended conditions inside the office	23 - 26	40 - 50	0.13 – 0.23

Table 15 Indoor conditions

Four types of diffusers are set in three orientations all south-facing and all cases running as constant wall temperature, but not all walls of office are exposed to outside. For each type of diffuser three cases are chosen, the first case just eastern

and southern walls, the second case is only the southern wall and the third case is the southern and western wall, and the ceiling in all cases is included.

The measurements for the displacement, grille diffuser had poles positioned in the shown middle cross section Figure 5.2 (a). On the other hand, the poles for the slot diffuser measurements were positioned in a plane closer to the diffuser as shown in Figure 5.2 (b).

5.2 Boundary Conditions

Some boundary conditions at the return and the internal heat sources of small office spaces for all cases as follows:

- *Outlet:*

The outlet is specified as pressure outlet, i.e., the gauge pressure at the outlet is specified as zero.

- *Thermal conditions:*

Temperature or heat flux at the walls is used to specify the thermal conditions for different objects in the flow field:

The thermal conditions of the following objects are specified as heat flux:

1. Computer 1: 171.43 W/m^2.
2. Computer 2: 274.6 W/m^2.
3. Human: 41.9 W/m^2.
4. Lamps: 37.78 W/m^2.

5.2.1 Modeling and simulation

5.2.1.1 Turbulence modeling

Applying that the Realizable k-ε models and the SST k-ω model can give reasonable prediction for ventilation flows coupled with heat transfer, these models are further evaluated in test cases.

5.2.1.2 Computation meshes

Because there are many flow obstacles in the flow field, using a structured mesh will result in lots of unnecessary mesh cells in the regions far from the walls, so an unstructured mesh is used instead. Depending on many testing meshes, it is founded that the size of cells is acceptable for all types listed in Table 16.

Sq.	Diffuser type	Cells number	Sq.	Diffuser type	Cells number
1	Displacement	1,480,232	3	Slot	1,071,118
2	Grille	499,952	4	Square	1,751,500

Table 16 Size of cells

5.2.1.3 Numerical schemes

The convection terms are discretized using the second-order upwind scheme. For the discretization of pressure, the PRESTO! (PREssure STaggering Option) scheme is used. The SIMPLEC scheme is used for the pressure-velocity coupling. When working with unstructured meshes, a high-order scheme is preferred for the discretization of convection terms to minimize the discretization errors.

5.3 Displacement Diffuser

5.3.1 Boundary conditions

- *Inlet diffuser:*

The airflow is discharged horizontally from the front surface, as shown in Figure 5.3. The supply air velocity is (0.35 m/s), the airflow rate is (0.0768 kg/s), and the temperature is (15.0^{o}C), and a turbulence intensity of 4% is specified. The turbulence quantities (k, ε or ω) at the inlet are calculated using equations (4.1) and (4.3).

5.3.2 Summary of boundary conditions

Table 17 shown below summarizes the boundary conditions for three cases at inlet and outlet and wall temperature to displacement diffuser.

Cases	Orientation	Air supply ACH (kg/s)	Air velocity (m/s)	Gross area (m^2)	Air temp. supply (ºC)	Air temp. return (ºC)
Case 1	Eastern, southern walls and ceiling	5.0 (0.0768)	0.11	1.1 × 0.53	15	24
Case 2	Southern and ceiling					
Case 3	Southern, western wall and ceiling					

Table 17 summarize boundary conditions

5.3.3 Simulation results

The air velocity and dimensionless temperature profiles using different models for this cases can be shown in Figures. 5.4 to 5.9.

The difference in the values of speed appeared in the area near the floor level at (p1), and possibly that is due to the treatment of the flow near the walls, which is expressed in the boundary layer knowing that the two models following the same method of treatment which enhanced wall treatments. For the rest of the values, there is a good agreement between them.

The predicted temperatures have some discrepancies with the measured data near floor, which highlight the difference in the temperature curves. After preview, Figures. 5.10 to 5.15 show a logical explanation for this difference, Figures. 5.8, 5.10 and 5.12 as a result of using the analysis by k-ε model and Figures. 5.9, 5.11 and 5.13 as a result of using the analysis by k-ω model has appeared difference in thermal gradient inside the room.

These results possibly agree with the analysis by k-ω model as reviewed in the chapter one (PP.10), where air supply type was classified as type D.

Figure (5.16) shows the results of the effect draft temperature (EDF) inside the occupied zone within the recommended ranges in the Iraqi Code of cooling [42], it is (-1.7 to 0), and different behavior observed in the curves due to the form described in contours, Figures. 5.10 to 5.15, and possible adoption of the data as evidence of the environment in the occupied zone.

5.4 Grille Diffuser

5.4.1 Boundary conditions

- *Inlet diffuser:*

The airflow is discharged horizontally from the front surface. The supply air velocity is (2.7 m/s), the airflow rate is (0.0768 kg/s), and the temperature is (15.0^{o}C), and a turbulence intensity of 4% is specified [13]. The turbulence quantities (k, ε or ω) at the inlet are calculated using equations (4.1) and (4.2).

5.4.2 Summary of boundary conditions

Table 18 shown below summarizes the boundary conditions for three cases at inlet and outlet and wall temperature to displacement diffuser.

Cases	Orientation	Air supply ACH (kg/s)	Air velocity (m/s)	Gross area (m^2)	Air temp. supply (ºC)	Air temp. return (ºC)
Case 1	Eastern, southern walls and ceiling	5.0 (0.0768)	1.25	0.28 × 0.18	15	24
Case 2	Southern and ceiling					
Case 3	Southern, western wall and ceiling					

Table 18 Boundary conditions:

5.4.3 Simulation results

Figures 5.19 to 5.24 show comparisons between predicted air velocity and temperature profiles using Realizable k-ε and SST k-ω models, respectively.

Figures 5.19 to 5.24 show good agreement results of which is good in terms a prediction of air velocity and temperature distribution, the consensus severe illustrated images are extracted from a program from Figures. 5.25 to 5.30.

Figure 5.31 shows the results of the effect draft temperature (EDF) inside the occupied zone within the recommended ranges in the Iraqi Code of cooling [42], it is (-1.7 to 0).

5.5 Slot diffuser

5.5.1 Boundary conditions

- *Inlet diffuser:*

The airflow is discharged horizontally from the front surface. The supply air velocity is (3.9 m/s), the airflow rate is (0.1410kg/s), and the temperature is (15.0^{o}C), and a turbulence intensity of 5% is specified [13]. The turbulence quantities (k, ε or ω) at the inlet are calculated using equations (4.1) and (4.2).

5.5.2 Summary of boundary conditions

Table 19 show below summarizes the boundary conditions for three cases at inlet and outlet and wall temperature to displacement diffuser.

Table 19 summarize boundary conditions:

Cases	Orientation	Air supply ACH (kg/s)	Air velocity (m/s)	Gross area (m^2)	Air temp. supply (ºC)	Air temp. return (ºC)
Case 1	Eastern, southern walls and ceiling	9.2 (0.1410)	1	1.15 × 0.1	15	24
Case 2	Southern and ceiling					
Case 3	Southern, western wall and ceiling					

Table 19 Summarize boundary conditions:

5.5.3 Simulation results

Figures 5.34 to 5.39 shown comparisons between predicted air velocity and temperature profiles using Realizable k-ε and SST k-ω models, respectively.

Figures 5.34 to 5.39 are shown applicable to results of air velocity and temperature distribution, the consensus severe illustrated images are extracted from a program from Figures. 5.40 to 5.45.

Figure 5.46 shows the results of the effect draft temperature (EDF) inside the occupied zone within the recommended ranges in the Turkey Code of cooling [35], it is (-1.7 to 0).

5.6 Square diffuser

5.6.1 Boundary conditions

- *Inlet diffuser:*

The airflow is discharged horizontally from the front surface. The supply air velocity is (5.2 m/s), the airflow rate is (0.0750 kg/s), and the temperature is (15.0^{o}C), and a turbulence intensity of 5% is specified [13]. The turbulence quantities (k, ε or ω) at the inlet are calculated using equations (4.1) and (4.2).

5.6.2 Summary of boundary conditions

Table 20 shown below summarizes the boundary conditions for three cases at inlet and outlet and wall temperature to displacement diffuser.

Cases	Orientation	Air supply ACH (kg/s)	Air velocity (m/s)	Gross area (m^2)	Air temp. supply (ºC)	Air temp. return (ºC)
Case 1	Eastern, southern walls and ceiling	4.9 (0.0750)	5.2	0.3 × 0.3	15	24
Case 2	Southern and ceiling					
Case 3	Southern, western wall and ceiling					

Table 20 Summarize boundary conditions:

5.6.3 Simulation results

Figures**.** 5.50 to 5.55 show comparisons between predicted air velocity and temperature profiles using Realizable k-ε and SST k-ω models, respectively.

Figures. 5.50 to 5.55 indicate give good results for prediction of air velocity and temperature distribution, illustrated images are extracted from a program from Figures. 5.56 to 5.61.

Figure 5.53 depicts the results of the effect draft temperature (EDF) inside the occupied zone within the recommended ranges in the Iraqi Code of cooling [42], it is (-1.7 to 0).

These four types of diffusers (displacement, slot, grille, square), as shown in Fig.(5.1), were simulated using k-ε and k-ω models. In this chapter, also same diffusers are suggestion but with different boundary conditions for suitable climate in Turkey building, this is done by referring to Turkey Code of cooling .

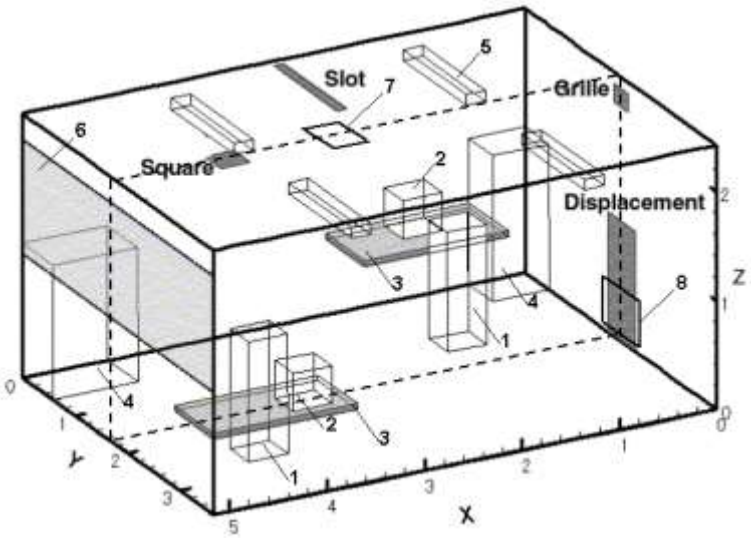

Figure 5.1 Element of test room and positions of the supply diffusers (1- person, 2- computer, 3- table, 4- cabinet, 5- fluorescent lamp, 6- window, 7- exhaust for the displacement diffuser, 8- exhaust for the mixing diffusers), [13].

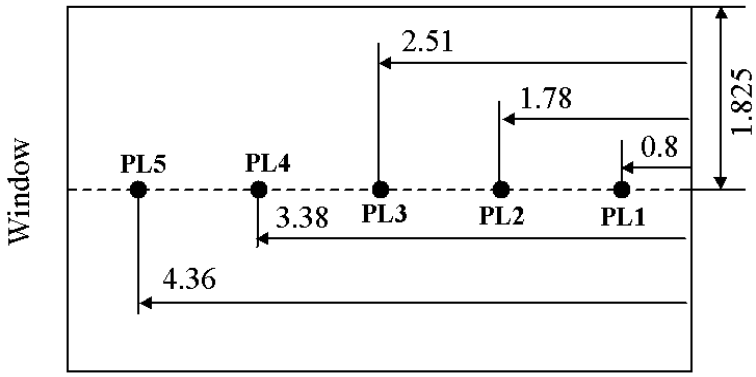

a

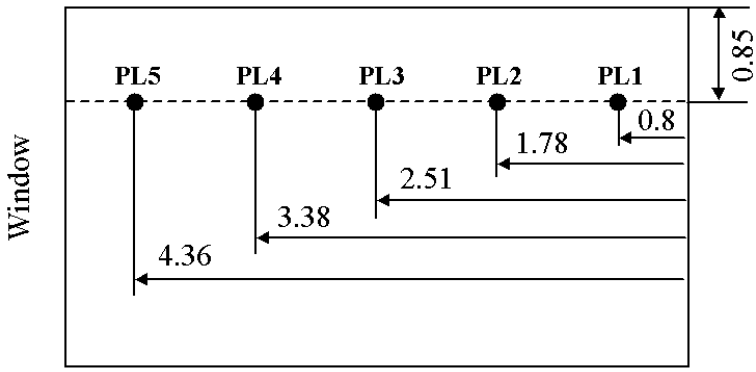

b

Figure 5.2 The positions of the measuring poles, a- The displacement ventilation test case,

b-The ceiling slot ventilation test case, [13].

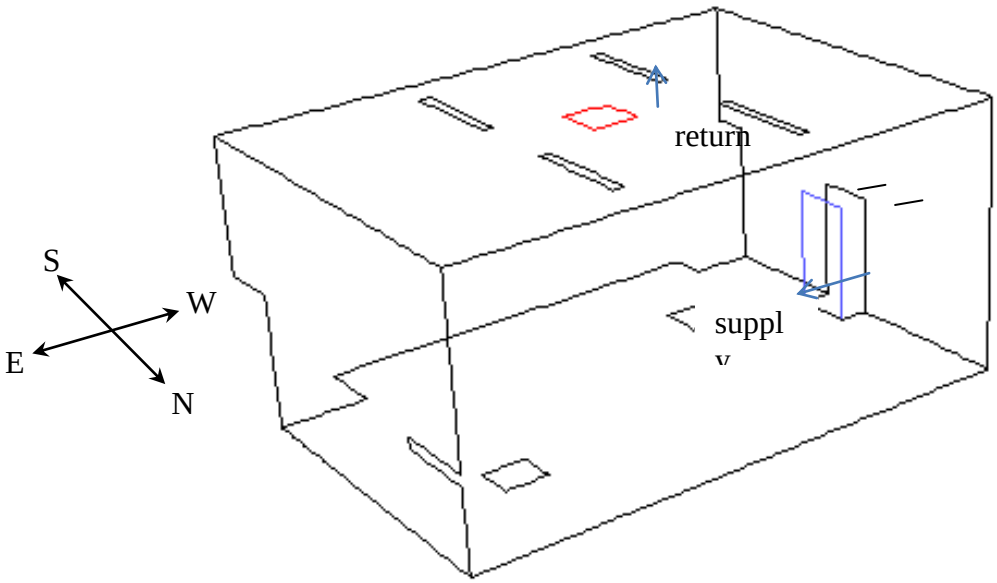

Figure 5.3 Configuration of the displacement ventilation test case.

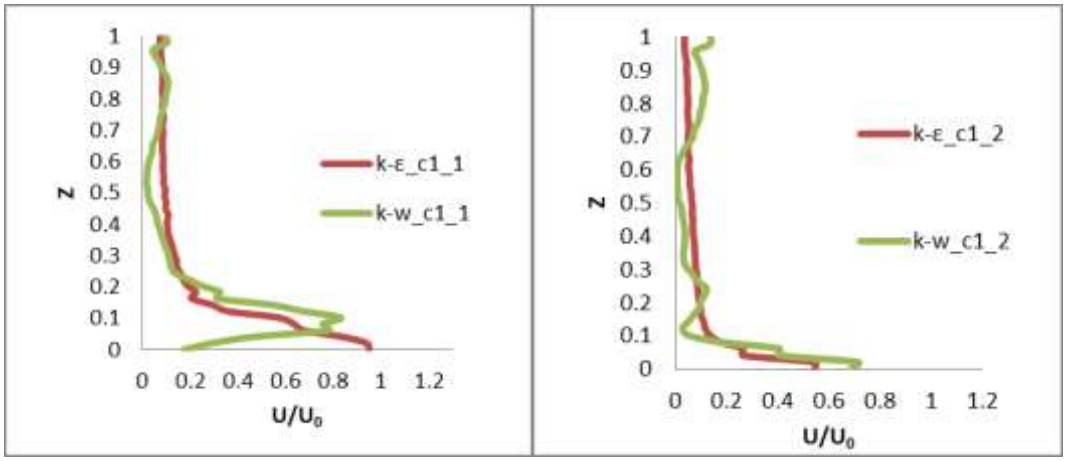

a b

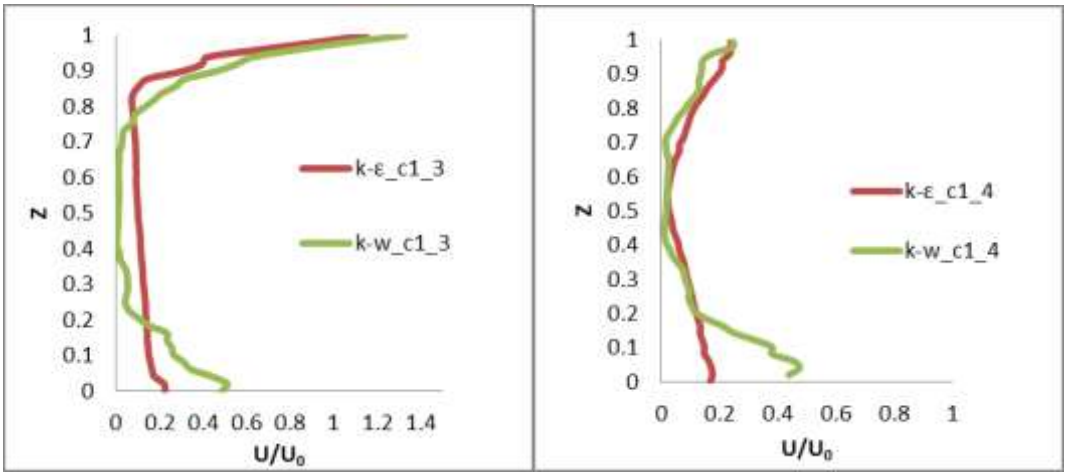

c d

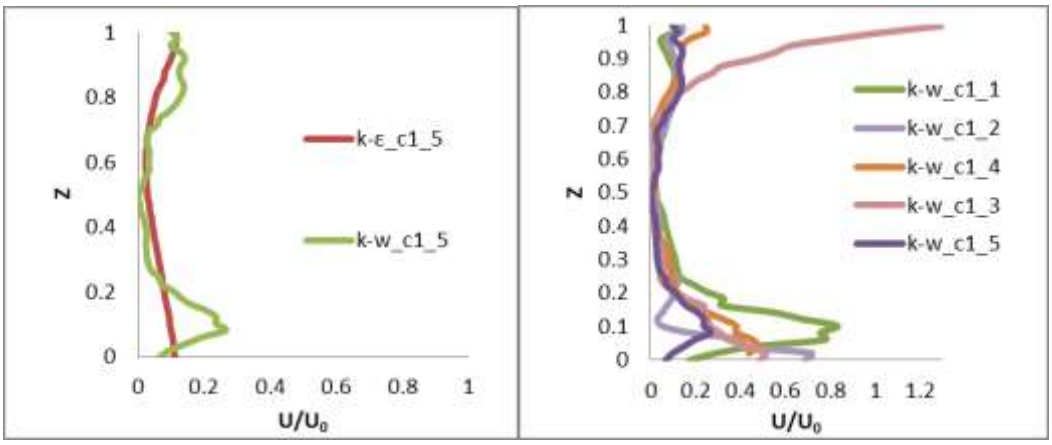

e f

Figure 5.4 Displacement diffuser (case 1) prediction of the air velocity by Realizable k-ε model with Enhancement Wall Treatment and SST k-ω, (*Z=height/total room height (H), U=velocity/supply velocity (U_0), H=2.43m, U_0=0.35m/s*).

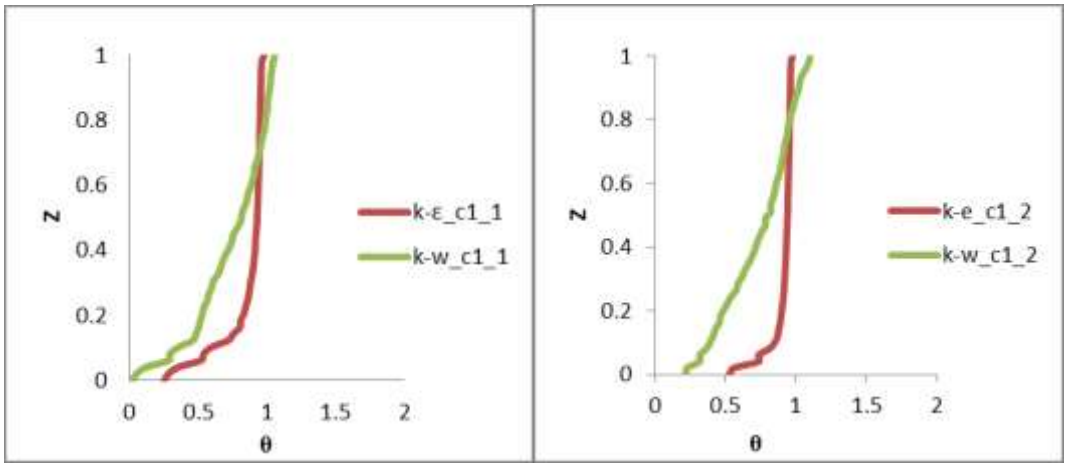

a b

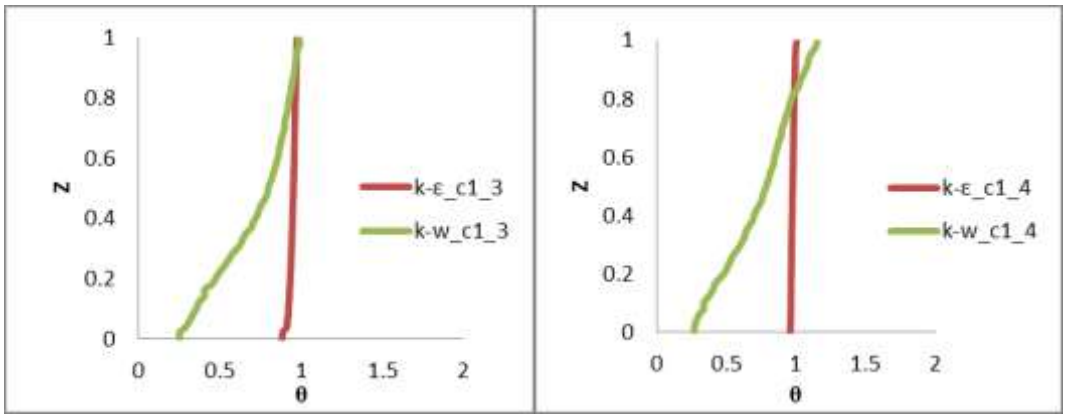

c d

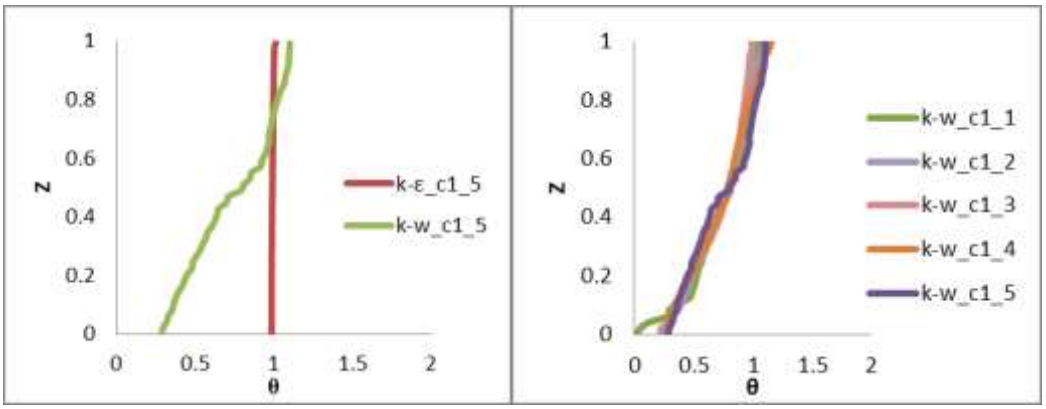

e f

Figure 5.5 Displacement diffuser (case 1) prediction of the air temperature by Realizable k-ε model with Enhancement Wall Treatment and SST k-ω, (Z=height/total room height (H), $\theta=(T-T_{in}/T_{out}-T_{in})$, H=2.43m, T_{in}=15.0ºC, T_{out}=24ºC).

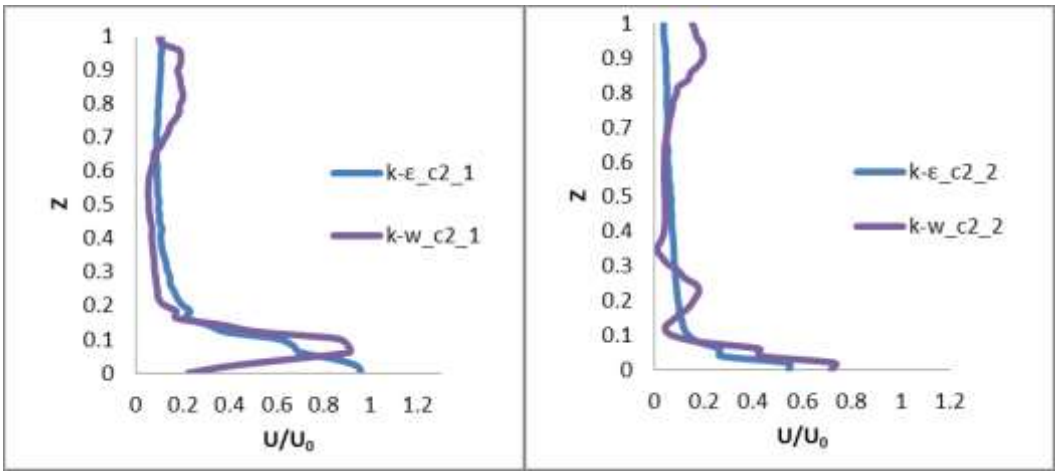

a b

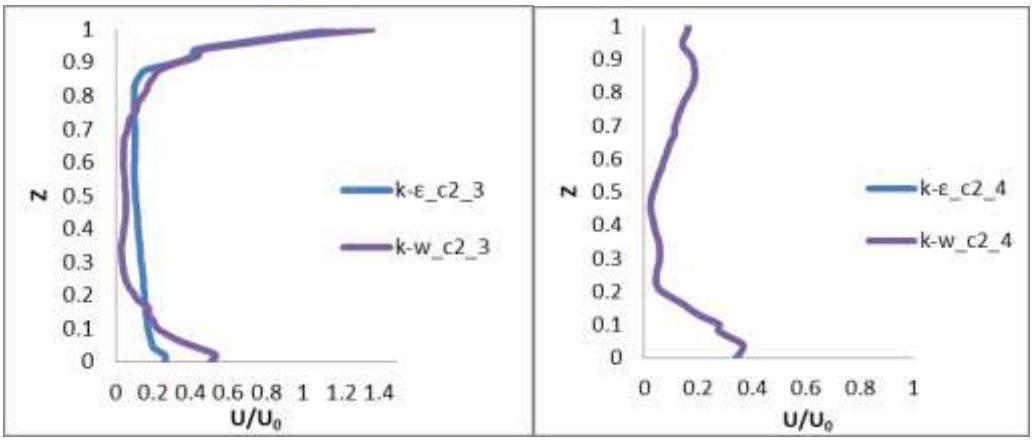

c d

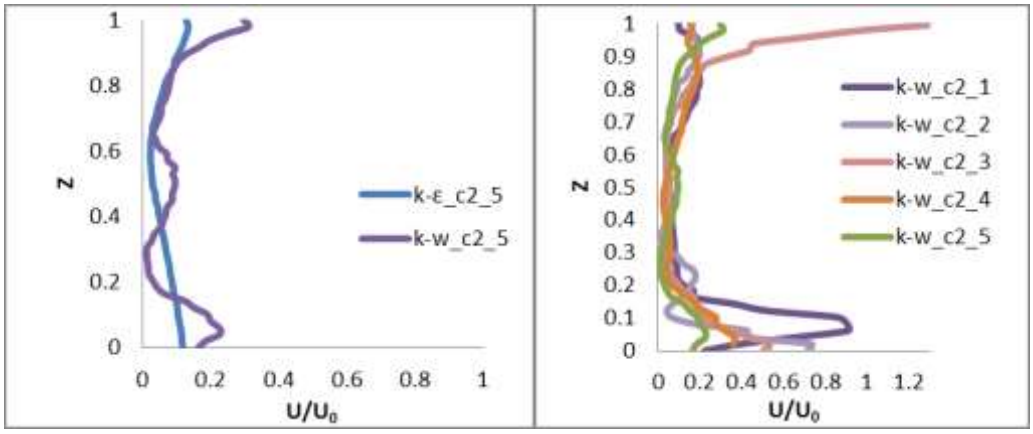

e f

Figure 5.6 Displacement diffuser (case 2) prediction of the air velocity by Realizable k-ε model with Enhancement Wall Treatment and SST k-ω, (*Z=height/total room height (H), U=velocity/supply velocity (U_0), H=2.43m, U_0=0.35m/s*).

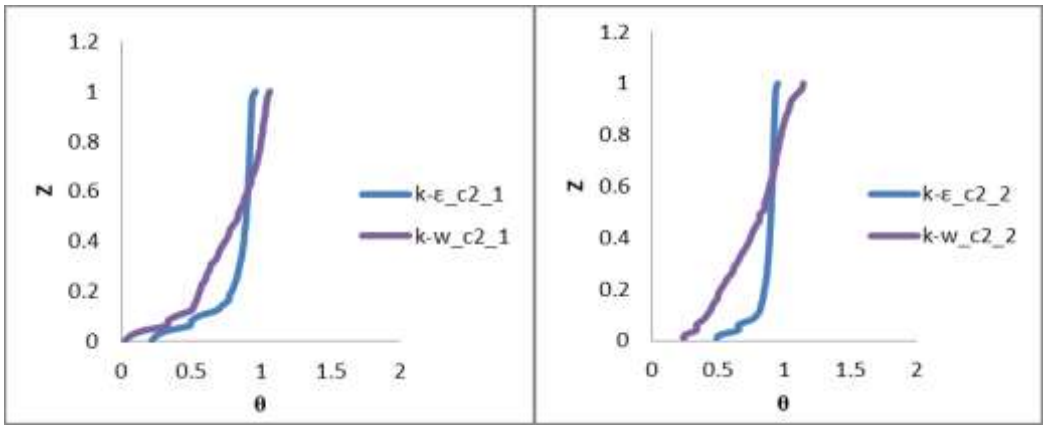

a b

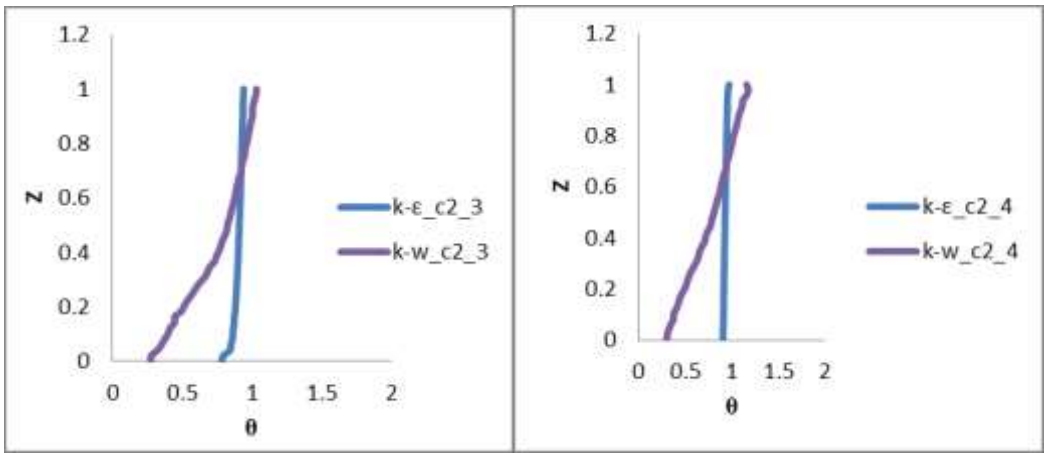

c d

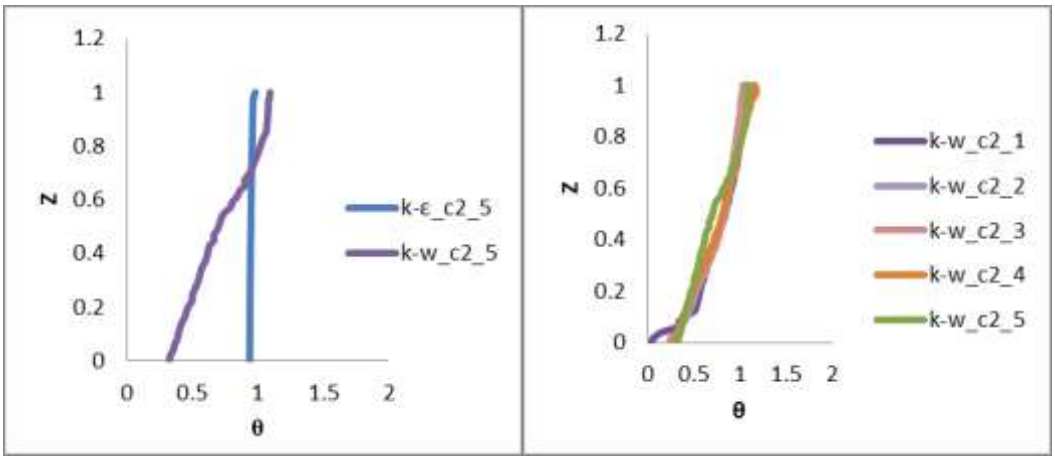

e f

Figure 5.7 Displacement diffuser (case 2) prediction of the air temperature by Realizable k-ε model with Enhancement Wall Treatment and SST k-ω, (Z=height/total room height (H), $\theta=(T-T_{in}/T_{out}-T_{in})$, H=2.43m, T_{in}=15.0ºC, T_{out}=24ºC).

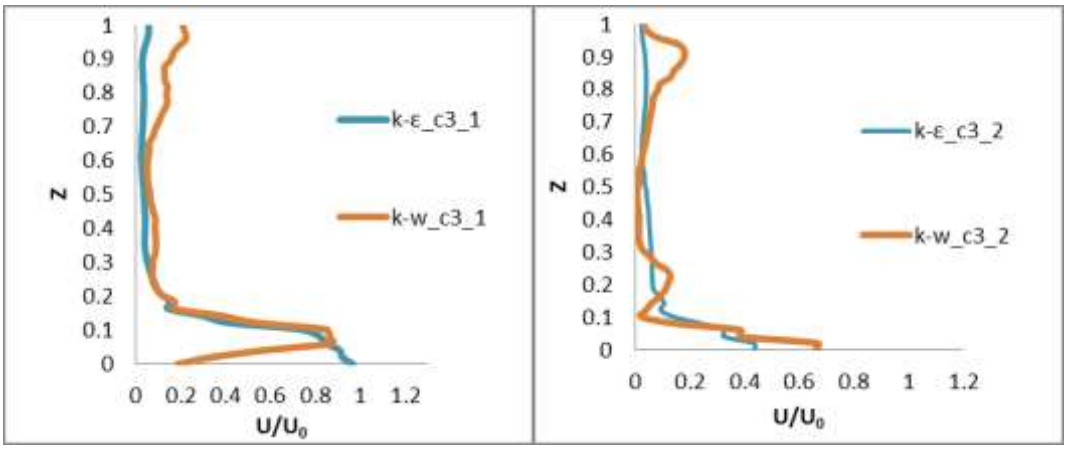

a b

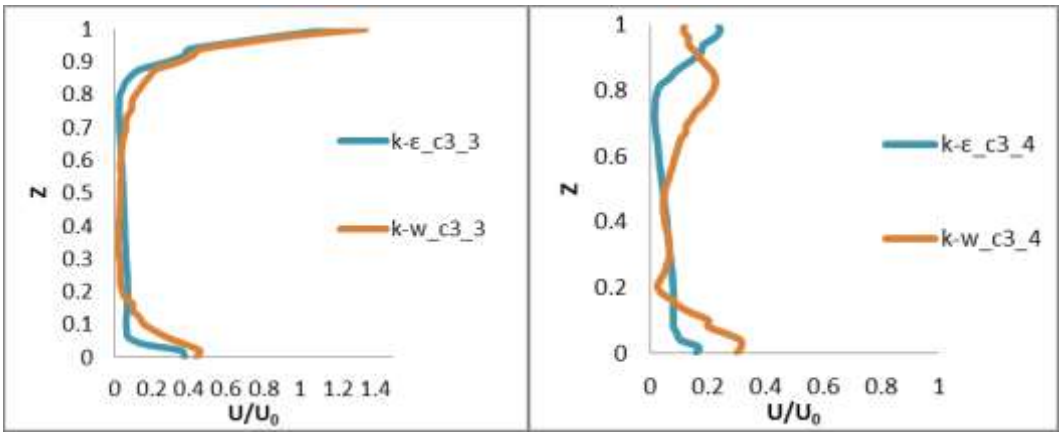

c d

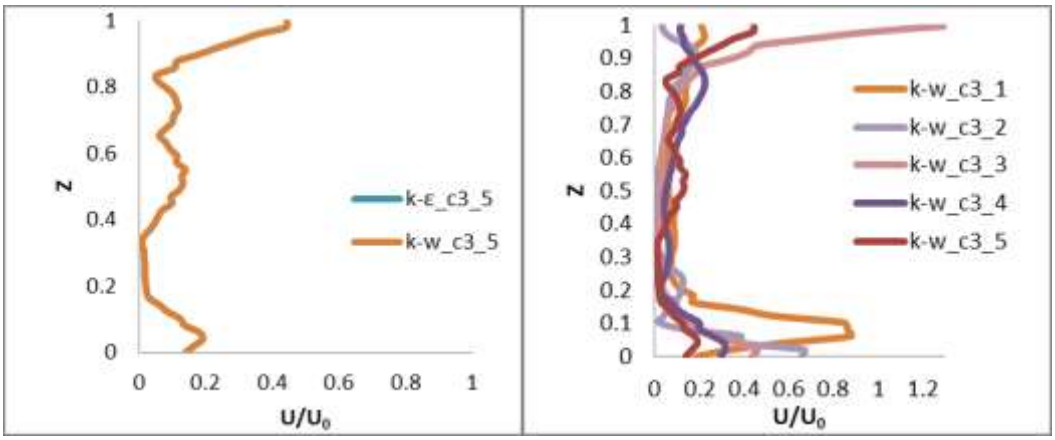

e f

Figure 5.8 Displacement diffuser (case 3) prediction of the air velocity by Realizable k-ε model with Enhancement Wall Treatment and SST k-ω, (*Z=height/total room height (H), U=velocity/supply velocity (U_0), H=2.43m, U_0=0.35m/s*).

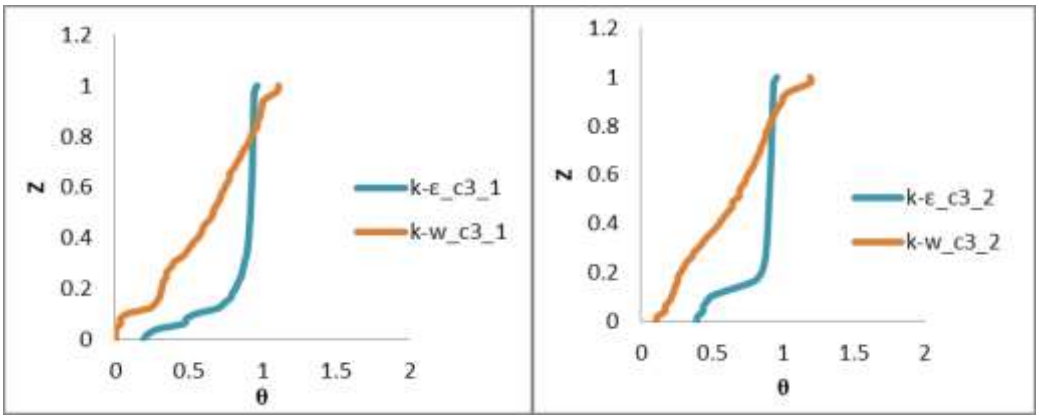

a b

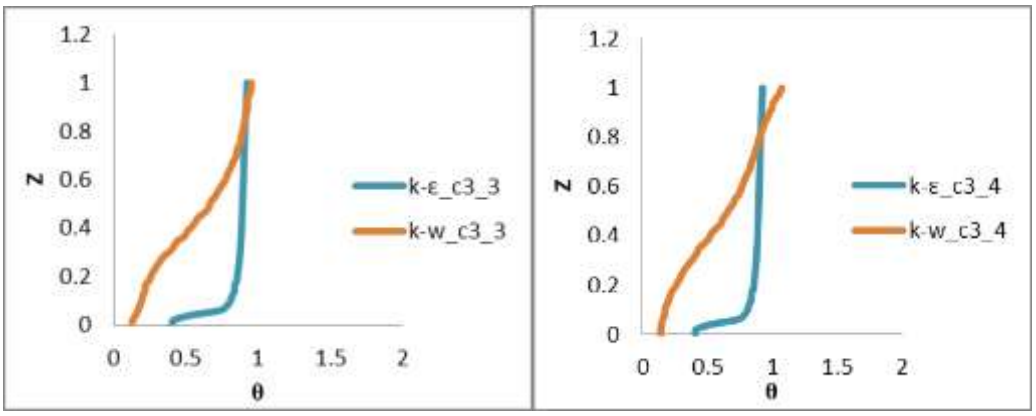

c d

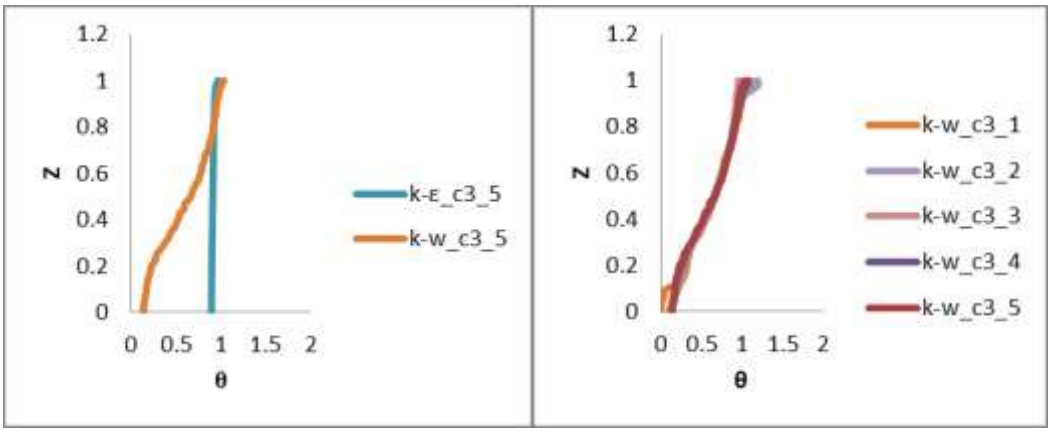

e f

Figure 5.9 Displacement diffuser (case 3) prediction of the air temperature by Realizable k-ε model with Enhancement Wall Treatment and SST k-ω, (Z=height/total room height (H), $\theta=(T-T_{in}/T_{out}-T_{in})$, H=2.43m, T_{in}=15.0ºC, T_{out}=24ºC).

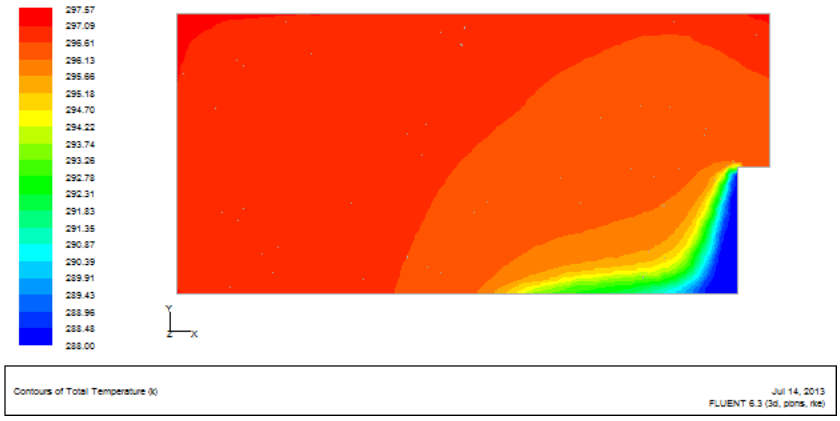

a

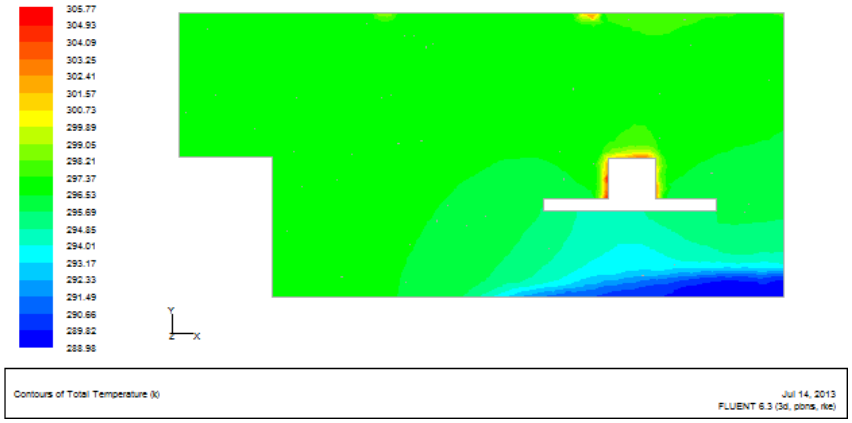

b

Figure 5.10 Distribution of calculation air temperature contours with k-ε, (case 1), (a) plane at z=1.825m, (b) plane at z=0.4m.

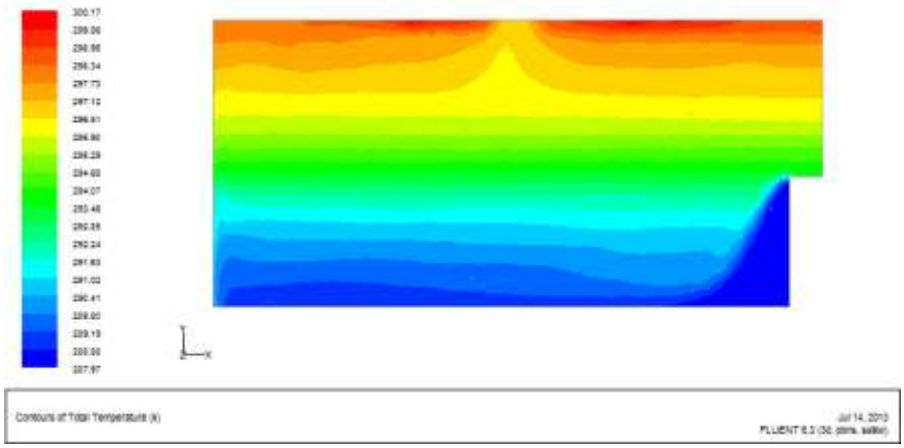

a

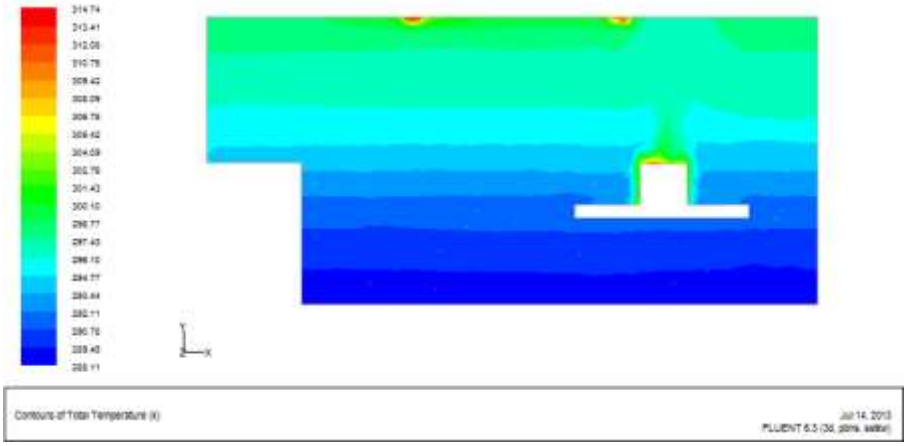

b

Figure 5.11 Distribution of calculation air temperature contours with k-ω, (case1), (a) plane at z=1.825m, (b) plane at z=0.4m.

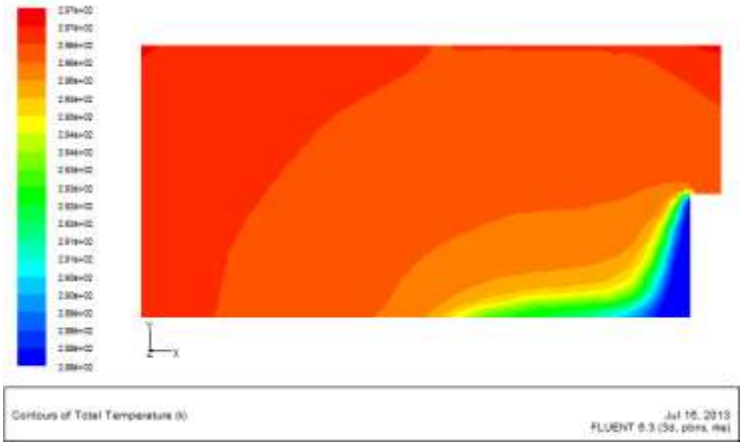

a

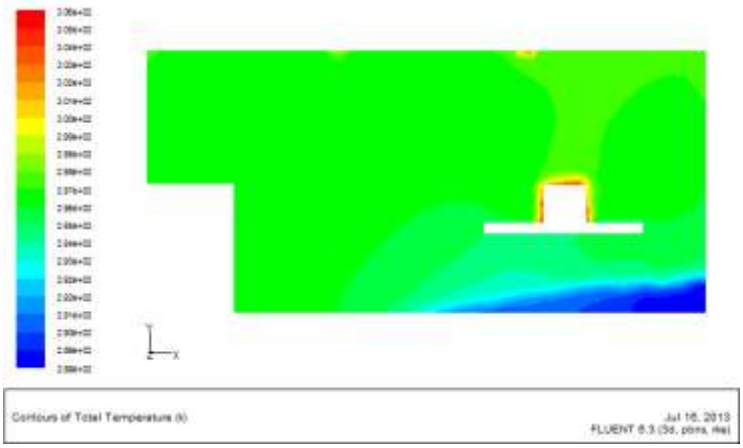

b

Figure 5.12 Distribution of calculation air temperature contours with k-ε, (case 2), (a) plane at z=1.825m, (b) plane at z=0.4m.

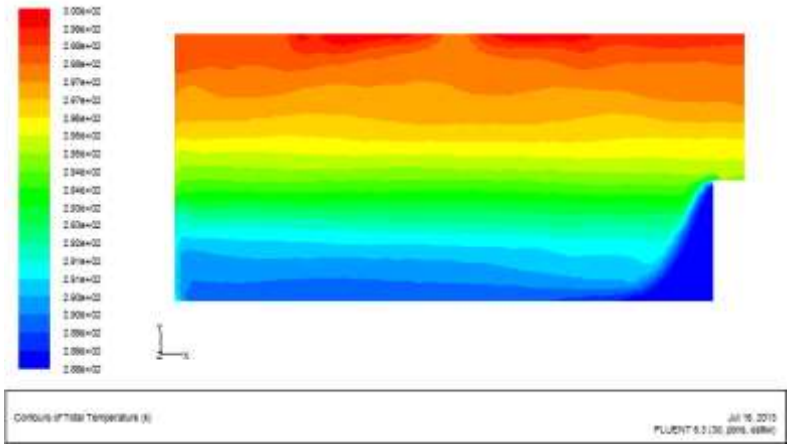

a

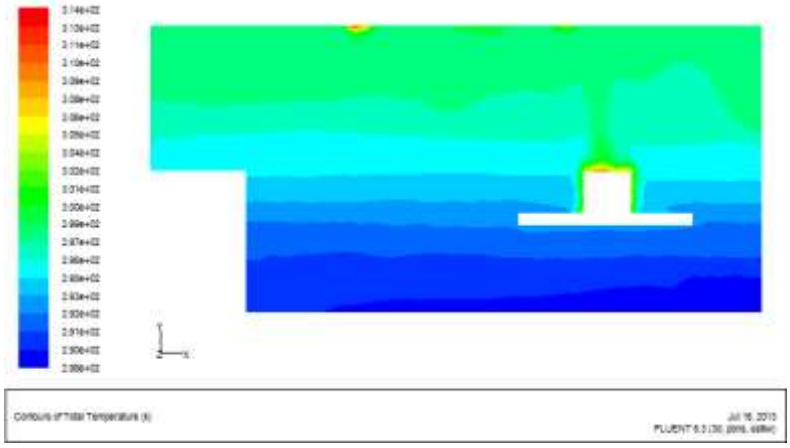

b

Figure 5.13 Distribution of calculation air temperature contours with k-ω, (case2), (a) plane at z=1.825m, (b) plane at z=0.4m.

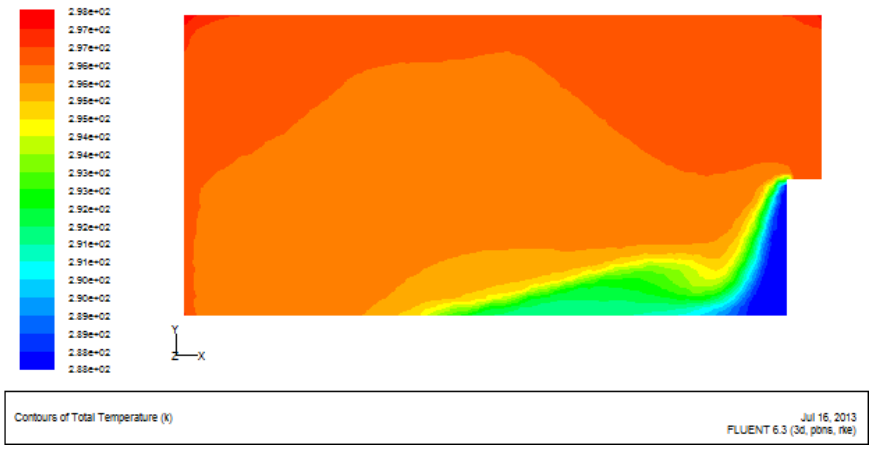

a

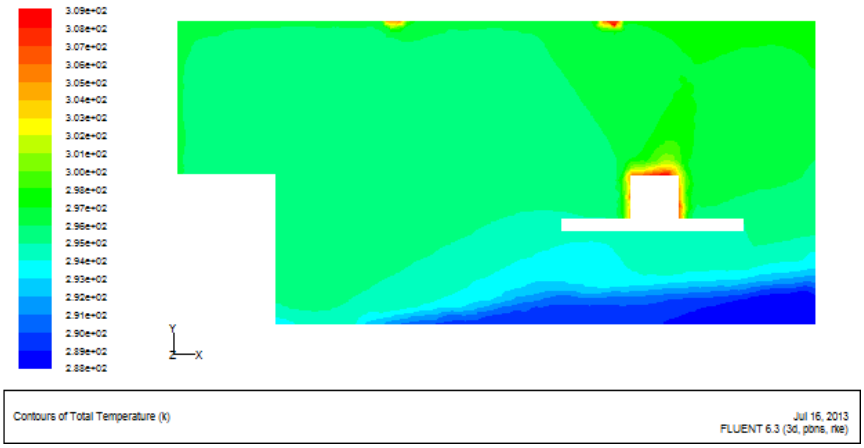

b

Figure 5.14 Distribution of calculation air temperature contours with k-ε, (case 3), (a) plane at z=1.825m, (b) plane at z=0.4m.

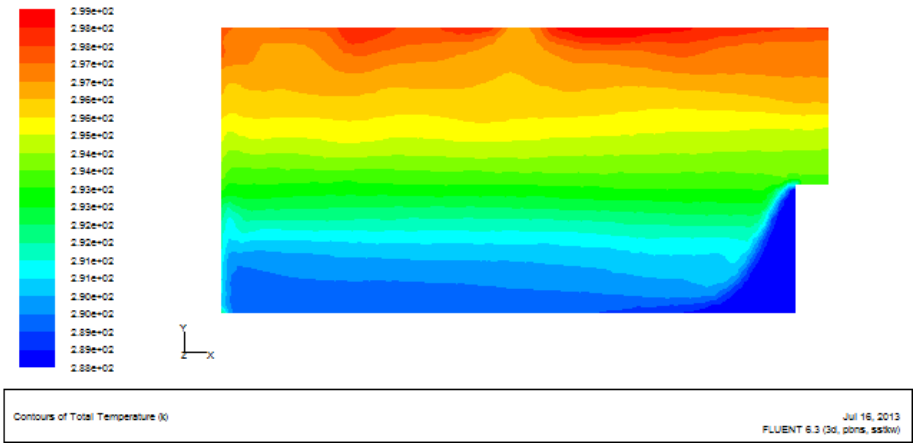

a

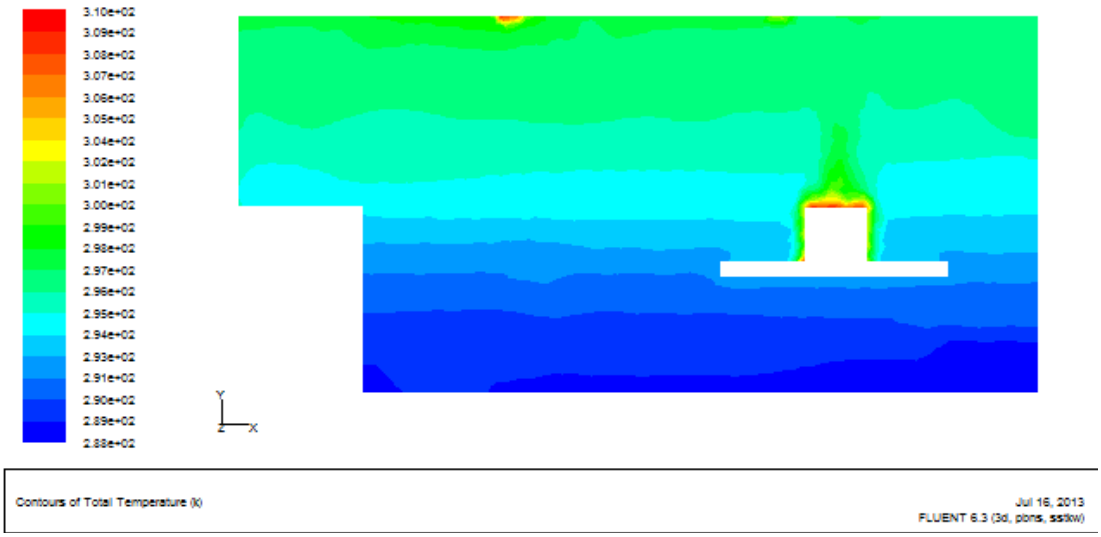

b

Figure 5.15 Distribution of calculation air temperature contours with k-ω, (case3), (a) plane at z=1.825m, (b) plane at z=0.4m.

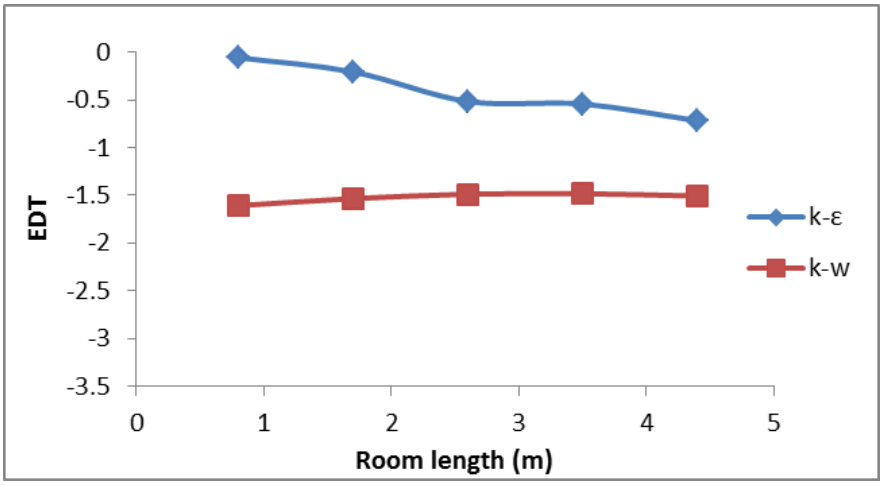

a

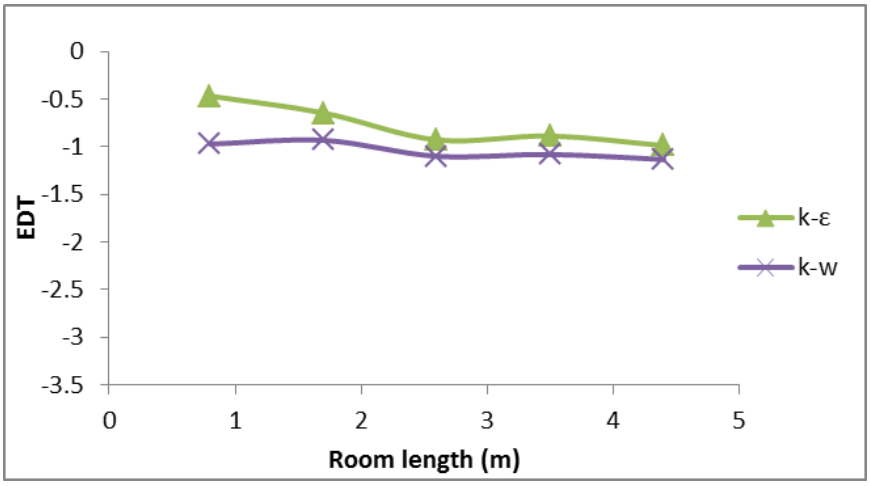

b

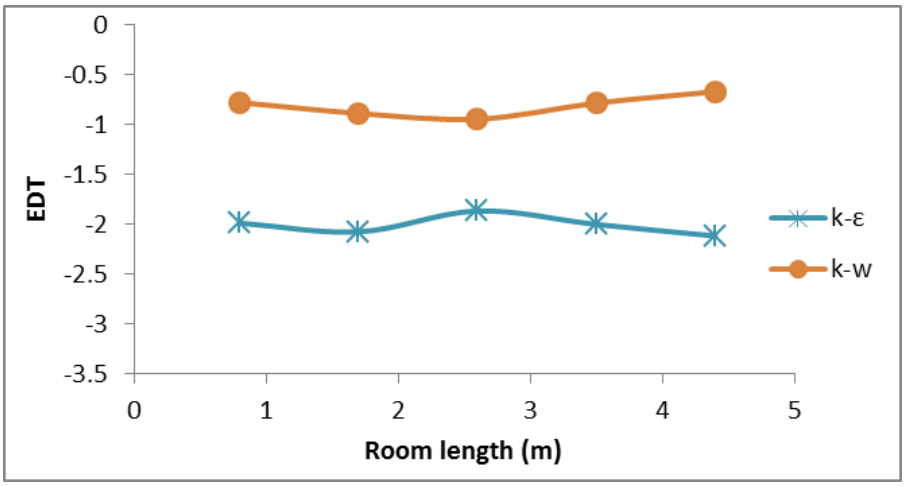

c

Figure 5.16 Effect draft temperature for k-ε and k-ω models, (a) case1, (b) case 2, (c) case 3.

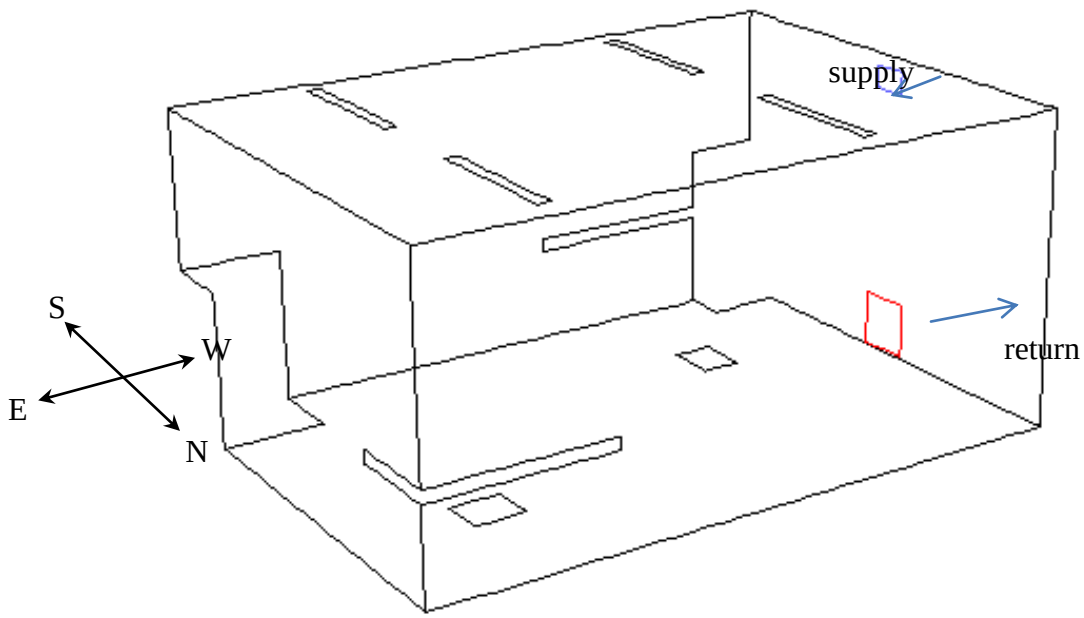

Figure 5.17 Configuration of grille ventilation test case.

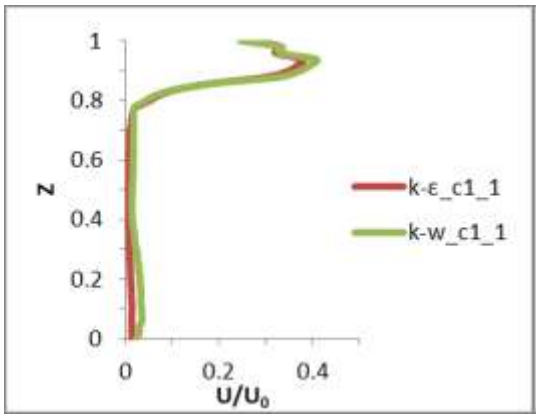

a

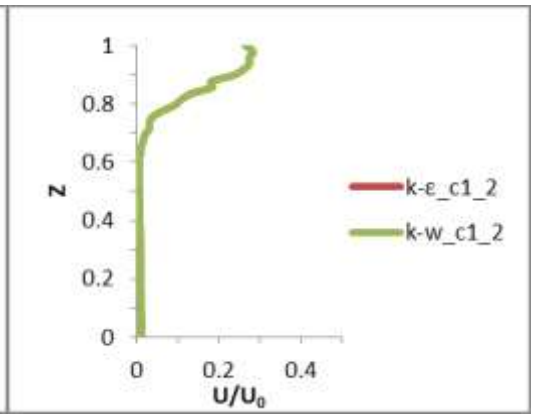

b

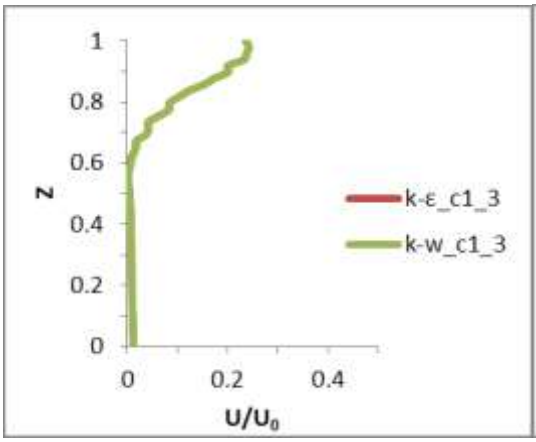

c

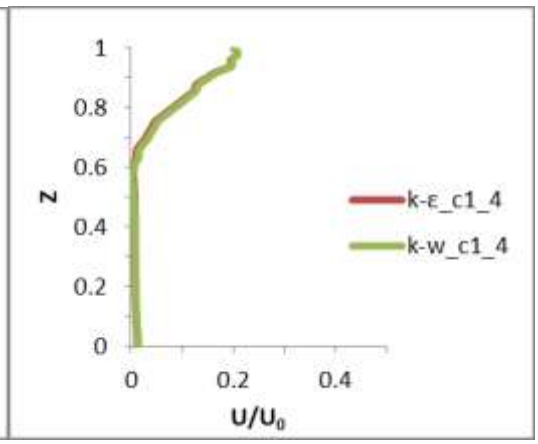

d

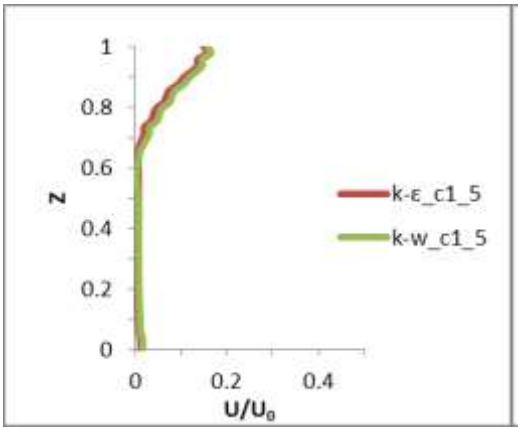

e

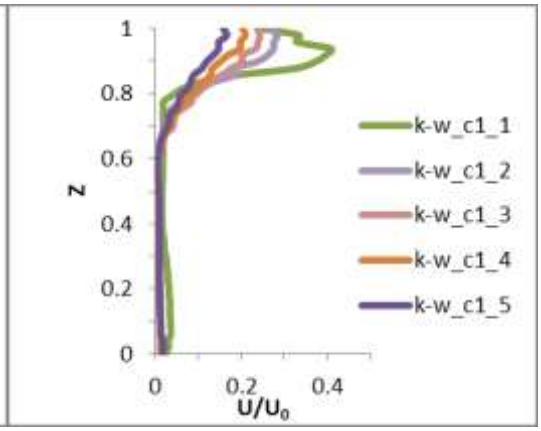

f

Figure 5.18 Grille diffuser (case 1) prediction of the air velocity by Realizable k-ε model with Enhancement Wall Treatment and SST k-ω, (*Z=height/total room height (H), U=velocity/supply velocity (U_0), H=2.43m, U_0=2.7m/s*).

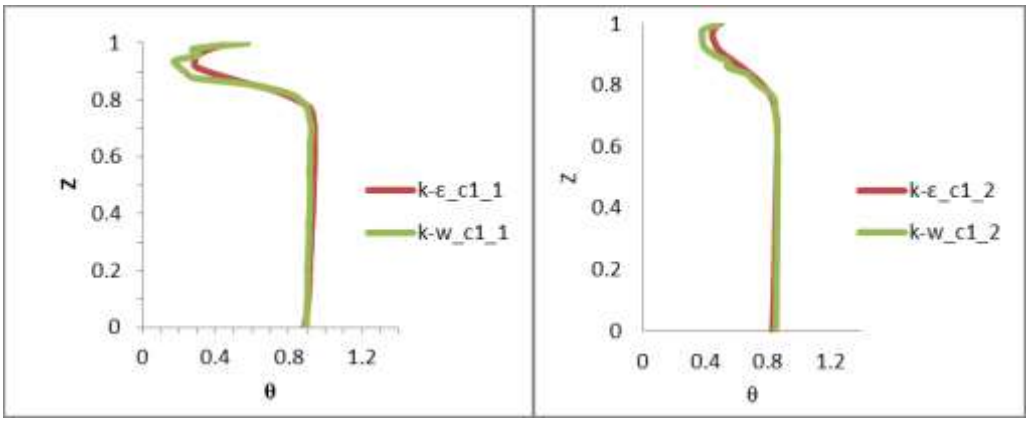

a

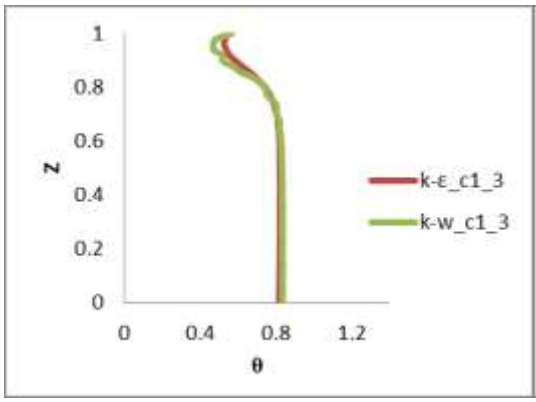

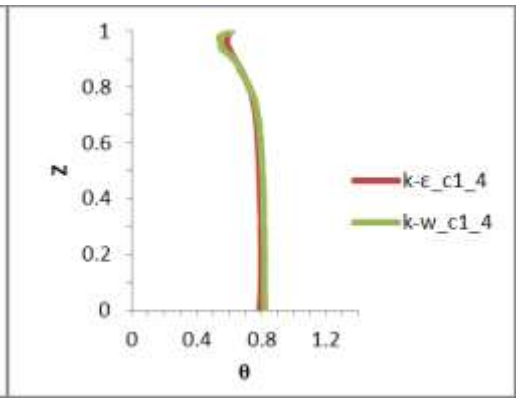

c d

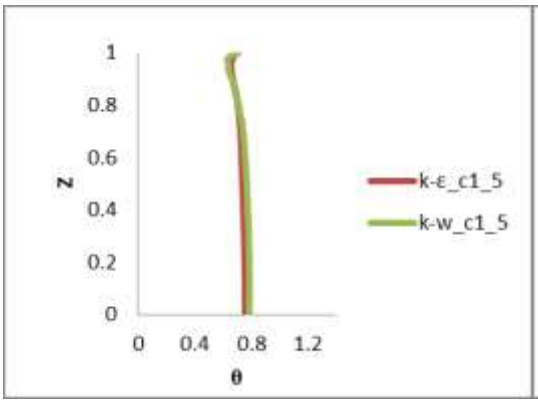

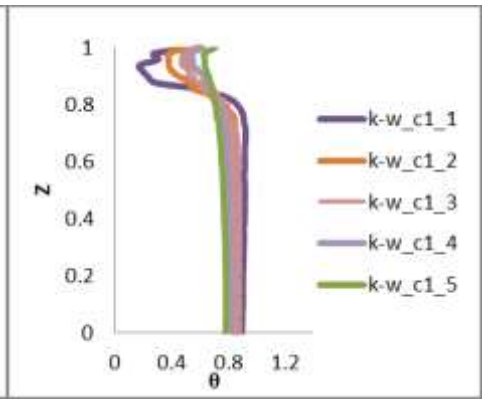

e f

Figure 5.19 Grille diffuser (case 1) prediction of the air temperature by Realizable k-ε model with Enhancement Wall Treatment and SST k-ω, (Z=height/total room height (H), θ=(T-Tin/Tout-Tin), H=2.43m, Tin=15.0ºC, Tout=24ºC).

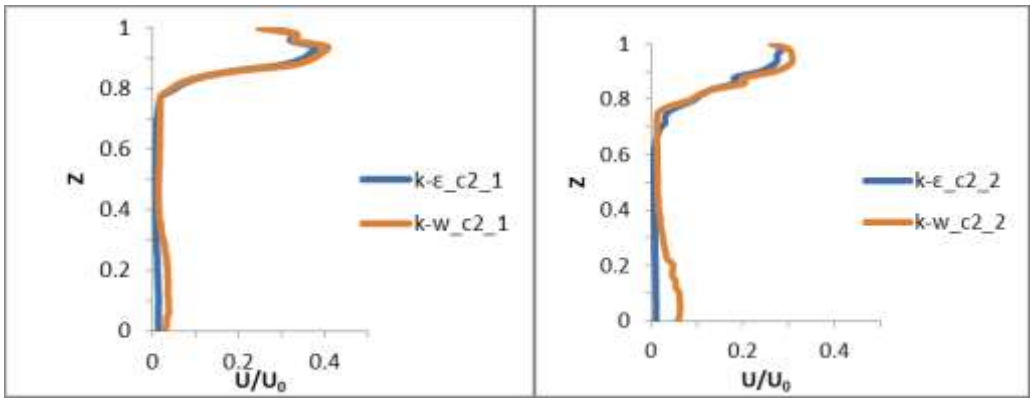

a

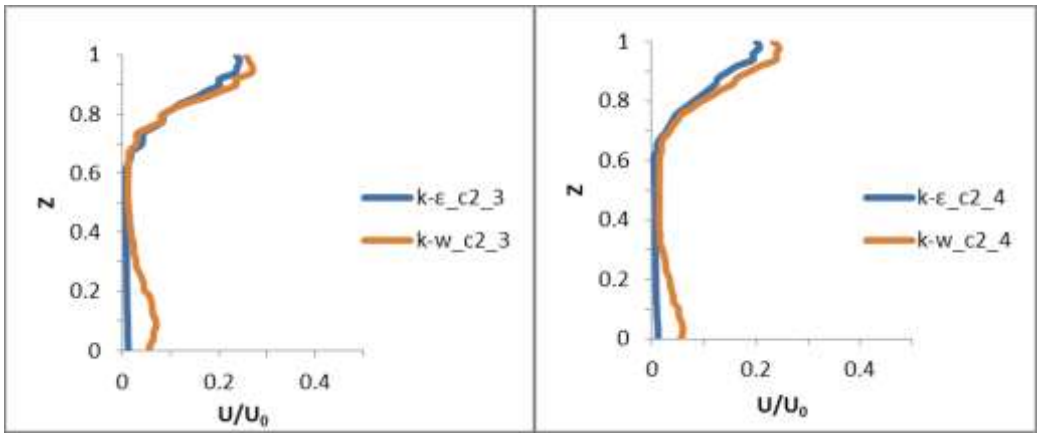

c d

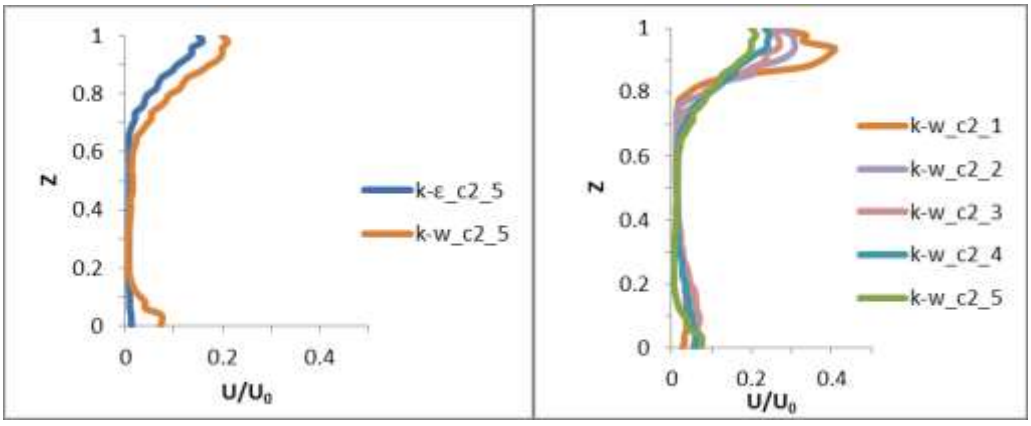

e f

Figure 5.20 Grille diffuser (case 2) prediction of the air velocity by Realizable k-ε model with Enhancement Wall Treatment and SST k-ω, (*Z=height/total room height (H), U=velocity/supply velocity (U_0), H=2.43m, U_0=2.7m/s*).

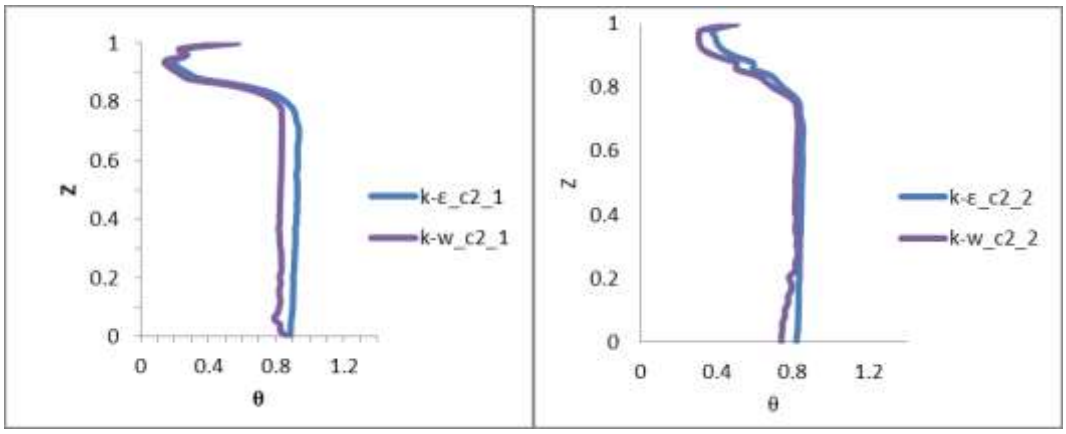

a b

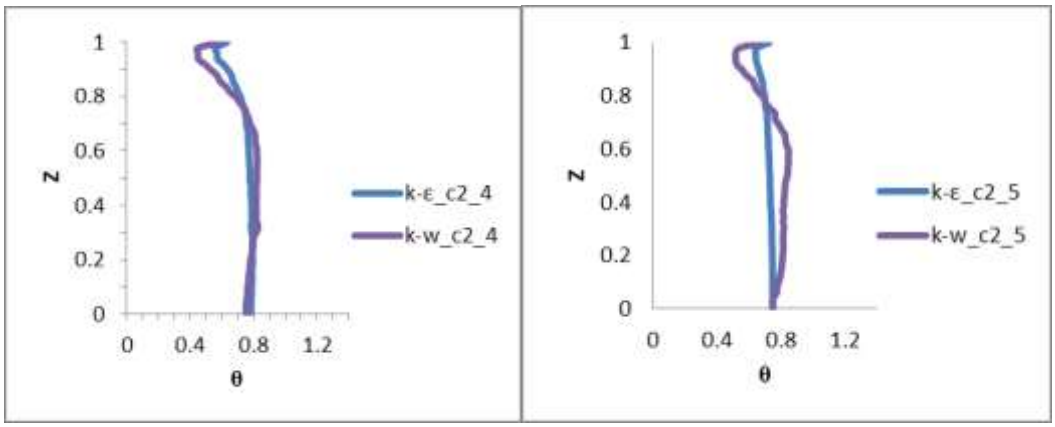

c d

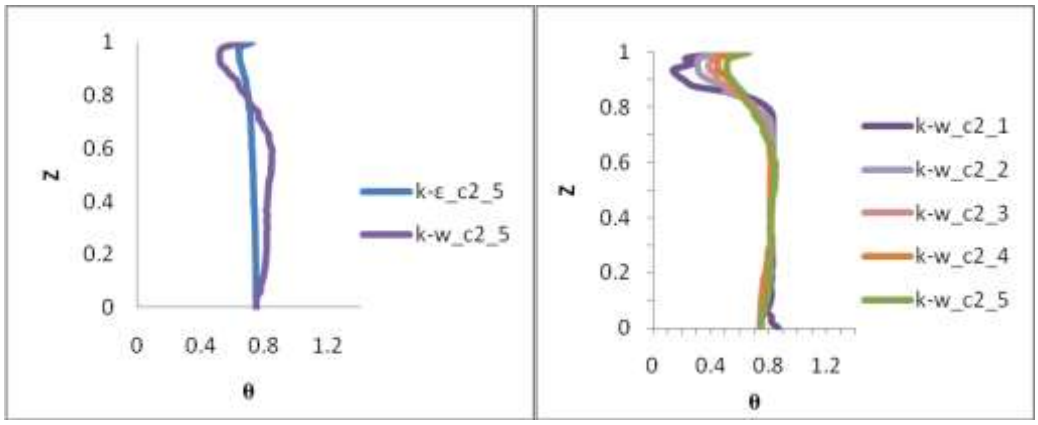

e f

Figure 5.21 Grille diffuser (case 2) prediction of the air temperature by Realizable k-ε model with Enhancement Wall Treatment and SST k-ω, (Z=height/total room height (H), $\theta=(T-T_{in}/T_{out}-T_{in})$, H=2.43m, T_{in}=15.0ºC, T_{out}=24ºC).

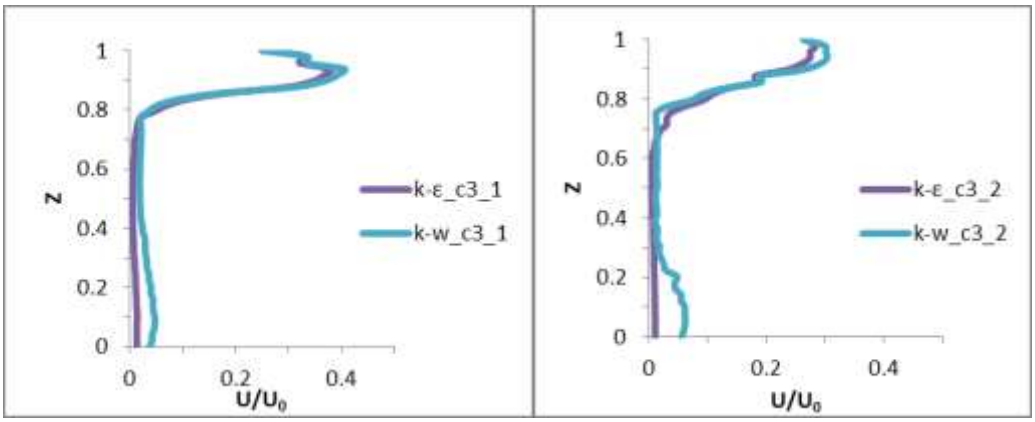

a

b

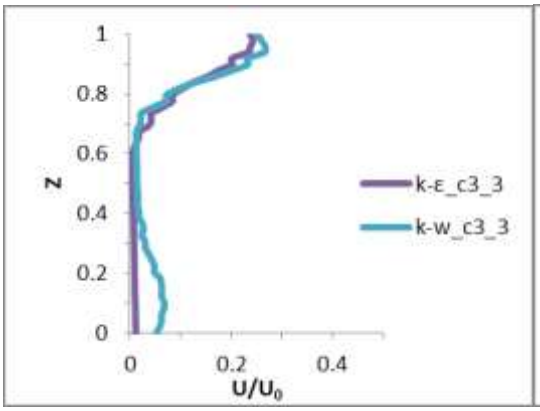

c

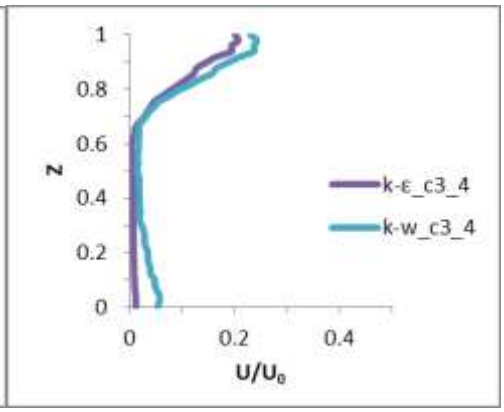

d

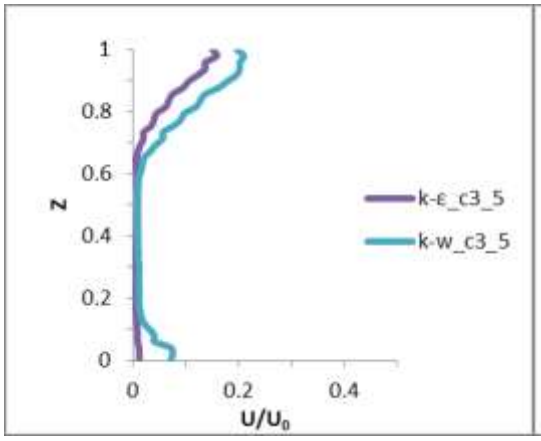

e

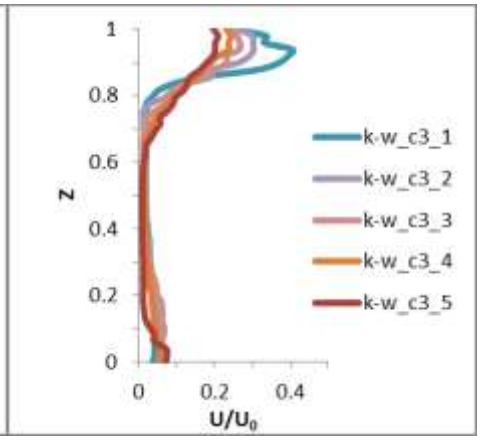

f

Figure 5.22 Grille diffuser (case 3) prediction of the air velocity by Realizable k-ε model with Enhancement Wall Treatment and SST k-ω, (*Z=height/total room height (H), U=velocity/supply velocity (U_0), H=2.43m, U_0=2.7m/s*).

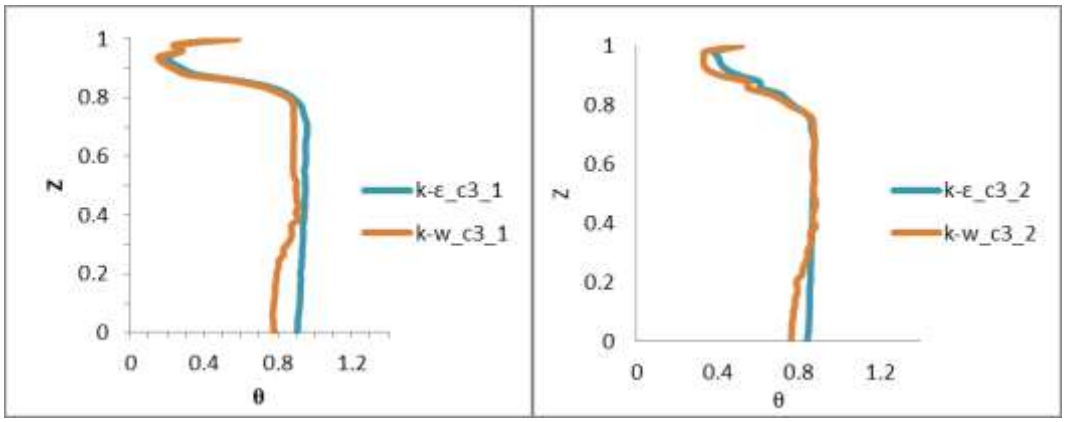

a

b

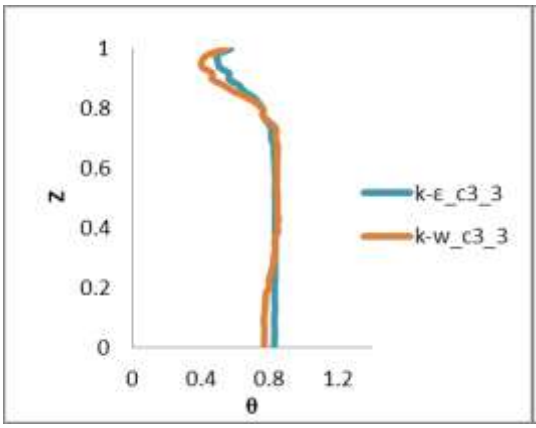

c

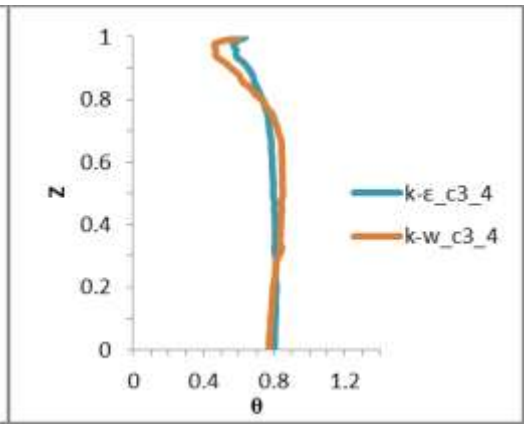

d

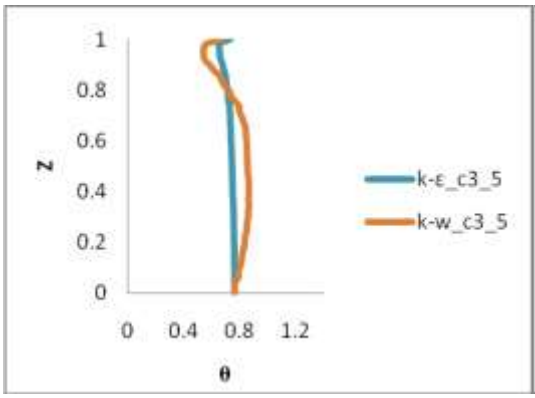

e

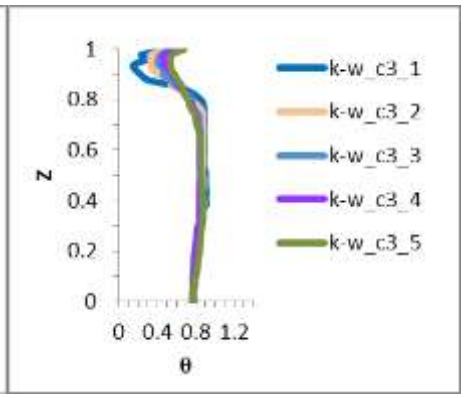

f

Figure 5.23 Grille diffuser (case 3) prediction of the air temperature by Realizable k-ε model with Enhancement Wall Treatment and SST k-ω, (Z=height/total room height (H), θ=(T-Tin/Tout-Tin), H=2.43m, Tin=15.0ºC, Tout=24ºC).

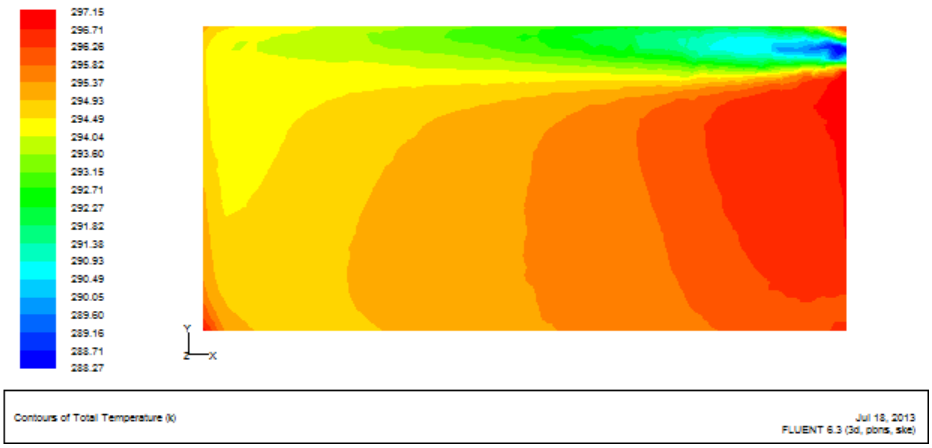

a

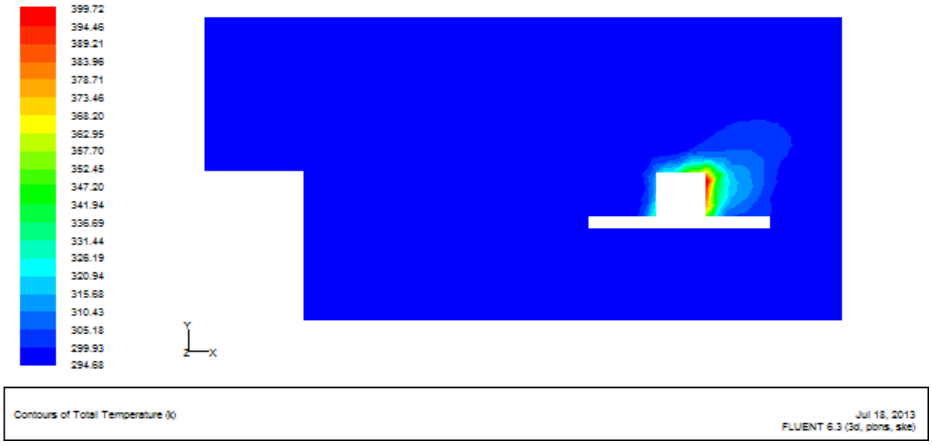

b

Figure 5.24 Distribution of calculation air temperature contours with k-ε, (case 1), (a) plane at z=1.825m, (b) plane at z=0.4m

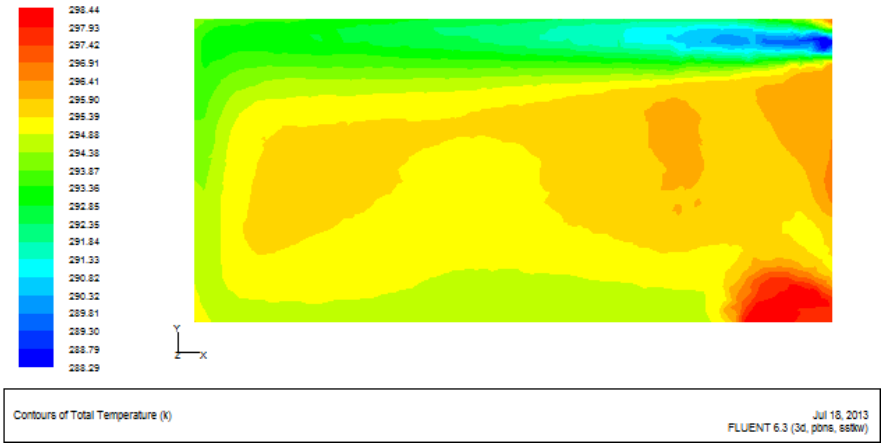

a

b

Figure 5.25 Distribution of calculation air temperature contours with k-ω, (case 1), (a) plane at z=1.825m, (b) plane at z=0.4m

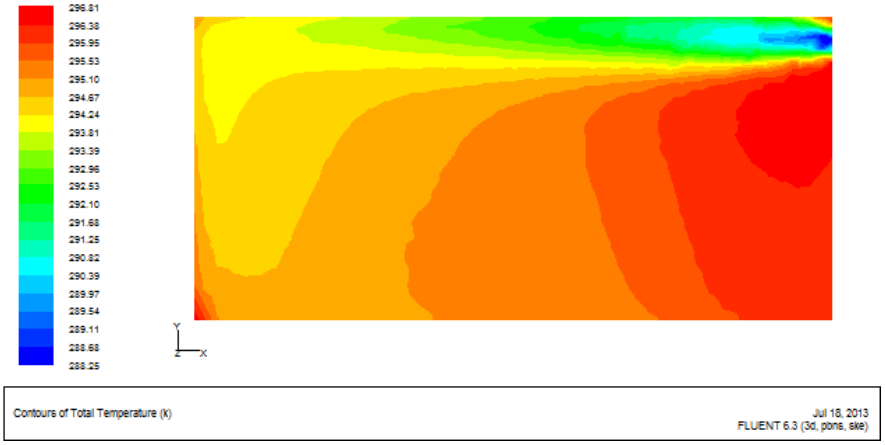

a

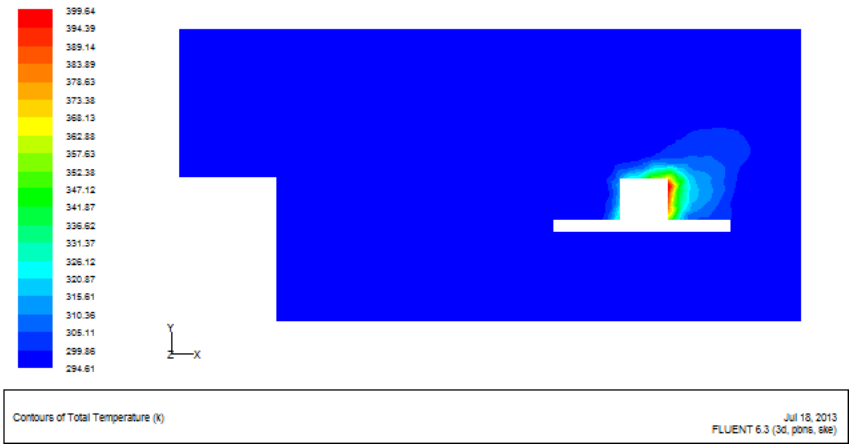

b

Figure 5.26 Distribution of calculation air temperature contours with k-ε, (case 2), (a) plane at z=1.825m, (b) plane at z=0.4m

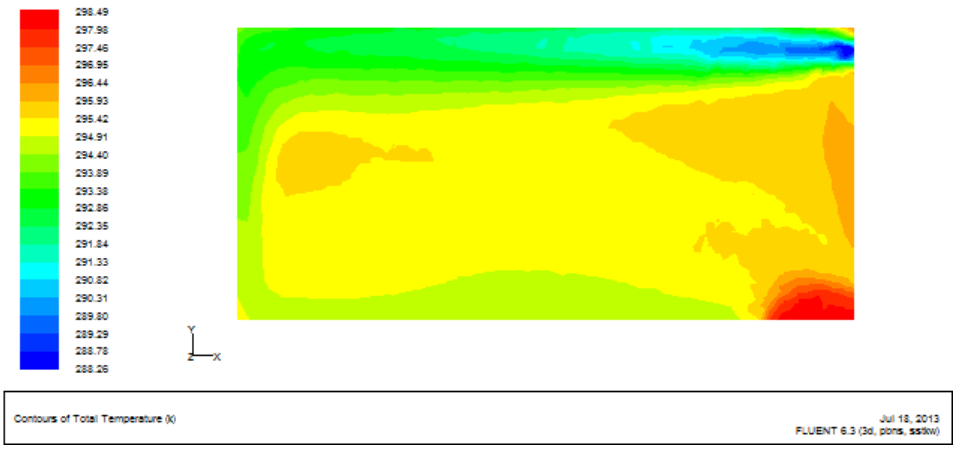

a

b

Figure 5.27 Distribution of calculation air temperature contours with k-ω, (case 2), (a) plane at z=1.825m, (b) plane at z=0.4m

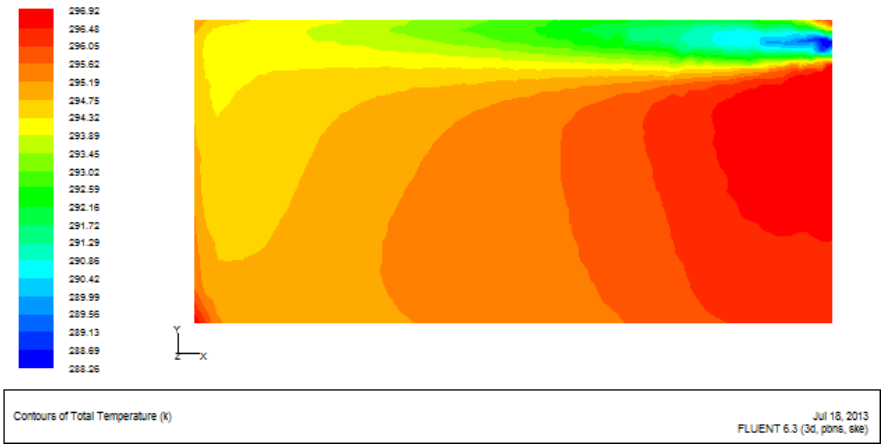

a

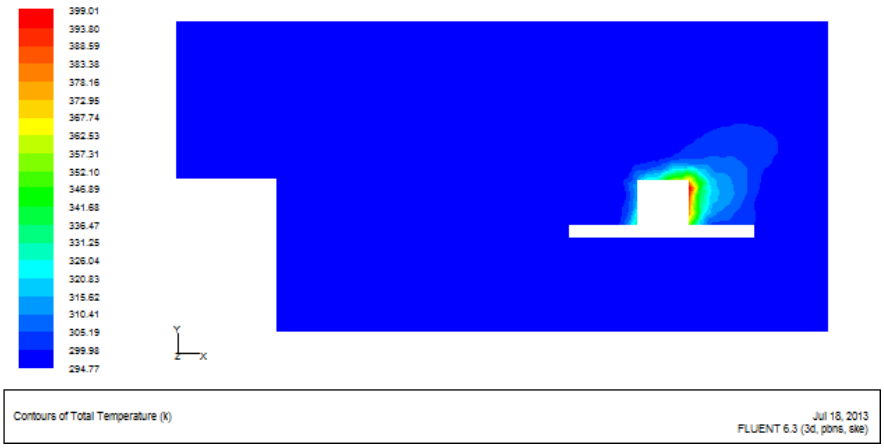

b

Figure 5.28 Distribution of calculation air temperature contours with k-ε, (case 3), (a) plane at z=1.825m, (b) plane at z=0.4m

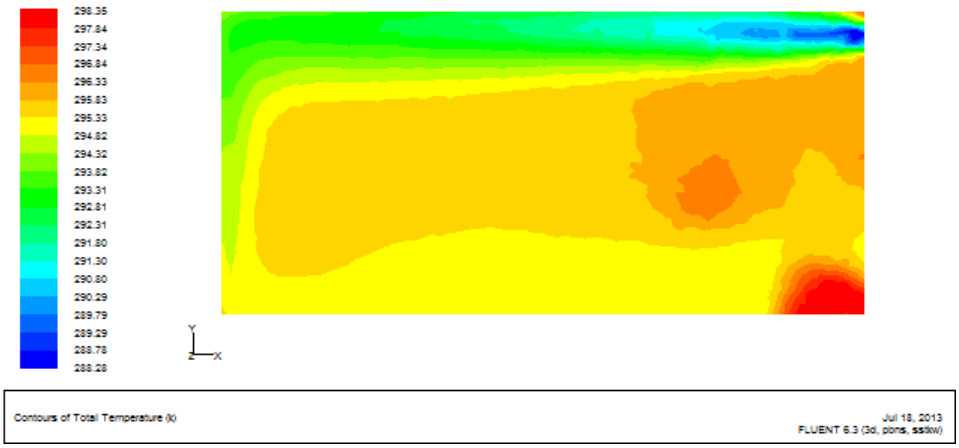

a

b

Figure 5.29 Distribution of calculation air temperature contours with k-ω, (case 3), (a) plane at z=1.825m, (b) plane at z=0.4m

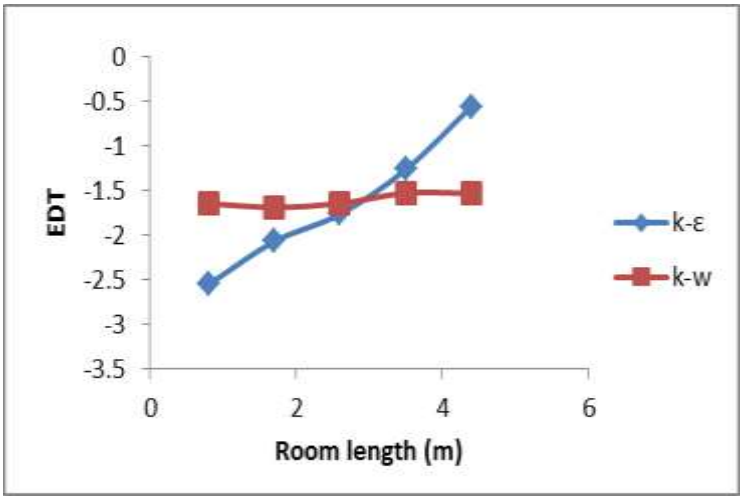

a

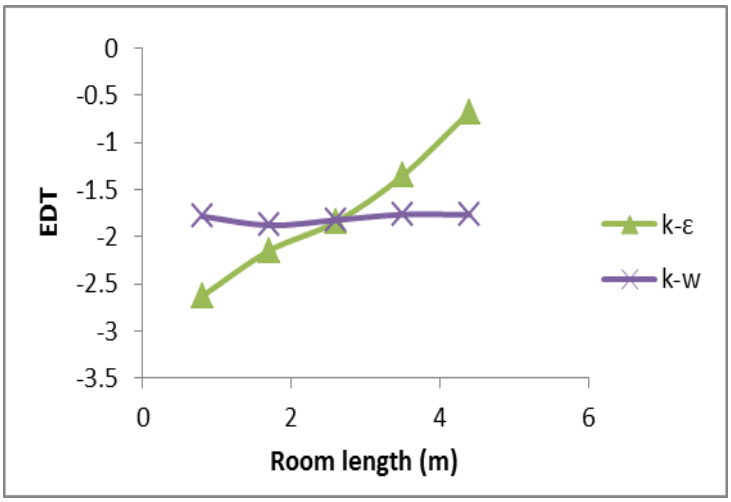

b

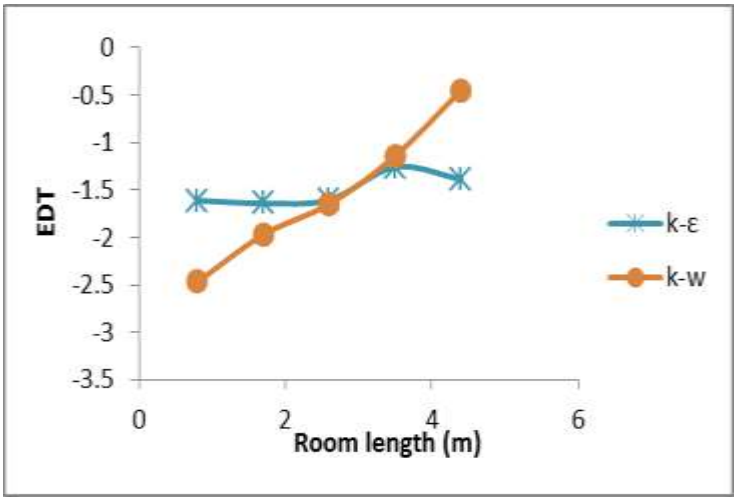

c

Figure 5.30 Grille effect draft temperature for k-ε and k-ω models, (a) case1, (b) case 2, (c) case 3.

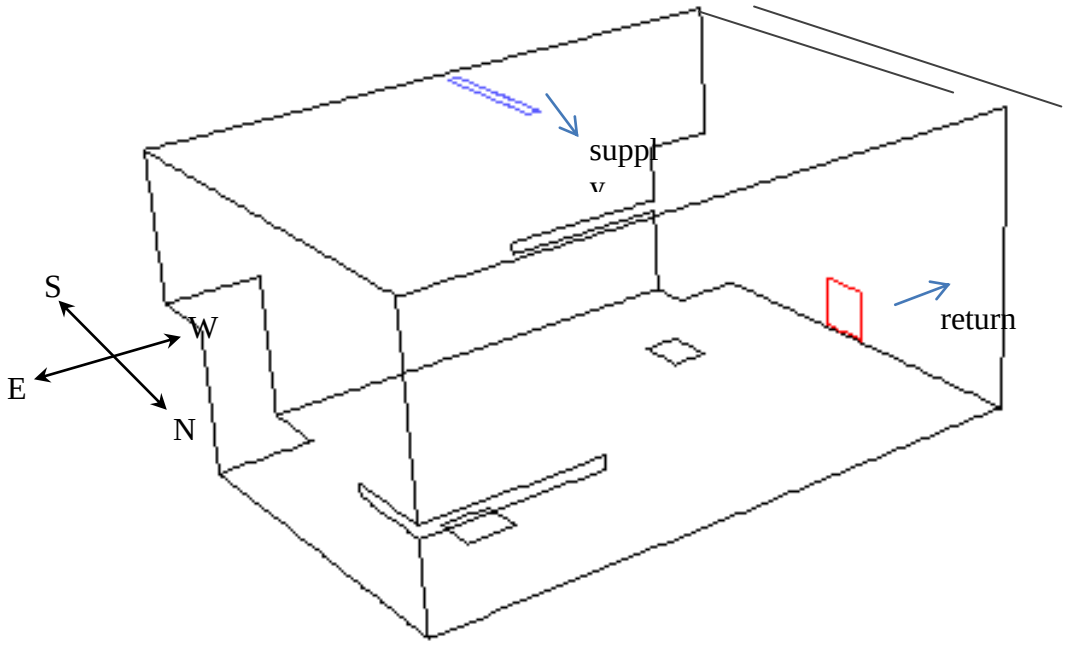

Figure 5.31 Configuration of ceiling slot ventilation test case

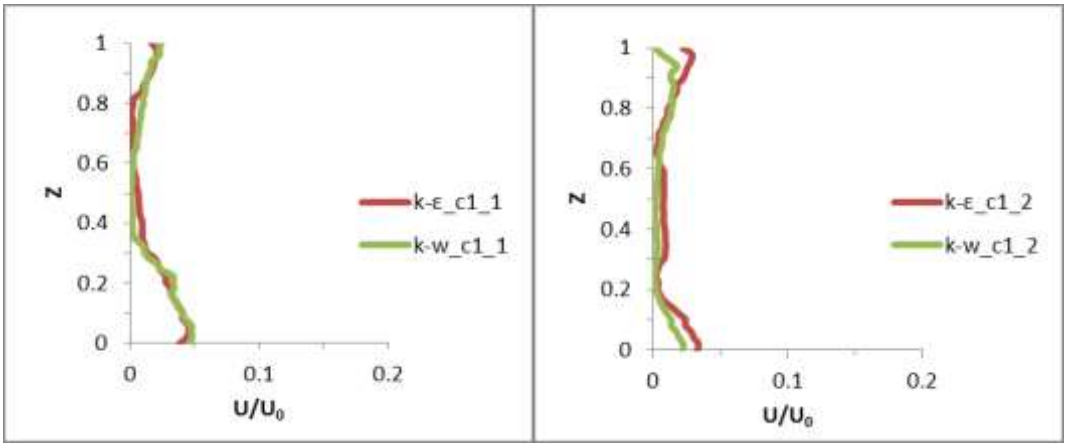

a b

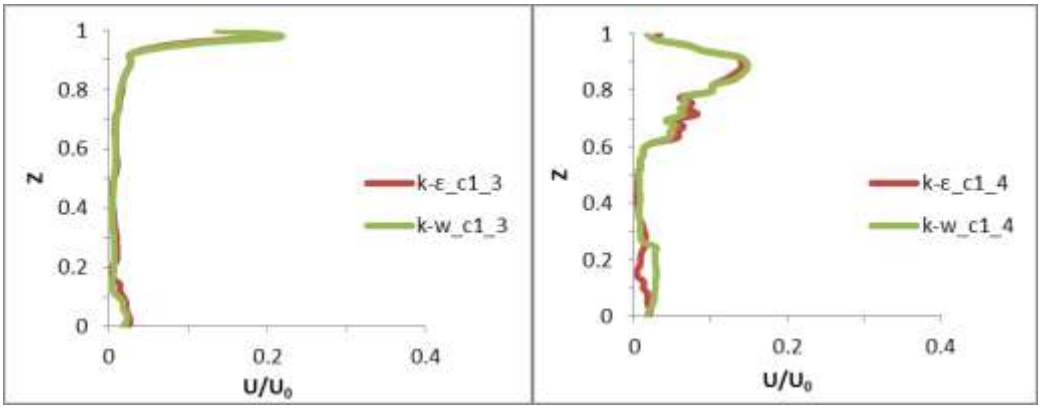

c d

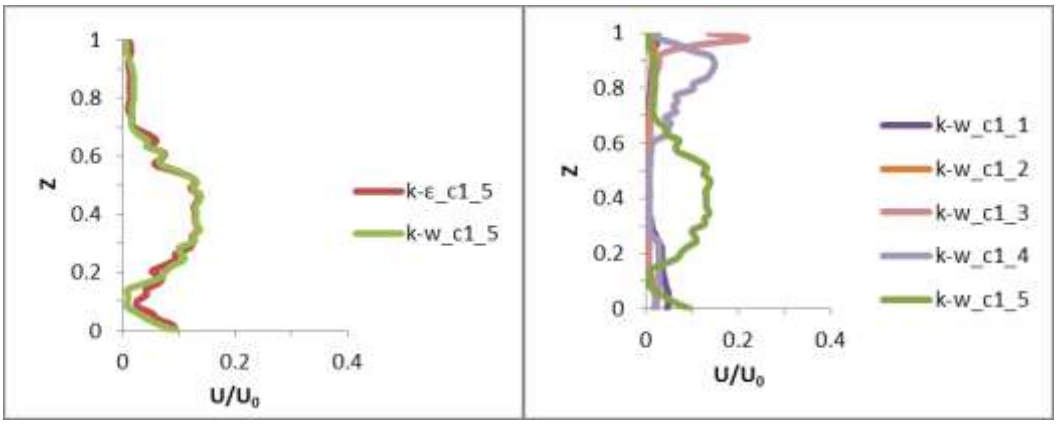

e f

Figure 5.32 Slot diffuser (case 1) prediction of the air velocity by Realizable k-ε model with Enhancement Wall Treatment and SST k-ω, (*Z=height/total room height (H), U=velocity/supply velocity (U_0), H=2.43m, U_0=3.9m/s*).

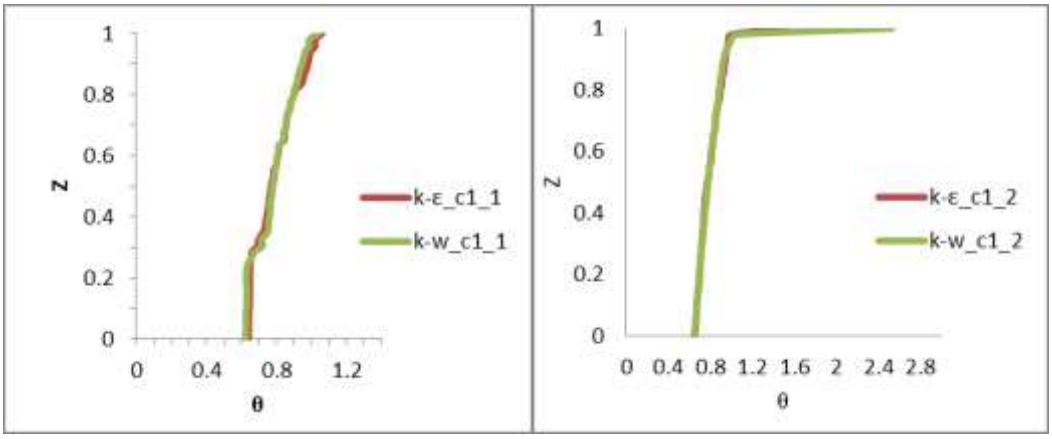

a b

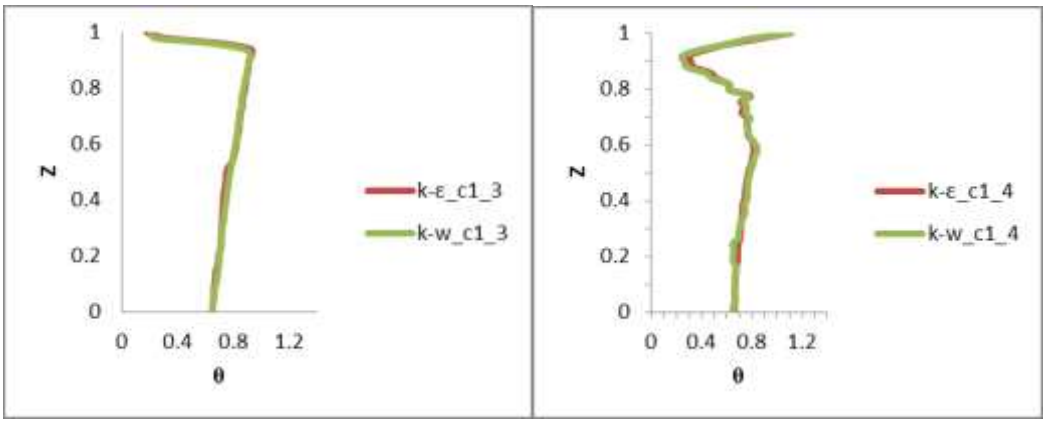

c d

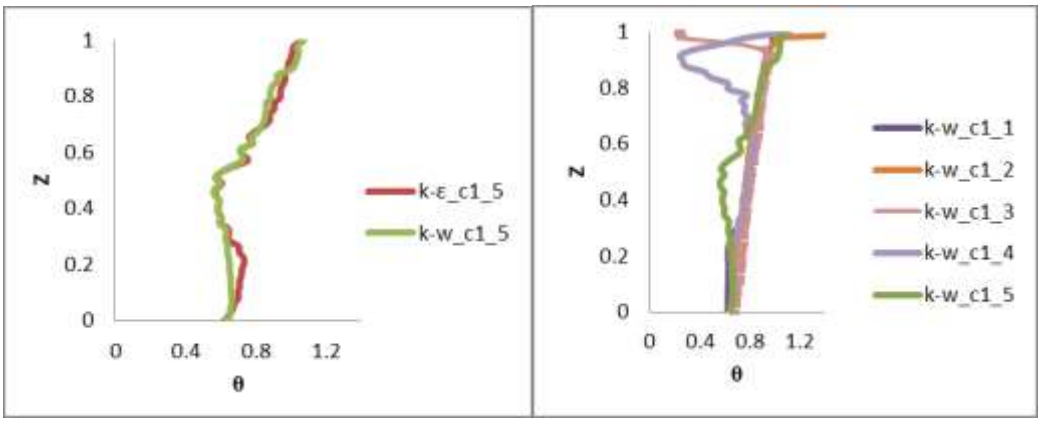

e f

Figure 5.33 Slot diffuser (case 1) prediction of the air temperature by Realizable k-ε model with Enhancement Wall Treatment and SST k-ω, (Z=height/total room height (H), θ=(T-Tin/Tout-Tin), H=2.43m, Tin=15.0ºC, Tout=24ºC).

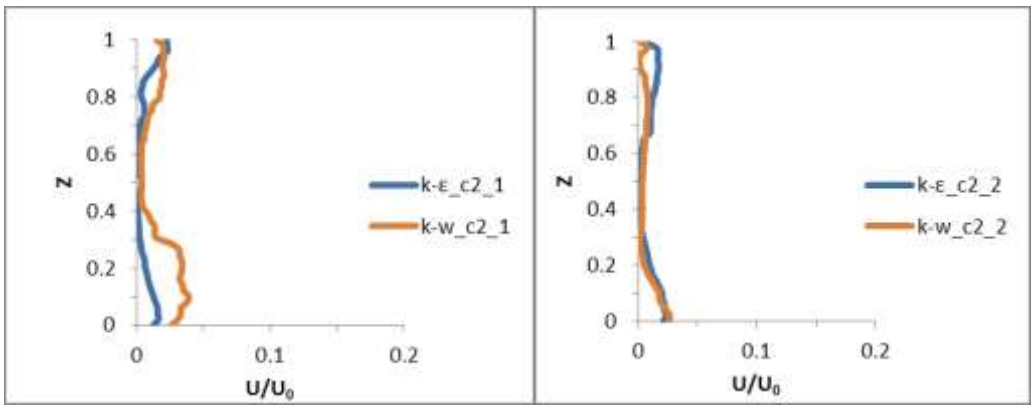

a b

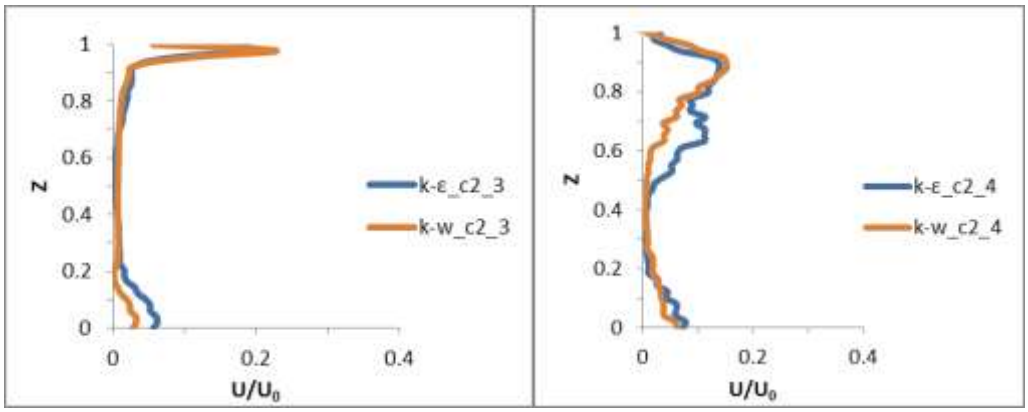

c d

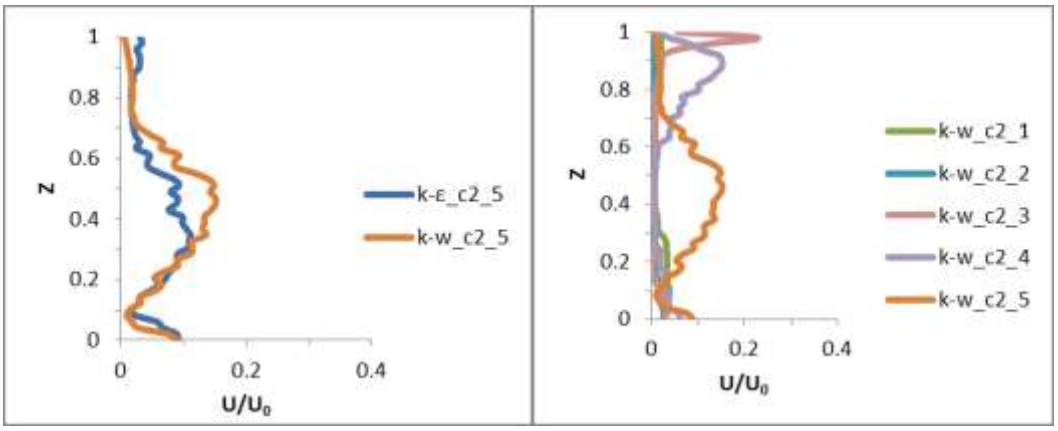

e f

Figure 5.34 Slot diffuser (case 2) prediction of the air velocity by Realizable k-ε model with Enhancement Wall Treatment and SST k-ω, (*Z=height/total room height (H), U=velocity/supply velocity (U_0), H=2.43m, U_0=3.9m/s*).

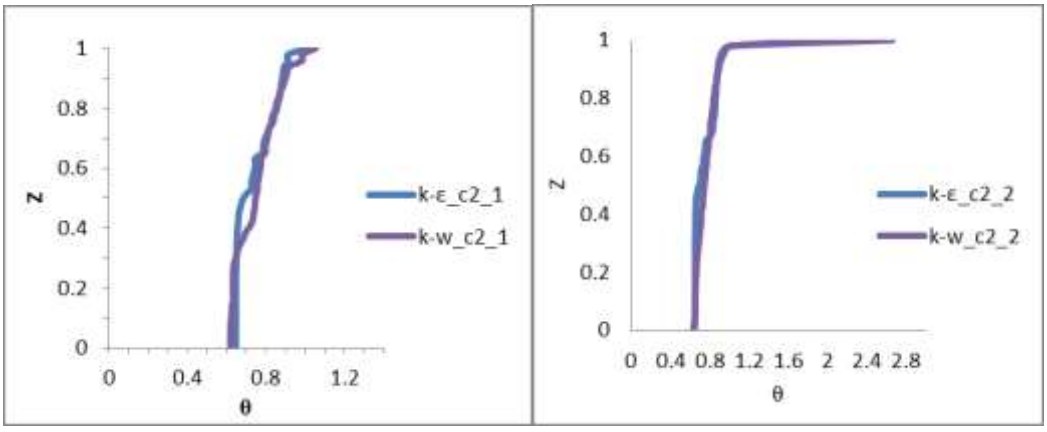

a b

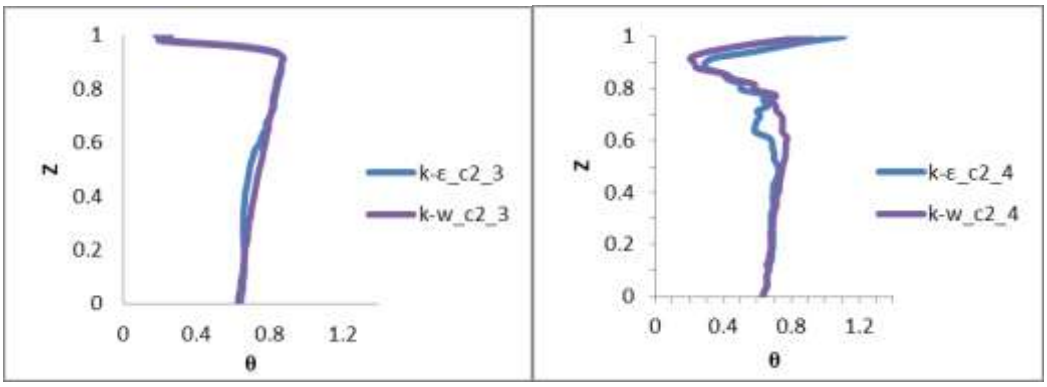

c d

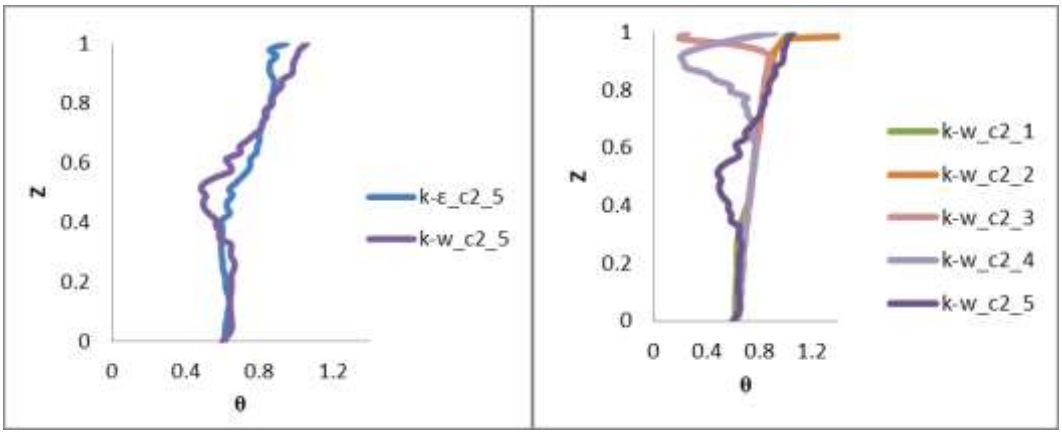

e f

Figure 5.35 Slot diffuser (case 2) prediction of the air temperature by Realizable k-ε model with Enhancement Wall Treatment and SST k-ω, (Z=height/total room height (H), θ=(T-Tin/Tout-Tin), H=2.43m, Tin=15.0ºC, Tout=24ºC).

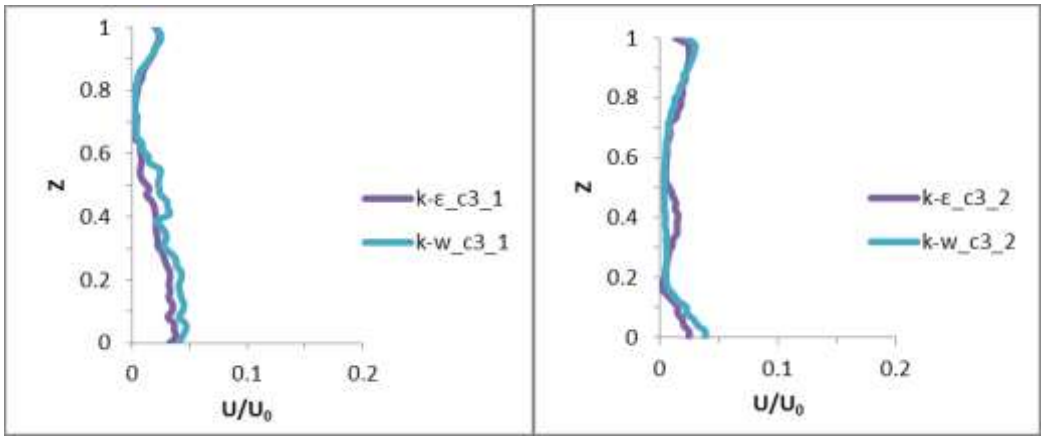

a b

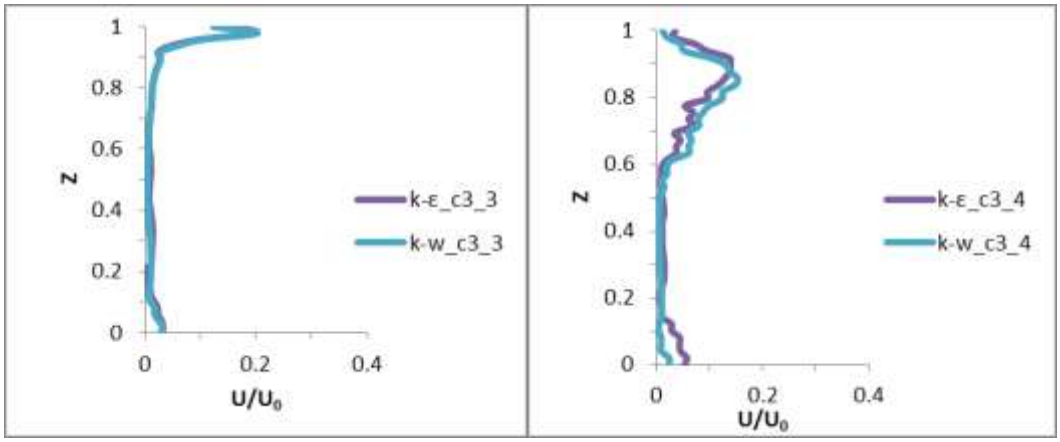

c d

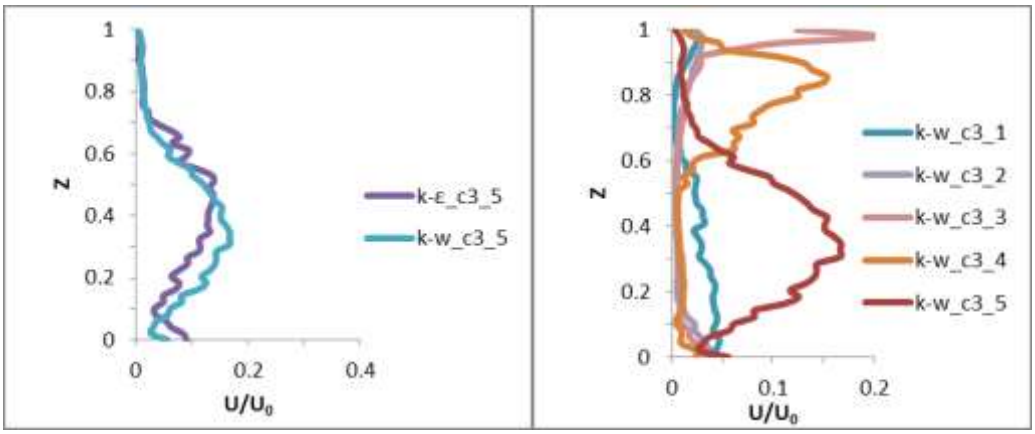

e f

Figure 5.36 Slot diffuser (case 3) prediction of the air velocity by Realizable k-ε model with Enhancement Wall Treatment and SST k-ω, (*Z=height/total room height (H), U=velocity/supply velocity (U_0), H=2.43m, U_0=3.9m/s*).

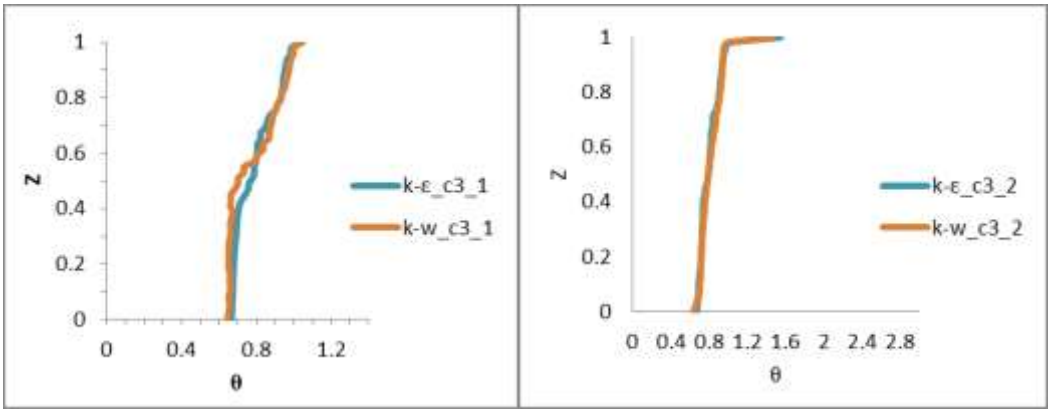

a b

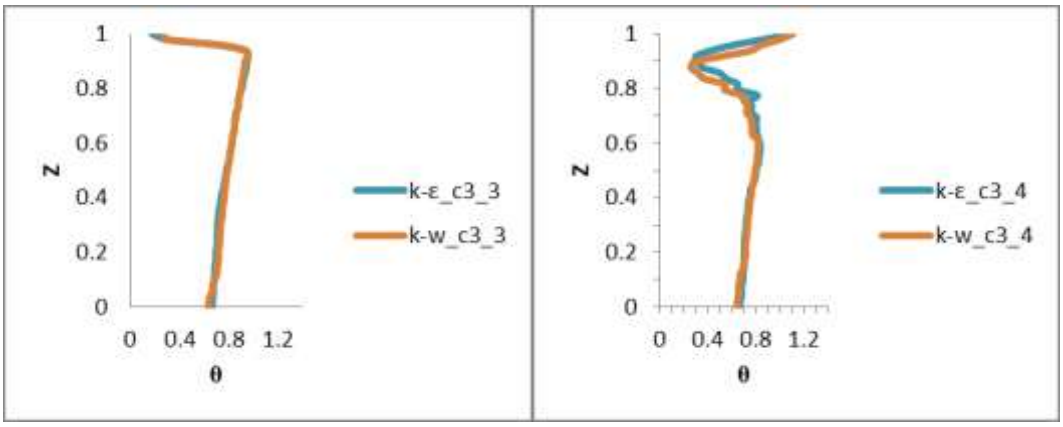

c d

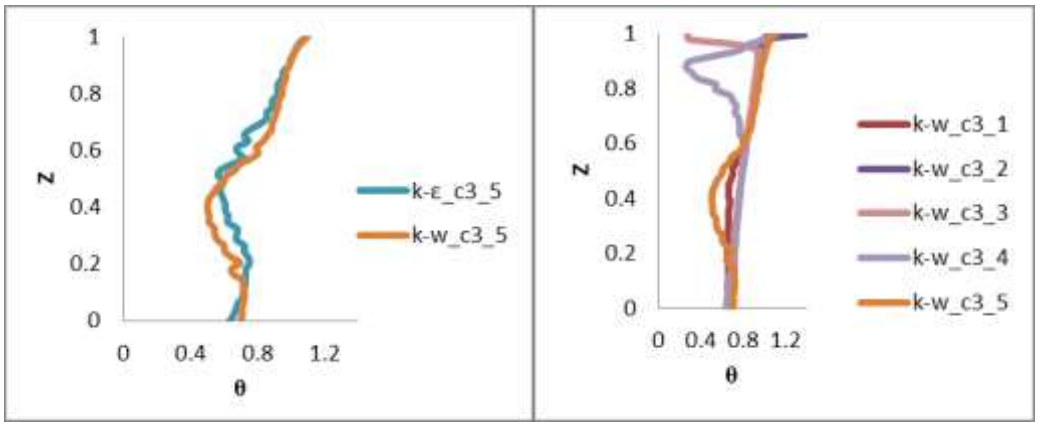

e f

Figure 5.37 Slot diffuser (case 3) prediction of the air temperature by Realizable k-ε model with Enhancement Wall Treatment and SST k-ω, (Z=height/total room height (H), θ=(T-Tin/Tout-Tin), H=2.43m, Tin=15.0ºC, Tout=24ºC).

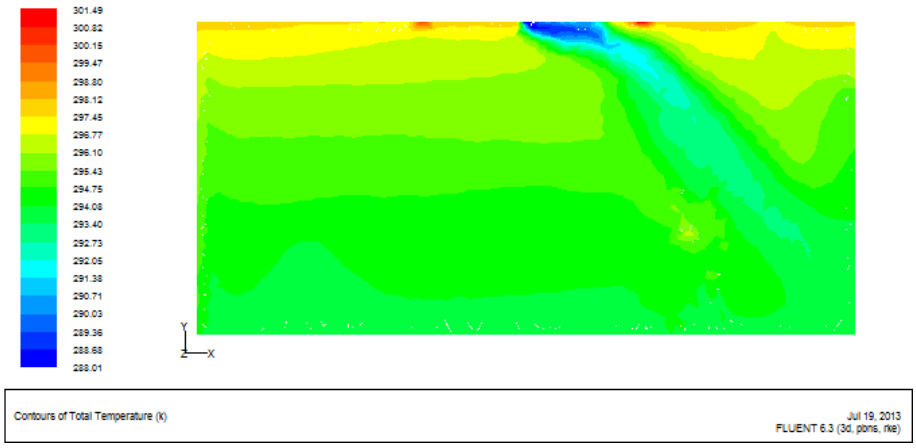

a

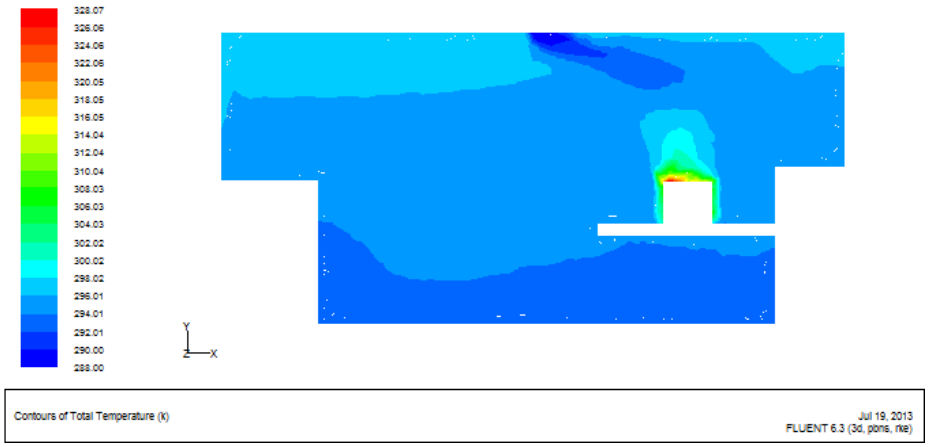

b

Figure 5.38 Distribution of calculation air temperature contours with k-ε, (case 1), (a) plane at z=1.825m, (b) plane at z=0.4m

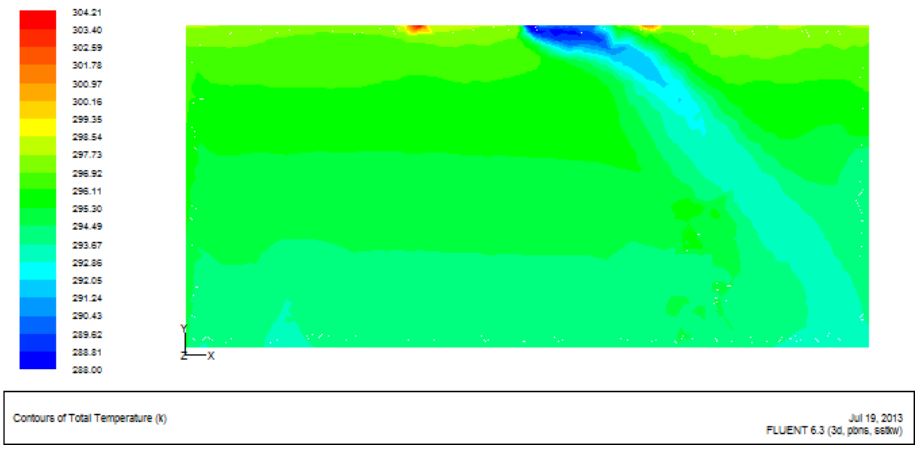

a

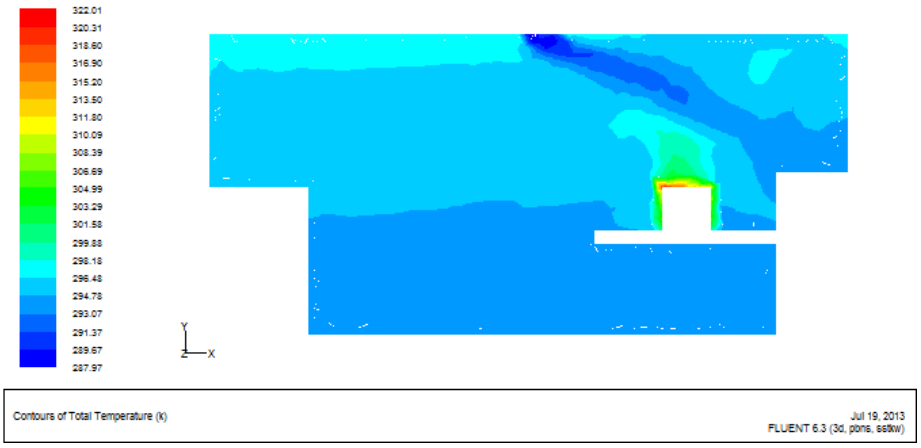

b

Figure 5.39 Distribution of calculation air temperature contours with k-ω, (case 1), (a) plane at z=1.825m, (b) plane at z=0.4m

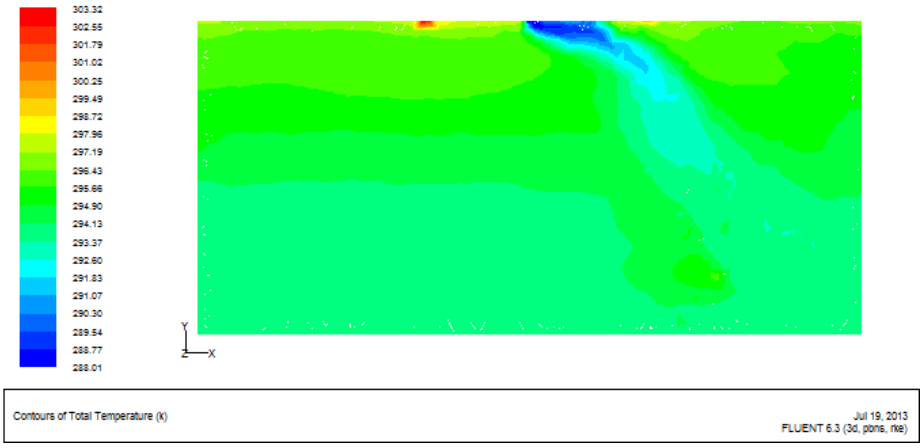

a

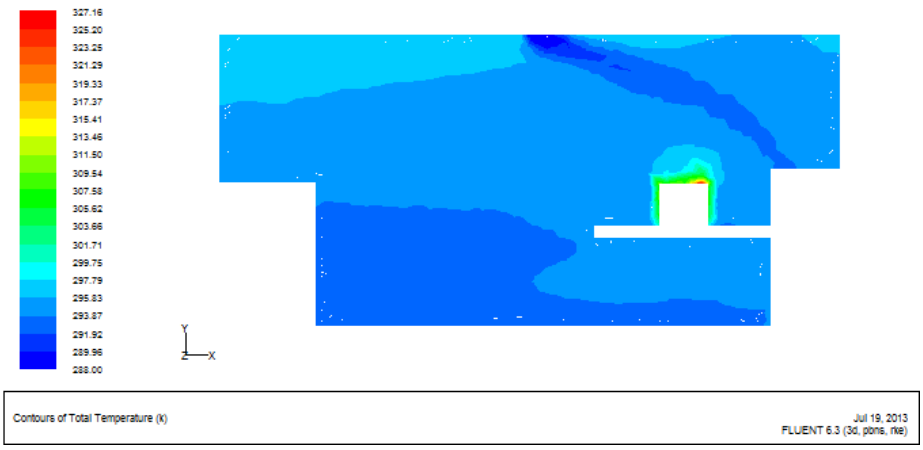

b

Figure 5.40 Distribution of calculation air temperature contours with k-ε, (case 2), (a) plane at z=1.825m, (b) plane at z=0.4m

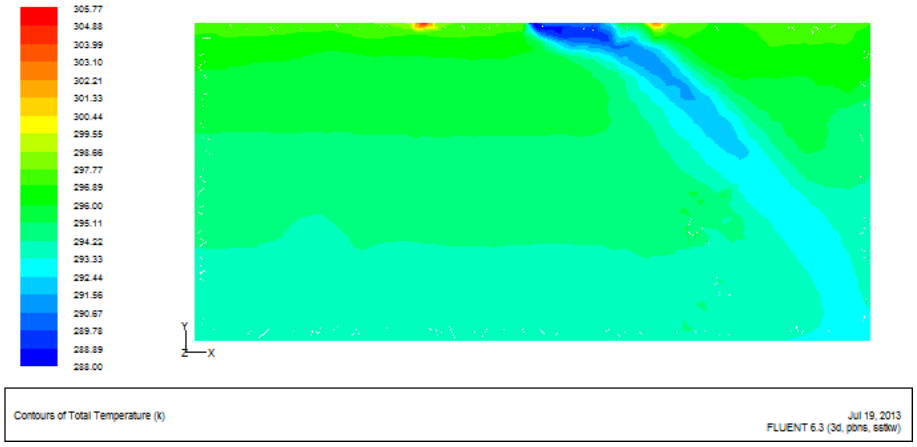

a

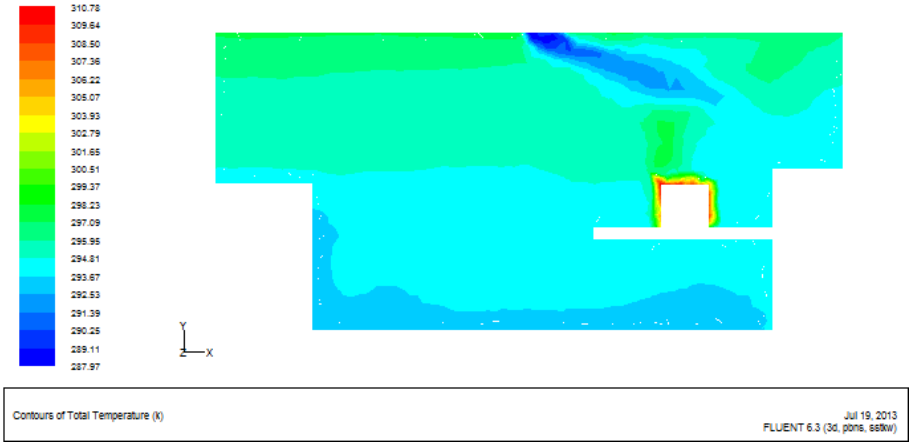

b

Figure 5.41 Distribution of calculation air temperature contours with k-ω, (case 2), (a) plane at z=1.825m, (b) plane at z=0.4m

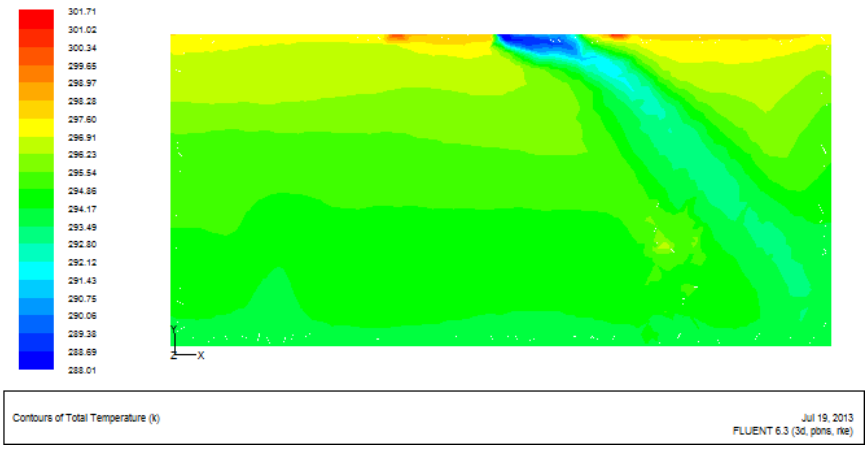

a

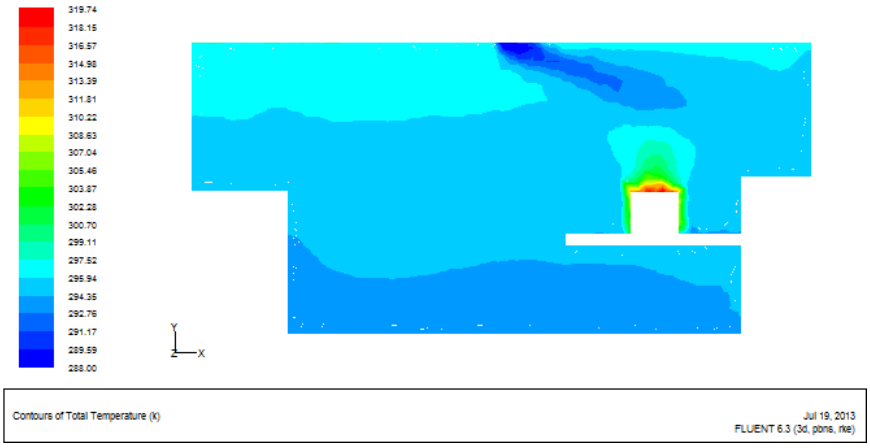

b

Figure 5.42 Distribution of calculation air temperature contours with k-ε, (case 3), (a) plane at z=1.825m, (b) plane at z=0.4m

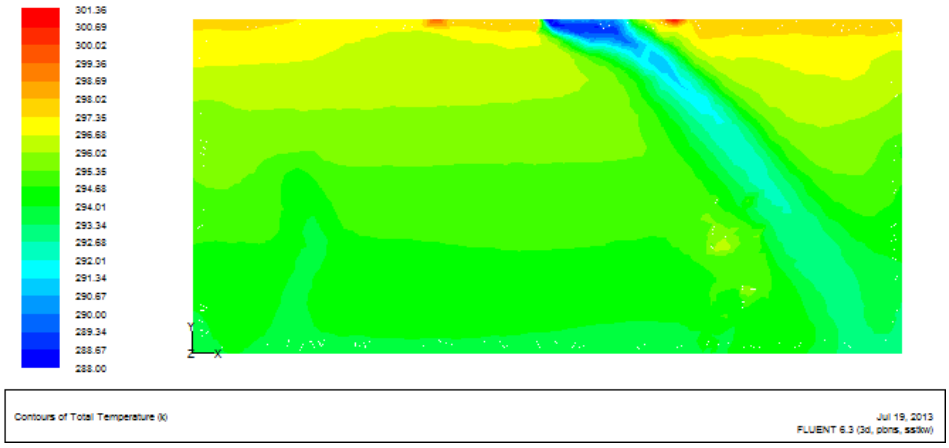

a

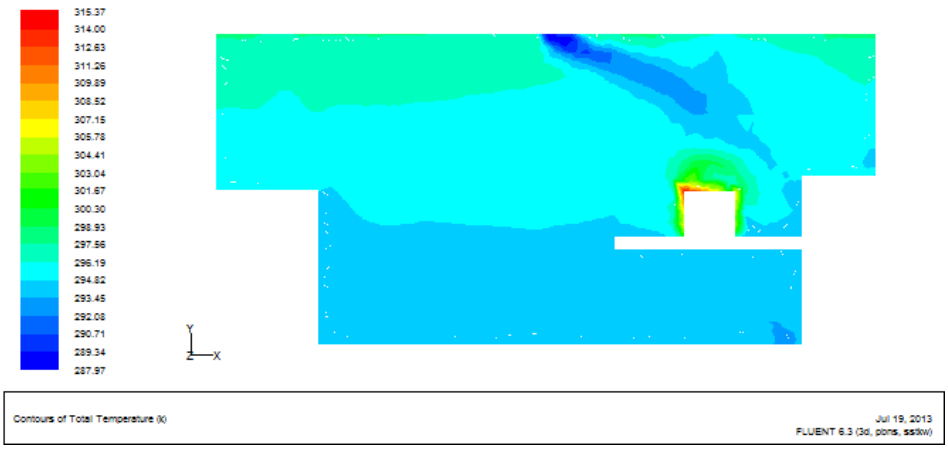

b

Figure 5.43 Distribution of calculation air temperature contours with k-ω, (case 3), (a) plane at z=1.825m, (b) plane at z=0.

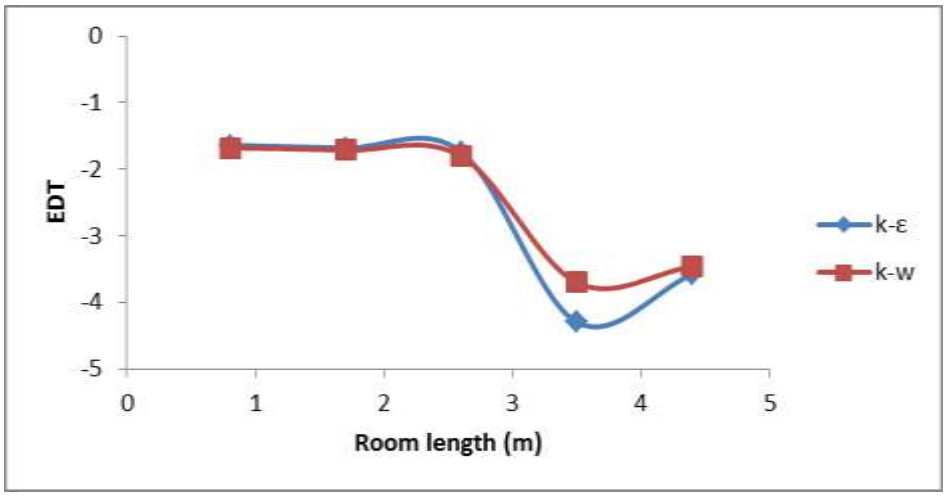

a

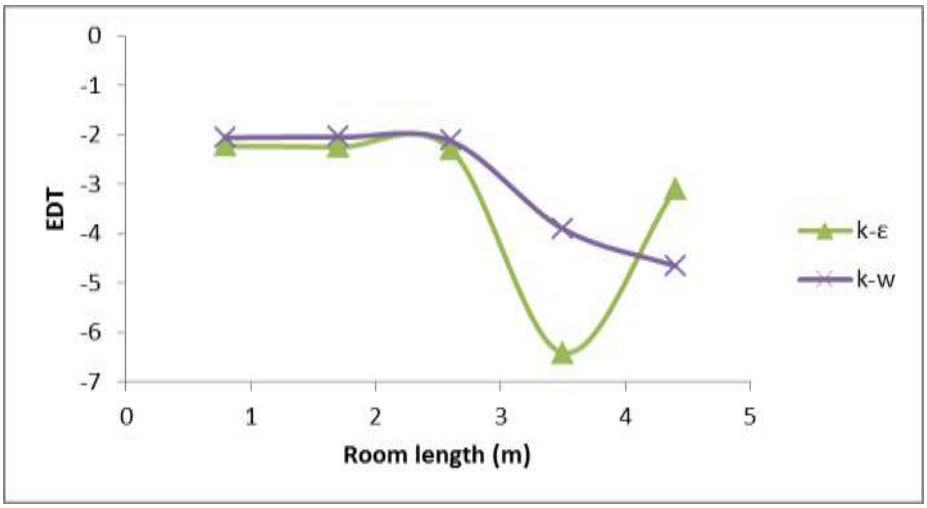

b

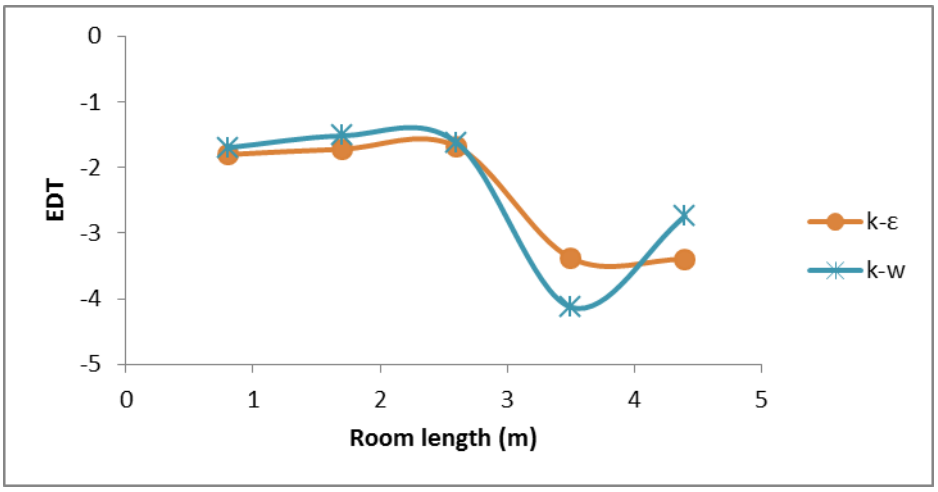

c

Figure 5.44 Slot effect draft temperature for k-ε and k-ω models, (a) case1, (b) case 2, (c) case 3.

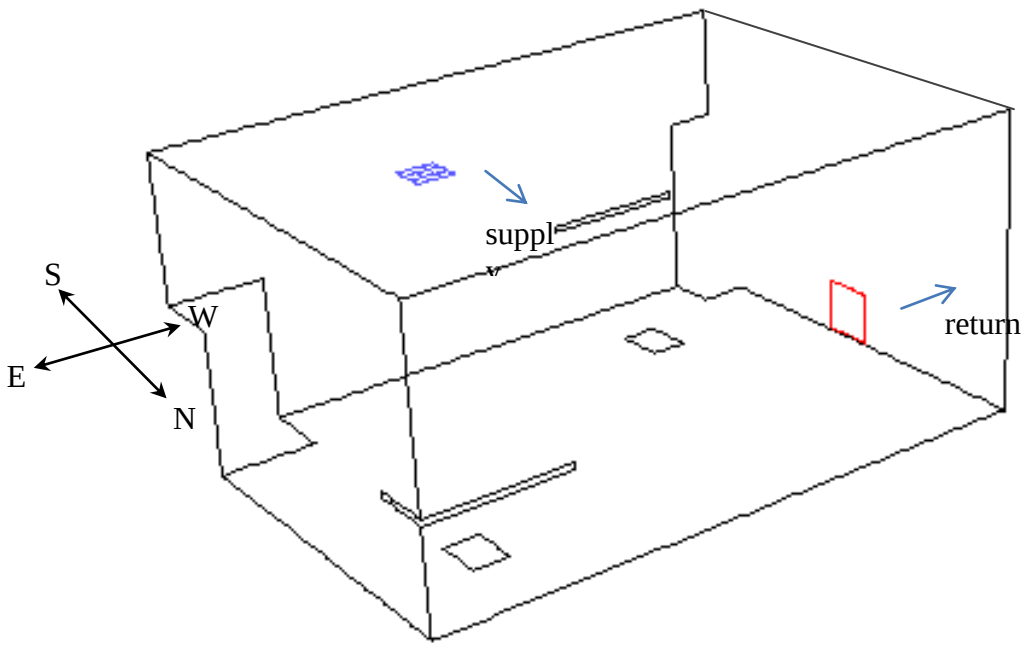

Figure 5.45 Configuration of ceiling slot ventilation test case.

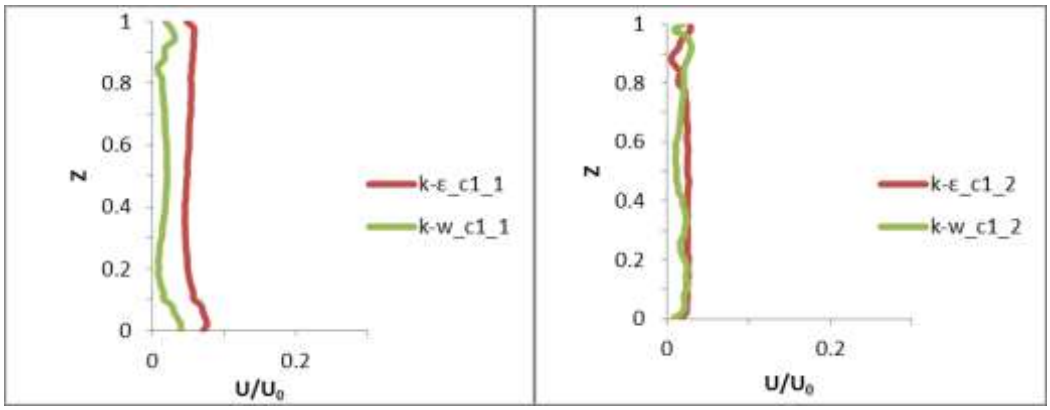

a

b

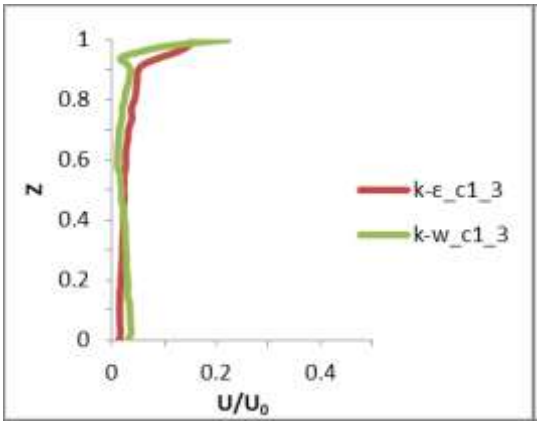

c

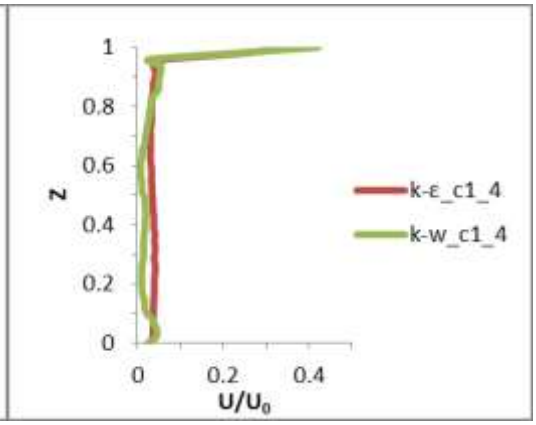

d

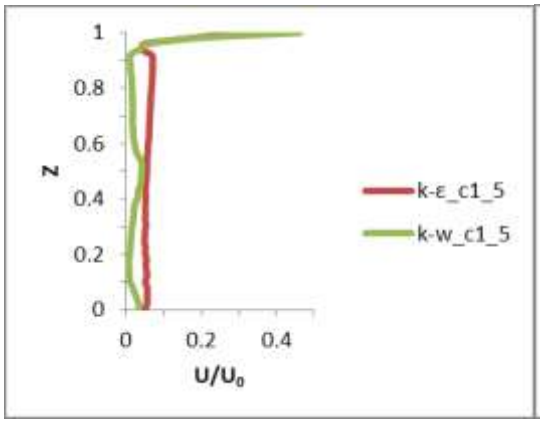

e

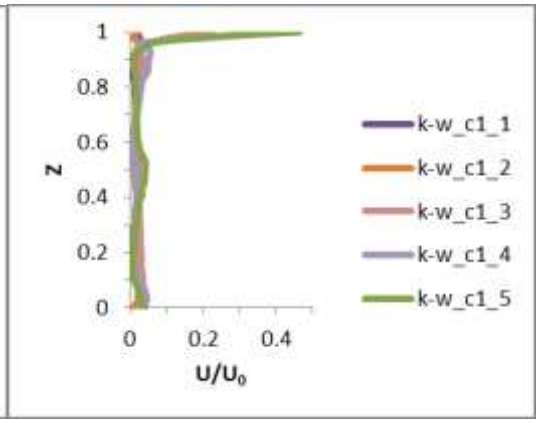

f

Figure 5.46 Square diffuser (case 1) prediction of the air velocity by Realizable k-ε model with Enhancement Wall Treatment and SST k-ω, (*Z=height/total room height (H), U=velocity/supply velocity (U_0), H=2.43m, U_0=5.2m/s*).

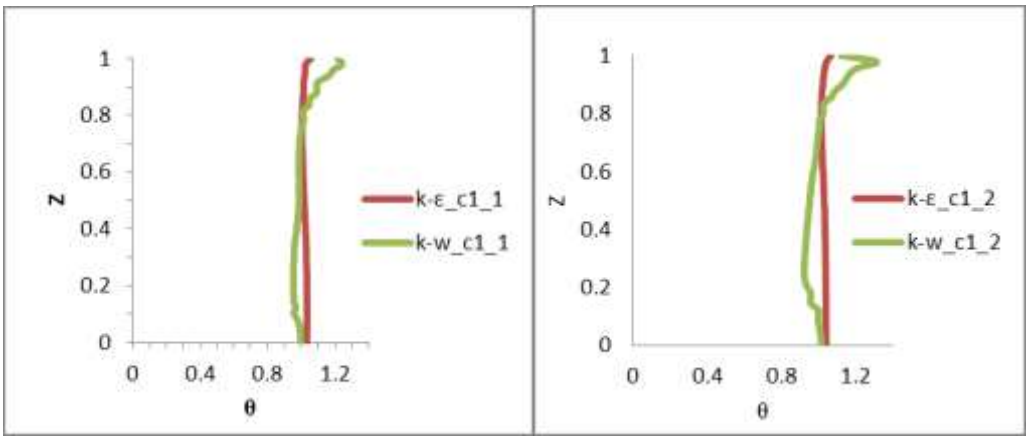

a

b

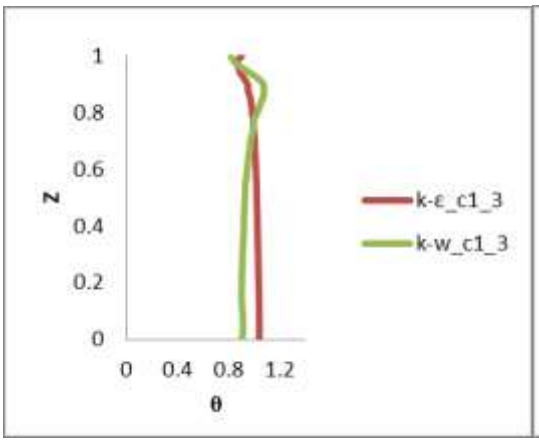

c

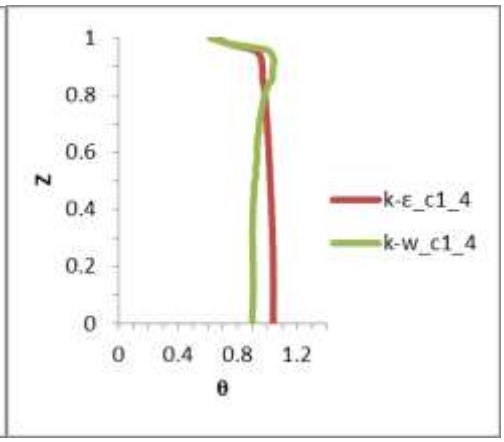

d

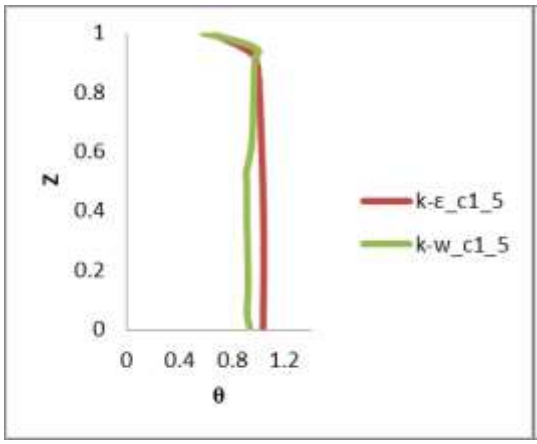

e

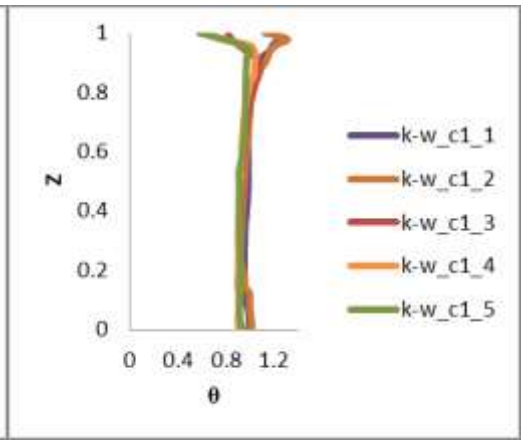

f

Figure 5.47 Square diffuser (case 1) prediction of the air temperature by Realizable k-ε model with Enhancement Wall Treatment and SST k-ω, (Z=height/total room height (H), θ=(T-Tin/Tout-Tin), H=2.43m, Tin=15.0ºC, Tout=24ºC).

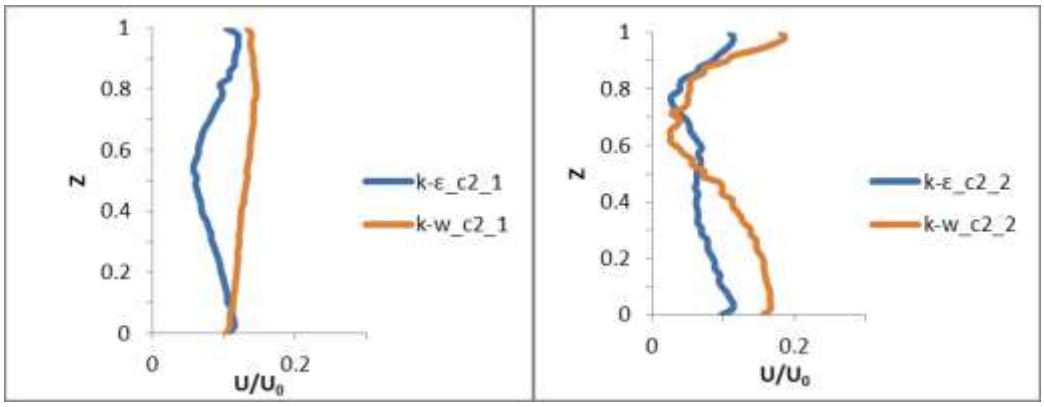

a

b

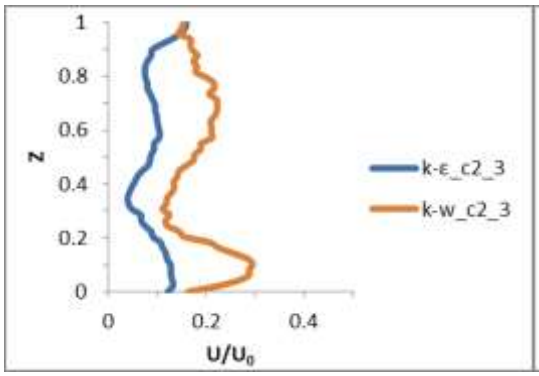

c

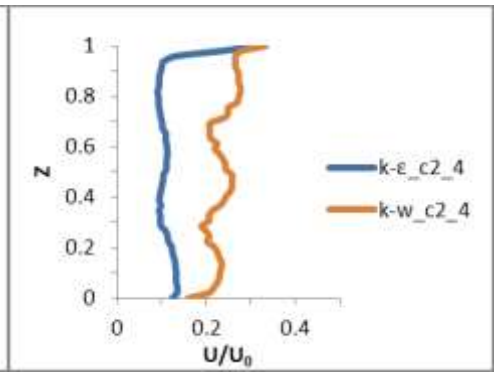

d

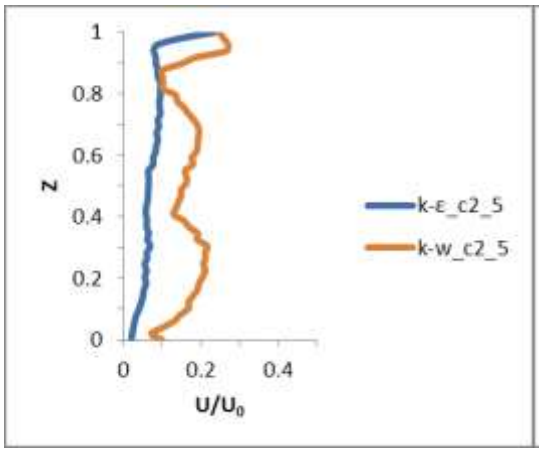

e

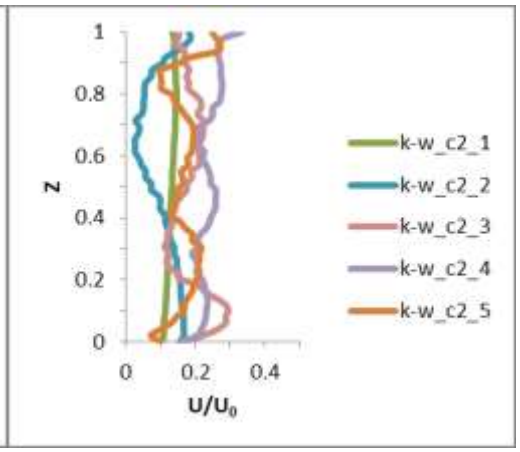

f

Figure 5.48 Square diffuser (case 2) prediction of the air velocity by Realizable k-ε model with Enhancement Wall Treatment and SST k-ω, (*Z=height/total room height (H), U=velocity/supply velocity (U_0), H=2.43m, U_0=5.2m/s*).

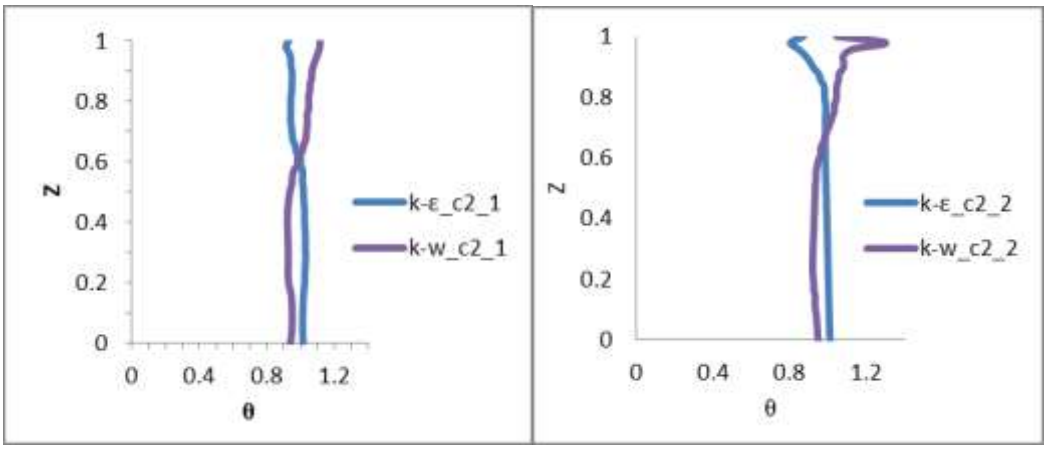

a

b

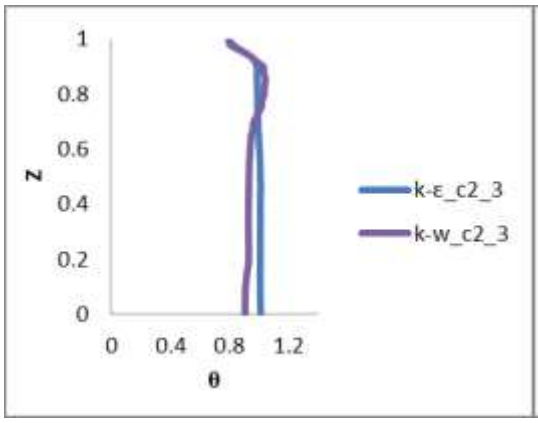

c

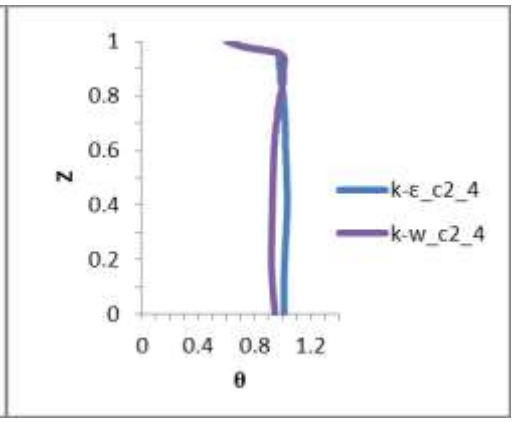

d

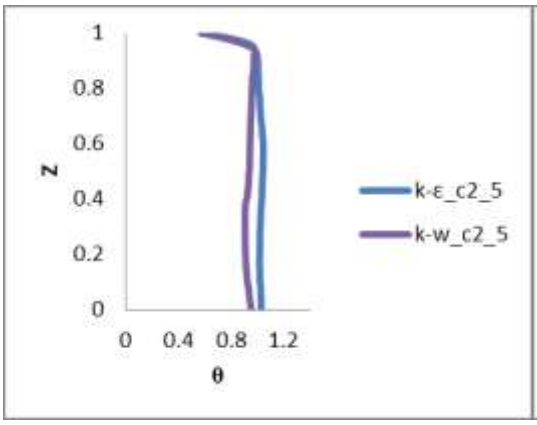

e

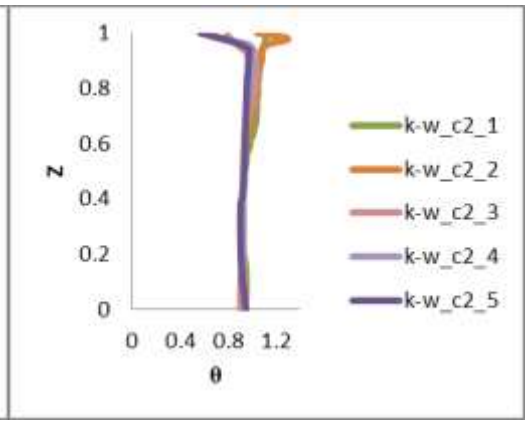

f

Figure 5.49 Square diffuser (case 2) prediction of the air temperature by Realizable k-ε model with Enhancement Wall Treatment and SST k-ω, (Z=height/total room height (H), θ=(T-Tin/Tout-Tin), H=2.43m, Tin=15.0ºC, Tout=24ºC).

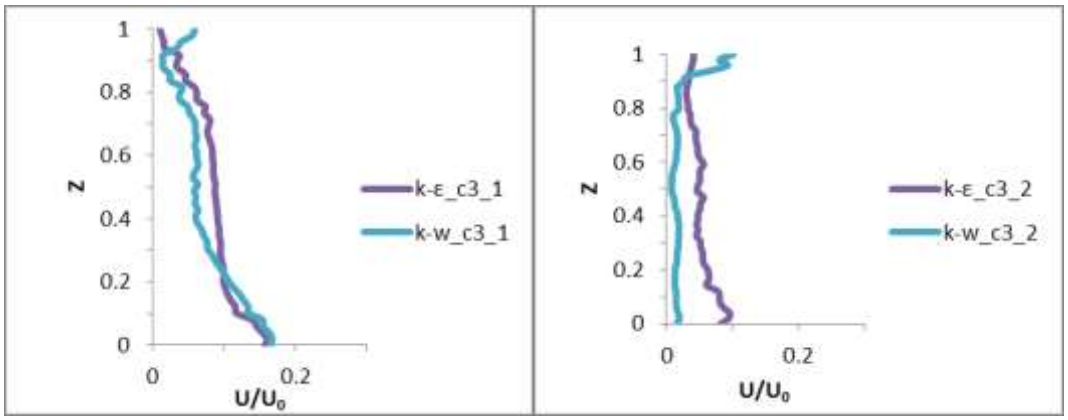

a

b

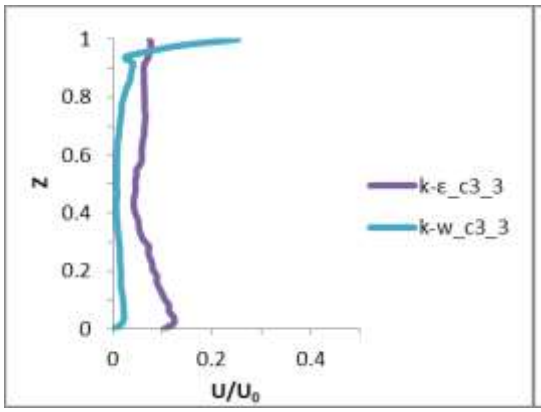

c

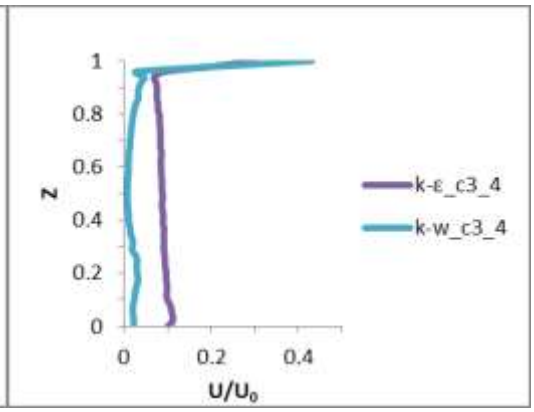

d

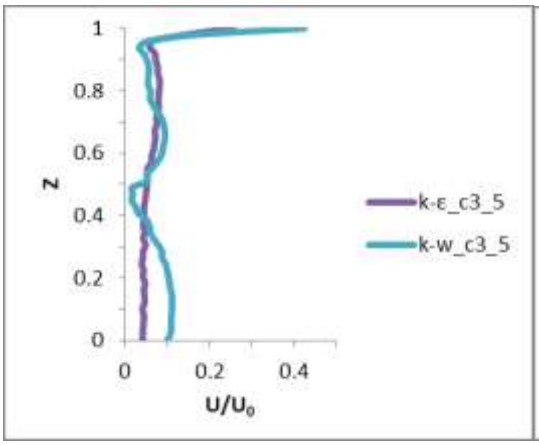

e

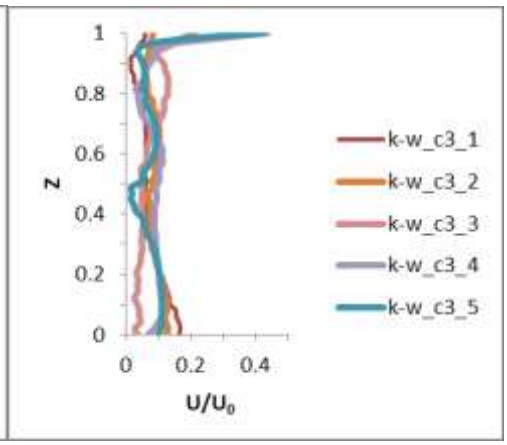

f

Figure 5.50 Square diffuser (case 3) prediction of the air velocity by Realizable k-ε model with Enhancement Wall Treatment and SST k-ω, (*Z=height/total room height (H), U=velocity/supply velocity (U_0), H=2.43m, U_0=5.2m/s*).

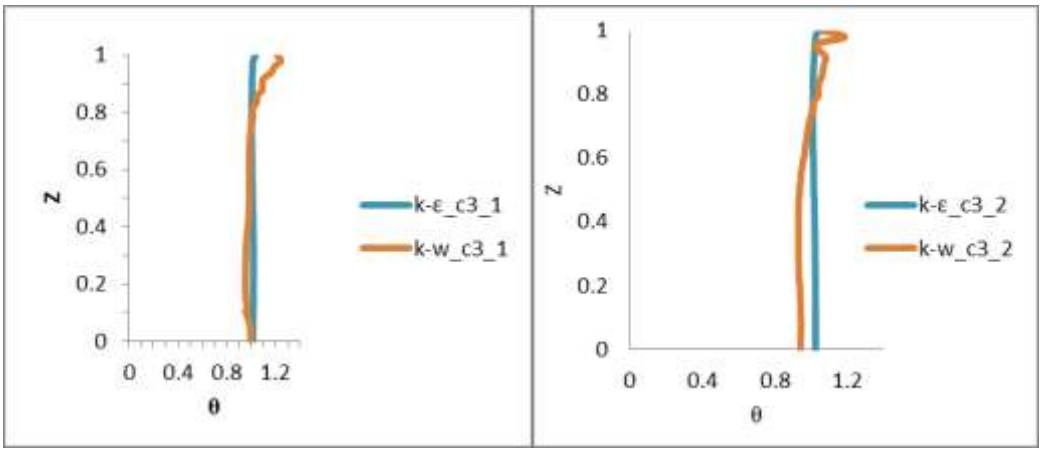

a

b

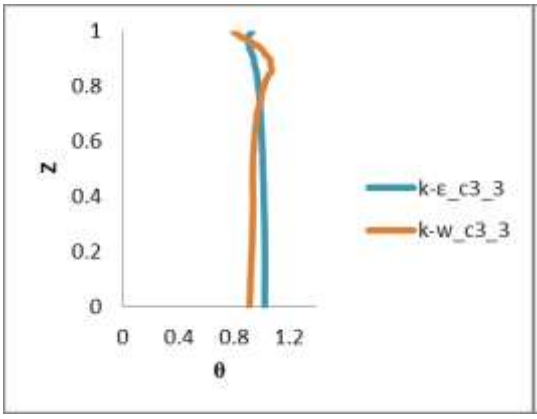

c

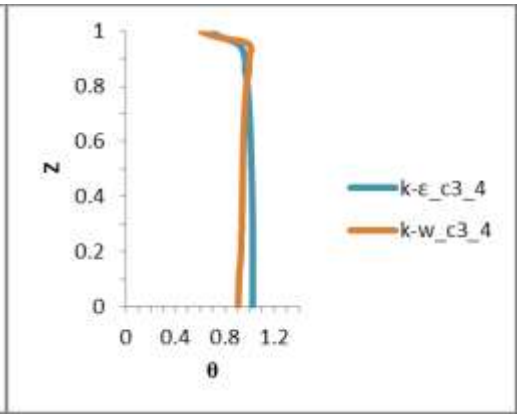

d

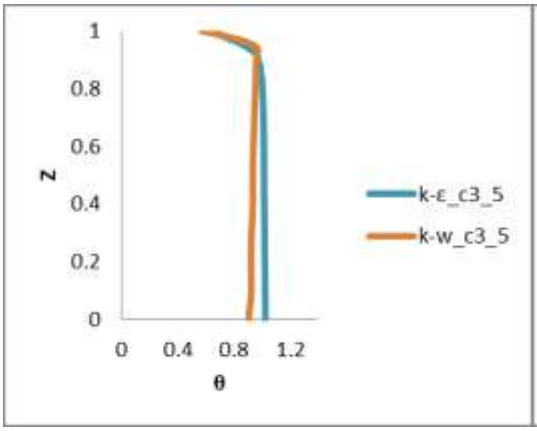

e

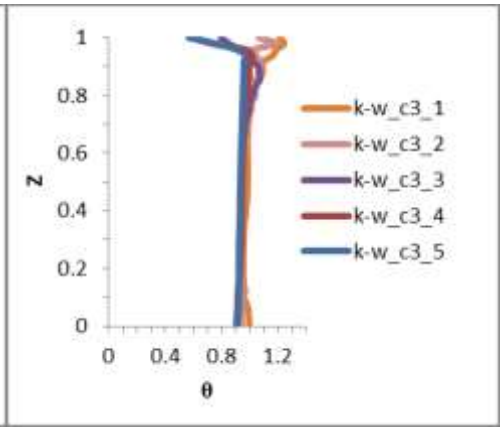

f

Figure 5.51 Square diffuser (case 3) prediction of the air temperature by Realizable k-ε model with Enhancement Wall Treatment and SST k-ω, (Z=height/total room height (H), $\theta=(T-T_{in}/T_{out}-T_{in})$, H=2.43m, T_{in}=15.0ºC, T_{out}=24ºC).

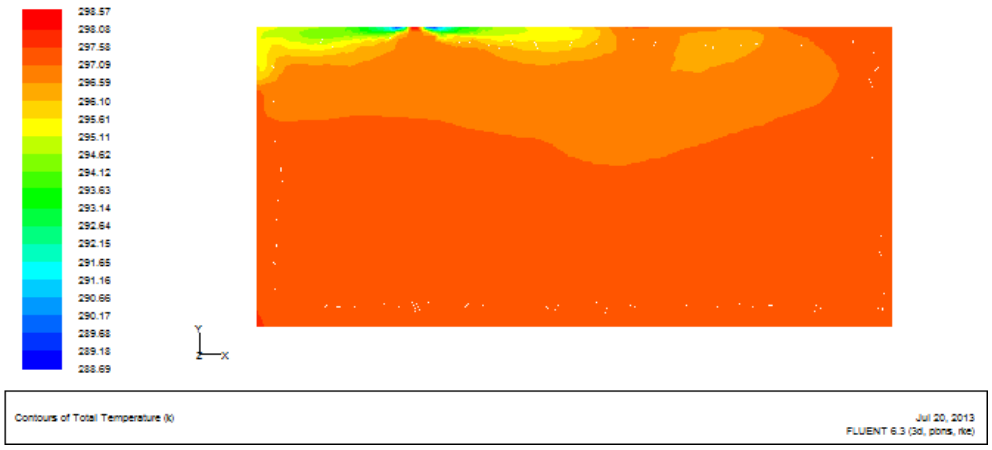

a

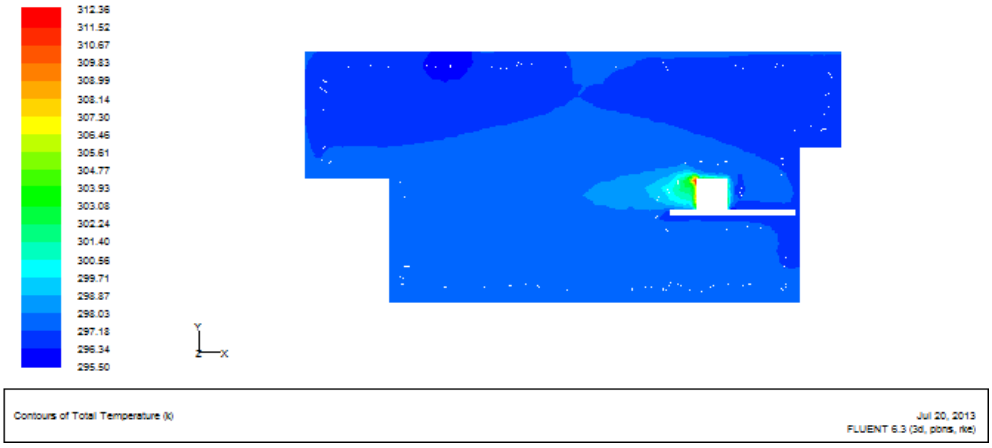

b

Figure 5.52 Distribution of calculation air temperature contours with k-ε, (case 1), (a) plane at z=1.825m, (b) plane at z=0.4m.

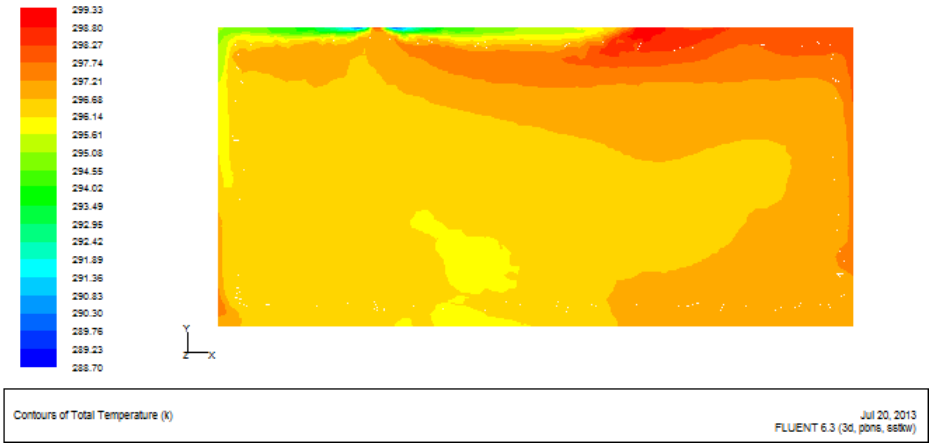

a

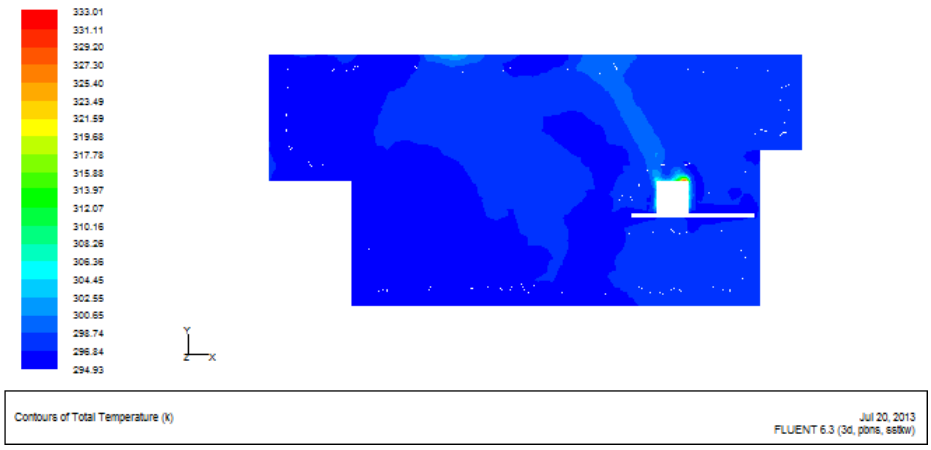

b

Figure 5.53 Distribution of calculation air temperature contours with k-ω, (case 1), (a) plane at z=1.825m, (b) plane at z=0.4m.

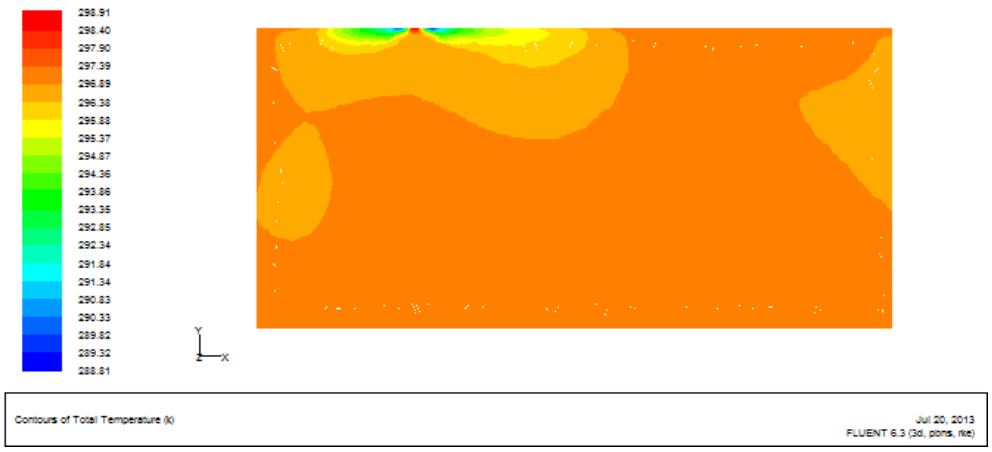

a

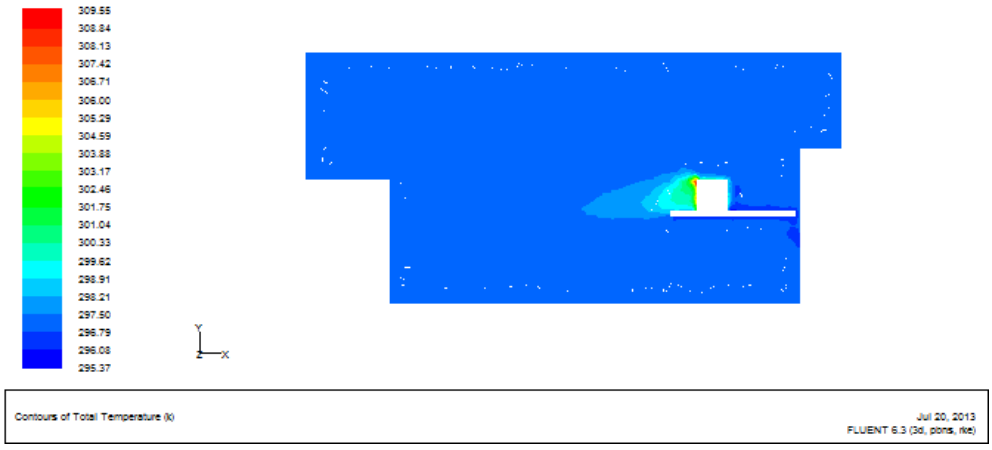

b

Figure 5.54 Distribution of calculation air temperature contours with k-ε, (case 2), (a) plane at z=1.825m, (b) plane at z=0.4m.

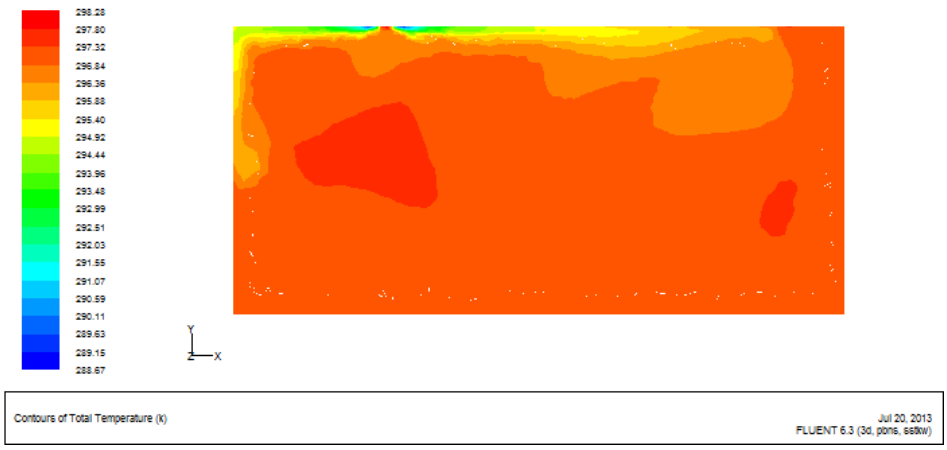

a

b

Figure 5.55 Distribution of calculation air temperature contours with k-ω, (case 2), (a) plane at z=1.825m, (b) plane at z=0.4m.

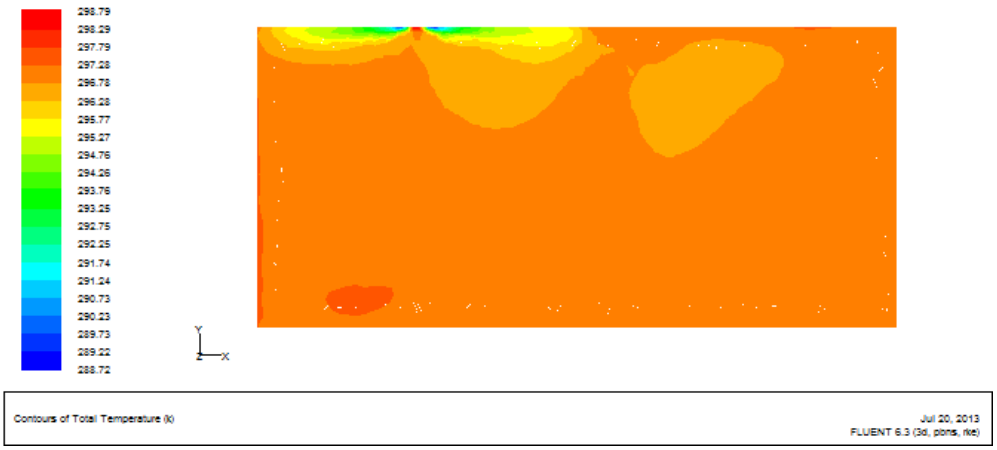

a

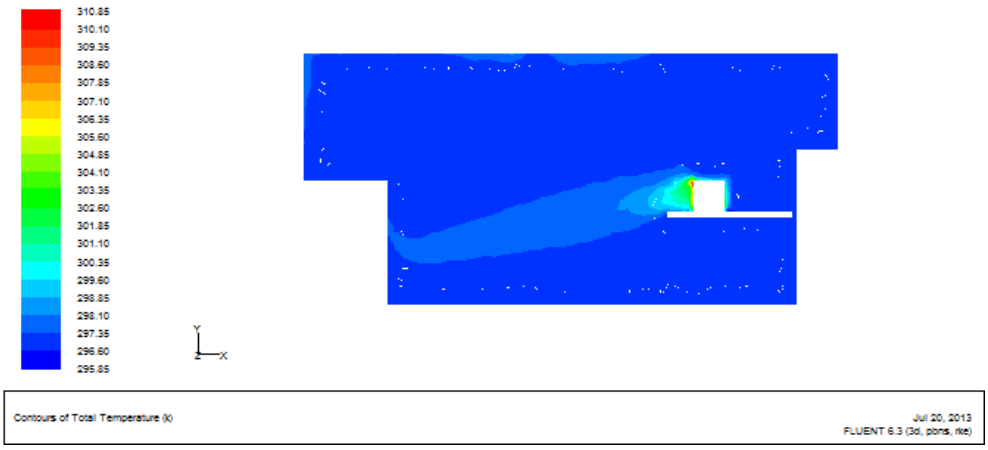

b

Figure 5.56 Distribution of calculation air temperature contours with k-ε, (case 3), (a) plane at z=1.825m, (b) plane at z=0.4m

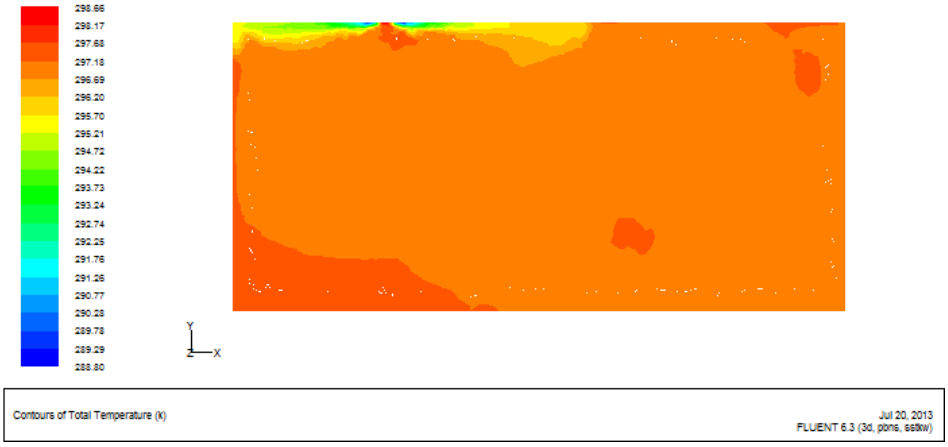

a

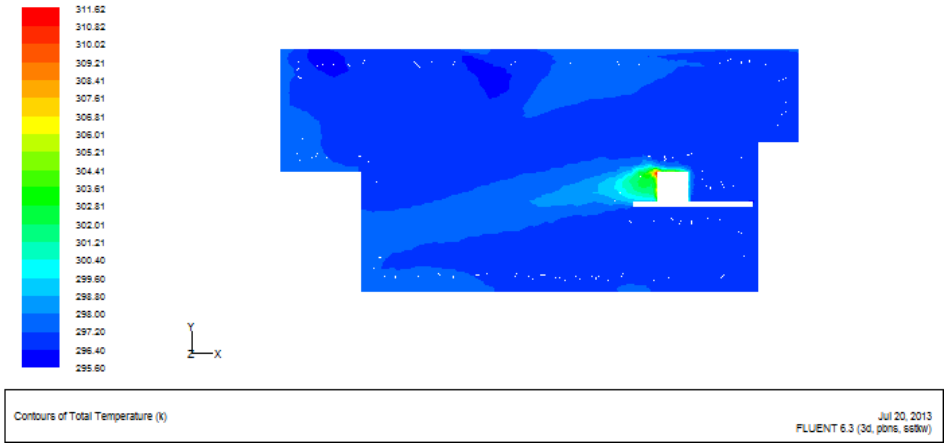

b

Figure 5.57 Distribution of calculation air temperature contours with k-ω, (case 3), (a) plane at z=1.825m, (b) plane at z=0.4 m.

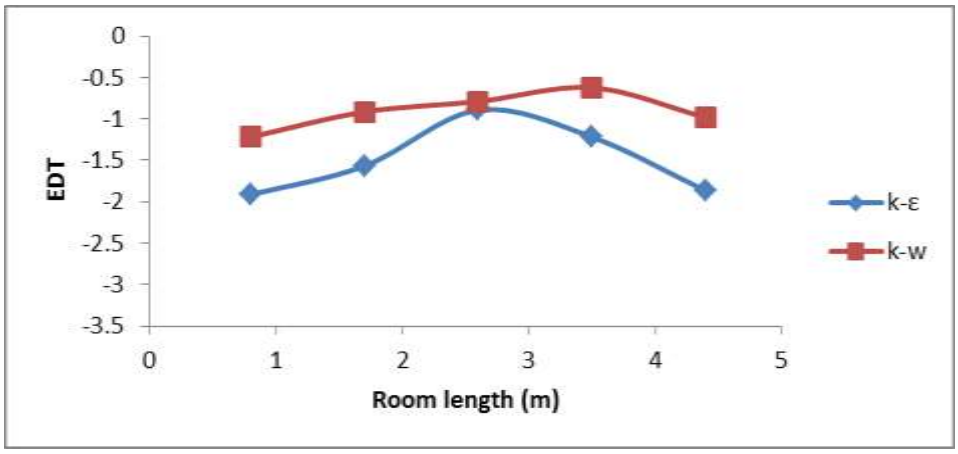

a

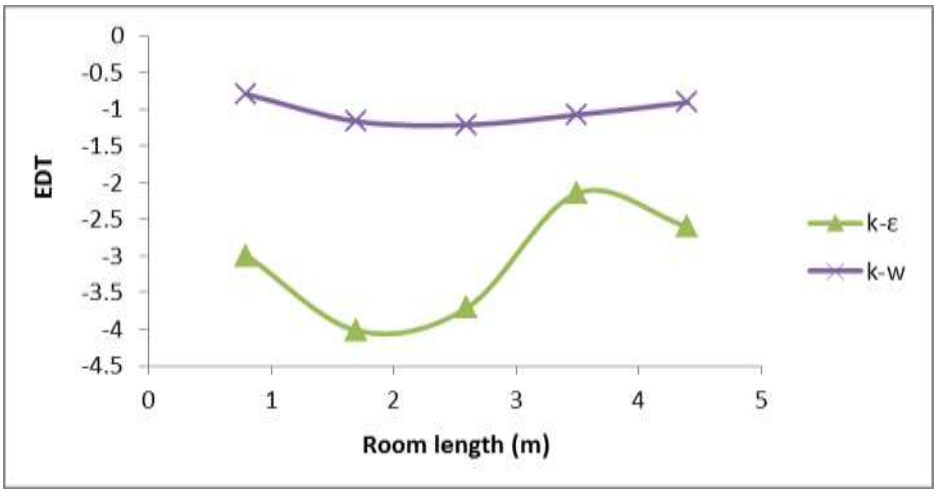

b

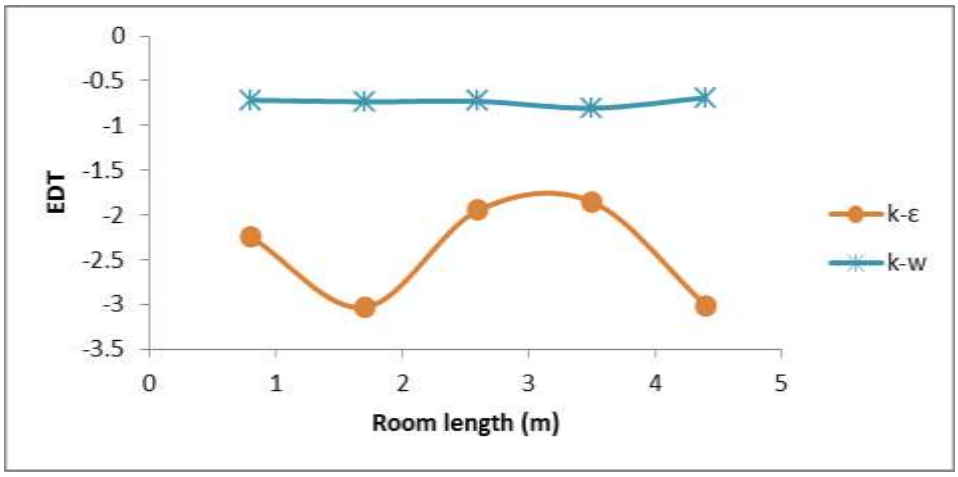

c

Figure 5.58 Slot effect draft temperature for k-ε and k-ω models, (a) case1, (b) case2, (c) case 3.

CHAPTER 6

CONCLUSION AND SUGGESTIONS FOR FUTURE WORKS

6.1 Conclusions

The study in this thesis focuses mainly on modeling of diffuser and prediction of airflow and temperature to the occupied zone under isothermal and non-isothermal heat transfer, the validation of turbulence models and modeling methods for their capability of correct prediction of some general ventilation flow problems often encountered in ventilated space.

The following conclusions are reached during this investigation:

1. It was found that the wall-function k-ε model gives a good agreement between the experimental and numerical data in the validation cases.
2. The comparison between the simulation results and experimental ones can verify the reliability of the computational model and provide theoretical basis for air organization design.
3. It can be seen that different models have different performances (advantages and drawbacks) for different problems; a model which works for one case doesn't necessarily mean that it will work for another case, and it is difficulty to validate the models with only 2D cases. More specifically, the following conclusions can be drawn:

- When dealing with practical ventilation flows with heat transfer and with complicated flow configurations, it seems that the SST k-ω model works better than the other k-ε equation turbulence models, it predicts better the recirculation flow and the flow separation which are often encountered in ventilated rooms with obstacles,
- The near wall treatment method is another very important issue for the correct prediction of indoor airflows; a validation is also needed to verify if the

chosen near-wall treatment method is capable of capturing the basic physics of the problem under consideration.

4. The CFD package is used for an air distribution simulation in the ventilated room which enables an analysis of different supply patterns. This analysis can be used to facilitate the easier choice and proper design of the positioning of vents in order to guarantee thermal comfort in the ventilated room.

5. This study evaluated the performance for four types outlet diffusers with various commonly used turbulence models for complex airflows and temperature distributions under forced ventilation conditions in Iraq with different condition buildings, may be showing that the displacement diffuser is better than other types in these cases.

6. The model accuracy has been analyzed in terms of the average temperatures at various levels. The present research indicates that all the turbulent models tested predict satisfactorily the main qualitative features of the flow and temperature distributions in Iraq with slightly better performance with the SST k-ω model that depend on the overall average error which is not exceed for displacement ventilation (19.87 % at velocity carves) and (14.20 % at temperature carve).

6.2 Suggestions for Future Works

1. The next challenging issue will also be its integration into existing building thermal analysis as effect on the airflow and temperature distribution in occupied zone.
2. A study for the same diffusers types through a development study for the effect of air humidity during the analysis and comparing the results with published ones.

Use of the method of analysis by CFD method for the work of an experimental study focusing on the effect of solar radiation on the walls and windows and how it influences the airflow and temperatures distribution.

REFERENCES

1. **C. P. Arora, 2005,** *"Refrigeration And Air Conditioning"*, Tata McGraw-Hill, second edition.

2. **Shan K. Wang, 2001,** *"Handbook Of Air Conditioning And Refrigeration"*, McGraw-Hill, second edition.

3. **W. P. Jones, January, 2001,** *"Air Conditioning Engineering"*, Elsevier Science & Technology Books, fifth edition.

4. **H. B. Awbi, 2003,** *"Ventilation Of Buildings"*, Spon Press, second edition.

5. **D. R. Oughton, and S. Hodkinson, 2008,** *"Faber And Kell's Heating And Air-Conditioning Of Buildings"*, tenth edition.

6. **Basman Mohamed Nabil El Hadidi, 1998,** *"A Computational Study Of Flow In Mechanically Ventilation Space"*, M.Sc. thesis, Faculty of Engineering, Cairo University.

7. **Fluent Inc. 2006,** Fluent 6.3.26 user's guide.

8. **ASHRAE Handbook, 2009,** *"Fundamentals Volume, American Society Of Heating "*, Refrigerating and Air-Conditioning Engineers, Inc., Atlanta, GA.

9. **F. C. McQuiston, J. D. Parker, and J. D. Spitler, 2005,** *"Heating, Ventilating, And Air Conditioning Analysis And Design"*, John Wiley & Sons Inc., Sixth Edition.

10. **Qingyan Chen, and Jelena Srebric, 2001,** *"Simplified Diffuser Boundary Conditions For Numerical Room Airflow Models"*, ASHRAE RP-1009, Final Report submitted to ASHRAE.

11. **E. M. Barber, T. Kusuda, P. J. Reynolds, and F. J. Powell, 1972,** "*A Study Of Air Distribution In Survival Shelters Using A Small-Scale Modeling Technique"*, Report to Office of Civil Defense Office of the Secretary of the Army, National Technical Information Service.

12. **Zhang, J. S., Christianson, L. L., Wu, G. J., and Riskowski, G. L, 1992**, "Detailed *Measurements Of Room Air Distribution For Evaluating Numerical Simulation Models"*, ASHRAE, vol.98, Part 1, Paper number 3548, 58-65.

13. **Aijun Wang, Yuanhui Zhang, Yigang Sun, and Xinlei Wang, 2006,** *"Experimental Study Of Ventilation Effectiveness And Air Velocity Distribution In An Aircraft Cabin Mockup"*, Building and Environment, 43, PP. (337–343).

14. **Peter V. Nielsen, 2007,** *"Comparison Between Different Air Distribution Systems"*, Aalborg University and International Centre for Indoor Environment and Energy, Denmark.

15. **T. Van Hooff, B. Blocken, T. Defraeye, J. Carmeliet, and G. J. F. Van Heijst, 2012,** *"PIV Measurements Of A Plane Wall Jet In A Confined Space At Transitional Slot Reynolds Numbers"*, Springer, Exp. Fluids, 53, PP. (499 – 517).

16. **Simon J. Rees, and Philip Haves, 2013,** *"An Experimental Study Of Air Flow And Temperature Distribution In A Room With Displacement Ventilation And A Chilled Ceiling"*, Building and Environment, 59, PP. (358-368).

17. **Liping Pang, Jie Xu, Lei Fang, Mengmeng Gong, Hua Zhang, and Yu Zhang, 2013,** *"Evaluation Of An Improved Air Distribution System For Aircraft Cabin"*, Building and Environment, 59, PP. (145-152).

18. **Yasushi Kondo, Shin-ichi Akabayashi, Osamu Nagase, and Akihiko Matsuda, 1998,** *"Numerical Simulation Of Ventilation Efficiency In Commercial Kitchen"*, International conference on air distribution in rooms, Stockholm, P.P (14 – 17).

19. **S. L. Sinha, R.C. Arora, and Subhransu Roy, 1999,** *"Numerical Simulation Of Two-Dimensional Room Air Flow With And Without Buoyancy"*, Energy and Buildings, 32, PP. (121–129).

20. **Pavel Charvat, Michal Jaros, Jaroslav Katolicky, and Petr Svorcik, 2001,** *"Numerical Modeling Of Airflow And Temperature Fields In A Glazed Attic"*, Seventh International IBPSA Conference, PP. (441-447).

21. **Fangting Song, Bin Zhao, Xudong Yang, Yi Jiang, Vipin Gopal, Gregory Dobbs, and Michael Sahm, 2006,** *"A New Approach On Zonal Modeling Of Indoor Environment With Mechanical Ventilation"*, Building and Environment, 43(3), PP.(278–286).

22. **Liyan Zhu, Rui Li, and Dongzhao Yuan, 2006,** "*Numerical Analysis Of A Cold Air Distribution System"*, the Sixth International Conference for Enhanced Building Operations, International Conference for Enhanced Building Operations China, IV-2-3.

23. **H. J. Steeman, A. Janssens, J. Carmeliet, and M. DePaepe, 2009,** *"Modelling Indoor Air And Hydrothermal Wall Interaction In Building Simulation: Comparison Between CFD And A Well-Mixed Zonal Model"*, Building and Environment, 44, PP. (572 – 583).

24. **Wei Cai, Xubo Yu, and Danjun Wang, 2010,** *"A CFD Simulation Of Cold Air Distribution System With Different Supply Patterns"*, 2nd International Conference on Computer Engineering and Technology, china, Computer Engineering and Technology (ICCET), 2nd International Conference,5, PP. (242-246).

25. **M. Cehlin, and B. Moshfegh, 2010,** *"Numerical Modeling Of A Complex Diffuser In A Room With Displacement Ventilation"*, Building and Environment, 45, PP. (2240-2252).

26. **Son H. Ho, Luis Rosario, and Muhammad M. Rahman, 2011,** *"Comparison Of Underfloor And Overhead Air Distribution Systems In An Office Environment"*, Building and Environment, 46, PP. (1415-1427).

27. **Sami A. Al-Sanea, M. F. Zedan, and M. B. Al-Harbi, 2012,** *"Effect Of Supply Reynolds Number And Room Aspect Ratio On Flow And Ceiling Heat-Transfer Coefficient For Mixing Ventilation"*, International Journal of Thermal Sciences, 54, PP. (176-187).

28. **Tengfei Zhang, Linlin Tian, Chao-Hsin Lin, and Shugang Wang, 2012,** *"Insulation Of Commercial Aircraft With An Air Stream Barrier Along Fuselage"*, Building and Environment, 57, PP. (97-109).

29. **Yan Huo, 1997,** *"Ventilation Impact On Indoor Air Quality Problems In Partitioned Offices"*, Ph. D thesis, Concordia University, Montreal - Canada.

30. **Bartak M, Cermak M, Clarke J A, Denev J, Drkal F, Lain M, Macdonald I A, Majer M, and Stankov P, 2001,** "*Experimental And Numerical Study Of Local Mean Age Of Air"*, Building simulation, PP. (773-780).

31. **Srebric, J. and Chen, Q., 2002,** *"Simplified Numerical Models For Complex Air Supply Diffusers,"* HVAC and R Research, 8(3), PP. (277-294).

32. **J. D. Posner, C. R. Buchanan, and D. Dunn-Rankin, 2003,** *"Measurement And Prediction Of Indoor Air Flow In A Model Room"*, Energy and Buildings 35, PP. (515-526).

33. **J. J. A. A. Akoua, F. Allard, C. Beghein, and B. Collignan, 2006,** *"Experimental And Numerical Studies On Indoor Air Quality In A Real Environment"*, Air Infiltration and Ventilation Centre Conference 25th Ventilation and retrofitting, PP. (203-214).

34. **Yu Mei, and Zhang Deng, 2009,** *"Numerical Simulation Of Air Distribution And Experimental Research Of Testing Room For Air Conditioning Unit"*, Computational Intelligence and Software Engineering (CiSE) International Conference, IEEE, PP. (1-4).

35. **Kisup Lee, Tengfei Zhang, Zheng Jiang, and Qingyan Chen, 2009,** *"Comparison Of Airflow And Contaminant Distributions In Rooms With Traditional Displacement Ventilation And Under-Floor Air Distribution Systems"*, ASHRAE Transactions, 115(2), PP. (306-325).

36. **Chen Q., Lee K., Mazumdar S., Poussou S., Wang L., Wang M., and Zhang, Z., 2010,** *"Ventilation Performance Prediction For Buildings: Model Assessment"*, Building and Environment,45(2), PP. (295-303).

37. **Glenn Reynders, Dirk Saelens, 2011,** *"Numerical And Experimental Evaluation Of Ventilation In Laboratories: A Case Study"*, International Conference 12th on Air Distribution in Rooms, PP. (1-8).

38. **Kiaus A. Hoffmann, 1989,** *"Computational Fluid Dynamics For Engineers"*, Austin, TX 78713-8148, USA, First Edition.

39. **Chen Q., Lee K., Mazumdar S., Poussou S., Wang L., Wang M., and Zhang, Z., 2010,** *"Ventilation Performance Prediction For Buildings: Model Assessment"*, Building and Environment,45(2), PP. (295-303).

40. **Dale A. Anderson, Jone C. Tannehell, and Richard H. Pletcher, 1984,** *"Computational Fluid Mechanics And Heat Transfer"*, The SOUTHEAST BOOK COMPANY, Reprinted.

41. **Peter V. Nielsen, 1990,** *"Specification Of A Two-Dimensional Test Case"*, The University of Aalborg, Denmark, research item 1.45.

CURRICULUM VITAE

PERSONAL INFORMATION

Surname, Name: Medhi CHOWAID

Date and Place of Birth: 14.01.1974

Marital Status: Married

Phone: 009647808511593

Email: me74k@yahoo.com

EDUCATION

Degree	**Institution**	**Year of Graduation**
M.Sc.	Çankaya Univ., Mechanical Engineering	2016
B.Sc.	University Of Technology, Mechanical Engineering	2003

T.C
YÜKSEKÖĞRETİM KURULU
ULUSAL TEZ MERKEZİ

TEZ VERİ GİRİŞİ VE YAYIMLAMA İZİN FORMU

Referans No	10099562
Yazar Adı / Soyadı	MEHDİ CHOWAID
Uyruğu / T.C.Kimlik No	IRAK / 0
Telefon	5388452081
E-Posta	me74k@yahoo.com
Tezin Dili	İngilizce
Tezin Özgün Adı	NUMERICAL STUDY OF INFLUENCE OF AIR CEILING DIFFUSERS ON ROOM AIR FLOW CHARACTERISTICS
Tezin Tercümesi	TAVAN DİFUZORLERİNİN ODADAKİ HAVA AKIM ÖZELLİKLERİNE ETKİSİ ÜZERİNE SAYISAL ÇALIŞMA
Konu	Makine Mühendisliği = Mechanical Engineering
Üniversite	Çankaya Üniversitesi
Enstitü / Hastane	Fen Bilimleri Enstitüsü
Anabilim Dalı	
Bilim Dalı	
Tez Türü	Yüksek Lisans
Yılı	2016
Sayfa	129
Tez Danışmanları	PROF. DR. TANER ALTUNOK 39904947814
Dizin Terimleri	
Önerilen Dizin Terimleri	Surface Diffraction, Edge Diffraction, Fringe Waves
Kısıtlama	Yok

Yukarıda bilgileri kayıtlı olan tezimin, bilimsel araştırma hizmetine sunulması amacı ile Yükseköğretim Kurulu Ulusal Tez Merkezi Veri Tabanında arşivlenmesine ve internet üzerinden tam metin erişime açılmasına izin veriyorum.

20.01.2016

İmza:.....

A2